Exploring the role of Wnt signalling in heart failure with preserved ejection fraction.

PAUL, M.A.

2022

Exploring the role of Wnt signalling in Heart Failure with preserved Ejection Fraction

Mhairi A. Paul

A thesis submitted in partial fulfilment of the requirements of

Robert Gordon University for the degree of

Doctor of Philosophy

This research was carried out in collaboration with

AstraZeneca (Mölndal, Sweden)

March 2022

Declaration

The thesis in candidature for the degree of Doctor of Philosophy has been composed entirely by myself. The work which is documented was carried out by myself unless expressly stated in the text. All sources of information contained within which have not arisen from the results generated have been specifically acknowledged.

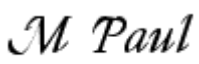

Mhairi Paul

Table of Contents

Acknowledgements

I would like to thank several people who have supported me throughout my PhD journey in Aberdeen.

First of all, the biggest thanks must go to my principal supervisor Dr Sarah Walsh for all her excellent support and guidance throughout my project. Sarah, you really go above and beyond with all the help you have given me throughout my project and for that I am eternally grateful. From going through the possibility of redundancies to working through a pandemic, it hasn't been the smoothest ride, however, we made it through. Even when I wanted to cry about results, you always had optimism that they actually really weren't that bad. I couldn't have asked for a better supervisor and I hope I have made the experience of your first PhD student an enjoyable one, as I have thoroughly enjoyed my project working with you. I would also like to thank the other members on my supervisory team, Prof. Cherry Wainwright for all your support and experience, and Dr Emma Hector for all your help with the molecular biology experiments. Thanks, must also go to my external supervisors, Prof. Stephen Leslie for continuing to read my thesis chapters, even though the clinical objective of my project was not able to be completed, and Dr Erik Ryberg for allowing the opportunity for me to work in the labs of AstraZeneca and for teaching me how to use the Corning® Epic® system. Finally, I must say a big thank you to all the members on my supervisory team mentioned above for proof reading my thesis and for giving me such an enjoyable experience throughout my PhD.

Thanks, must also go to all the technical staff for all their assistance in the labs and help with ordering consumables. A special thanks to Andrea MacMillan for always helping out with any queries or problems.

Thanks, must also go to the Medical Research Council and AstraZeneca for providing the funding for my 4-year studentship that allowed me to carry out and complete my PhD Project.

To my biggest supporters, my family, especially my Mum. Thank you for your continued support over the years and for supporting my decision to move to Aberdeen to do a PhD. I couldn't have done it without all your love and support.

Thanks to all the friends that I have made in Aberdeen, especially Hazel, Priscila, Teo and Sam. I can honestly say I have made friends for life and you have made my time in Aberdeen such a memorable and happy time for me. Also, a big thanks to my lifelong friends, Carol and Alison, for always being on the end of the phone whenever I needed a chat.

Jill, a big thanks to you for being such a great friend and listening to all my worries throughout my PhD and the phone calls every day. I can't thank you enough for your support and all your help with everything.

Publications

Abstract for Poster Presentation

Paul M, Hector E, Ryberg E, Leslie S, Wainwright C and Walsh S (2020). Wnt signalling contributes to cardiomyocyte hypertrophy. *British Journal of Pharmacology.* 177(11): 2539-2539P025. DOI: 10.1111/bph.15035 (British Pharmacological Society Conference, London, 2019).

Abstract for Oral Communication

Paul M, Hector E, Wainwright C, Ryberg E, Leslie S and Walsh S (2021). Investigation of Wnt signalling in a 'two-hit' experimental model of diastolic heart failure. *British Journal of Pharmacology.* 178(2): 422-422P046. DOI: 10.1111/bph.15316 (British Pharmacological Society Conference, Online, 2020).

Abstract

Heart failure with preserved ejection fraction (HFpEF) accounts for approximately 16% of heart failure cases according to the European Society of Cardiology long-term outpatient regiustry, with survival rates failing to improve due to the lack of effective treatments and the increasing prevalence of comorbidities. It has been widely documented throughout the literature that Wingless/int1 (Wnt) signalling plays a role in the development of both cardiomyocyte hypertrophy and cardiac fibrosis, which are key features of HFpEF. Useful *in vivo* models of HFpEF are lacking, however a recently published 'two-hit' (metabolic and mechanical stress) *in vivo* model of HFpEF shows promise. However, targeting Wnt signalling as a potential therapeutic intervention in this HFpEF model has not been investigated thus far. Therefore, the present study was carried out to investigate whether pharmacological inhibition of Wnt signalling could improve detrimental structural and/or functional changes associated with HFpEF. The present study aimed to 1) examine the role of Wnt signalling in cardiomyocyte hypertrophy; 2) investigate whether Wnt signalling contributes to the development of HFpEF using an *in vivo* model of the condition; and 3) determine whether the administration of a Wnt inhibitor (Wnt-c59) alters the maladaptive structural and/or functional changes associated with HFpEF. Initial *in vitro* experiments using H9c2 cells determined the optimum experimental conditions for AngII (1μM) induced cardiomyocyte hypertrophy. Furthermore, subsequent experiments determined that AngII induced cardiomyocyte hypertrophy is mediated, at least in part, via activation of canonical Wnt signalling, and this thesis is the first to demonstrate this pro-hypertrophic pathway in human cardiomyocytes. A role for Wnt signalling in the pathogenesis of HFpEF (a condition characterised by cardiac hypertrophy) was then examined in an *in vivo* model of the condition induced by the chronic administration of a high fat diet and N_{ω}-nitro-L-arginine methyl ester (L-NAME; 0.5g/L) to mice for 7 weeks. Findings from this study demonstrated that this mouse model of HFpEF was characterised by hypertension, cardiac hypertrophy and fibrosis, diastolic dysfunction (measured via pressure volume loop analysis), but there was no evidence demonstrating activation of canonical Wnt signalling in the hearts of these animals. Thus, on the basis of this study, a role for canonical Wnt signalling in the development of HFpEF is not supported. Notwithstanding this, treatment of HFpEF mice with Wnt-c59 (5mg/kg/day) did ameliorate diastolic dysfunction via mechanisms that may contribute to increased ventricular compliance such as BNP induced phosphorylation of titin and/or favourable regulation of the ratio of collagen subtype expression, however this requires further investigation. In conclusion this study has identified a hypertrophic role for Wnt signalling *in vitro*, indicating a link between renin angiotensin-aldosterone system (RAAS) activation and the initiation of Wnt signalling. Furthermore, in the 'two-hit' model of HFpEF there was no evidence of activation of canonical Wnt signalling, however treatment of HFpEF mice with Wnt-

c59 did ameliorate diastolic dysfunction via mechanisms that may contribute to increased ventricular compliance.

Keywords: HFpEF; Wnt signalling; cardiac function; hypertension; cardiomyocyte hypertrophy; Wnt-c59

Abbreviations (Alphabetical Order)

A

ACC/AHA	American College of Cardiology/ American Heart Association
ACE	Angiotensin-Converting Enzyme
ACTA1	Skeletal α-actin
AGT	Angiotensinogen
α-MHC	Alpha Myosin Heavy Chain
AMVMs	Adult Mouse Ventricular Myocytes
AngII	Angiotensin II
ANP	Atrial Natriuretic Peptide
AP	Action Potential
AP-1	Activator Protein 1
APC	Adenomatous Polyposis Coli Protein
ARBs	Angiotensin Receptor Blockers
ARVMs	Adult Rat Ventricular Myocytes
α-SMA	Alpha-smooth Muscle Actin
AT_1R	Angiotensin II Type 1 Receptor
AT_2R	Angiotensin II Type 2 Receptor
ATP	Adenosine 5′-triphosphate
AU	Arbitrary Units
AUC	Area Under the Curve

A wave	Atrial Contraction

B

β-catenin	Beta-catenin
BCP	1-bromo-3-chloropropane
BHF	British Heart Foundation
β-MHC	Beta Myosin Heavy Chain
BMI	Body Mass Index
BNP	B-type Natriuretic Peptide
BP	Blood Pressure
BSA	Bovine Serum Albumin
BSU	Biological Services Unit
BW	Body Weight

C

Ca^{2+}	Calcium
CAD	Coronary Artery Disease
CaMKII	Calmodulin-dependent Protein Kinase II
CaN	Calcineurin
CC	Closed Chest PVL
CCDN1	Cyclin D1
cDNA	Complementary Deoxyribonucleic Acid
cGMP	Cyclic Guanosine Monophosphate
cGMP-PKG	Cyclic Guanosine Monophosphate-protein kinase G
CHO	Chinese Hamster Ovary
CK1α	Casein Kinase 1α

CNP	C-type natriuretic peptide
CO	Cardiac Output
Col1	Collagen type I
Col3	Collagen type III
CRD	Cysteine-rich Domain
CREB	cAMP Responsive Element Binding Protein 1
CTD	Carboxy-terminal Domain
cTnI	Cardiac Troponin I
cTnT	Cardiac Troponin T
CVD	Cardiovascular Disease

D

DAAM1	Dvl associated activator of morphogenesis 1
DAG	Diacylglycerol
DBP	Diastolic Blood Pressure
DCM	Dilated Cardiomyopathy
DGK	Diglycerol Kinase
dH_2O	Deionised H_2O
DKK	Dickkopf
DM	Diabetes Mellitus
DMEM	Dulbecco's Modified Eagle Medium
DMR	Dynamic Mass Redistribution
DMSO	Dimethyl Sulfoxide
DNA	Deoxyribonucleic Acid
DOCA	Deoxycorticosterone Acetate
DOCP	Desoxycorticosterone Pivalate

DPBS	Dulbecco's Phosphate Buffer Solution
dPBS	Dulbecco's Phosphate Buffered Saline
Drp1	Dapper 1
DT	Deceleration Time
Dvl	Dishevelled

E

E_a	Aterial Elastance
ECACC	European Collection of Authenticated Cell Cultures
E wave	Early Diastolic Filling
E/A Ratio	The E-wave and the A wave ratio
EC	Excitation-contraction coupling
ECG	Electrocardiogram
ECM	Extracellular Matrix
EDP	End-Diastolic Pressure
EDPVR	End-Diastolic Pressure Volume Relationship
EDV	End-Diastolic Volume
EF	Ejection Fraction
ELISA	Enzyme-linked Immunosorbent Assay
eNOS	Endothelial Nitric Oxide Synthase
ERK1/2	Extracellular-signal-regulated Kinase ½
ESP	End-Systolic Pressure
ESPVR	End-Systolic Pressure Volume Relationship
ESV	End-Systolic Volume
ET-1	Endothelin-1
ET_A	Endothelin A receptor

F

FBS	Fetal Bovine Serum
FCS	Fetal Calf Serum
FGF	Fibroblast Growth Factor
Fn1	Fibronectin
FZD	Frizzled

G

GC-A	Guanylyl Cyclase A
GC-B	Guanylyl Cyclase B
GI	Gastrointestinal
GOI	Gene of Interest
GPx	Glutathione Peroxidase
GSH	Glutathione
GSK-3β	Glycogen Synthase Kinase 3 Beta
GTP	Guanosine-5'-triphosphate

H

H_2O_2	Hydrogen Peroxide
HBSS	Hanks Balanced Salt Solution
HCMs	Human Cardiac Myocytes
HEPES BSS	HEPES Buffered Balanced Salt Solution
hESCs	Human Embryonic Stem Cells
HF	Heart Failure
HFD	High Fat Diet
HFpEF	Heart Failure with preserved Ejection Fraction

HFrEF	Heart Failure with reduced Ejection Fraction
hiPSC-CMs	Human Induced Pluripotent Stem Cell Cardiomyocytes
HKG	Housekeeping Gene
HR	Heart Rate
HRP	Horseradish Peroxidase
HTN	Hypertension

I

I.P.	Intraperitoneal
ICR	Institute of Cancer Research
IL-6	Interleukin-6
IL-8	Interleukin-8
iNOS	Inducible Nitric Oxide Synthase
IP_3	Inositol trisphosphate
iPSCs	Induced Pluripotent Stem Cells
IVC	Inferior Vena Cava

J

JNK	c-Jun-N-terminal kinase

L

LA	Left Atrial
L-NAME	N_ω-Nitro-L-arginine methyl ester hydrochloride
LRP5/6	Low Density Lipoprotein Receptor Related Proteins
LTCC	L-type Calcium channels
LV	Left Ventricle

LVEDP	Left Ventricular End-Diastolic Volume
LVEDV	Left Ventricular End-Diastolic Volume
LVESV	Left Ventricular End-Systolic Volume
LVH	Left Ventricular Hypertrophy

M

MABP	Mean Arterial Blood Pressure
MAPKs	Mitogen Activated Protein Kinases
MGM	Myocyte Growth Medium
MI	Myocardial Infarction
miPSC-CMs	Mouse Induced Pluripotent Stem Cell Cardiomyocytes
MKPs	MAPK phosphatases
MMPs	Matrix Metalloproteinases
MMP2	Matrix Metalloproteinase 2
MRI	Magnetic Resonance Imaging
MTT	(3-(4,5-dimethylthiazol-2-yl)-2,5-diphenyltetrazolium bromide) tetrazolium
Myh6	Myosin Heavy Chain 6
Myh7	Myosin Heavy Chain 7
Myl2	Myosin Light Chain 2

N

Na^+	Sodium
NAD^+	Nicotinamide Adenine Dinucleotide
NADPH	Nicotinamide Adenine Dinucleotide Phosphate
NCAP	National Cardiac Audit Programme
NCX	Sodium-calcium Exchanger

NEAT-HFpEF	Nitrate's Effect on Activity Tolerance in Heart Failure with Preserved EF
NFAT	Nuclear Factor of Activated T Cells
NF_KB	Nuclear Factor Kappa Beta
NHS	National Health Service
NICE	National Institute for Clinical Excellence
NIH	National Institutes of Health
nNOS	Neuronal Nitric Oxide Synthase
NO	Nitric Oxide
NOS	Nitric Oxide Synthase
NPR-C	Natriuretic Peptide Receptor-3
NPs	Natriuretic Peptides
NRVMs	Neonatal Rat Ventricular Myocytes
NTD	Amino Terminal Domain
NT-proBNP	N terminal pro-BNP
NYHA Class	New York Heart Association functional classification

O

$O_{2^{\cdot -}}$	Superoxide
OC	Open Chest PVL
OCT	Optimal Cutting Temperature
OH	Hydroxyl Radical

P

PBS	Phosphate Buffered Saline
PCP	Planar Cell Polarity
PCR	Polymerase Chain Reaction

PDE5	Phosphodiesterase-5
pEF	Preserved Ejection Fraction
pGC	Particular Guanylate Cyclase
pGC-A	Particulate Guanylyl Cyclase A receptor
PKA	Protein Kinase A
PKC	Protein Kinase C
PKG	Protein Kinase G
PLC	Phospholipase C
pm	Picometer
PMSF	Phenylmethylsulfonyl Fluoride
PORCN	Porcupine
PVL	Pressure Volume Loop

Q

qPCR	Quantitative Polymerase Chain Reaction
qRT-PCR	Quantitative Reverse Transcription-Polymerase Chain Reaction

R

RA	Retinoic Acid
RAAS	Renin-Angiotensin-Aldosterone System
RAR/RXR	Retinoic acid receptor/retinoid X receptor
RESSA	Research Ethics: Student and Supervisor Appraisal
RGU	Robert Gordon University
RNA	Ribonucleic Acid
ROCK	Rho-associated Protein kinase
ROS	Reactive Oxygen Species

RT-PCR	Reverse Transcription-polymerase Chain Reaction
RVU	Relative Volume Units
RyR2	Ryanodine Receptor 2

S

SAMP	Accelerated Senescence Model
SBP	Systolic Blood Pressure
SD	Standard Diet
SEM	Standard Error of the Mean
SERCA	SR Ca^{2+}-adenosine triphosphatase
sFRPs	Secreted Frizzled Related Protein
sGC	Soluble Guanylate Cyclase
SGLT2	Sodium/glucose cotransporter 2
SOD	Superoxide Dismutase
SR	Sarcoplasmic Reticulum
SV	Stroke Volume

T

T2DM	Type 2 Diabetes Mellitus
TAC	Transverse Aortic Constriction
TAE	Tris-acetate-EDTA
TBE	Tris-Borate-EDTA
TCF/LEF	T Cell Factor/ Lymphoid Enhancer Factor
TE	Tris-EDTA
TGF-β	Transforming Growth Factor Beta
TIMPs	Tissue Inhibitor of Metalloproteinases

TL	Tibia Length
TMB	Tetramethylbenzidine
TNFα	Tumour Necrosis Factor Alpha
TNS	Trypsin Neutralising Solution

V

Vp	Parallel Conductance Value
vs.	Versus
VSMC	Vascular Smooth Muscle Cell

W

WAT	White Adipose Tissue
WHO	World Health Organisation
WIF1	Wnt Inhibitory Factor
WISP1	Wnt inducible Signalling Protein 1
Wnt	Wingless/Int1

Table of Figures

Chapter 1: General Introduction

Chapter 2: Materials and Methods

Chapter 3: Optimisation of an *in vitro* model of cardiomyocyte hypertrophy

Chapter 4: Investigating the role of Wnt3a in cardiomyocyte hypertrophy

Chapter 5: Characterisation of a "two-hit" experimental model of HFpEF

Chapter 6: Investigating the effect of inhibition of Wnt signalling in a "two-hit" experimental model of HFpEF

Chapter 7: General Discussion

List of Tables

Chapter 1: General Introduction

Chapter 2: Materials and Methods

Chapter 3: Optimisation of an *in vitro* model of cardiomyocyte hypertrophy

Chapter 5: Characterisation of a ‘two-hit’ experimental model of HFpEF

Chapter 6: Investigating the effect of inhibition of Wnt signalling in a ‘two-hit’ experimental model of HFpEF

Chapter 1: General Introduction

1.1. Cardiovascular Physiology

1.1.1. Excitation-contraction coupling

One of the most vital processes in the heart is excitation-contraction (EC) coupling which enables the chambers of the heart to both contract and relax. Every contractile cycle in cardiomyocytes is started by the production of an action potential (AP) by pacemaker cells in the sinoatrial node. The AP is rapidly transmitted throughout the heart via conduction fibres and from cell to cell through gap junction intracellular channels. Both ventricular and atrial cardiomyocytes are connected to each other by a chain of intercalated discs composed of gap junctions that conduct the AP directly between the cytoplasm of adjacent cells. The EC coupling cycle involves the following series of steps: 1) depolarisation of the plasma membrane and its membrane invaginations by the AP; 2) transduction of the depolarisation signal to the sarcoplasmic reticulum (SR) membrane; 3) activation of calcium (Ca^{2+}) release from the SR and subsequent global increase in intracellular Ca^{2+}; 4) transient interaction of Ca^{2+} with contractile proteins resulting in muscle contraction; and 5) return of intracellular Ca^{2+} concentration back to levels at resting conditions leading to muscle relaxation (Smyrnias *et al*. 2012).

1.1.2. Frank-Starling Law/Mechanism

In the late 19th century, it was observed by Otto Frank that the strength of ventriclar contraction was elevated when the ventricle was stretched prior to contraction. This finding was further studied by Ernest Starling in the early 20th century who discovered that increasing venous return to the heart which increased the filling pressure (left ventricular end-diastolic pressure; LVEDP) of the ventricle, subsequently led to increased stroke volume (SV; Abraham *et al.* 2016). On the contrary, decreasing venous return reduces SV. Therefore, the Frank-Starling Law/Mechanism refers to the ability of the heart to alter its force of contraction and therefore SV in response to changes in venous return. The Frank-Starling mechanism arises as a result of the length-tension relationship observed in cardiac muscle. Cardiac muscle contraction is increased by the stretching of muscle fibres (myofibrils), which increases Ca^{2+} sensitivity. In particular the sensitivity of troponin for binding Ca^{2+} increases, resulting in the increased release of Ca^{2+} from the SR. In addition to the increase in Ca^{2+}, there is a decrease in the spacing between thin and thick filaments when a cardiac muscle fibre is stretched, resulting in the formation of an increased number of actin-myosin cross-bridges. The sarcomere length (which is determined by the degree of stretch placed on the individual fibres by ventricular filling) at the time of muscle cell activation by Ca^{2+} influences the force the muscle fibre generates (Chung *et al*. 2016).

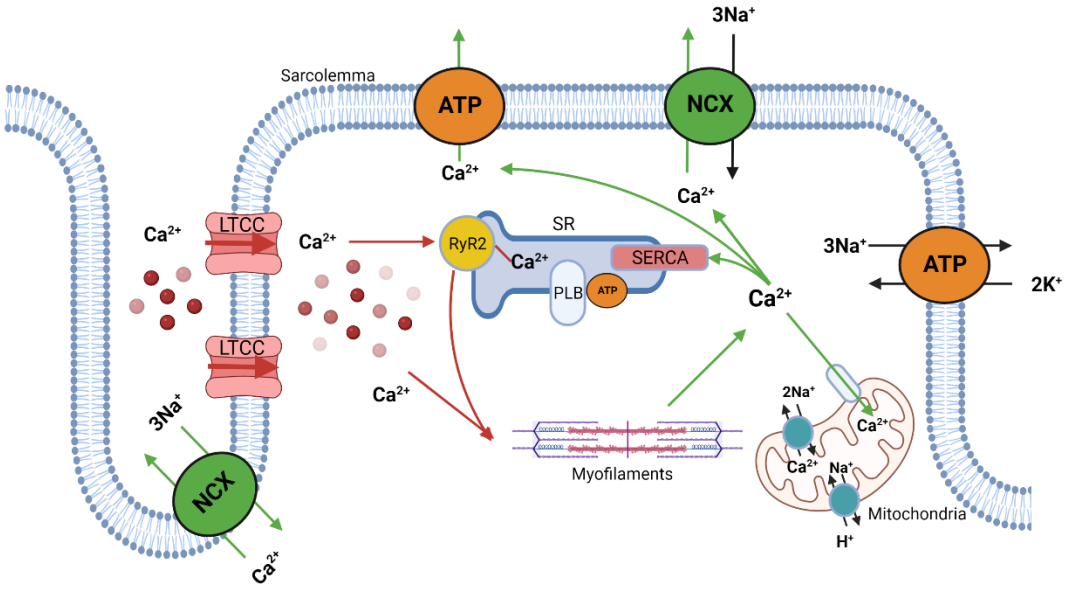

Figure 1.1. The transport of Ca^{2+} in ventricular cardiomyocytes for contraction and relaxation. Contraction is initiated by an AP exciting the sarcolemma, which opens L-type calcium channels (LTCC) in the cell membrane and transverse tubules, subsequently allowing Ca^{2+} to enter the cell, and leading to a large increase of Ca^{2+} in the dyadic space (region bounded by the t-tubule and SR). This influx of Ca^{2+} activates the ryanodine receptor 2 (RyR2) located on the SR inducing Ca^{2+}- induced Ca^{2+} release. The newly released Ca^{2+}, which is in the cytosol of the cell, stimulates contraction of the cardiomyocyte by binding to the myofilament protein troponin C (i.e. the Ca^{2+} sensor for induction of contraction). To allow the cell to relax, SR Ca^{2+}-adenosine triphosphatase (SERCA) drives Ca^{2+} from the cytosol of the cell into the SR. A further reduction of cytosolic Ca^{2+} is also achieved via the sodium-calcium exchanger (NCX) which works in forward mode to pump a Ca^{+} ion out of the cell in exchange for $3Na^{+}$ ions. Ca^{2+} is then subsequently unbound from troponin C resulting in relaxation (Bers 2002).

Therefore, the pressure generated by cardiac muscle fibres is linked to the end-diastolic volume (EDV) of the left and right ventricles. If the Frank-Starling mechanism did not exist and right and left ventricular outputs were not equal, blood would collect in the pulmonary circulation (if the right ventricle produced more output than the left) or the systemic circulation (if the left ventricle (LV) produced more output than the right).

Preload is the term used to describe the initial stretching of the cardiomyocyte prior to contraction and is influenced by venous return. When there is an increase in venous return to the heart, both EDV and end-diastolic pressure (EDP) are increased, which stretches the sarcomeres and therefore increases preload. Conversely, preload is decreased in conditions characterised by reduced ventricular compliance such as cardiac hypertrophy or impaired relaxation. Furthermore, changes in preload can profoundly affect SV. Afterload is the amount of pressure the ventricles must overcome to open the aortic valve and eject the blood into the systemic circulation and is influenced by both aortic pressure and systemic vascular resistance. Any changes in afterload will affect end-systolic volume (ESV), SV, and EDP. An increase in systemic vascular resistance and aortic pressure increases afterload, subsequently decreasing SV and increasing ESV. Afterload does not directly alter preload, however preload changes in response to changes in afterload i.e. afterload increases ESV which when combined with venous return increases EDV and subsequently preload (Vincent 2008).

1.2. Cardiovascular Disease

Cardiovascular disease (CVD) is an umbrella term used to describe a number of linked pathologies that affect the heart and circulation and includes stroke, coronary artery disease (CAD), myocardial infarction (MI), type 2 diabetes mellitus (T2DM) and heart failure (HF). It has been reported that CVD is the leading cause of death worldwide, with an estimated 17.7 million people dying as a result of this condition in 2015 (World Health Organisation (WHO), 2017). In relation to the UK, 25% of all deaths are caused by CVD which accounts for approximately 168,000 deaths per year (British Heart Foundation (BHF) Statistics 2021), with a reported financial burden of over 750 million pounds spent treating CVD within the National Health Service (NHS) in Scotland alone in 2012/2013 (Bhatnagar *et al.* 2015). Throughout an average human lifetime, the heart will undergo 2.8 billion cycles of contraction and relaxation (Monfredi *et al*. 2013), where a precise sequence is choreographed to ensure the effective circulation of blood around the body. During this time, many of the biophysical properties of the heart change, making it more susceptible to injury and disease (Carrick-Ranson *et al*. 2012;

Lakatta *et al*. 2014), consequently both the risk and prevalence of CVD is higher in the ageing population (Rodgers *et al*. 2019). With life expectancy increasing (National Institutes of Health (NIH) 2016) and the burden on the NHS growing, the development of strategies aimed at both the prevention and improved management of CVD is of paramount importance.

1.3. Heart Failure (HF)

1.3.1. Definition of HF

HF is a clinical syndrome where myocardial pump function is insufficient for sustaining and supporting a patient's physiological demands. It can be caused by both structural and functional defects in the myocardium resulting in the heart failing to pump a sufficient volume of blood to the lungs and around the body (Kemp and Conte 2012). In 2017, the global number of HF cases was 64 million (Bragazzi *et al*. 2021) and in the UK alone it is estimated that as many as 920,000 people are living with HF in the UK (BHF Statistics 2021). This alarming increase in the prevalence of this disease is in part due to increases in both population size and life expectancy, but is primarily due to one or more pathophysiological conditions. The most frequent causes of HF include hypertension (HTN), MI, CAD, and T2DM, while less common aetiologies include myocarditis, valvular disease, cardiomyopathies, infections, systemic toxins, and cardiotoxic drugs (Kemp and Conte 2012). In this setting, the failing heart initiates several compensatory mechanisms including activation of the neurohormonal system which leads to LV remodelling (characterised by increased ventricular volume and wall thickness) in order to increase cardiac output (CO) and maintain adequate tissue perfusion. However, over a period of time these compensatory measures can no longer sustain the physiological needs of the patient and the heart begins to decline. As the heart begins to fail, symptoms start to arise which include peripheral oedema and ascites from reduced venous return and dyspnoea from pulmonary congestion. Other symptoms include fatigue, lack of appetite, and nausea (NHS 2018).

1.3.2. Risk factors for developing HF

Common risk factors associated with HF include smoking, obesity, stress, high blood pressure (BP), and high cholesterol. For many years it was thought that heart disease predominantly affected men, however in reality the incidence of this disease in women is greater, particularly as they age (Bhatnagar *et al*. 2015). Age is a key risk factor for HF and is partly due to the increased exposure to numerous insults including obesity, smoking, HTN, and chronic diseases. Increasing age is also linked to gradual changes in myocardial tissue, including

decreased LV relaxation, elevated myocardial and arterial stiffness, and decreased contractility. The aging heart also displays an increase in LV mass in response to peripheral vascular stiffness and increased haemodynamic load (North and Sinclair 2012). As people age there is an increasing incidence in the number of patients displaying HF as shown in Figure 1.2.

1.3.3. Aetiology of HF

The primary aetiology of HF appears to vary between different countries (Ziaeian and Fonarow 2016), however patients tend to have multiple overlapping disorders (listed in Table 1.1.), which all contribute to the development of HF. The predominant aetiological factors leading to HF are often dependent on the population being studied with CAD and HTN being the most common causes of HF in the developed world, while valvular heart disease and nutritional cardiac disease are much more frequent in the developing world.

1.3.4. Classifications of HF stages

As HF is a progressive syndrome, it requires continuous assessment to evaluate the severity. To be able to assess the severity, clinicians require valid assessment systems in accordance with national clinical practice guidelines. The New York Heart Association functional classification (NYHA class) or the American College of Cardiology/American Heart Association (ACC/AHA) are assessment schemes typically used by clinicians to assess HF. The NYHA class is based on the signs presented by the patients (Table 1.2.), while the ACC/AHA stages are assessed on the extent of damage to the heart (Figure 1.3.; Athilingam *et al*. 2013). Clinicians may use the two assessment tools individually or use both together to make clinical treatment decisions. Both these classification systems have strengths and weaknesses with conflicting evidence regarding whether the NYHA classes and the ACC/AHA stages are correlated to cognitive and physical function (Raphael *et al*. 2007). However, there is evidence acknowledging that the NYHA classification system is still a valuable and reliable tool in the clinical setting (Bredy *et al*. 2018).

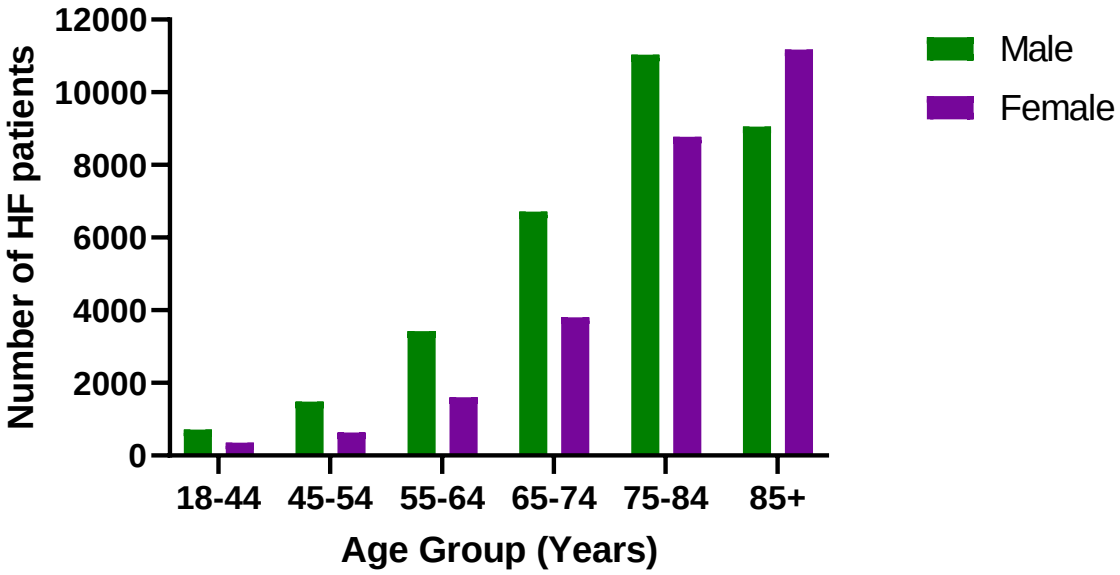

Figure 1.2. Age and gender demographics of patients with HF on first admission. (Adapted from National Institute for Cardiovascular Outcomes Research (NICOR), 2019/2020).

Table 1.1 Aetiology of HF. (Adapted from Lip *et al*. 2000).

Aetiology of Heart Failure
There is no agreed or satisfactory classification for the cause of HF, with much overlap between potential categories.
1- Coronary artery disease **i. Myocardial infarction** **ii. Ischaemia**
2- Hypertension
3- Cardiomyopathy **i. Dilated (congestive)** **ii. Hypertrophic/obstructive** **iii. Restrictive –e.g. amyloidosis, sarcoidosis and Obliterative**
4- Valvular and congenital heart disease **i. Mitral valve disease** **ii. Aortic valve disease** **iii. Atrial septal defect, ventricular septal defect**
5- Arrhythmias **i. Tachycardia** **ii. Bradycardia** **iii. Loss of atrial transport – e.g. atrial fibrillation**
6- Alcohol and drugs **i. Alcohol** **ii. Cardiac depressant drugs (β-blockers, calcium antagonists)**
7- "High output" failure **i. Anaemia, thyrotoxicosis, arteriovenous fistulae, Paget's disease**
8- Pericardial disease **i. Constrictive pericarditis** **ii. Pericardial effusion**
9- Primary right heart failure **i. Pulmonary hypertension – e.g. pulmonary embolism** **ii. Tricuspid incompetence**

Table 1.2. The NYHA classification system of HF. (Adapted from Davis *et al*. 2000).

Class	Symptoms
Class I (Asymptomatic)	• No limitation of physical activity. Ordinary physical activity does not cause symptoms (under fatigue, palpitations, shortness of breath or angina pectoris). • This can be suspected only if there is a history of heart disease that is confirmed by investigation such as echocardiography.
Class II (Mild)	• Slight limitation of physical activity. • In milder Class II disease, strenuous exercise causes symptoms but patients can continue to have an almost normal lifestyle and employment. • In more severe Class II cases, patients can be short of breath on one flight of stairs and be unable to work except at a desk.
Class III (Moderate)	• Marked limitation of physical activity. • Comfortable at rest, but fatigue, palpitations or shortness of breath results from mild physical exertion • Walking on the flat indoors and washing and dressing produce symptoms.
Class IV (Severe)	• Unable to carry out any physical activity without discomfort. • Patients are breathless at rest and mostly housebound. • If any physical activity is undertaken, discomfort is increased.

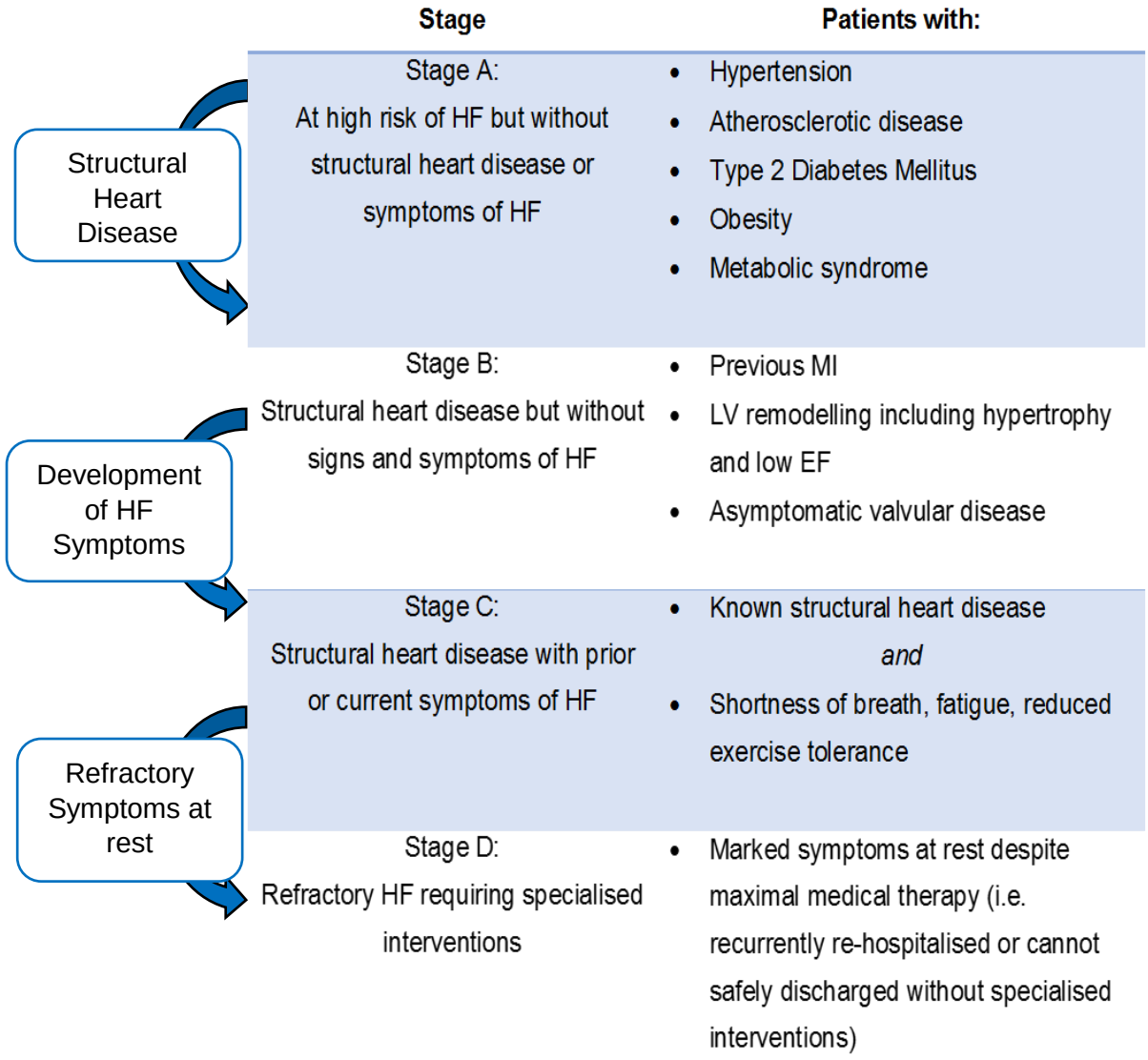

Figure 1.3. Stages in the development of HF – the ACC/AHA classification. (Adapted from Jessup *et al.* 2009).

1.3.5. Diagnosis of HF

Diagnosis can often be difficult in the early stages of HF due to symptoms being non-specific, therefore it's difficult to discriminate between HF and other medical conditions. Symptoms and signs of HF are detailed in Table 1.3. Several of the symptoms associated with HF occur as a result of both sodium and water retention, therefore are not specific to the condition. Although elevated jugular pressure and displacement of the apical impulse are classed as more specific signs of HF, it is difficult to detect these signs in patients. Another challenge in the detection of HF is the difficulty of diagnosing signs and symptoms in obese individuals, in the elderly, and in patients with chronic lung disease (Diez-Villanueva and Alfonso 2016; Celutkiene *et al*. 2017). Therefore, effective diagnostic tests are essential to confirm the presence of HF.

1.3.5.1. General Diagnostic Tests

The most frequently used diagnostic tools in patients with suspected HF are the echocardiogram/echocardiography and electrocardiogram (ECG). Cardiac magnetic resonance imaging (MRI) is also a useful diagnostic tool and arguably better than echocardiography and ECG, however access to MRI is limited due to the high cost associated with it. Echocardiography uses ultrasound in the 2-7MHz range which provides information about the structure and the function of the heart. All imaging techniques can provide an ejection fraction (EF), however the versatility of echocardiography makes it unique in terms of its provision of volumes, ventricular function, diastolic function, haemodynamics, and detection of valvular disease. The main ultrasound modalities used are M-mode, two dimensional, three dimensional, spectral Doppler, and colour Doppler echocardiography. M-mode echocardiography is the simplest type which creates a trace of the heart rather than a detailed picture of heart structures. It is useful for viewing the heart's pumping chambers, thickness of heart walls, or the size of the heart itself. Doppler echocardiography is a method used to measure and assess the flow of the blood through the heart's valves and chambers, with colour doppler being an enhanced form which designates different colours to the direction of blood flow. Two-dimensional echocardiography is used to visualise the actual motion of the heart structures with three-dimensional echocardiography capturing images with great detail and live images to allow for a more accurate assessment of heart function. Heart failure with reduced ejection fraction (HFrEF; also known as systolic HF) is relatively straightforward to diagnose by echocardiography and is characterised by a reduced EF (<40%) and a dilated LV. Heart failure with preserved ejection fraction (HFpEF; also known as diastolic HF) is harder to diagnose as not only are both HF symptoms and a preserved EF (>50%) present, there are also functional or structural signs of diastolic dysfunction or LV hypertrophy (LVH), respectively.

Table 1.3. Signs and symptoms typical of HF. (Adapted from Ponikowski *et al*. 2016).

Symptoms	Signs
Typical	**More Specific**
Breathlessness (Orthopnoea, Paroxysmal nocturnal dyspnoea) Reduced exercise tolerance Fatigue, tiredness, increased time to recover after exercise Ankle swelling	Elevated jugular venous pressure Hepatojugular reflux Third heart sound Laterally displaced apical impulse
Less Typical	**Less Specific**
Nocturnal cough Wheezing Bloated feeling Loss of appetite Confusion (especially in the elderly) Depression Palpitations Dizziness Syncope (temporary loss of consciousness) Bendopnea (shortness of breath when leaning forward)	Weight gain (>2kg/week) Weight loss (in advanced HF) Tissue wasting (cachexia) Cardiac murmur Peripheral oedema Pulmonary crepitations (crackling sound in lungs) Reduced air entry and dullness to percussion at lung bases Tachycardia (heart rate that exceeds the normal rate) Irregular pulse Tachypoea (abnormal rapid breathing) Ascites Cold extremities Narrow pulse pressure

To evaluate diastolic dysfunction the following measurements are of particular importance: the ratio between the E-wave and the A-wave (E/A ratio), estimating LV filling pressure via e', and measurement of deceleration time (DT; Nagueh *et al*. 2016). Mitral doppler echocardiography can also evaluate the characteristics of diastolic trans-mitral-valve blood flow by measuring the peak velocities of blood flow during early diastolic filling (E wave) and atrial contraction (A wave) and calculate a ratio. In healthy patients, the E wave velocity is greater than the A wave velocity giving a ratio of around 1.5. In patients with early signs of diastolic dysfunction, impaired relaxation due to the heart becoming stiffer is present and thus the E/A wave ratio is less than 1. However as diastolic dysfunction worsens and the left ventricular pressure rises, the E/A ratio increases to 2 or above (Gutierrez and Blanchard 2004). Example E/A waves are shown in Figure 1.4. DT is the period of time from the peak of the E wave to its projected baseline and normally ranges between 150ms and 240ms, with a normal E-wave exhibiting a rapid acceleration (ascending part) and rapid deceleration (descending part). The DT indicates the time taken for equalising the pressure difference between the left atrium and LV. If LV compliance or left atrial (LA) pressure is increased, the DT will decrease (Nagueh *et al*. 2016). The E/e' ratio, which is determined by dividing the peak E-wave by the peak e' velocity, can estimate LVEDP. A normal E/e' ratio is considered <15, while diastolic dysfunction via impaired ventricle relaxation increases the E/e' ratio. A practical approach to assess and grade diastolic dysfunction is shown below in Figure 1.5.

While an echocardiogram provides information regarding both the anatomy and function of the heart, the standard 12 lead ECG enables the assessment of heart rhythm and electrical conduction and can also provide evidence of LVH. A schematic of a normal ECG is shown in Figure 1.6. An analysis by O'Neal et al. (2017) examining the differential predictive abilities of ECG abnormalities to determine if patients are at risk of HFrEF or HFpEF identified that markers associated with HFrEF included evidence of abnormal ventricular depolarisation (prolonged QRS duration, delayed time to intrinsicoid deflection), axis deviation (left and right), abnormal ventricular repolarisation (ST/T-wave abnormalities), and conduction disease (left bundle-branch block). In patients with HFpEF, a higher resting heart rate (HR) and abnormal P-wave axis were seen with an abnormal QRS-T axis being associated with both subtypes (O'Neal *et al*. 2017). An illustration of an ECG wave indicating LVH is shown in Figure 1.7. However, routine biochemical and haematological investigations are also important to diagnose HF (McMurray *et al*. 2012).

A

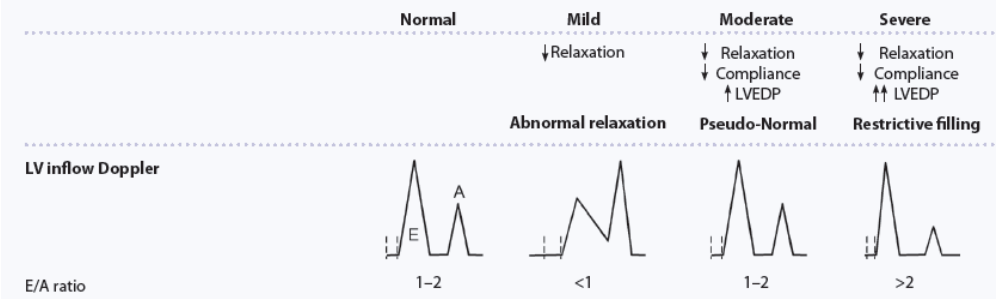

B

Normal

C

HFpEF

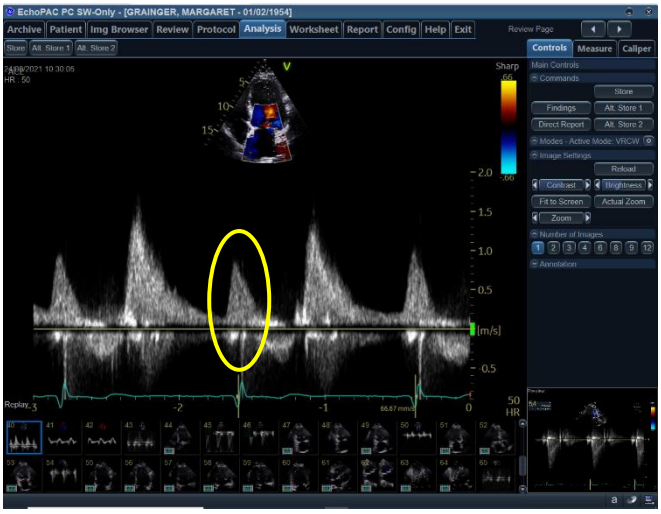

Figure 1.4. Examples of E and A waves in normal and HFpEF patients. (A) The E/A ratios and waves shown in healthy patients and patients with increasing severity of diastolic dysfunction adapted from Masani et al. (2011). (B) An echocardiogram illustrating a healthy patient's E (circled in red) and A (circled in green) waves. (C) A patient displaying signs of diastolic dysfunction with a decrease in the A wave (circled in yellow). Images (B and C) were provided by Professor Stephen Leslie from Raigmore Hospital, Inverness.

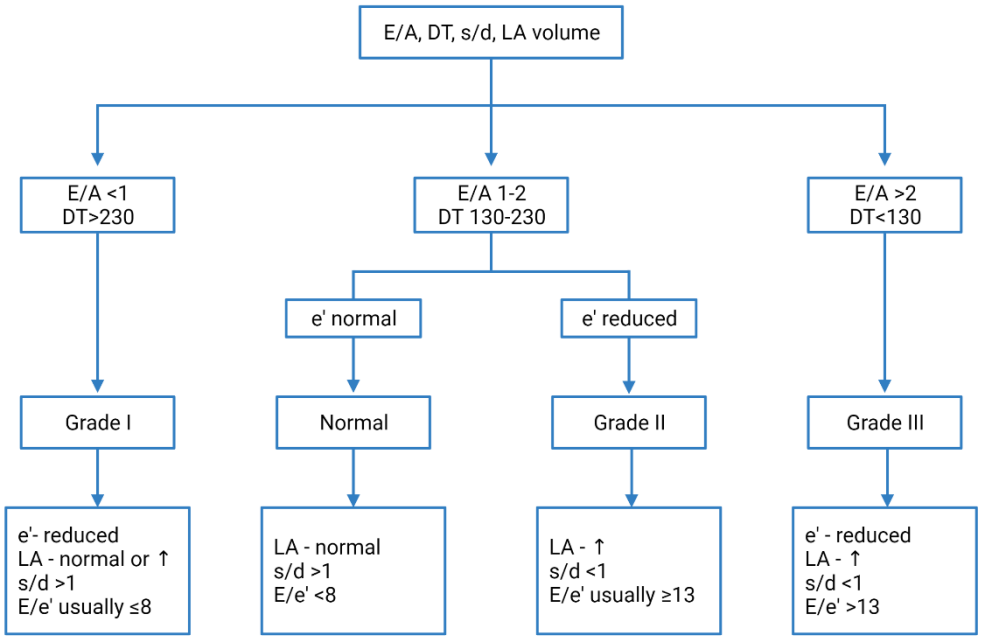

Figure 1.5. Practical approach to assess and diagnose diastolic function. E/A ratio – ratio of the E wave/A wave. DT – deceleration time (ms). e'- velocity of early myocardial relaxation on tissue Doppler imaging (cm/s). LA – left atrial volume. s/d – ratio of pulmonary vein peak systolic/peak diastolic velocity. E/e' – ratio of mitral valve E wave/myocardial relaxation velocity. Adapted from (Mathew *et al*. 2013).

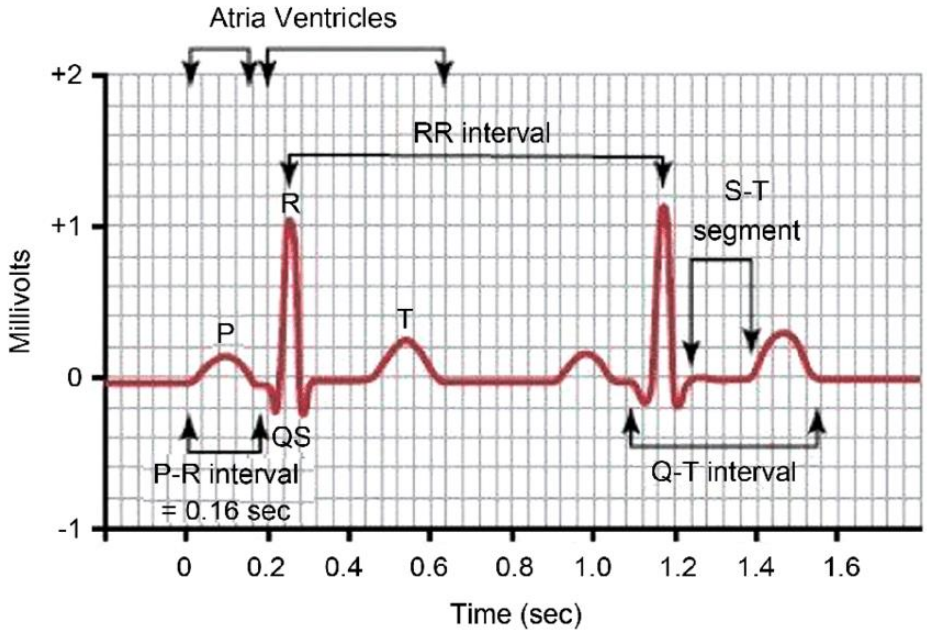

Figure 1.6. Diagram depicting a normal ECG. P wave- the depolarisation of the right and left atria (contraction). QRS complex – right and left ventricular depolarisation. ST-T wave – ventricular repolarisation. P-R interval – duration from onset of atrial depolarisation (P wave) to onset of ventricular depolarisation (QRS complex). Q-T interval – duration of ventricular depolarisation and repolarisation. RR interval – duration of ventricular cardiac cycle. PP interval – duration of atrial cycle (Breijo-Márquez 2018).

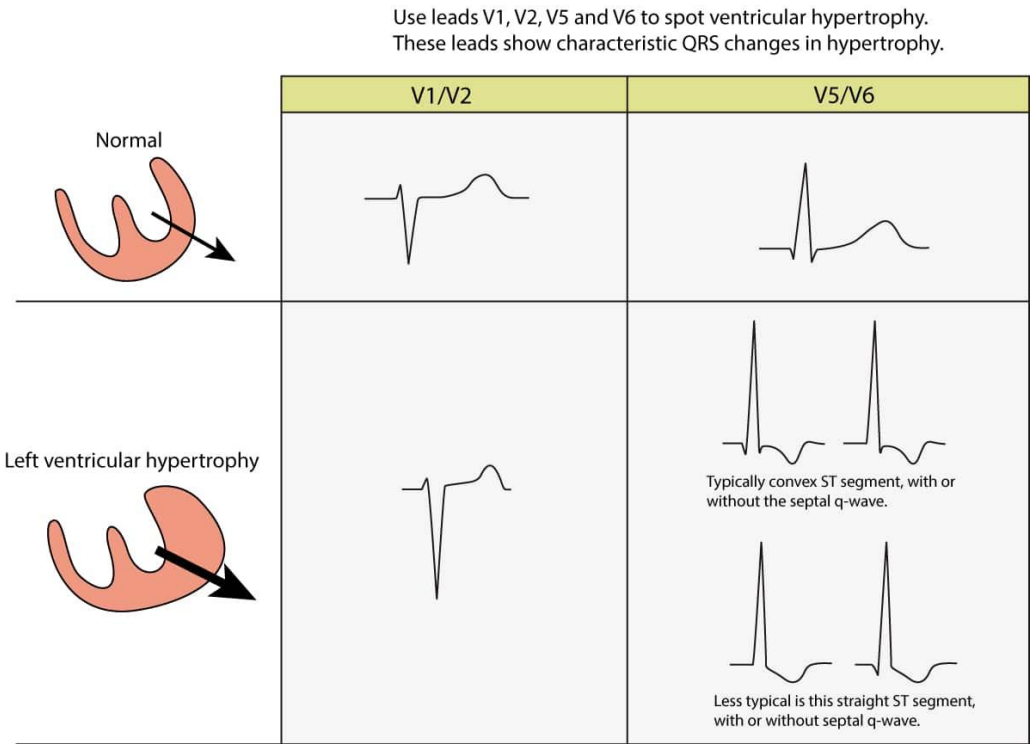

Figure 1.7. Changes in ECG wave indicating LVH. The electrical vector of the LV is increased which results in large R-waves in left-sided leads (V5/V6) and deep S waves in right-sided chest leads (V1/V2) (adapted from ECG and Echo Learning).

1.3.5.2. General diagnostic tests: Natriuretic Peptides

As previously mentioned, the symptoms of HF are often non-specific and thus many patients with suspected HF referred for echocardiography have no clear evidence of a cardiac abnormality. In this instance an additional diagnostic test is conducted which involves measuring the circulating concentration of natriuretic peptides (NPs). B-type natriuretic peptide (BNP) and N-terminal proBNP (NT-proBNP) are well established clinically validated biomarkers that have been shown to increase the diagnostic accuracy of HF (Fu *et al*. 2018). Further information on NPs and the clinical significance of them as biomarkers for HFpEF is discussed in Chapter 3, section 3.1.3.3. Researchers have found that increasing severity of HF, classified by the NYHA classes, correlated directly with increasing concentrations of BNP (Maisel *et al*. 2002). NT-proBNP is equivalent to BNP in its diagnostic value, however it is cleared via different mechanisms and has a longer half-life than BNP. Nevertheless, the expression of NT-proBNP is similar to BNP in that it increases with the severity of HF. In the International Collaborative of NT-proBNP (ICON) study patients with acutely decompensated HF had statistically higher NT-proBNP levels compared to patients without HF (Januzzi *et al*. 2006). As a diagnostic tool, the European Society of Cardiology states that a BNP level of >35pg/ml and/or NT-proBNP >125pg/ml can indicate chronic HF, while higher values (>100pg/ml for BNP and/or for NT-proBNP >300pg/ml) indicate acute HF (Ponikowski *et al*. 2016). NP values are higher in elderly people (Fu *et al*. 2018), therefore there are age-adjusted cut off values for NT-proBNP with cut-off values of >450pg/ml, >900pg/ml and >1800pg/ml for patients <50 years, >50 years, and >75 years old, respectively (Januzzi *et al*. 2006; Tanase *et al.* 2019).

1.3.6. Types of HF

HF can affect either the left or right ventricle of the heart, however LV HF is the predominant form of the disease and can be sub-divided into two types i.e. HFrEF (also known as systolic HF) or HFpEF (also known as diastolic HF). HFrEF occurs when the heart is too weak to efficiently pump blood around the body, while HFpEF occurs when the LV becomes stiff and cannot fill correctly during the diastolic filling phase. A way of identifying which of the two forms of HF is present is by determining the EF in combination with diagnostic tests described in section 1.3.5. EF is a measure of the ability of the LV to adequately eject blood during systole and is calculated using both the LVEDV and left ventricular end-systolic volume (LVESV) via equation 1 shown below:

Equation 1: **EF (%) = (LVEDV-LVESV)/LVEDV x 100**

The normal physiological range for EF in healthy individuals is between 50-70%, however this can be altered in the various types of HF as described in the following sections. Although EF is an established clinical measure it still has its limitations with variability and reproducibility of data being the first limitation, and EF being load dependent being the second. This results in a loss of reproducibility with repeated measures in the same individual resulting in a 5-7-point variability. The second important factor is that EF is a parameter of chamber function (expressing the emptying of the LV) instead of an index of contractile function, therefore the measurement is strongly influenced by LV geometry and load. The relationship between EF and EDV is inversely proportional and is regulated by LV geometry. In the early stages of HF, preload and afterload increase exerting opposing effects on EF with the net effect of a normal EF despite the developing eccentric hypertrophy and dilatation. As the disease progresses and the ventricular remodelling becomes more extensive patients develop either one or the other type of HF as described in the subsequent section (Cikes and Solomon 2016).

1.3.6.1. Heart Failure with reduced Ejection Fraction (HFrEF)

The clinical definition for HFrEF is a clinical syndrome associated with congestive symptoms and/or symptoms of low CO due to impaired ventricular pump function (reduced EF) and it is characterised by an EF <40% (McDonagh *et al.* 2021). The European Society of Cardiology long-term outpatient registry reports that 60% of patients have HFrEF (McDonagh *et al*. 2021), with the main causes being MI, CAD, valvular diseases, HTN, and T2DM. Systolic dysfunction refers to impaired ventricular contraction also known as loss of inotropy. The loss of cardiac inotropy (decreased contractility) results in a decrease in SV and a compensatory increase in preload due to incomplete emptying, subsequently leading to an increase in ventricular EDV and pressure. An increase in blood volume is also evident in HFrEF which also contributes to increased ventricular filling, EDV, and pressure. Ventricular dilatation is also apparent due to ventricular remodelling and a loss of contractility causes a reduction in SV. A reduced EF results in less blood being ejected per stroke leading to an increase in the residual volume of blood in the ventricle.

Although a large percentage of patients are diagnosed with HFrEF, both morbidity and mortality of patients have improved over the years with the administration of neuro-hormonal antagonists. Numerous studies have demonstrated that the use of angiotensin receptor blockers (ARBs), beta-adrenoceptor blockers, angiotensin-converting enzyme (ACE) inhibitors, aldosterone blockers and/or cardiac resynchronisation improves mortality and morbidity in patients with HFrEF (Jessup *et al*. 2009) and consequently they are now mainstay

therapies. More recently a new drug preparation (LCZ696) that combines an ARB (Valsartan) and a neprilysin inhibitor (Sacubitril) has recently emerged to have a greater effect than ACE inhibitors in reducing hospitalisations and the risk of death associated with HFrEF (McMurray *et al*. 2014). In contrast, the use of ionotropic agents (beta-agonists, phosphodiesterase type 3 inhibitors, and Ca^{2+} sensitisers) to improve systolic function were found to have no benefit and proved to be detrimental to patients with HFrEF (Konstam *et al*. 2011; Bistola *et al*. 2019). Any medication used to treat HF should be administered in conjunction with diuretics in patients with signs and symptoms of congestion. In addition, due to comorbidities like HTN, T2DM, and dyslipidaemia being common features of HF, treatment directed at these comorbidities can also improve the condition considerably.

1.3.6.2. Heart Failure with preserved Ejection Fraction (HFpEF)

It became evident that HF occurs in patients with a whole range of EFs, including an EF ≥50%, which is classed as within the normal range (Iwano and Little 2013). This condition is referred to as HFpEF and is characterised by reduced compliancy of the LV, which occurs as a consequence of detrimental structural alterations including cardiomyocyte hypertrophy and varying degrees of myocardial interstitial fibrosis (van Heerebeek and Paulus 2016). The criteria for HFpEF includes signs and symptoms of HF, an EF ≥50%, evidence of structural and/or functional abnormalities consistent with the presence of LV diastolic dysfunction/raised LV filling pressures, and raised NPs (McDonagh *et al*. 2021). The European Society of Cardiology long-term outpatient registry has reported approximately 16% of all HF cases are diagnosed as HFpEF (McDonagh *et al.* 2021) and it is predicted to rise further due to increasing life expectancy and the elevated incidences of obesity, HTN, T2DM, and atrial fibrillation (Bhuiyan and Maurer 2011; Dunlay *et al*. 2017). Approximately 90% of patients with HFpEF are ≥60 years of age and studies suggest that the high prevalence in this group is due in part to 1) adverse vascular remodelling which occurs as a consequence of vascular smooth muscle cell (VSMC) death, chronic inflammation, calcification, mechano-stimuli, and/or epigenetic events, and 2) age-related increases in collagen cross-linking in the vasculature which leads to increased rigidity and a greater resistance to degradation (Snedeker and Gautieri 2014) as both pathophysiological events are associated with advancing age (Lacolley *et al*. 2018). Loss of elasticity and increased stiffness due to fibrosis in vessels demands greater force to accommodate blood flow, resulting in an increase in systolic blood pressure (SBP), increased cardiac work load, and subsequent cardiac hypertrophy (Harvey *et al*. 2016). In particular, age-related adverse vascular remodelling results in an increase in afterload, subsequently leading to the ventricle increasing its wall thickness and decreasing chamber diameters. This

remodelling reduces internal wall stress, however reduces ventricular compliance leading to diastolic dysfunction (LaCombe *et al*. 2021).

It has emerged that twice as many women are being diagnosed with HFpEF than men which may in part be attributed to women having a higher risk of developing one or more of the comorbidities associated with HFpEF and also having a longer life expectancy (Borlaug and Redfield 2011). In comparison to men, women have differences in cardiac structure and function which includes smaller LV chambers and a higher resting HR to maintain CO despite their lower SV. Moreover, women also have both elevated systolic and diastolic LV elastance (stiffness) compared with men, a difference which is further exacerbated with ageing (Redfield *et al*. 2005). There is also evidence to support a contributing role of menopause to the development of HFpEF as data has shown that in response to diminished levels of oestrogen the renin-angiotensin-aldosterone system (RAAS) is activated, increasing reactive oxygen species (ROS) production, which leads to a reduction in nitric oxide (NO) bioavailability and increased collagen synthesis (Beale *et al*. 2018). Another possible explanation as to why more women suffer from HFpEF could be due to their higher incidence of multimorbidity (i.e. presence of several co-morbidities) compared with men (Conrad *et al*. 2018). Comorbidities associated with HFpEF include HTN, T2DM, CAD, and obesity. Oestrogen which is a hormone naturally produced in women plays a vital role in protection against CAD and helps control cholesterol levels reducing the risk of fatty plaques building up inside artery walls. As people age, blood vessels become stiffer caused by high BP and during and after menopause women gradually produces less oestrogen increasing the risk of narrowing arteries due to a build-up of plaques. This could explain why women have a 3-fold higher risk of becoming hypertensive in comparison to men who are reported to have a 2-fold risk with increasing age. In response to HTN, women are more likely to develop HFpEF due to the resultant concentric hypertrophy, while men are more likely to develop HFrEF due to the presence of eccentric hypertrophy. Another key contributor to the predominance of HFpEF in women, is that they are at a greater risk of developing T2DM (Kautzky-Willer *et al*. 2016), which has been shown to induce adverse remodelling in the heart. Finally, obesity has been shown to affect more women globally than men (Garawi *et al*. 2014) and obese women display a larger LV mass and relative wall thickness.

1.4. Pathophysiology of HFpEF

Numerous pathophysiological mechanisms have been proposed to contribute to both the functional and morphological alterations in HFpEF and several are described below.

1.4.1. Morphological changes associated with HFpEF

The two major structural changes associated with HFpEF are cardiomyocyte hypertrophy and cardiac fibrosis which can both be included under the umbrella term 'cardiac remodelling'. Cardiomyocytes, the contractile cell of the heart, make up one third of the total cell population and account for approximately 70-80% of the heart's total mass (Mehrotra *et al*. 2013). The majority of cardiomyocytes lose the ability to proliferate at birth or soon after, and as a consequence growth of the heart during adolescence/adulthood predominantly occurs via an increase in cardiomyocyte size (Foglia and Poss 2016). Cardiac hypertrophy can be defined as an increase in heart mass, which is closely interlinked to its functional load. In the setting of HTN, the heart must work harder to meet the physiological needs of the body. To compensate for the elevated wall stress, the muscle cells within the heart expand, resulting in an increase in size and mass (Frey *et al*. 2004). There are two main types of LVH, concentric and eccentric, with concentric LVH occurring due to increased afterload (e.g. HTN), whereas eccentric LVH is often observed in conditions of LV volume overload (e.g. valve regurgitation or physiological conditions such as pregnancy or in response to exercise; Lovic *et al*. 2017). At a morphological level, concentric hypertrophy is characterised by increases in both the cross-sectional area of cardiomyocytes (i.e. an increase in their width) and LV mass, and an unchanged LV chamber volume, whereas in eccentric hypertrophy cardiomyocytes elongate through addition of sarcomeres, LV mass increases, and there is an accompanying increase in LV chamber volume (Bisping *et al*. 2014). Figure 1.8. illustrates the appearance of an LV which has undergone concentric hypertrophy. In addition to concentric hypertrophy, HFpEF is also characterised by interstitial cardiac fibrosis induced by activation of fibroblasts. The main function of fibroblasts is to produce collagen, a component of the extracellular matrix (ECM), which maintains cardiac structure and enables coordinated contraction and relaxation of the ventricular muscle to maintain perfusion of the vital organs. In addition to collagen, fibroblasts also generate a number of cytokines, peptides and enzymes, including matrix metalloproteinases (MMPs) and their inhibitors, tissue inhibitor of metalloproteinases (TIMPs), which regulate ECM turnover and homeostasis (Fan *et al*. 2012). In the setting of HFpEF, hyperactivity of cardiac fibroblasts results in additional production and deposition of ECM proteins (i.e. fibronectin (Fn1) and collagens) in the myocardium leading to an accumulation of fibrous connective tissue (Bonnans *et al*. 2014), increased LV stiffness, and diastolic dysfunction.

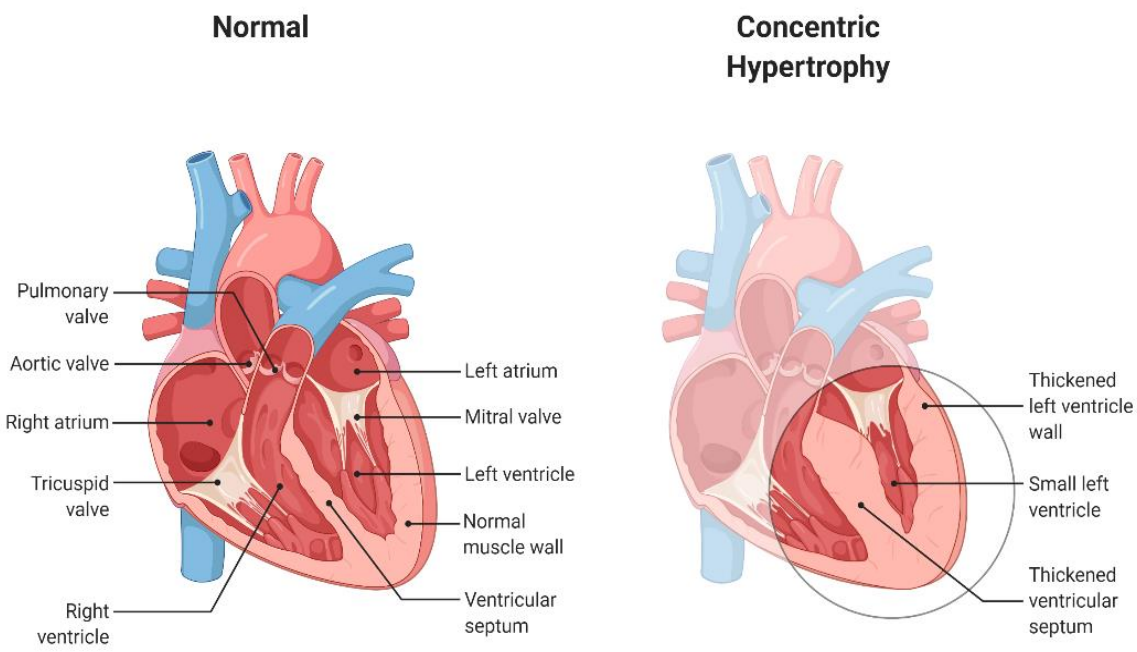

Figure 1.8. Graphical illustration of LV concentric hypertrophy. Image created with BioRender.

1.4.2. Activation of the renin-angiotensin-aldosterone system (RAAS)

One of the most prominent factors that has emerged as playing an important role in the development of HFpEF is activation of the RAAS (Sciarretta *et al*. 2009). The RAAS moderates the differentiation and proliferation of cellular growth which can promote both cardiomyocyte hypertrophy and cardiac fibrosis (described in Figure 1.9.). Angiotensin II (AngII) is the key effector peptide in the RAAS that can facilitate cell differentiation and growth through systemic (endocrine) and local (paracrine and autocrine) effects (Piastowska-Ciesielska *et al*. 2014). AngII regulates cellular growth and hypertrophy via the activation of mitogen activated protein kinases (MAPKs), which include c-Jun-N-terminal kinase (JNK), p38 MAPK, and extracellular-signal-regulated kinase 1/2 (ERK1/2; Son *et al*. 2011). ERK1/2 is the predominant kinase involved in the Ang II-mediated hypertrophic response in both VSMCs and cardiomyocytes and increased levels of both total and phosphorylated ERK1/2 have been observed in the myocardial tissue of mice with cardiac hypertrophy (Hu *et al*. 2017). Furthermore, in the presence of an increased production of ROS, due to increased cellular stress, AngII has also been shown to induce the activation of JNK and p38 MAPK via apoptosis signal-regulating kinase-1 resulting in cardiac hypertrophy in mice (Izumiya *et al*. 2003). Finally, the upregulation of the AngII type 1 receptor (AT_1R) has been shown to increase TGF-β which has been shown as a potent stimulant of cardiac myocyte growth (Gray *et al*. 1998). In addition to cardiac hypertrophy, mediators of the RAAS can also directly activate receptors on cardiac fibroblasts to increase their pro-fibrotic function and induce myocardial fibrosis. The RAAS is mainly activated through the binding of AngII to the AT_1R and the interaction of aldosterone and its mineralocorticoid receptor (reviewed by Cannavo *et al*. 2018). Binding to these receptors stimulates fibroblasts to produce fibrillary collagen type I (Col1) and collagen type III (Col3), which gradually accumulates, resulting in a derangement of tissue structure i.e. fibrosis. A persistent activation of the RAAS stimulates and maintains the ECM which is accountable for increased myocardial stiffness and reduced diastolic function. AngII and aldosterone can also influence fibrosis through the activation of TIMPs and MMPs (reviewed by Jia *et al*. 2018).

1.4.2.1. RAAS and Inflammatory Cytokines

The RAAS has also been shown to promote cardiac remodelling by activating subclinical tissue inflammation through paracrine actions (Pacurari *et al*. 2014). In arterial HTN, elevated levels of both AngII and aldosterone induce the expression of several different cytokines which contribute to the development and progression of cardiac perivascular and interstitial fibrosis, cardiomyocyte hypertrophy, and diastolic dysfunction. In particular, overactivation of the RAAS leads to the production and release of the cytokines tumour necrosis factor-α (TNF-α) and interleukin-6 (IL-6), and growth factors such as transforming growth factor β (TGF-β), all of

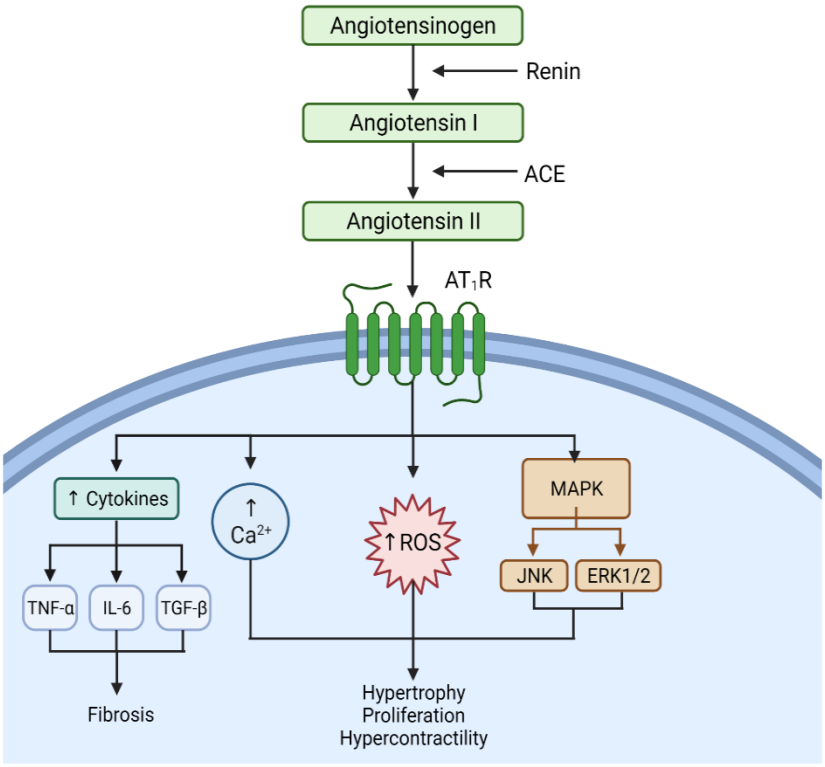

Figure 1.9. The effect of activation of the RAAS on morphological changes in HFpEF. AngII is produced by the conversion of angiotensinogen (AGT) to angiotensin I (AngI) by renin, and then cleaved by angiotensin converting enzyme (ACE) to produce AngII. AngII acts on the G-protein-coupled receptor, AT_1R. AngII can then activate MAPK (JNK and ERK1/2), increase ROS production and intracellular calcium, all of which contribute the development of cardiac hypertrophy. AngII can also upregulate the expression of cytokines (TNF-α, IL-6, and TGF-β) which initiate and maintain inflammation locally and stimulate fibroblasts to produce excess collagen. (Adapted from St. Paul *et al.* 2020).

which initiate and maintain inflammation locally and stimulate fibroblasts to produce excess collagen. TGF-β has emerged as the most influential growth factor in this setting due to it being a fibroblast-activating growth factor. Induced activation of AT_1R by AngII leads to the production of TGF-β, which subsequently activates the Smad3 signalling pathway resulting in enhanced expression of MMPs and TIMPs.

1.4.3. Hypophosphorylation of titin

Another physiological mechanism that contributes to cardiac remodelling in HFpEF involves the giant skeletal protein titin. In cardiomyocytes, titin functions as a bidirectional spring and provides stability to the other myofilaments. In an adult human heart, titin is present in two isoforms: a longer and more compliant N2BA isoform and a shorter and stiffer N2B isoform. The N2BA:N2B ratio is altered in different forms of heart disease, however generally the ratio increases in eccentric remodelling and decreases in concentric remodelling (LeWinter and Meyer 2013), the latter leading to increased stiffness of the ventricular muscle. Myocardial cyclic guanosine monophosphate-protein kinase G (cGMP-PKG) signalling is essential for normal cardiovascular physiology as it maintains cardiomyocyte compliance and prevents maladaptive hypertrophy. This pathway involves generation of the second messenger, cGMP, via NO induced activation of soluble guanylate cyclase (sGC) and/or activation of particular guanylate cyclase (pGC) by NPs such as BNP. Once produced, cGMP activates PKG which subsequently phosphorylates a large number of target proteins including titin. Under physiological conditions, the N2B isoform of titin undergoes phosphorylation by PKG which results in a decrease in cardiomyocyte passive tension. In addition to PKG, protein kinase A (PKA) also phosphorylates the N2B isoform reducing ventricular stiffness and further promoting relaxation of the myocardium via the phosphorylation of troponin I (Layland *et al*. 2005). However, due to the obesity, HTN, and/or T2DM induced proinflammatory state present in the hearts of patients with HFpEF, dysfunctional endothelial cells produce excessive amounts of ROS which consequently reduces the NO bioavailability for adjacent cardiomyocytes (Bishu *et al*. 2011; Falcao-Pires *et al*. 2011; Hamdani *et al*. 2013). Limited NO then decreases the production of cGMP, therefore limiting PKG activity in cardiomyocytes, resulting in hypophosphorylation of the N2B isoform of titin leading to subsequent concentric LV remodelling and stiffer cardiomyocytes (LeWinter and Meyer 2013). In a rat model of obesity and high metabolic risk, it was demonstrated that hypophosphorylation of cardiac titin was associated with increased myocardial stiffness (Hamdani *et al*. 2013). In human LV myocardial samples taken from patients with both HFrEF and HFpEF, hypophosphorylation of the stiff N2B titin isoform was responsible for increasing passive stiffness in cardiomyocytes (Borbely *et al*. 2009), which could be corrected with the *in vitro* administration of PKA or PKG,

which was also shown in a hypertensive dog HFpEF model (Bishu *et al*. 2011). In patients with HFpEF, titin was not only hypophosphorylated, but there was also a decrease in PKG and cGMP, which subsequently activates PKG (Van Heerebeek *et al*. 2012).

1.4.4. Alterations in Ca^{2+}

Another mechanism proposed to play a role in initiating diastolic dysfunction in HFpEF is alterations is Ca^{2+} signalling. Cardiac contractile/relaxation function is tightly regulated by cyclic release and reuptake of Ca^{2+} to and from the cytoplasm of cardiomyocytes, in a process known as EC coupling (described previously in section 1.1.1.). In HFpEF, an increase in intracellular sodium (Na^{+}) in cardiomyocytes increases the late Na^{+} current, therefore the Na^{+} conductance responsible for rapid depolarisation of cardiomyocytes does not completely inactivate during the AP. This leads to an increase in Na^{+} entry into the cell cytoplasm, which reduces the driving force for extrusion of Ca^{2+}, therefore favours Ca^{2+} influx via the NCX. As a consequence of this elevated intracellular Ca^{2+} actin-myosin filament interaction is increased during diastole, subsequently leading to increases in diastolic tension (Pourrier *et al*. 2013). Oxidative stress induced changes in Ca^{2+} homeostasis has also been shown to contribute to diastolic dysfunction via ROS induced S-nitroslylation of the RyR, which leads to diastolic SR Ca^{2+} leaks and impaired relaxation of cardiomyocytes (Gonzalez *et al*. 2010).

1.4.5. Oxidative Stress

Oxidative stress can be defined as an overproduction of ROS relative to the level of antioxidants. ROS are oxygen-based chemicals which include free radicals such as superoxide ($O_{2^{-}}$) and the hydroxyl radical (OH) and also non-radicals which are able to generate free radicals such as hydrogen peroxide (H_2O_2). ROS production is associated with oxygen consumption, therefore cells that have high oxygen consumption rates are more prone to oxidative stress. Cardiomyocytes have a particularly high level of oxygen consumption and thus an increased susceptibility to oxidative stress. ROS production within the heart is primarily achieved by the mitochondria, nicotinamide adenine dinucleotide phosphate (NADPH) oxidases, xanthine oxidase, and uncoupled nitric oxide synthase (NOS). In the vasculature, ROS are produced by all vascular layers, including smooth muscle, endothelium, and adventitia, with the endothelium having an important role in the regulation of vascular tone, modulation of inflammation and promotion or inhibition of vascular growth and platelet coagulation and aggregation. ROS has been shown to be implicated in cell damage, cell apoptosis and necrosis (Moris *et al*. 2017). In HFpEF, high levels of ROS overpower cellular antioxidant defence mechanisms resulting in adverse cardiac and skeletal remodelling. ROS

can directly weaken the electrophysiology and the contractile mechanism of cardiomyocytes by altering proteins that are central to EC coupling, such as LTCCs, potassium channels, sodium channels, and the NCX. In addition, ROS can also change the activity of SERCA, as well as decreasing myofilament Ca^{2+} sensitivity. Furthermore, ROS can also induce an energy deficit by altering the function of proteins involved in energy metabolism and also has a pro-fibrotic function by inducing fibroblast proliferation and the activity of MMPs resulting in extracellular remodelling (van der Pol *et al*. 2019). Under pathological conditions, the electron transport chain of the mitochondria stimulates the formation of large quantities of O_2^- which has been shown to contribute to cardiomyocyte damage and larger MI injury after acute MI (Perrelli *et al*. 2011). In response to mechanical stretch, both AngII and endothelin-1 (ET-1) increase ROS due to the increased expression and activity of NADPH oxidase (Wen *et al*. 2012; Mushtaq *et al*. 2015). TNF-α has also been shown to induce cardiomyocyte hypertrophy through nuclear factor-kappa B (NF-κB) activation via the generation of ROS (Higuchi *et al*. 2002). As a result of cardiac injury, NOS becomes uncoupled and structurally unstable leading to an increased generation of ROS. In mice, elevated levels of ROS resulted in LV dilatation, contractile dysfunction, and LV remodelling (Takimoto *et al*. 2005). Consequently, to prevent oxidative damage cells express a number of enzymatic scavengers of ROS including superoxide dismutase (SOD), catalase, glutathione peroxidase (GPx), nicotinamide adenine dinucleotide (NAD^+), and glutathione (GSH; Pignatelli *et al*. 2018). Studies have shown a significant decrease in the activity of SOD (Lu *et al*. 2008) and GPx (Verk *et al*. 2017) in animal models of HF.

1.5. Treatment of HFpEF

HFpEF is associated with significant morbidity and mortality rates and to date no particular treatment has demonstrated significant improvements in HFpEF patients, especially in contrast to the efficacy of treatments used to treat HFrEF. There has been a number of clinical trials for potential treatments for HFpEF, however the majority of results have been negative. The current lack of successful treatments for HFpEF are likely due to the heterogeneous nature of the disease resulting in several different phenotypes and multifactorial pathophysiologies (reviewed by Ilieșiu and Hodorogea 2018). In the early stages of HFpEF, the most effective treatment relates to targeting the risks factors associated with the disease, which include HTN, T2DM, and CAD. HTN is one of the main adaptable risk factors for HFpEF and treatment of HTN has been shown to reduce the development of HFpEF, especially in older patients (Wright *et al*. 2015), while the potential utility of anti-diabetic drugs, such as sodium/glucose cotransporter 2 (SGLT2) inhibitors (Packer 2018) and dipeptidyl peptidase-4 inhibitors

(Yamamoto *et al*. 2017), is currently being investigated in large clinical trials. New therapies targeting the pathophysiological pathways of HFpEF (at both the cellular and molecular level) are currently being investigated and are discussed in the following sub-sections. A recently published study identified that SGLT2 inhibitors, Empagliflozin in particular, reduced the risk of cardiovascular death or hospitalisation in HFpEF patients, regardless of the presence or absence of diabetes (Anker *et al.* 2021). This is the first successful clinical trial in HFpEF to provide a clear clinical benefit.

1.5.1. Exogenous Nitrates

Nitrates have been investigated as a potential treatment for HFpEF as they enhance peripheral venous capacitance, therefore decreasing ventricular load and LV filling pressures. At a molecular level, exogenous nitrates activate sGC increasing cGMP synthesis resulting in vasodilation. However, studies to date have failed to demonstrate a beneficial effect of nitrates in HFpEF. In particular, the Nitrate's Effect on Activity Tolerance in Heart Failure with Preserved EF (NEAT-HFpEF) trial failed to demonstrate any beneficial effects of isosorbide mononitrate on exercise tolerance in HFpEF patients (Zakeri *et al*. 2015). Furthermore, findings from a study by Lim et al. (2017) extend those of the NEAT-HFpEF trial demonstrating that not only is the use of nitrates not associated with any improvements in HFpEF patients, but that there use appears to be associated with increased combined all-cause mortality. Furthermore, although nitrates may improve endothelial function, research has provided evidence that long-acting nitrates can unexpectedly enhance oxidative stress and local endothelin activation (Oelze *et al*. 2013). Therefore, based on the results from several clinical trials, nitrates are not recommended as a treatment for HFpEF patients.

1.5.2. Phosphodiesterase-5 Inhibitors

As the enzyme phosphodiesterase-5 (PDE5) is upregulated in cardiac hypertrophy, significant interest has now been focused on the therapeutic potential of PDE5 inhibitors in HFpEF. PDE5 inhibitors block the intracellular catabolism of cGMP by phosphodiesterases, increasing cGMP activity, and enhancing the vascular and myocardial effects of NO leading to vasodilation (Hutchings *et al*. 2018). In a small study involving 44 patients with HFpEF (EF >50%), pulmonary HTN and recent onset dyspnoea, the PDE5 inhibitor Sildenafil improved LV remodelling and diastolic function, and decreased pulmonary HTN in comparison with placebo after 12 months (Guazzi 2014). However, these promising results with Sildenafil have not been replicated in other clinical trials with larger participant numbers (Andersen *et al*. 2013). In particular, a greater number (113) of participants were included in the RELAX trial and given

Sildenafil for 24 weeks, however the treatment failed to improve the clinical status and exercise capacity of HFpEF patients (Redfield *et al*. 2013).

1.5.3. Combined Angiotensin Receptor Blocker (ARB) and Neprilysin Inhibitor

The combination of an ARB with a neprilysin inhibitor is a new therapeutic class of agents developed to modulate the RAAS. LCZ696, the first drug in the class, is a combination of Valsartan, an AT_1R blocker and Sacubitril, a neprilysin inhibitor. LCZ696 acts by suppressing the RAAS and potentiating the protective effects of atrial natriuretic peptide (ANP). Neprilysin is the primary enzyme that degrades NPs, therefore inhibiting it with sacubitril, increases the bioavailability of NPs which exert vasodilator, natriuretic, and anti-proliferative effects. Early clinical trials demonstrated positive findings with LCZ696 in patients with HFrEF (McMurray *et al.* 2014; Desai *et al.* 2015; Solomon *et al.* 2016) and thus it was subsequently investigated as a potential therapeutic agent in HFpEF. A phase II trial assessed the effect of LCZ696 on circulating levels of NT-proBNP (used as a marker of LV wall stress) in patients with HFpEF (Solomon *et al*. 2012) and demonstrated that NT-proBNP levels were significantly lower at 12 weeks in the LCZ696 treatment group when compared with the Valsartan group. However, a subsequent clinical trial demonstrated that the drug didn't reduce hospitalisations or deaths in HFpEF patients and so they are still without a viable treatment (Solomon *et al*. 2019). Although many trials have been completed to find a treatment for HFpEF, these potential treatments have not been successful and thus HFpEF remains a disease with significant morbidity and hospitalisation without an effective therapy.

1.6. Wnt Signalling

The specification, differentiation, and coordinated behavior of tissues in the human body all involve a network of tight cell-to-cell communication. To allow all these processes within the body to work efficiently, they are controlled by secreted signalling molecules that belong to small gene families. Protein families which have particular importance in this setting are Hedgehog, Wingless/int1 (Wnt), TGF-β, and fibroblast growth factor (FGF) due to their pleiotropic actions during both development and maintenance of most tissues (Bovolenta *et al*. 2008; Kahn 2014). Wnt signalling plays an essential role in the differentiation, proliferation, function, and apoptosis of cells, and thus plays a critical role in the regulation of development, growth, and homeostatic processes (Ring *et al*. 2014). However, aberrant Wnt signalling has been associated with many cancers (Polakis 2012), CVD (Hermans and Blankesteijn 2015), and T2DM (Ip *et al*. 2012). The Wnt proteins are a large family of 19 palmitoylated secreted glycoproteins (Wnt1, Wnt2, Wnt2b, Wnt3, Wnt3a, Wnt4, Wnt5a, Wnt5b, Wnt6, Wnt7a, Wnt7b,

Wnt8a, Wnt8b, Wnt9a, Wnt9b, Wnt10a, Wnt10b, Wnt11, and Wnt16) that initiate at least three different signalling pathways, one canonical or beta-catenin (β-catenin) dependent pathway, and two non-canonical or β-catenin independent pathways (i.e. planar cell polarity (PCP) and Wnt/Ca^{2+} pathways) via cell surface transmembrane proteins. Wnts are secreted from cells by the protein Wntless (Yu and Virshup 2014; Galli *et al*. 2016) and are structurally composed of two domains, an amino terminal domain (NTD) and carboxy-terminal domain (CTD). The NTD is composed of ten cysteine residues forming five disulfide bridges, in a cluster of α-helices, while the CTD contains six disulfide bridges and a two strand β-sheet (Janda *et al*. 2012). Once Wnt proteins are secreted they interact with glycosaminoglycans in the ECM which control their diffusion, distribution, and signal transduction (Takada *et al*. 2017).

1.6.1. Frizzled receptors

Frizzled (FZD) receptors are a family of 10 transmembrane receptors that are expressed on the plasma membrane of numerous cell types throughout the body including the cardiovascular system and act as the main targets for transducing Wnt signalling. Table 1.4 details documented interactions between FZD receptors and Wnt ligands and the tissues that they are predominantly expressed in. These receptors belong to the Class F G protein-coupled receptor family and are comprised of 7 hydrophobic transmembrane helices and display an extracellular cysteine-rich domain (CRD) in their N-terminal (Pei and Grishin 2012). Although, FZD receptors are the main proteins responsible for binding Wnt ligands, there are additional molecules that are involved in the mediation of Wnt signalling. These include low-density lipoprotein-receptor-related proteins (LRP5 and LRP6) that work as FZD co-receptors and the tyrosine kinase receptors (Ror and Ryk), which contain a CRD similar to that of FZDs (MacDonald and He 2012). Activation of Wnt signalling is then further regulated by different endogenous antagonists including Cerberus, Wnt inhibitory factor (WIF1), Sclerostin, and members of the Dickkopf (Dkk) and secreted frizzled related protein (sFRP) families. Dkk and Sclerostin proteins restrict Wnt activity and antagonise canonical signalling by binding to LRP5 or LRP6, while in contrast WIF1, Cerberus, and sFRPs attenuate Wnt signalling via binding to the Wnt ligands (Cruciat and Niehrs 2013).

1.6.2. Canonical Wnt Signalling Pathway

The β-catenin dependent Wnt signalling pathway has been the most studied to date and is characterised by the intracellular accumulation of β-catenin that in turn regulates the expression of key developmental genes (MacDonald *et al*. 2009). Target genes for β-catenin include c-Myc, c-Jun, and cyclin D1 (CCND1), which are all involved in regulating cell cycle

Table 1.4. Organ/cellular location of FZD receptors and known interactions with Wnt ligands. (Adapted from Dawson *et al.* 2013. Expression and subcellular location taken from Protein Atlas).

FZD Receptor	RNA predominantly expressed in	Protein predominantly expressed in	Cellular Location	Wnt Signalling Pathway	Wnt Ligand
FZD_1	Endocrine tissue	Lung Small intestine Liver Bone marrow Placenta	Plasma Membrane	Canonical	Wnt1 Wnt2 Wnt3 Wnt3a Wnt8
FZD_2	Uterus Retina	Breast Smooth muscle	Nucleoplasm	Canonical/non-canonical	Wnt3a Wnt5a
FZD_3	Brain	Expressed in most cytoplasmic tissue	Intracellular membrane	Non-Canonical	Wnt1
FZD_4	Adipose tissue	GI tract Pancreas Kidney	Plasma membrane	Canonical/non-canonical	Wnt2 Wnt5a Wnt8
FZD_5	Intestine Liver	GI tract Placenta Brain	Membrane	Non-canonical	Wnt5a Wnt7a Wnt8 Wnt11
FZD_6	Endocrine tissue	Expressed in most cytoplasmic tissue	Plasma membrane	Negative Regulator	Wnt4
FZD_7	Brain Smooth muscle	Brain Female tissue Lung	Vesicles	Canonical/non-canonical	Wnt5a Wnt8 Wnt11
FZD_8	Spleen	Brain Lung Liver Kidney	Endoplasmic reticulum	Canonical	Wnt8
FZD_9	Skeletal muscle	Unknown	Membrane	Canonical	Wnt2
FZD_{10}	Esophagus Lymphoid tissue	Unknown	Nucleoplasm	N/A	Wnt8

progression and proliferation (Wisdom *et al*. 1999; Yang *et al*. 2006; Bretones *et al*. 2015). In the absence of Wnt activation, β-catenin is phosphorylated by a complex known as the "destruction complex", which prepares β-catenin for subsequent degradation by the ubiquitin proteasome pathway. The destruction complex is composed of glycogen synthase kinase 3β (GSK-3β), Axin, casein kinase 1α (CK1α), protein phosphatase 2A and adenomatous polyposis coli protein (APC; Stamos and Weis 2013). Phosphorylated β-catenin is then proteolytically degraded as shown in Figure 1.10. To activate the β-catenin dependent signalling pathway, a Wnt ligand binds to a complex consisting of both a FZD receptor and LRP5/6, the latter acting as a co-receptor essential for Wnt signalling. Post stimulation with a Wnt ligand, the activated FZD receptor/LRP5/6 complex binds to the cytoplasmic protein Dishevelled (Dvl), which leads to the recruitment and subsequent disintegration of the destruction complex at the plasma membrane and an accumulation of cytosolic β-catenin. β-catenin is then translocated from the cytoplasm to the nucleus where it binds to T cell factor/lymphoid enhancer factor (TCF/LEF) transcription factors on target genes (i.e. CCND1, c-Myc, Wnt inducible signalling protein 1 (Wisp1), etc.). CCND1 is a cell cycle regulator that controls proliferation of cardiomyocytes (Yang *et al*. 2006), c-Myc is a proto-oncogene that regulates cell cycle progression in numerous cell types (Bretones *et al*. 2015), and Wisp1 is a member of the connective tissue growth factor family involved in various biological processes including cell adhesion and proliferation (Jung *et al*. 2017). Collectively an increase in the transcription of these genes promotes both cardiac hypertrophy and fibrosis, the two main detrimental structural alterations in HFpEF (Xiao *et al*. 2001; Colston *et al*. 2007).

1.6.3. Non-canonical Signalling Pathways

In addition to the β-catenin dependent signalling pathway, non-canonical signalling pathways can also be activated by Wnt proteins as shown in Figure 1.11. The PCP pathway regulates cell orientation in relation to neighboring cells and involves the activation of the small G proteins Rac and Rho. This pathway is initiated by binding of the Wnt ligand to the FZD receptor/tyrosine kinase-like receptor (i.e. Ror and Ryk) complex, followed by Dvl-mediated activation of Rac and Rho (reviewed by Abou and Mani 2017). JNK and Rho-associated protein kinase (ROCK) are subsequently activated by Rho and Rac leading to changes in actin polymerisation and the activation of the transcription factors activator protein 1 (AP-1) and Jun (Green *et al*. 2014). AP-1 is an important transcription factor which forms both homodimers and heterodimers with Jun (v-Jun, c-Jun, JunB, and JunD) that control a range of cellular processes involving apoptosis, differentiation, proliferation, and cell migration (Ye *et al*. 2014). The Wnt/Ca^{2+} pathway involves binding of the Wnt ligand to the FZD receptor which induces an elevation in intracellular Ca^{2+}, subsequent activation of both protein kinase C (PKC) and

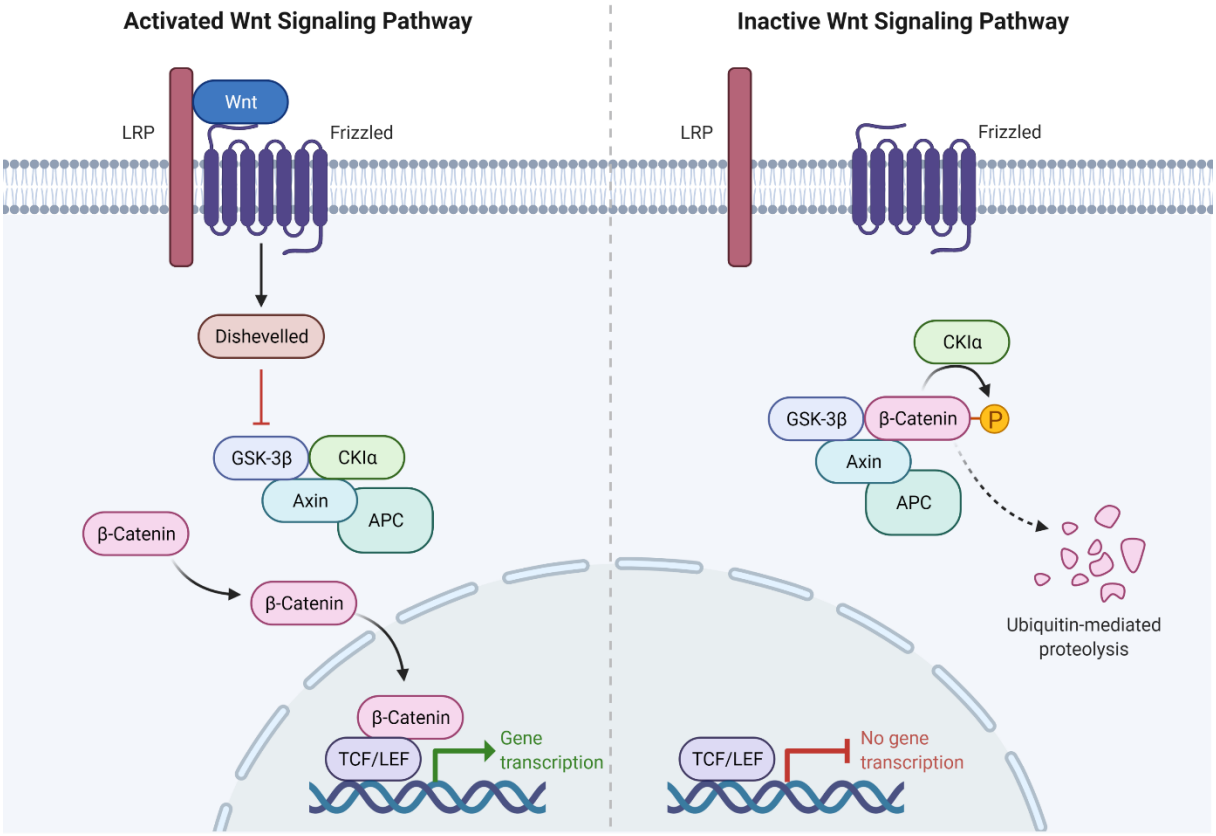

Figure 1.10. Schematic representation of the β-catenin dependent Wnt signalling pathway. In the inactive state, β-catenin is phosphorylated and broken down by the destruction complex composed of GSK-3β, Axin, APC, and CK1α. However, when this pathway is activated Wnt, FZD, and LRP5/6 form a complex which recruits the Dvl protein to the plasma membrane leading to the destruction complex being dissociated. This results in the accumulation of β-catenin which migrates to the nucleus forming a complex with TCF/LEF transcription factors resulting in gene expression. (Adapted from BioRender).

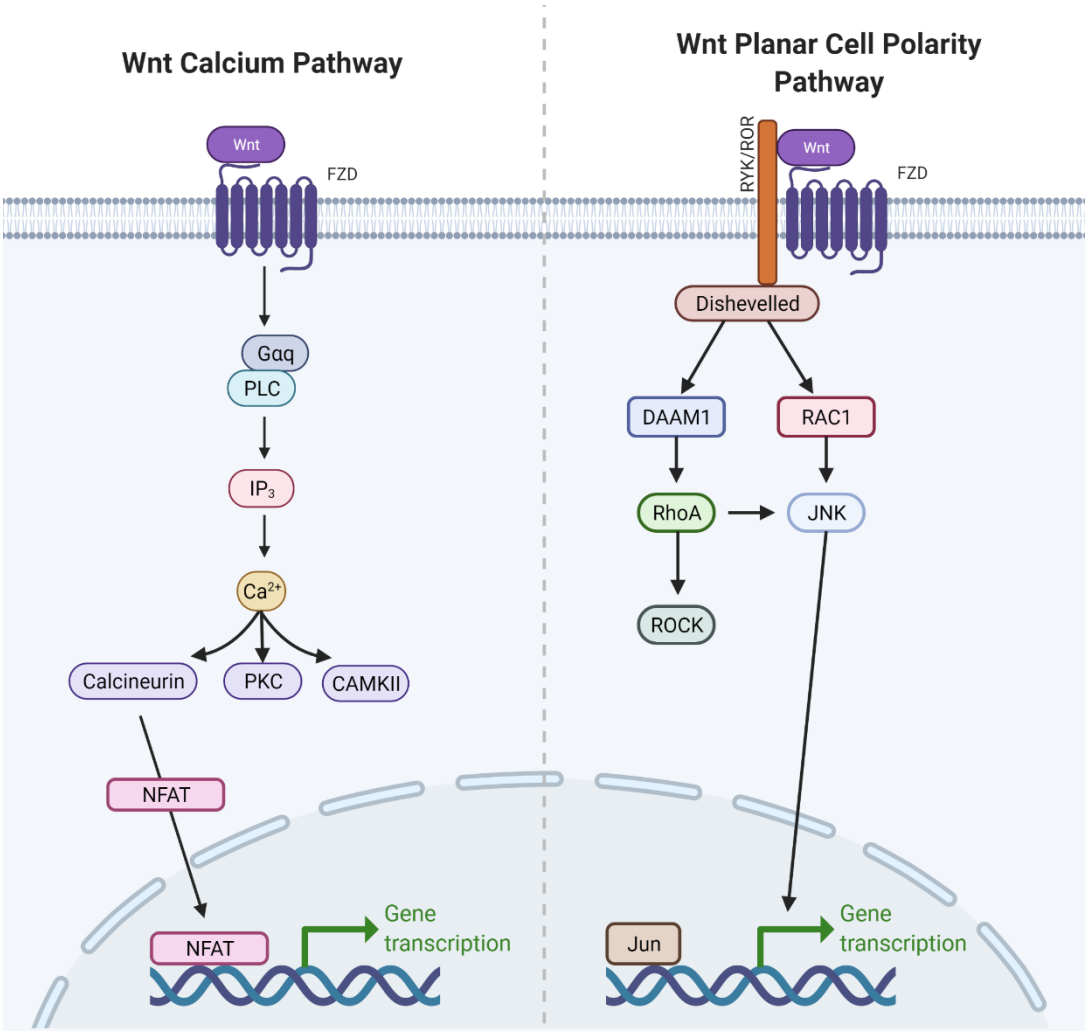

Figure 1.11. An overview of the non-canonical Wnt signalling pathways. The Ca^{2+} signalling pathway is activated via Wnt binding to a G protein-coupled FZD resulting in the activation of phospholipase C (PLC). This then leads to an increase in inositol triphosphate (IP_3) production and stimulation of intracellular Ca^{2+} release. The Ca^{2+} cascade involves the activation of PKC, calmodulin-dependent protein kinase II (CaMKII) and changes in gene transcription via the calcineurin-NFAT mechanism. The PCP pathway is initiated by Wnt binding to a FZD receptor and the Ryk/Ror co-receptor. This recruits the Dvl protein leading to the activation of the RhoA (by de-inhibition of Dvl associated activator of morphogenesis 1 (DAAM1)) and RAC signalling cascades. The activation of these two pathways causes cytoskeletal modifications and changes in gene expression via the JNK pathway. (Adapted from BioRender).

calmodulin-dependent protein kinase II (CaMKII), and induction of the transcription factors NF-κB and cAMP Responsive Element Binding Protein 1 (CREB). The increase in Ca^{2+} also activates cytosolic phosphatase calcineurin (CaN), which subsequently phosphorylates nuclear factor of activated T cells (NFAT). Activation of NFAT leads to the transcription of several genes in both cardiac and skeletal muscle cells (De 2011).

1.6.4. Secreted Frizzled Related Proteins (sFRPs)

sFRPs are the largest family of endogenous inhibitors of Wnt signalling and are responsible for regulating both canonical and non-canonical Wnt signalling in early development and a variety of diseases. The sFRP family comprises of five secreted glycoproteins (sFRP1, sFRP2, sFRP3, sFRP4, and sFRP5), which are approximately 300 amino acids in length and can fold into two independent domains. The amino terminus contains a secretion signal peptide followed by a FZD type CRD. The CRD domain contains 10 conserved cysteine residues and displays 30-50% sequence similarity to the CRD of FZD receptors (Xavier *et al*. 2014). sFRPs can inhibit Wnt signalling by either binding directly to the Wnt ligand preventing the latter from binding to a FZD receptor or by directly binding to the FZD receptor to form a non-functional complex which prevents the activation of Wnt induced signalling. It has been suggested that sFRPs are not just Wnt-binding proteins (i.e. Wnt antagonists), but they can also antagonise one another's activity (Carstensen-Kirkberg *et al*. 2017), bind directly to FZD receptors themselves activating them (Cruciat and Niehrs 2013), and provide axon-guidance information (Onishi *et al*. 2014). Furthermore, they have been shown to interact with other receptors and matrix molecules interfering with bone morphogenetic protein signalling (Luo *et al*. 2015) by acting as proteinase inhibitors (Lee *et al*. 2006). Their expression is altered in different types of cancers (Polakis 2012), bone pathologies (Tornero-Esteban *et al*. 2015), retinal degeneration (Yi *et al*. 2007), and CVD (Sklepkiewicz *et al*. 2015; Nakamura *et al*. 2016), which indicates that their activity is fundamental for tissue homeostasis.

1.6.5. Wnt Signalling and Cardiovascular Disease

As mentioned previously Wnt signalling plays an important role in heart development and little if any role in the adult heart under normal physiological conditions, however several components of this signalling system are activated in CVD.

1.6.6. Wnt Signalling and Myocardial Infarction

Activation of Wnt signalling has been demonstrated in response to MI with the expression of the canonical Wnt ligands, Wnt2, Wnt4, Wnt10b, and Wnt11, all being increased in the infarcted area during granulation tissue formation (Aisagbonhi *et al*. 2011). Furthermore, Duan et al. (2012) reported the upregulation of Wnt1 after acute ischaemic injury in mice and suggested that the latter promoted the differentiation of epicardial cells into fibroblasts. In a separate study, serum levels of Wnt1 were reported to increase 11-fold post MI in mice (Aisagbonhi *et al*. 2011), while conversely in another study a reduction in circulating Wnt1 was demonstrated to be associated with premature MI (Goliasch *et al*. 2012). Furthermore, within the first 7 days post MI the expression of Wnt4, Wnt7a, and Wnt10b were all shown to upregulated in the heart while the expression of Wnt7b was downregulated (Barandon *et al*. 2003; Duan *et al*. 2012). Conversely, a cardioprotective role for Wnt11 against hypoxia induced injury in cardiomyocytes post MI has been suggested (Zuo *et al*. 2012), while increased survival was demonstrated in skeletal muscle derived stem cells overexpressing Wnt11 (Xiang *et al*. 2011). However, the majority of evidence suggests a potential detrimental role for Wnt signalling in MI. In particular, endogenous inhibitors of Wnt signalling have been shown to exert protective effects after ischaemic injury, with sFRP2 activating mesenchymal stem cells and promoting cardiac repair via the inhibition of canonical Wnt signalling (Alfaro *et al*. 2010; He *et al*. 2010a). Research has indicated that transgenic mice overexpressing sFRP1 have reduced infarct size and improved cardiac function following MI (Barandon *et al.* 2003) and that sFRP1 exerts its protective effects by altering the balance of pro- and anti-inflammatory cytokine expression, reducing neutrophil infiltration, and subsequently attenuating scar formation post infarction (Barandon *et al*. 2011). Furthermore, sFRP5 has been shown to mediate anti-inflammatory effects after ischaemic injury by potentially antagonising the non-canonical Wnt5a/JNK signalling pathway (Nakamura *et al*. 2016). More recently, research by Yang et al. (2017) demonstrated that the novel porcupine (PORCN) inhibitor, CGX1321 (which inhibits the secretion of all Wnt proteins), reduced MI injury by limiting fibrosis and stimulating regeneration via the promotion of cardiomyocyte proliferation. Taken together, the upregulation of Wnt proteins following ischaemic injury and the cardioprotective effects reported with Wnt inhibitors supports a detrimental role for Wnt signalling in MI injury.

1.6.7. Wnt Signalling and Cardiac Hypertrophy

The onset of HFpEF is usually accompanied by cardiac hypertrophy which occurs in response to the HTN induced increased afterload and/or pathophysiological mechanisms induced by co-morbidities i.e. obesity, T2DM etc. Cardiac hypertrophy is characterised by an increase in cardiomyocyte size as well as thickening of the LV wall (Tham *et al*. 2015). At the beginning

this growth is an adaptive response to maintain cardiac function, however over a prolonged period of time with sustained stress on the heart it becomes maladaptive leading to the expression of fetal isoforms of contractile proteins (Cox and Marsh 2014) and cardiomyocyte enlargement. One physiological system thought to play a key role in the induction of cardiomyocyte hypertrophy is the RAAS with AngII being the key effector peptide. AngII promotes hypertrophy through binding to the AT_1R which stimulates multiple signal transduction pathways such as tyrosine kinases, MAPKs and ERKs (previously described in section 1.4.2.). A more recent pathway shown to induce cardiomyocyte hypertrophy is Wnt signalling which is discussed in further detail in both Chapter 4, section 4.1.1. and Chapter 6, section 6.1.1. The upregulation of RAAS and Wnt signalling results in the transcription of c-fos, c-jun and c-Myc and the re-expression of the fetal genes skeletal α-actin (ACTA1) and ANP and the growth of cardiomyocytes. The relationship between the RAAS and canonical Wnt signalling and their role in cardiac hypertrophy is discussed in detail in Chapter 4, section 4.1.1. and Chapter 6, section 6.1.1.

1.6.8. Wnt Signalling and Fibrosis

Cardiac fibrosis is primarily a protective mechanism which is beneficial for wound healing and tissue generation, however continuous ECM deposition can eventually lead to impaired cardiac function. Fibrotic scarring in the heart generally occurs after an MI, but fibrosis also occurs in response to a number of other conditions including hypertensive heart disease, idiopathic dilated cardiomyopathy (DCM), and diabetic hypertrophic cardiomyopathy. Research has shown that there is an increase in the synthesis and deposition of cardiac Col1 in patients after MI (Querejeta *et al*. 2004) and increased circulating Col1 is associated with the incidence of HFpEF (Duprez *et al*. 2018). Cardiac fibrosis is characterised by changes in matrix composition and quality due to remodeling of the ECM, which can negatively affect heart muscle function. Under physiological conditions, cardiac fibroblasts do not express fiber proteins (i.e. Col1 and Col3, elastin, Fn1 and/or alpha-smooth muscle actin (α-SMA)), however following injury (i.e. MI) and/or chronic stress (i.e. HTN/T2DM related oxidative stress and/or inflammation) fibroblasts are activated and differentiate into myofibroblasts that produce excessive amounts of these structural protein fibers. A more recent pathway shown to induce cardiac fibrosis is Wnt signalling which is discussed in further detail in Chapter 6, section 6.1.2. Canonical Wnt signalling has not only been shown to be activated in cardiac fibrosis but also in renal and pulmonary fibrosis. Renal expression of Wnt4 has been shown to be increased in a mouse model of kidney fibrosis (Surendran *et al*. 2002), while Dkk1, a Wnt antagonist, reduced both β-catenin accumulation and renal interstitial fibrosis in a mouse model of obstructive nephropathy (He *et al.* 2009). In pulmonary fibrosis, the expression of Wnt1, Wnt3a, and Wnt5a

were all significantly upregulated in the lungs of both humans and experimental models (Konigshoff *et al*. 2008; Aumiller *et al*. 2013; Newman *et al*. 2016). Finally, in pulmonary fibroblasts, sFRP1 has been shown to reduce TGF-β1 induced collagen production supporting a potential anti-fibrotic role for this protein (De Langhe *et al*. 2014).

1.6.9. Wnt Signalling and Comorbidities

Patients diagnosed with HFpEF have a higher prevalence of comorbidities such as HTN, obesity, and T2DM.

1.6.9.1. Hypertension (HTN)

HTN is one of the most prevalent risk factors associated with HFpEF. Nearly 10 million people are diagnosed with HTN in the UK with a further potential 6-8 million people living with undiagnosed HTN (BHF Statistics 2021). BP is measured as both SBP which refers to BP during myocardial contraction and diastolic blood pressure (DBP) which to refers to BP during myocardial relaxation. Clinically, HTN is defined as a persistent raised BP of >140/90mmHg (National Institute for Clinical Excellence (NICE), 2011) with a normal BP being approximately 120/80mmHg. HTN in patients is defined by BP categories and the following AAC/AHA guidelines: normal BP (SBP <120mmHg and DBP <80mmHg), elevated BP (SBP 120-129mmHg and DBP <80mmHg), stage 1 HTN (SBP 130-139mmHg and DBP 80-89mmHg), and stage 2 HTN (SBP ≥140mmHg and DBP ≥ 90mmHg; Flack and Adekola 2020).

In healthy individuals, BP is regulated by the RAAS, arterial baroceptors, endothelial cells, ANP, and mineralocorticoid and glucocorticoid steroids. However, dysfunction in any of these processes can lead to HTN through either increased CO or increased systemic vascular resistance (Williams 2015). As patients get older blood vessels become more rigid with ageing resulting in a reduction in vasodilation and an increase in systemic vascular resistance which ultimately results in HTN (Jani and Rajkumar 2006). Research has shown that HTN on its own can increase vascular resistance (Mayet and Hughes 2003) and HFpEF patients have abnormal macrovascular and microvascular function (Ali *et al*. 2019). Balmain et al. (2007) also investigated arterial compliance and microvascular vasodilator function in HFpEF patients, HFrEF patients, and healthy individuals and found increased arterial stiffness only in the HFpEF group. Canonical Wnt signalling has been shown to induce multiple RAAS genes including those encoding angiotensinogen (AGT), renin, ACE, and the AT_1R, while administration of the Wnt signalling inhibitor, ICG-001, reduces RAAS gene induction both *in*

vitro and *in vivo* (Zhou *et al*. 2015). In a more recent study, a reciprocal role for RAAS induced activation of Wnt signalling was demonstrated when treatment with AngII stimulated the expression of multiple Wnt ligands (Zhao *et al*. 2018). In an experimental model of HTN, β-catenin accumulation was significantly increased in the nuclei of cardiomyocytes from hypertensive compared with normotensive rats (Zheng *et al*. 2013). Furthermore, administration of ICG-001 reduced both SBP and DBP in hypertensive rats infused with AngII to levels similar to control rats (Zhao *et al*. 2018; Xiao *et al*. 2019). Taken together, the evidence suggests that the RAAS and Wnt signalling system perpetuate each other's activity and consequently both contribute to the pathogenesis of HTN and associated diseases i.e. HFpEF.

1.6.9.2. Obesity

Obesity is another common co-morbidity that is associated with HFpEF and approximately 27% of adults in the UK are classed as obese (Body mass index; BMI>30) with a further 35% classed as overweight (BMI 25-30; BHF Statistics 2021). Approximately 80% of patients with HFpEF are obese (Haass *et al*. 2011) and there is a significant association between BMI and LV diastolic function (Rosenbaum *et al*. 2018). It has also been reported that there is a greater risk of HFpEF with increased BMI and insulin resistance in comparison to HFrEF, with the risk factors being more prevalent in women than men (Savji *et al*. 2018). Obesity has been documented to contribute to the development of HFpEF via the activation of RAAS, the release of pro-inflammatory adipokines, the generation of oxidative stress, and based on recent evidence potentially via the activation of Wnt signalling. Research has shown that β-catenin expression is significantly increased in the subcutaneous white adipose tissue (WAT) of both obese patients and mice fed on a high fat diet (HFD; Chen *et al*. 2020). Moreover, β-catenin has been demonstrated to be more highly expressed in mature adipocytes compared with preadipocytes, which may suggest that β-catenin plays an important role in mature adipocyte function and potentially fat accumulation within these cells (Chen *et al*. 2020). In addition, canonical Wnt signalling has been shown to regulate adipogenesis and control adipocyte differentiation (Bennett *et al*. 2002; Ross *et al*. 2000). Data suggests that the activation of both canonical and non-canonical Wnt signalling occurs in obesity as Wnt5a expression has also been shown to be significantly elevated in both subcutaneous and visceral WAT from obese patients (Fuster *et al*. 2015). In adipose tissue, Wnt5a is not only produced by infiltrating macrophages (Pereira *et al.* 2008; Mill *et al.* 2014) but the latter can also be activated by Wnt5a in an autocrine fashion resulting in the secretion of pro-inflammatory mediators (Pereira *et al.* 2008; Kim *et al.* 2012; Maiti *et al.* 2012). These pro-inflammatory mediators can then act on adjacent adipocytes to induce Wnt5a expression further exacerbating the inflammation in the adipose tissue (Catalan *et al.* 2014). Clinical data has also demonstrated that serum levels of

Wnt5a are positively correlated with IL-6 (Relling *et al*. 2018) and both circulating levels and visceral fat expression of Wnt5a are increased in obese patients compared with lean individuals (Schulte *et al*. 2012; Catalan *et al*. 2014; Fuster *et al*. 2015; Farb *et al*. 2016; Akoumianakis *et al.* 2019). Conversely, evidence from the literature relating to the role of endogenous Wnt inhibitors in the setting of obesity is considerably more disparate and entirely dependent on the individual sFRP. In obese individuals, the expression of sFRP1 was reduced in subcutaneous WAT, while the expression of sFRP2, sFRP3, and sFRP4 were all upregulated (Ehrlund *et al*. 2013). Similarly, research by Lagathu et al. (2010) demonstrated that sFRP1 expression in subcutaneous WAT is reduced in morbidly obese patients, while genetic deletion of sFRP1 resulted in increased adiposity, increased inflammatory responses, and glucose homeostasis irregularities in transgenic mice fed a HFD (Gauger *et al*. 2013). In addition, sFRP4 deletion in mice also led to greater weight gain in response to a HFD (Mastaitis *et al*. 2015). Research has shown that overweight and obese patients have significantly lower levels of sFRP5 in comparison to lean individuals (Ouchi *et al*. 2010; Hu *et al*. 2013) and, in addition, sFRP5 acts as an anti-inflammatory adipokine that positively modulates metabolic dysfunction in obesity (Ouchi *et al.* 2010). Taken together, this suggests a prominent role for Wnt signalling in obesity.

1.6.9.3. Diabetes Mellitus (DM)

More than 3.9 million adults currently living in the UK have been diagnosed with DM and one third of all adults with DM die from either heart or circulatory disease (BHF Statistics 2021). DM is characterised by hyperglycaemia (elevated glucose in the circulation) which can occur as a consequence of either insufficient insulin secretion, insulin resistance, or excessive glucagon secretion. There are two types of DM, Type 1 DM and T2DM, the former is an autoimmune disease which is characterised by dysfunctional pancreatic beta-cells, while the latter is much more common and is due to impaired glucose regulation caused by a combination of insulin resistance and dysfunctional pancreatic beta-cells (reviewed by Blair 2016). Approximately 45% of patients with HFpEF have T2DM (McHugh *et al*. 2019) and in the Framingham Study T2DM was associated with a 2-fold risk of HF in men and a 4-fold risk in women (Kannel and McGee 1979). In a diabetic mouse model, the expression of Wnt1, Wnt2b, Wnt3, Wnt3a, Wnt8a, Wnt10b, Wnt16, and FZD_9 were all found to be upregulated in comparison to controls (Zhou *et al*. 2012). While in diabetic patients, Wnt2b, β-catenin, TCF7L2 (a gene that is strongly linked with T2DM and is a direct downstream target of β-catenin), CCND1, and c-Myc were all found to be upregulated in islet cells (Lee *et al*. 2008). Similar to obesity, sFRP4 has been shown to be increased in diabetic patients with elevated circulating levels reported to act as a biomarker for T2DM (Hoffmann *et al*. 2014). The utility of

sFRP4 as a biomarker for T2DM was further substantiated in a study by Mahdi et al. (2012), which demonstrated that individuals with high circulating levels of sFRP4 were 5 times more likely to develop T2DM, since sFRP4 had the potential to decrease the secretion of insulin (Mahdi *et al*. 2012). Finally, Hu et al. (2013) reported that circulating levels of sFRP5 were lower in diabetic patients compared to patients with normal glucose tolerance.

1.7. Hypothesis

It has been widely documented throughout the literature that Wnt signalling plays a role in not only a number of the co-morbidities associated with HFpEF but also in the development of both cardiomyocyte hypertrophy and cardiac fibrosis, key features of the condition. However, targeting Wnt signalling as a potential therapeutic intervention in HFpEF has not been investigated thus far. Therefore, the present study was carried out to investigate whether pharmacological inhibition of Wnt signalling could improve detrimental structural and/or functional changes associated with HFpEF.

1.7.1. Aims and Objectives

The main aims of this project were to 1) examine the role of Wnt signalling in cardiomyocyte hypertrophy; 2) investigate whether Wnt signalling contributes to the development of HFpEF using an *in vivo* model of the condition; and 3) determine whether the administration of a Wnt inhibitor (Wnt-c59) alters the maladaptive structural and/or functional changes associated with HFpEF.

The specific objectives of this thesis were:

- Objective 1: To optimise an *in vitro* model of AngII induced cardiomyocyte hypertrophy in H9c2 cells.
- Objective 2: To investigate the hypertrophic potential of Wnt3a in H9c2 cells and determine whether any observed findings translate to a human cell model of cardiomyocyte hypertrophy.
- Objective 3: To determine whether Wnt signalling is activated in an *in vivo* model of HFpEF and/or whether the administration of a Wnt inhibitor (Wnt-c59) could reverse some of the key structural/functional features associated with HFpEF.

Chapter 2: Materials and Methods

2.1. Materials

The reagents used throughout this project were purchased from the companies listed in Table 2.1.

Table 2.1. Sources of reagents and diets used in this project.

Product	Company and Address
1-Bromo-3-chloropropane, 99%, ACROS Organic	Fisher Scientific, Leicestershire, UK
Acetic Acid	Sigma-Aldrich, Dorset, UK
Agarose	Sigma-Aldrich, Dorset, UK
Angiotensin II (5mg)	Tocris Bioscience, Abingdon, UK
AngII Enzyme Immunoassay kit	Sigma-Aldrich, Dorset, UK
Applied Biosystems™ High-Capacity cDNA Reverse Transcription Kit	Fisher Scientific, Leicestershire, UK
Applied Biosystems™ RNase Inhibitor	Fisher Scientific, Leicestershire, UK
ATP	Sigma-Aldrich, Dorset, UK
Bradford Reagent	Fisher Scientific, Leicestershire, UK
Brain Natriuretic Peptide EIA Kit	Sigma-Aldrich, Dorset, UK
Bovine Serum Albumin (BSA)	Sigma-Aldrich, Dorset, UK
Buffered Zinc Formalin	Fisher Scientific, Leicestershire, UK
Candesartan	Cayman Chemical, USA
Cell Lysis Buffer	Cell Signalling Technology, UK
Cellpath Optimal Cutting Temperature (OCT) embedding matrix	Fisher Scientific, Leicestershire, UK
Control Diet (D12450J)	Research Diets, USA
Cor.At® 1M iPS Kit	NCardia, Cologne, Germany
Detach Kit	PromoCell, Germany
Dimethyl Sulfoxide (DMSO)	Fisher Scientific, Leicestershire, UK
Dulbecco's Phosphate Buffered Saline (dPBS)	Sigma-Aldrich, Dorset, UK
Ethanol, Absolute (200 Proof), Molecular Biology Grade	Fisher Scientific, Leicestershire, UK
exACTGene Mini DNA Ladder 25bp-650bp	Fisher Scientific, Leicestershire, UK
Fisher BioReagents exACTGene DNA Ladders	Fisher Scientific, Leicestershire, UK
Gel loading dye	Promega, Southampton, UK
Gel Red 0.5ml	Bioscience, Cambridge, UK
Gelatin from porcine skin	Sigma-Aldrich, Dorset, UK
Gibco DPBS with Calcium and Magnesium	Fisher Scientific, Leicestershire, UK
Gibco™ Dulbecco's Modified Eagle Medium (DMEM), high glucose, pyruvate, no glutamine	Fisher Scientific, Leicestershire, UK
Gibco™ Fetal Bovine Serum (FBS), qualified, heat inactivated, E.U.-approved, South America Origin	Fisher Scientific, Leicestershire, UK

Gibco™ Fibronectin Bovine Protein, Plasma (1mg)	Fisher Scientific, Leicestershire, UK
Gibco™ Penicillin-Streptomycin-Glutamine (100X)	Fisher Scientific, Leicestershire, UK
Gibco™ Trypsin-EDTA (0.25%), Phenol red	Fisher Scientific, Leicestershire, UK
H9c2 (2-1) Cell Line from rat	Sigma-Aldrich, Dorset, UK
Hank's Balanced Salt Solution (HBSS)	Sigma-Aldrich, Dorset, UK
HEPES	Invitrogen, UK
High Fat Diet (D12492)	Research Diets, USA
Human Cardiac Myocytes (HCM)	PromoCell, Germany
HyClone™ Hank's Balanced Salt Solution	Fisher Scientific, Leicestershire, UK
Invitrogen™ TRI Reagent™ Solution	Fisher Scientific, Leicestershire, UK
Invitrogen™ UltraPure™ Tris-Borate-EDTA (TBE) Buffer,10X	Fisher Scientific, Leicestershire, UK
Isopropanol	Sigma-Aldrich, Dorset, UK
Ketamine (Narketan)	Vetoquinol UK Ltd, Northamptonshire, UK
Menzel-Glaser Cover Glasses	Fisher Scientific, Leicestershire, UK
Menzel-Glaser Superfrost Slides	Fisher Scientific, Leicestershire, UK
Mouse Wnt3a DuoSet ELISA	R&D Systems, Abingdon, UK
Mouse Total β-catenin DuoSet ELISA	R&D Systems, Abingdon, UK
Myocyte Growth Medium (MGM)	PromoCell, Germany
National Diagnostics Histo-clear II	Scientific Laboratory Supplies Ltd, Nottingham, UK
National Diagnostics HistoMount	Scientific Laboratory Supplies Ltd, Nottingham, UK
National Diagnostics OmniMount	Scientific Laboratory Supplies Ltd, Nottingham, UK
N_{ω}-Nitro-L-arginine methyl ester hydrochloride (L-NAME)	Fisher Scientific, Leicestershire, UK
PBS Tablets	Fisher Scientific, Leicestershire, UK
PMSF	Fisher Scientific, Leicestershire, UK
PrecisionPLUS R & SY qPCR Master Mix	Primer Design,
Promega Blue/Orange Loading Dye 6x	Fisher Scientific, Leicestershire, UK
Protease Inhibitor Cocktail	Sigma-Aldrich, Dorset, UK
QuantiTect SYBR Green PCR Kit (200)	Qiagen, Manchester, UK
Recombinant Human sFRP1 Protein, Carrier Free (25ug)	R&D Systems, Abingdon, UK
Recombinant Human Wnt3a Protein, Carrier Free (10ug)	R&D Systems, Abingdon, UK
Recombinant Human/Mouse Wnt5a Protein, Carrier Free (10ug)	R&D Systems, Abingdon, UK
REDTaq® ReadyMix™ PCR Reaction Mix	Sigma-Aldrich, Dorset, UK
Retinoic acid (100mg)	Sigma-Aldrich, Dorset, UK
Sample Diluent Concentrate 1 (5X)	R&D Systems, Abingdon, UK
Shandon Eosin-Y	Fisher Scientific, Leicestershire, UK
Shandon Gills Haematoxylin	Fisher Scientific, Leicestershire, UK
Sirius Red in Picric Acid Solution	Atom Scientific, Cheshire, UK

Sucrose	Fisher Scientific, Leicestershire, UK
SupplementMix	PromoCell, Germany
Tris-EDTA buffer solution	Sigma-Aldrich, Dorset, UK
Trypan Blue	Sigma-Aldrich, Dorset, UK
Water (RNase/DNase free)	Fisher Scientific, Leicestershire, UK
Wnt-c59	Cayman Chemical, USA
Xylazine (Rompun)	Bayer Healthcare, UK

2.1.1. Composition of Drugs and Solutions

- **1% Acetic acid solution:** 1ml of acetic acid and 99ml of deionised water (dH_2O)
- **1x TBE Buffer:** 100ml of 10x TBE Buffer in 900ml of dH_2O
- **95% Ethanol solution:** 95ml of absolute ethanol and 5ml of dH_2O
- **5% FBS DMEM:** 25ml FBS in 500ml of DMEM
- **2% Agarose gel:** 1g agarose in 50ml of 1x TBE buffer
- **Anaesthesia:** Mixture of 120mg/kg ketamine and 16mg/kg xylazine administered at a dose of 100µl per 10g body weight
- **Angiotensin II stock (1mM):** 5mg in 2.4ml of dPBS
    - All further dilutions were prepared in 5 or 10% FBS DMEM
- **Candesartan stock (27.5mg/ml):** 27.5mg in 1ml of 100% DMSO
    - 85µl of Candesartan stock was added to 340µl of 100% DMSO
    - *Candesartan working solution:* 400µl of diluted Candesartan stock was added to 39.6ml of water containing L-NAME (0.5g/L) and 2% Sucrose (for palatability)
- **Heparinised saline (100U/ml):** 1000U/ml heparin sodium diluted with 0.9% saline
- **Hypertonic saline (15%):** 75g of sodium chloride in 500ml of dH_2O
- **L-NAME solution:** 0.5g of L-NAME per 1L dH_2O
- **Phosphate buffered saline (PBS):** 1 PBS tablet dissolved in 100ml of dH_2O
- **Retinoic acid (RA) stock (10mM):** 100mg of RA in 33.28ml of 100% DMSO
    - Subsequent dilutions of RA stock were prepared using DMEM
- **sFRP1 Stock (10µg/ml):** 25µg of sFRP1 in 2.5ml of dPBS
    - All further dilutions were prepared using 5% FBS DMEM
- **Wnt3a Stock (10µg/ml):** 10µg of Wnt3a in 1ml of dPBS
    - All further dilutions were prepared using 5% FBS DMEM
- **Wnt-c59 Stock *in vitro* (10mM)**: 10mg of Wnt-c59 in 2.64ml of 100% DMSO
    - All further dilutions were prepared using 5% FBS DMEM
- **Wnt-c59 Stock *in vivo* (27.5mg/ml)**: 27.5mg of Wnt-c59 in 1ml of 100% DMSO
    - 85µl of Wnt-c59 stock was added to 340µl of 100% DMSO

- *Wnt-c59 working solution:* 400µl of diluted Wnt-c59 stock was added to 39.6ml of water containing L-NAME (0.5g/L) and 2% Sucrose (for palatability)

2.2. Cell culture studies

For cell culture studies both rat myoblast H9c2 cells and primary human cardiac myocytes (HCMs) were used as rodent and human cardiomyocyte models, respectively.

2.2.1. Rat myoblast H9c2 cells

H9c2 cells are a proliferative myoblast cell line originally derived from embryonic BD1X rat ventricular tissue (Kimes and Brandt 1976), which have been used extensively as an *in vitro* experimental model in cardiomyocyte hypertrophy studies, cytotoxicity studies, and cell proliferation studies. Cells were shipped in standard growth media supplemented with 5% dimethyl sulfoxide (DMSO) and stored in the liquid nitrogen vapour phase until required.

2.2.1.1. Culture of H9c2 cells from frozen stock

A frozen cryovial of H9c2 cells was thawed in a water bath at 37°C for 2 minutes until all the contents of the cryovial had defrosted. Cells were then added to a T75 flask containing 12ml of pre-warmed standard Dulbecco's Modified Eagle Medium (DMEM) supplemented with 10% fetal bovine serum (FBS), 100U/ml penicillin, 100µg/ml streptomycin and 2mM L-glutamine (subsequently referred to as standard DMEM). Cells were cultured overnight in a humidified atmosphere at 37°C under 5% CO_2 to allow attachment to the flask surface, medium was then replaced with fresh standard DMEM to remove any remaining cryopreservant (DMSO). H9c2 cells were routinely maintained under these conditions with media changes carried out every 2-3 days, until they were ready for subculture or required for experimentation.

2.2.1.2. Subculturing of H9c2 cells

Cells were maintained in culture until they became 60-70% confluent before sub-culturing to ensure that the cells maintained their myoblastic phenotype. The media was poured off the cells and 10ml of sterile pre-warmed Hanks Balanced Salt Solution (HBSS) was added to remove any remaining media. This step was repeated before 5ml of 0.25% tryspin-EDTA was added and flasks incubated for 5 minutes at 37°C under 5% CO_2. Cells were observed under a Leica DMIL microscope (Leica Biosystems, Newcastle, UK) to ensure all cells had detached, with the flasks being gently tapped if some cells remained attached. The contents of the flask

were poured in to a 50ml centrifuge tube. The flask was then rinsed with 10ml of standard DMEM to collect any remaining cells and neutralise the trypsin following addition to the 50ml tube containing the cell suspension. The cell suspension was then centrifuged at 200xg for 5 minutes, media was poured off, and the cell pellet was resuspended in 1ml of standard DMEM. Following cell counting (see section 2.2.1.3.) H9c2 cells were seeded in T75 flasks at a cell density of between 200,000-300,000 cells.

2.2.1.3. Cell counting

The number of cells was verified using a double chamber haemocytometer shown in Figure 2.1. Following disruption of the cell pellet in 1ml of standard DMEM, 15µl of the cell suspension was added to a microcentrifuge tube containing 15µl of Trypan blue (0.4%) solution and the tube was incubated at 37ºC for 5 minutes. This created a dilution factor of 2 to be used in equation 2, as the cells were placed in a 1 in 2 dilution with Trypan blue. Trypan blue was used to check the viability of cells by measuring the ratio of unstained cells (viable cells) versus (vs) the stained cells (non-viable cells). 10µl of the cell suspension and Trypan blue mixture was added to the haemocytometer and the cell count was determined by counting the cells within a set area of 16 squares within the 4 larger quadrants of the haemocytometer.

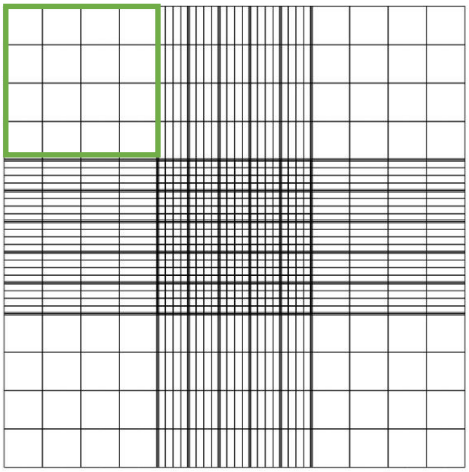

Figure 2.1. Example of a haemocytometer.

Clear viable cells were counted in all 4 larger outer quadrants (highlighted in green) and combined giving the total number of cells (N). To determine the average number of cells per quadrant this value (N) was divided by 4 giving A_N and this value was used to calculate the overall concentration of viable cells per ml (V) using the following equation:

Equation 2: $\mathbf{V = (A_N) \times 10^4 \times dilution\ factor}$

2.2.1.4. Harvesting of H9c2 cells for RNA extraction

To prepare cells for ribonucleic acid (RNA) extraction, cells were detached from the growth flask using trypsin and pelleted as previously described in section 2.2.1.2. The cell pellet was resuspended in 1ml of Tri-reagent solution and gently pipetted up and down to break up the cell pellet, then the solution was transferred to a sterile 1.7ml RNase/DNase free microcentrifuge tube. RNA was either extracted (as described in section 2.3.) straight away or the tubes were placed in a freezer at -20°C for future extraction.

2.2.1.5. Cryopreservation of H9c2 cells

Additional cells that were not required for immediate experiments were cryopreserved for later use. To freeze the cells, the cell pellet was collected as previously stated in section 2.2.1.2. Cells were resuspended in freezing media (standard DMEM with 5% DMSO), transferred into a cryovial and placed in a Corning CoolCell LX freezing container overnight at -80°C. The following day the cells were moved to a liquid nitrogen container for long term storage.

2.2.2. Human Cardiac Myocytes (HCMs)

Primary HCMs isolated from the ventricles of adult hearts were obtained from PromoCell and used in the present study to assess the translational potential of any effects observed in the rat myoblast cell line (H9c2 cells). One of the benefits of using these HCMs, compared to freshly isolated rod-shaped myocytes, is their ability to proliferate allowing long term experiments to be conducted making them a useful *in vitro* model for cardiovascular based research. However, caution must be exercised when interpreting any findings relating to these cells as their proliferative capacity is due to their undifferentiated state and similarity to cardiac progenitor cells as evidenced by their expression of markers of early stage differentiation (i.e. GATA-4 and sarcomeric alpha-actin). Based on supplier information these cells can be differentiated to a more mature phenotype which express markers of late differentiation (i.e. sarcomeric alpha-actinin and slow muscle myosin) and form myotube-like structures following prolonged time in culture (>60 days), however preliminary studies conducted in our lab found limited viability of cells after 21 days of culture. On this basis and the observation that all previously published literature using these HCMs used them in their undifferentiated state (Nehra *et al.* 2013; Chen *et al.* 2016; Srivastava *et al.* 2016) all studies documented here were conducted with the undifferentiated HCMs. HCMs were shipped in a cryogenic vial containing 500,000 viable cells and stored in the liquid nitrogen vapour phase until required.

2.2.2.1. Culture of HCMs from frozen stock

To prepare the medium for culturing HCMs, one vial of PromoCell SupplementMix was defrosted at room temperature and added to a bottle of PromoCell Myocyte Growth Medium (MGM). Final supplement concentrations in the MGM are detailed in Table 2.2. A vial of HCMs was removed from liquid nitrogen and placed in a water bath at 37ºC for 2 minutes until the contents of the cryovial had defrosted. Cells (250,000) were then seeded in T25 flasks containing 5ml of MGM and cultured overnight in a humidified atmosphere at 37°C under 5% CO_2 to allow attachment. Media was then replaced with fresh MGM to remove any remaining cryopreservant (DMSO). HCM cells were routinely maintained under these conditions, with media changes carried out every 2-3 days, until they were ready for subculture or required for experimentation.

Table 2.2. Final supplement concentrations of medium after addition of SupplementMix to MGM.

Supplement	Concentration
Fetal Calf Serum	0.05ml/ml
Epidermal Growth Factor (recombinant human)	0.5ng/ml
Basic Fibroblast Growth Factor (recombinant human)	2ng/ml
Insulin (recombinant human)	5µg/ml

2.2.2.2. Subculturing of HCMs

Cells were maintained in culture until they became 80-90% confluent before sub-culturing. To detach HCMs a PromoCell DetachKit consisting of three components: Trypsin/EDTA (0.04%/0.03%); HEPES Buffered Balanced Salt Solution (HEPES BSS; containing 30nM HEPES, D-glucose, NaCl, KCl, Na-Phosphate and phenol red); and trypsin neutralising solution (TNS; composed of 0.05% trypsin inhibitor from soybean and 0.1% bovine serum albumin (BSA)) was used. The three solutions that form the DetachKit were brought up to room temperature 30 minutes before use. The medium was poured off the culture flask and 100µl HEPES BSS per cm^2 of culture flask surface was added to wash the cells and then discarded. To detach the cells 100µl Trypsin/EDTA was added per cm^2 of flask surface and incubated at room temperature for approximately 10 minutes. If any remaining cells were still attached the flask was gently tapped to loosen them. TNS (100µl per cm^2) was then added to the flask to neutralise the Trypsin/EDTA solution, the contents transferred to a 50ml falcon tube, and subsequently centrifuged at 220xg for 3 minutes. The supernatant was then discarded and the cell pellet was resuspended in 1ml of pre-warmed (37ºC) MGM. Cells were counted following the method outlined in section 2.2.1.4 and seeded at a cell density of 10,000 cells per cm^2 in either T25 or T75 flask containing 5ml or 15ml of pre-warmed MGM, respectively.

2.2.2.3. Harvesting of HCMs for RNA extraction

To prepare cells for RNA extraction, cells were detached using trypsin and pelleted as previously described in section 2.2.2.2. The cell pellet was resuspended in 1ml Tri-reagent solution and gently pipetted up and down to break up the cell pellet, then transferred into sterile RNase/DNase free 1.7ml microcentrifuge tubes. RNA was either extracted (as described in section 2.3.) straight away or the tubes were placed in a freezer at -20°C for future extraction.

2.3. Gene expression studies

2.3.1. RNA extraction from both tissues and cells

Rodent tissues were harvested, washed in PBS, placed in 1ml of Tri reagent and subsequently homogenised. Following homogenisation of the tissue, samples were spun at 12,000xg for 10 minutes to pellet remaining tissue debris and the supernatant transferred to clean RNase/DNase free microcentrifuge tubes. For RNA extraction from cells, both cell types were harvested and resuspended in 1ml of Tri reagent as described in sections 2.2.1.4. (H9c2 cells) and 2.2.2.3. (HCMs). 100µl of 1-bromo-3-chloropropane (BCP) per 1ml of Tri-reagent solution was then added to each microcentrifuge tube containing the supernatant from either the homogenised tissue or cell samples. To mix the solution, the tubes were shaken vigorously for 15 seconds and incubated at room temperature for 15 minutes. The tubes were then centrifuged at 12,000xg for 15 minutes at 4°C resulting in phase separation and the RNA containing clear aqueous phase then transferred to clean RNase/DNase free microcentrifuge tubes. To precipitate nucleotides in the samples, 500µl of isopropanol was added, samples vortexed for 10 seconds then left to incubate at room temperature for 10 minutes. After the incubation time the samples were centrifuged at 12,000xg for 8 minutes at 4^{o}C to produce the RNA pellet. The supernatant was removed, the RNA pellet washed with 75% ethanol, and then centrifuged at 7,500xg for 5 minutes at 4^{o}C. The ethanol was removed, the pellet air-dried for 20-30 minutes at room temperature, and then reconstituted in RNase/DNase free water according to the size of the pellet (5-20µl for non-visible/small pellets and up to 50µl for large pellets). The RNA pellet was frozen overnight at -80°C and the RNA concentration measured the following day.

2.3.2. Measuring RNA Concentration

The RNA samples were taken out of the -80°C freezer and placed on a heat block at 65°C for 10 minutes. To zero the spectrophotometer, 200µl RNase/DNase free water was added to a cuvette. After 10 minutes the RNA samples were removed from the heat block and gently flicked, then 2µl of RNA was added to 198µl of RNase/DNase free water in a centrifuge tube.

This was then vortexed, transferred to a cuvette, and placed in the spectrophotometer. RNA concentration was determined using the absorbance reading at 260nm and the following equation:

Equation 3: **RNA Concentration (µg/µl) = OD260 x 40µg x dilution factor ÷ 1000**

RNA quality was assessed via the absorbance readings at 260/280nm which allows an estimation of both protein and organic compound contamination in the sample. RNA was then diluted with RNase/DNase free water to either 25ng/µl (cells) or 50-100ng/µl (tissue) for the generation of complementary deoxyribonucleic acid (cDNA) via reverse transcription immediately, or placed in the freezer at -80°C for long term storage.

2.3.3. cDNA Reverse Transcription

To convert RNA to cDNA, a cDNA reverse transcription kit was purchased from Fisher Scientific. A master mix was prepared with the components indicated in Table 2.3., vortexed, then placed on ice before preparing the reaction mixture.

Table 2.3. Components to prepare the cDNA reverse transcription master mix.

Component	Volume/1 Reaction (µl)
10x RT Buffer	2.0
25x dNTP Mix (100mM)	0.8
10x RT Random Primers	2.0
MultiScribe Reverse Transcriptase	1.0
RNase Inhibitor	1.0
Nuclease-free H_2O	3.2

To prepare the cDNA reaction, 10µl of master mix was added to a PCR tube followed by the addition of 10µl of RNA (either 25ng/µl of cell RNA or 50-100ng/µl of tissue RNA). The samples were mixed by pipetting up and down then briefly centrifuged to eliminate any air bubbles. To perform reverse transcription the samples were transferred to a Biometra T3000 Thermocycler using the cycle conditions indicated in Table 2.4.

Table 2.4. Cycle conditions for cDNA reverse transcription.

	Step 1	Step 2	Step 3	Step4
Temperature (°C)	25	37	85	4
Time (min)	10	120	5	Pause

2.3.4. Polymerase Chain Reaction (PCR)

PCR is a technique which amplifies a single deoxyribonucleic acid (DNA) molecule into millions of copies in a relatively short period of time through a process involving three steps. The first step is denaturation, in which the double stranded DNA molecule is heated up to separate the strands. This is followed by the annealing stage, where short DNA molecules known as primers bind to the flanking regions of target DNA and the final stage is extension, in which the DNA polymerase extends the 3' end of each primer along the template strands. This process is repeated to create exact copies of the target DNA. Primers used for PCR were purchased from both Qiagen and Sigma Aldrich and reconstituted in 1.1ml of Tris-EDTA (TE) buffer solution (QuantiTect primers) or RNase/DNase free water (volume necessary to achieve a final concentration of 100µM; Sigma primers), respectively. Each primer was aliquoted out into 50µl volumes and stored at -20°C. A master mix was prepared for each primer as per Table 2.5.

Table 2.5. Components to prepare PCR master mix.

Reagent	Volume (µl)
RedTaq Ready Mix	25
Primer	2
RNase/DNase free H_2O	19

To prepare the reaction mixture 4µl of cDNA was added to a PCR tube followed by 46µl of master mix described in Table 2.5. Tubes were briefly centrifuged, samples placed in a thermocycler (Biometra T3000), and subjected to the cycle conditions described in Table 2.6.

Table 2.6. Cycle conditions for PCR.

Temperature (°C)	Time (mins)	Cycles
95	15	1
94	0.5	40
55	0.5	
72	0.5	

2.3.4.1. Agarose Gel Electrophoresis

Gel electrophoresis is a technique that separates DNA fragments by size (length in base pairs) and in this instance was used to confirm specificity of binding (as evidenced by the appearance of bands of the predicted/correct size). An electric field is used to attract the negatively charged DNA through an agarose gel towards a positive electrode. The approximate length of a DNA fragment can be determined by running the samples alongside a DNA ladder (used to determine PCR product sizes). A 2% agarose gel was prepared by adding 1g of agarose to 50ml of 1x Tris/Borate/EDTA (TBE) buffer. The solution was heated up until the agarose dissolved, left to cool slightly, and then 5µl of Gel Red was added. The agarose solution was poured into a gel tank, left to set following the addition of a comb to create wells, subsequently placed in the electrophoresis tank, and submerged in 1x TBE buffer. 2µl of 6x loading dye was added to 0.5ml microcentrifuge tubes followed by the addition of 10µl of the PCR product. To prepare the DNA ladder, 4µl of 6x loading dye and 20µl of the exACTGene Mini DNA Ladder (25bp-650bp) was added to a microcentrifuge tube. All samples were briefly centrifuged, then 10µl of each sample was loaded onto the gel. Two volumes (5µl and 10µl) of DNA ladder were tested and samples were subjected to electrophoresis for 1 hour at 80V. Gels were visualised and images captured using the PeqLab Fusion Fx7 system.

2.3.5. Quantitative Polymerase Chain Reaction (qPCR)

qPCR is a method used to amplify and quantify a target DNA sequence. It follows the same DNA amplification principle as PCR, with the addition that it produces a fluorescent signal which reflects the quantity of product produced in each cycle. In the present study, cDNA was either used neat or diluted to give a final concentration of 50ng/ul. For QuantiTect primers, a QuantiTect SYBR Green PCR kit was used and a master mix containing 10µl of SYBR green, 2µl of a specific primer, and 6µl RNase/DNase free water was prepared for each reaction. Primers obtained from Sigma were first diluted to 10µM in deionised H_2O (dH_2O), then a master mix was prepared using 10µl of Primer Design SYBR green, 0.5µl of each of the forward and reverse primers, and 7µl of RNase/DNase free water for each reaction. To prepare a mastermix with Qiagen primers, 2µl of primer was added to 10µl of Quantitect SYBR green and 7µl of RNase/DNase free water for each reaction. Finally, 2µl of cDNA was added to wells of a MicroAmp® Fast Optical 96-well reaction plate, followed by 18µl of the relevant qPCR reaction master mix. qPCR was then performed using a 7900HT Fast Real-Time PCR system (Applied Biosystems, Warrington, UK) as per the experimental conditions described in either Table 2.7. (QuantiTect primers) or Table 2.8. (Sigma primers). Individual primer information/sequences are detailed in the relevant chapters.

Table 2.7. Cycle conditions for qPCR followed by melting curve conditions for QuantiTect primers.

Step	Temperature (°C)	Time (minutes)	Number of Cycles
Initial Activation Step	95	15	1
Denaturation	94	0.5	40
Annealing	55	0.5	
Elongation	72	0.5	
Melting Step	94	0.25	1
	60	0.25	
	95	0.25	

Table 2.8. Cycle conditions for qPCR followed by melting curve conditions for Sigma primers.

Step	Temperature	Time (minutes)	Number of Cycles
Hot Start	95°C	2	1
	95°C	0.25	40
Annealing (Data Collection)	60°C	2	
Melting Step	95°C	0.25	1
	60°C	0.25	
	95°C	0.25	

2.3.5.1. Primer Efficiency

To assess primer efficiency a series of cDNA concentrations ranging from 0.01ng-100ng were analysed. Average Ct values were calculated for each concentration and a semi-logarithmic analysis plot created using linear regression (GraphPad Prism). Gradients between -3.1 and -3.6 were considered acceptable as they reflect a primary efficiency of between 90-110%. Another important measure of primer efficiency is the correlation coefficient R^2 which is obtained from the standard curve and is a measure of the linearity of the qPCR reaction. In the present study, an R^2 value of ≥0.98 was deemed additional confirmation of good primer efficiency. To calculate the % primer efficiency the following equation was used:

Equation 4: **% Primer Efficiency = (10 x (-1/gradient) -1) x 100**

2.3.5.2. Calculating relative gene expression using primer efficiency

The expression of all genes of interest (e.g. ANP, BNP etc.) were normalised in the first instance to that of the housekeeping gene (HKG), Gapdh, and subsequently to controls (in order to compare treatments). To measure changes in gene expression between treatments, the Pffafl relative expression ratio was used (Pfaffl 2001). The relative expression ratio is calculated from primer efficiencies of genes and the crossing point deviation of an unknown sample vs control. To begin, primer efficiencies were calculated for the HKG and each gene of interest (GOI) (as described in section 2.3.5.1.), these values subsequently converted to real time PCR efficiency (E) values (using Equation 5), and then used to calculate gene expression.

Equation 5: **E value = (% Primer Efficiency/100) +1**

To calculate the ΔCt for both HKG and GOI, the Ct values for individual samples (controls and treatment) were averaged and then subtracted from the overall average Ct value for the control HKG and GOI, respectively (see Equation 6).

Equation 6:

$$\Delta Ct_{HKG} = \text{Overall Ct average (control samples)}_{HKG} - \text{Average Ct for each sample}_{HKG}$$

$$\Delta Ct_{GOI} = \text{Overall Ct average (control samples)}_{GOI} - \text{Average Ct for each sample}_{GOI}$$

The GOI expression ratio for individual samples was then calculated using equation 7:

Equation 7: $$\text{Gene expression ratio} = (E_{GOI})^{\Delta Ct\ GOI} / (E_{HKG})^{\Delta Ct\ HKG}$$

2.4. *In vitro* cardiomyocyte hypertrophy studies

2.4.1. *In vitro* models of cardiomyocyte hypertrophy

2.4.1.1. H9c2 cells

H9c2 cells (maintained in culture as per section 2.2.1.1. and harvested as per section 2.2.1.4) were seeded at a density of 150,000 cells per T25 flask in 4ml of standard DMEM and maintained in a humidified atmosphere of 5% CO_2 at 37°C in an incubator for 24 hours. The following day the media was removed and replaced with serum free DMEM (100U/ml penicillin, 100µg/ml streptomycin and 2mM L-glutamine) and cells were serum starved for 24 hours. Cells

were stimulated with a hypertrophic agent for 24 hours in fresh 5% FBS DMEM. RNA was then extracted from treated cells and cDNA prepared as described in sections 2.3.1. to 2.3.3. and the mRNA expression of the fetal genes, ANP and BNP, measured via qPCR (as per section 2.3.5.) to detect the presence of hypertrophy i.e. an upregulation of fetal gene expression.

2.4.1.2. HCMs

HCMs (maintained in culture as per section 2.2.2.1. and harvested as per section 2.2.2.3) were seeded at a density of 250,000 cells per T25 flask in 5ml MGM and cultured in a humidified atmosphere of 5% CO_2 at 37ºC in an incubator for 48 hours. After 48 hours cells were stimulated with a hypertrophic agent for 24 hours in fresh MGM. To detect the presence of hypertrophy, RNA was extracted from treated cells and converted to cDNA as described in sections 2.3.1 to 2.3.3 and the mRNA expression of BNP (hypertrophic marker) was measured via qPCR (as per section 2.3.5).

2.4.2. Determining active biological concentrations of Wnt signaling mediators using Corning® Epic® Technology

Corning Epic® is a high throughput label-free technology that is used for the investigation of ligand-receptor signaling responses in different cell types. Receptor activation can be determined by dynamic mass redistribution (DMR), which allows the detection of biological responses within cells to various stimuli via the optical measurements of changes in refracted wavelength (illustrated in Figure 2.2.). H9c2 cells were cultured, as per section 2.2.1.1. in T175 flasks until they reached 60-70% confluence then harvested (as per section 2.2.1.4.) and resuspended in media at a density of 250,000 cells/ml. The cells were then seeded at 10,000 cells per well in an Epic® 384 well Fn1 coated cell assay microplate using a Multi-drop Combi cell dispenser (Thermo Electron Corporation, UK). The microplate was then placed in an incubator at 37°C in 5% CO_2 to allow the cells to attach overnight. The following day, a compound microplate was prepared with varying concentrations of agonist/antagonist. All pharmacological agents were made up at x4 concentration to account for the 1:4 dilution following addition to the microplate containing cells. Once prepared, all pharmacological agents and negative control (i.e. wash buffer comprised of HBSS containing HEPES (20mM) and 0.01% BSA; pH 7.4) were then added (30µl/well) to the relevant wells of the compound microplate. The microplate containing the cells was first gently washed with wash buffer using an ELx Microplate washer (Bio-Tek, Sweden) and then 30µl of wash buffer added to each well. The microplate was then placed in the Corning Epic Benchtop Imaging System (Corning, UK) at 26°C for 1 hour to allow the cells to reach thermal equilibrium (minimising the effect of

temperature on assay variability) prior to the addition of the compounds. Baseline measurements were recorded every 30 seconds for 3 minutes, then the microplate was removed, and the relevant compounds (10µl) were added to the appropriate wells using a Biomek NM laboratory automated workstation (Beckman Coulter, Sweden). The microplate was then placed back into the Epic system and DMR activity within the cells measured every 30 seconds for a time period of 1 hour. To analyse the data each DMR activity reading was plotted against time.

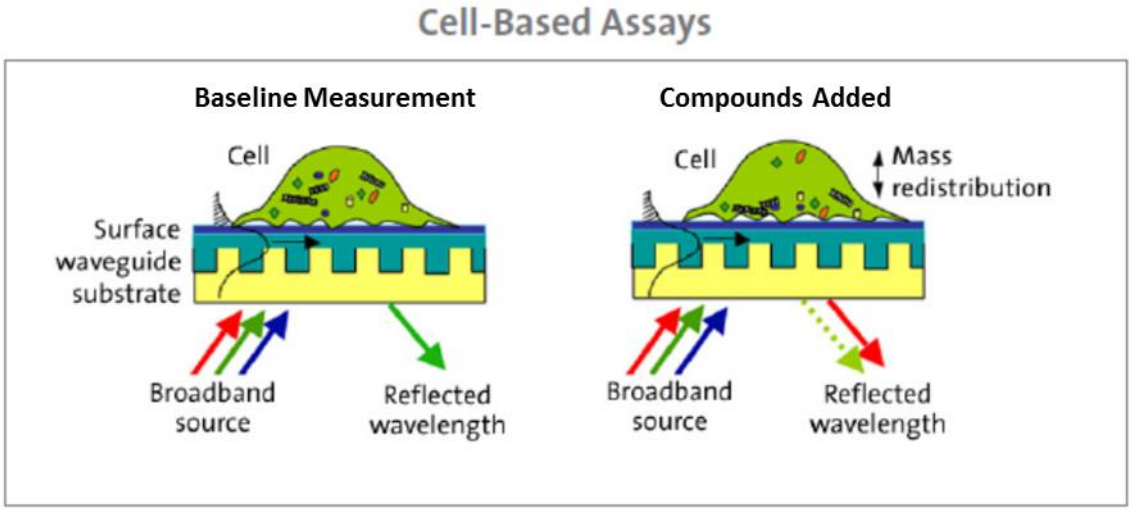

Figure 2.2. The methodology of Corning Epic Technology. When compounds are added to the cell, this can produce a change in mass within the cell, also causing index of refraction changes, resulting in a picometer wavelength shift. This is measured and reported as a dynamic mass redistribution (DMR) change (Adapted from Corning Epic Technology 2012).

2.4.3. Measurement of secreted BNP in cell culture media via ELISA

Enzyme-linked immunosorbent assay (ELISA) is a microplate-based assay that detects and measures proteins, antibodies, hormones, and peptides. The BNP Enzyme Immunoassay kit (cat# RAB086; Sigma-Aldrich, Dorset, UK) used in the present study is a quantitative assay that measures BNP peptide based on the principle of Competitive Enzyme Immunoassay. This assay works by spiking samples and standards with a known concentration of biotinylated BNP peptide, which are then added to the plate resulting in the biotinylated BNP peptide competing with endogenous (unlabeled) BNP to bind to the anti-BNP antibody. Any bound biotinylated BNP reacts with horseradish peroxidase (HRP)-streptavidin resulting in a chromogenic reaction. The intensity of the colour/absorbance is directly proportional to the quantity of

captured biotinylated BNP peptide and inversely proportional to the amount of endogenous BNP in the standards and samples. This ELISA kit has reactivity specific to rat, mouse and human BNP and was used as per the manufacturer's instructions. In brief, all wells of a 96-well plate were coated with 100µl of anti-BNP antibody (primary antibody) and the plate incubated overnight at 4°C. The wells were then washed with buffer to remove any unbound anti-BNP antibody and all standards and samples spiked with biotinylated BNP peptide. The samples and standards were then added to the plate and incubated for 2.5 hours at room temperature to allow the biotinylated BNP to compete with the endogenous (unlabeled) BNP for binding to the anti-BNP antibody. Wells were then washed and 100µl of HRP-streptavidin solution added for 45min at room temperature with gentle shaking. After the wash step, bound biotinylated BNP interacts with HRP-streptavidin, which will subsequently catalyse a colour development reaction. Surplus HRP-streptavidin solution was removed, wells washed repeatedly, 100µl of 3,3',5,5'-tetramethylbenzidine (TMB) One-Step Substrate Reagent added to each well, and the plate incubated in the dark with gently shaking for 30min. Finally, 50µl of Stop Solution was added to each well and the absorbance of the plate read immediately at 450nm using a microplate reader (BioTek MQX200 uQuant). A standard curve for BNP (0-1,000pg/ml) was plotted using four-parameter logistic regression in GraphPad Prism 8 with percentage absorbance (calculated as per equation 8) plotted on the y-axis and BNP concentration plotted on the x-axis and this was used to determine the concentration of endogenous BNP peptide in experimental samples.

Equation 8: **Percentage absorbance (B/B_0%) = (B–blank OD)/(B_0–blank OD)**

B = OD of sample or standard

B_0 = OD of zero standard (total binding)

2.5. *In vivo* Studies

2.5.1. Animal Ethics and Husbandry

Animal studies were conducted in accordance with the Animals (Scientific Procedures) Act 1986 under Home Office project license numbers 60/4231 and PP0376978 and personal license number I8DBF2161. Prior to any *in vivo* experiments being conducted, research ethics were obtained by the submission of a Research Ethics: Student and Supervisor Appraisal (RESSA) form to the Robert Gordon University (RGU) animal ethics committee for approval. Male C57Bl/6J mice were purchased from Charles River Laboratories (Edinburgh, UK) and group housed at RGU, with a maximum capacity of 4 mice per cage. Mice were housed within the Biological Services Unit (BSU) in a temperature and humidity (19-23ºC and 45-65%,

respectively) controlled room set on a 12-hour light/dark cycle (7am-7pm) and maintained in accordance with the husbandry guidelines set by the UK Home Office. All dietary interventions and surgical procedures were conducted within the BSU. Prior to the commencement of any experiments, mice were allocated a period of 7 days where they could acclimatise to their surroundings once they arrived within the BSU. All *in vivo* work is reported in accordance with the ARRIVE guidelines (Percie du Sert *et al*. 2020).

2.5.2. Pressure Volume Loop Analysis

Pressure volume loop (PVL) analysis was used to investigate cardiac function which is divided into two phases, systole (contraction) and diastole (relaxation). Simultaneous measurement of both pressure and volume *in vivo* creates a loop that represents the relationship between intraventricular pressure and volume throughout the entire cardiac cycle (Figure 2.3.). To record this relationship, a conductance catheter is inserted into the LV either via the carotid artery (closed chest; CC) or the apex of the heart (open chest; OC). The catheter is composed of four platinum electrodes which are arranged in two pairs with the pressure sensor located between the two pairs of electrodes. Following placement in the heart, the electrode pairs (proximal and distal) should be situated beneath the aortic valve and at the apex of the LV to facilitate continuous flow of the signal from the proximal probes to the distal probes creating an electric field. The analogue signal generated by the conductance catheter is then converted to a digital signal via the MPVS-Ultra Single Segment Foundation system (Millar Instruments, Texas, USA), cardiac function recorded using LabChart software (ADInstruments, Oxford, UK), and assessed using PVAN Ultra™ software (Millar Instruments, Texas, USA).

2.5.2.1. Calibration of the conductance catheter

To calibrate the catheter, the latter was connected to the MPVS-Ultra Single Segment Foundation system and the accompanying PowerLab (ADInstruments, Oxford, UK). Before calibration, the catheter (SPR-839; Millar Instruments, Texas, USA) was placed in warm (37^{o}C) saline (0.9% NaCl in water (w/v)) for approximately 30 minutes. Both the pressure and volume signals recorded in LabChart (ADInstruments, Oxford, UK) were then calibrated using fixed voltage signal references for pressure (0, 25, and 100mmHg) and volume (29.6 and 72µl) contained within the MPVS *Ultra* Control Interface (MPVS *Ultra* Software; Millar Instruments, Texas, USA).

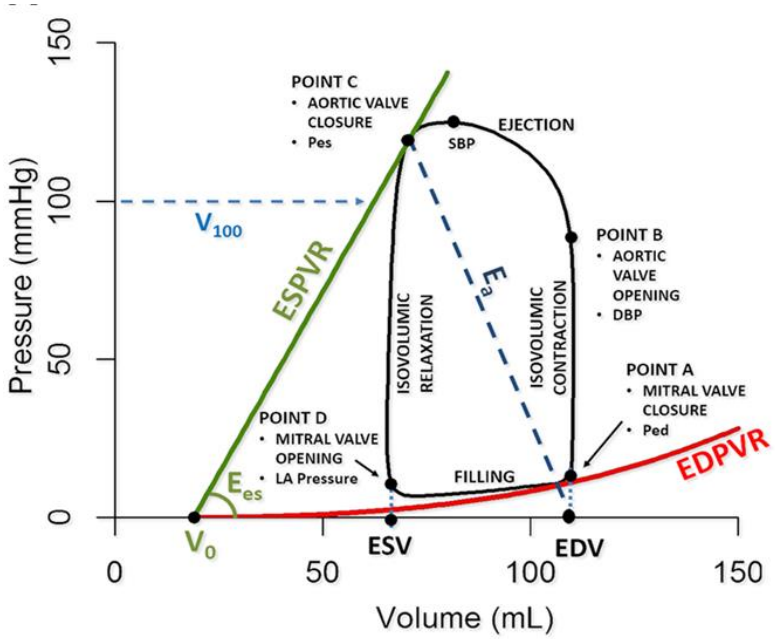

Figure 2.3. A typical PV loop. Isovolumic contraction (A-B), ejection (B-C), isovolumic relaxation (C-D) and filling (D-A), all components of a normal cardiac cycle. EDPVR – end-diastolic pressure volume relationship; ESPVR – end-systolic pressure volume relationship; ESV – end systolic volume; EDV – end diastolic volume. (Bastos *et al.* 2020).

2.5.2.2. Surgical procedure for insertion of conductance catheter for BP and PVL measurements

Male C57Bl/6J mice were weighed and then anaesthetised via intraperitoneal injection (i.p.) of a mixture of ketamine (120mg/kg; Narketan, Vetoquinol UK Ltd, Northamptonshire, UK) and xylazine (16mg/kg; Rompun, Bayer, Dublin, Ireland) at a concentration of 100µl per 10g body weight (BW). Once the animal was immobile it was moved on to a heat pad to maintain its body temperature at 37ºC and the depth of anaesthesia assessed every 15 minutes by testing the pedal withdrawal reflex. Once the animal was fully anaesthetised (deemed as a loss of the pedal withdrawal reflex) a rectal probe was inserted to ensure core body temperature was maintained between 37-38°C using a heat pad (RightTemp mouse body temperature monitor; Kent Scientific Corporation, Connecticut, USA). Adequate maintenance of body temperature is critical when operating on anaesthetised mice as a low body temperature can reduce the animal's HR to almost half of its normal rate leading to depressed cardiovascular function and the recording of non-physiologically accurate data (Hankenson *et al.* 2018). To allow administration of a hypertonic saline (15% NaCl w/v) bolus the right jugular vein was cannulated with flame stretched Portex polythene tubing (0.58mm ID x 0.96mm OD; Smiths Medical International Ltd, Kent, UK). To measure BP, the neck was opened, the right carotid artery isolated, and a 1.4Fr pressure conductance catheter inserted into the artery to record baseline measurements of SBP and DBP. Once BP measurements had been obtained, the catheter was advanced into the LV in those experiments in which closed chest (CC) PVL analysis was attempted. In experiments using open chest (OC) PVL analysis, the catheter was gently removed from the carotid artery, the latter securely tied off to prevent any blood loss, and the catheter inserted into the LV as described in the following text. To conduct OC PVL analysis, mice were artificially ventilated via tracheostomy using the Rovent® Jr ventilation system (Kent Scientific Corporation, Connecticut, USA). The ventilation system calculates the respiration rate and tidal volume based on the animal's BW, therefore each individual animal's BW was correctly inputted into the ventilation system before the tracheostomy took place. To make an incision into the chest, the chest wall was cut using a cauteriser (Bovie Change-A-Tip™; Interfocus Ltd, Linton, UK) at both sides of the xiphoid process to reveal the underside of the diaphragm. A cauteriser was used to minimise blood loss and maintain physiological cardiac function. Once the heart was in view, the pericardium was removed and a suture was placed loosely around the inferior vena cava (IVC) to conduct IVC occlusions after baseline PVL measurements were recorded. To insert the conductance catheter into the LV, the apex of the LV was punctured using a 27-gauge needle to create a hole for the passage of the catheter. Once the catheter was securely in the LV, it was moved very slightly until the largest SV was observed using the PVL recording software (LabChart) and baseline/load dependent measures of cardiac function recorded throughout the entire experiment. To obtain load

independent measures of cardiac function i.e. end-systolic pressure volume relationship (ESPVR) and end-diastolic pressure volume relationship (EDPVR) etc., IVC occlusions were conducted by lifting the suture to transiently occlude the vena cava resulting in a gradual decrease in the venous return to the heart. Both load dependent and independent cardiac function was subsequently analysed using PVAN Ultra™ software (Millar Instruments, Texas, USA) and all data calibrated using both parallel conductance and blood calibration values as subsequently described in sections 2.5.2.3. and 2.5.2.4., respectively.

2.5.2.3. Parallel Conductance

Parallel conductance is a term that refers to the conductivity of the heart muscle that encloses the left ventricular blood pool. Ideally the catheters' electrodes should only register the conductance signal within the blood, however some of this signal can also radiate into the cardiac muscle, which also acts as a conductor. Therefore, to prevent the overestimation of the blood volume in the LV, the parallel conductance value (V_P) was determined via the administration of a bolus dose of hypertonic saline (15% NaCl; 10µl) to the heart via the venous cannula in each experiment. The PV loops generated during this calibration were exported into PVAN Ultra^{TM} software and the V_P value calculated. To calculate the correct volume within the LV, the conductance across the ventricular wall (i.e. V_P) was subtracted from the blood conductance within the LV (calibrated conductance).

2.5.2.4. Blood volume calibration

Blood volume calibration is required as during PVL experiments volume is measured in relative volume units (RVU), and therefore needs to be converted to µl for data analysis. A calibration cuvette containing wells of known volumes (Millar Instruments, Texas, USA) was placed in a heating chamber at 37°C. Once PVL analysis had been completed, blood was collected via cardiac puncture and immediately transferred into the wells of the cuvette. The catheter was then placed in each well for 5-10 seconds with the MPVS-Ultra Single Segment Foundation System recording changes in RVU. The RVU data was then plotted on the y-axis, the known volumes of the wells plotted on the x-axis, and the data analysed using linear regression to calculate both the slope and the y-intercept which were subsequently used for the conversion of RVU data to µl in PVAN Ultra^{TM} software.

2.5.3. Plasma and Tissue Harvesting

Following the completion of the *in vivo* protocol, blood and tissues were collected from all mice for subsequent molecular, biochemical and histological analysis. Whole blood was collected from anaesthetised mice via cardiac puncture using a syringe containing heparinised saline (final heparin concentration of 20U/ml of blood) attached to a 29G needle; the blood was then transferred to a microcentrifuge tube and stored on ice prior to centrifugation to obtain plasma. Once the blood had been collected, the heart was immediately removed by cutting the connecting blood vessels to ensure that circulation had stopped and to confirm death of the animal before removing other tissues. Tissues that were chosen to be removed from the mice were the heart, lungs, liver, kidneys and WAT (epididymal fat pads). After removal the tissues were washed in sterile PBS, blotted to remove excess liquid and then weighed. All tissues were then placed in microcentrifuge tubes and flash frozen in liquid nitrogen. Whole blood was centrifuged at 2,000xg for 10 minutes at room temperature to obtain plasma, which was then transferred to a microcentrifuge tube and snap frozen in liquid nitrogen. All plasma and tissue samples were subsequently stored at -80°C for further analysis at a later stage.

2.5.4. Measurement of circulating levels of AngII in mouse plasma via ELISA

The AngII Enzyme Immunoassay kit (cat# RAB0010; Sigma-Aldrich, Dorset, UK) used in the present study is a quantitative assay that measures AngII based on the principle of Competitive Enzyme Immunoassay (the concept of which was previously described in section 2.4.3.). In brief, all wells of a 96-well plate were coated with 100µl of anti-AngII antibody (primary antibody) and the plate incubated overnight at 4°C. The wells were then washed with buffer to remove any unbound anti-AngII antibody and all standards and samples spiked with biotinylated AngII peptide. The plasma samples and standards were then added to the plate and incubated for 2.5 hours at room temperature to allow the biotinylated AngII to compete with the endogenous (unlabeled) AngII for binding to the anti-AngII antibody. Wells were then washed and 100µl of HRP-streptavidin solution added for 45min at room temperature with gentle shaking. Surplus HRP-streptavidin solution was removed, wells washed repeatedly, 100µl of TMB One-Step Substrate Reagent added to each well, and the plate incubated in the dark with gently shaking for 30min. Finally, 50µl of Stop Solution was added to each well and the absorbance of the plate read immediately at 450nm using a microplate reader (BioTek MQX200 uQuant). A standard curve for AngII (0-1,000pg/ml) was plotted using four-parameter logistic regression in GraphPad Prism 8 with percentage absorbance (calculated as per equation 9) plotted on the y-axis and AngII concentration plotted on the x-axis and this was used to determine the concentration of endogenous AngII peptide in experimental samples.

Equation 9: **Percentage absorbance (B/B_0%) = (B–blank OD)/(B_0–blank OD)**

B = OD of sample or standard

B_0 = OD of zero standard (total binding)

2.5.5. Measurement of Wnt3a and total β-catenin expression in murine tissues via ELISA

The Wnt3a and total β-catenin DuoSet ELISA kits quantify Wnt3a and total β-catenin protein using the solid phase sandwich ELISA technique which detects the antigen of interest (Wnt3a/β-catenin) using a microplate coated with a capture antibody (primary antibody directed against Wnt3a/β-catenin). In the present study, both Wnt3a and total β-catenin expression were measured in murine tissues via ELISA and normalized to the protein concentration of those tissues as described in detail below.

2.5.5.1. Protein extraction from murine tissues

To extract protein from murine tissues, tissue was harvested as stated in section 2.5.3. and subsequently placed in lysis buffer for subsequent homogenisation. The homogenisation buffer was prepared using cell lysis buffer (10x) (as described in Table 2.9.). To protect the protein from enzyme degradation a protease inhibitor cocktail and phenylmethylsulfonyl fluoride (PMSF), a serine protease inhibitor, were also added to the final lysis buffer at the volumes stated in Table 2.9. Tissue was removed from the -80ºC freezer, placed on ice and lysis buffer added at a volume of 1ml per 100mg of tissue. The tissue was homogenised in the lysis buffer in short bursts of 15 seconds and then spun at 14,000xg at 4ºC for 10 minutes to collect any remaining cell debris. The supernatant containing the protein was transferred to a chilled clean microcentrifuge tube and stored at -20ºC until samples were ready to be analysed.

Table 2.9. Components comprising 1ml of lysis buffer for the extraction of protein. A ratio of 1ml of lysis buffer to 100mg of tissue was used.

Component	Volume (µl)
Lysis Buffer (10x)	200
Protease Inhibitor Cocktail (1:100)	10
PMSF (100mM)	10
Water	780

2.5.5.2. Protein quantification using the Bradford Assay

To quantify the protein present in tissue samples the method originally described by Bradford (Bradford 1976) was used. The Bradford assay is a colorimetric assay based on an absorbance shift of the Coomassie Brilliant Blue G-250 dye. Under acidic conditions the dye changes from red to blue if there is protein present resulting in a shift in absorbance of the dye from 470nm to 595nm. The samples can then be read using a spectrophotometer and, using a standard curve with known concentrations of protein, the concentration of protein in experimental samples can be determined. Tissue sample supernatants were diluted 1:10 with PBS and a standard curve using BSA prepared with serial dilutions ranging from 0.03125mg/ml up to 5mg/ml diluted in PBS. To each well of a 96-well plate 200µl of Bradford reagent (0.01% Coomassie Brilliant Blue G-250, 5% methanol, 8.5% phosphoric acid) was added, followed by 10µl of each standard or sample in triplicate. The plate was then placed on a Biometra W12 tumbling table for 10 minutes and then read at 595nm using a microplate reader (BioTek MQX200 uQuant). Readings were averaged and a negative blank reading (Bradford reagent with 10µl of PBS) was deducted from all absorbance values. A standard curve was then created from the known BSA standards and linear regression (GraphPad Prism 8) used to determine the quantity of protein in the experimental samples.

2.5.5.3. Wnt3a DuoSet ELISA kit

The Wnt3a DuoSet ELISA kit (cat# DY1324B; R&D Systems, Abingdon, UK) detects both natural and recombinant mouse Wnt3a and was used as per manufacturer's instructions. In brief, all wells in a 96-well plate were coated with 100µl of capture antibody diluted in plate coating buffer supplied by the kit to a working concentration of 2µg/ml, the plate was sealed and incubated overnight at room temperature. The following day the plate was washed with wash buffer and the plate was blocked with 300µl of block buffer (1% BSA in PBS), which was prepared via a 1 in 10 dilution of the reagent diluent concentrate 2 provided by the kit. The block buffer was incubated for a minimum of 1 hour at room temperature. Wells were then washed and the plate was ready for the addition of standards and samples. For the dilution of standards and samples, a reagent diluent (0.1% BSA and 0.05% Tween 20 in Tris-buffered Saline (20mM Trizma base, 150mM NaCl)) was prepared and subsequently filtered. To create Wnt3a standards of varying concentrations, the Wnt3a stock provided by the kit was reconstituted with 0.5ml of reagent diluent to give a final concentration of 340ng/ml. This was then further diluted with reagent diluent to produce standards ranging from 156pg/ml up to 10,000pg/ml. 100µl of standard or sample was added to each well in duplicate, the plate sealed with an adhesive strip, and then incubated for 2 hours at room temperature. After 2 hours the plate was washed, 100µl of detection antibody (diluted to a working concentration of 500ng/ml

with reagent diluent) added to each well, the plate re-sealed, and incubated for a further 2 hours at room temperature. The plate was then washed and 100µl of Streptavidin-HRP B (diluted 1:40 with reagent diluent) was added to each well, the plate wrapped in tin foil to protect the contents from the light, and incubated at room temperature for 20 minutes. The plate was then washed and 100µl of substrate solution (1:1 mixture of colour reagent A and colour reagent B prepared in a tube wrapped in tin foil) was added to each well, the plate was rewrapped in tin foil, and incubated at room temperature for 20 minutes. Finally, 50µl of stop solution was added to each well and the plate was gently tapped to ensure thorough mixing. The optical density of each well was then determined by reading the absorbance of the plate at 450nm using a microplate reader (BioTek MQX200 uQuant). Due to wavelength corrections not being available the optical density was also read at 540nm, with the latter readings being subtracted from the readings recorded at 450nm which corrects for any optical imperfections in the plate. To get the final optical density readings, the blank (reagent diluent) was subtracted from each standard and sample reading. A standard curve was then created from the known standards and using linear regression the concentration of Wnt3a present in the experimental samples was extrapolated from the standard curve using GraphPad Prism 8.

2.5.5.4. Total β-catenin DuoSet ELISA kit

The Total β-catenin DuoSet IC ELISA kit (cat# DYC1329; R&D Systems, Abingdon, UK) detects both phosphorylated and unphosphorylated β-catenin and was used as per manufacturer's instructions. All wells in a 96-well plate were coated with 100µl of capture antibody diluted in plate coating buffer supplied by the kit to a working concentration of 4µg/ml and incubated overnight at room temperature. The next day the plate was washed with wash buffer and blocked with 300µl of block buffer (1% BSA & 0.05% NaN_3 in PBS). The block buffer was incubated for 2 hours at room temperature and then the wells were washed in preparation for the addition of standards and samples. For the dilution of samples and standards, a sample diluent concentrate was purchased from R&D systems, diluted 1:5 with dH_2O and labelled as IC diluent #4. To prepare the β-catenin standards, the β-catenin standard provided by the kit was first diluted to the highest standard concentration of 20,000pg/ml with IC diluent #4 concentrate. A range of β-catenin standards (313-20,000pg/ml) were then produced via serial dilution of the standard stock with IC diluent #4 in order to construct a standard curve. 100µl of each standard or sample was then added to wells in either duplicate or triplicate, the plate sealed with an adhesive strip, and then incubated for 2 hours at room temperature. Following incubation, the plate was washed, 100µl of detection antibody was added to each well, the plate re-sealed and incubated for a further 2 hours at room temperature. To prepare the detection antibody, reagent diluent concentrate 2 (provided by the kit) was diluted 1 in 10 with

dH_2O to make IC diluent #1 (1% BSA in PBS). The detection antibody was then diluted to a working concentration of 1µg/ml with IC diluent #1. Following incubation with the detection antibody, the plate was washed and 100µl of Streptavidin-HRP B (diluted 1:200 with IC diluent #1) added to each well, the plate wrapped in tin foil to protect the contents from the light, and incubated at room temperature for 20 minutes. The plate was then washed and 100µl of substrate solution (1:1 mixture of colour reagent A and colour reagent B prepared in a tube wrapped in tin foil) was added to each well, the plate was rewrapped in tin foil, and incubated at room temperature for 20 minutes. Finally, 50µl of stop solution was added to each well and the plate was gently tapped to ensure thorough mixing. The optical density of each well was then determined by reading the plate at 450nm using a microplate reader (BioTek MQX200 uQuant). Due to wavelength corrections not being available the optical density was also read at 540nm, with the latter readings being subtracted from the readings recorded at 450nm which corrects for any optical imperfections in the plate. To get the final optical density readings, the blank (IC diluent #4) was subtracted from each standard and sample reading. A standard curve was then created from the known standards and using linear regression the concentration of total (phosphorylated and unphosphorylated) β-catenin present in the experimental samples was extrapolated from the standard curve using GraphPad Prism 8.

2.6. Histology

2.6.1. Cryosectioning of ventricular tissue

Hearts were removed from the -80ºC freezer and placed in the cryotome (Shandon Cryotome FSE) where chamber, specimen and cryobar temperatures were set at -20ºC, -20ºC, and -50ºC, respectively. Before the heart tissue was embedded into the individual cryomoulds, the tissue was acclimatised to the chamber temperature for 30 minutes. After 30 minutes, a few drops of Optimal Cutting Temperature (OCT) medium were placed at the bottom of the cryomould and allowed to partially freeze before the heart was positioned with the ventricles touching the bottom of the mould as this was the side to be sectioned. Once the heart was secure, OCT medium was added until the tissue was completely covered avoiding the formation of air bubbles and allowed to fully set (approximately 1 minute). Transverse sections (6µm thickness) of the heart were cut and mounted onto glass slides, left to dry for 30 minutes, and then subsequently stored at -80ºC until histological staining commenced. Before staining, slides were removed from storage and left at room temperature for 5 minutes. To fix the tissue, slides were submerged in buffered zinc formalin for 15 minutes, then rinsed in running tap water for 5 minutes, air dried, and placed at 4ºC until stained.

2.6.2. Picrosirius Red Staining

Picrosirius red is a strong, linear anionic dye that under light microscopy stains collagen red and stains muscle fibres and cytoplasm yellow. Cardiac sections were stained manually using the protocol stated in Table 2.10. Once sections were stained, they were left to dry and a coverslip was mounted onto each slide using HistoMount mounting solution. Entire heart sections were imaged at a magnification of x25 using a Canon EOS 110D camera attached to a Leica DMIL microscope (Leica Biosystems, Newcastle, UK). Images were then relabelled by another lab user to enable blinded analysis and collagen deposition quantified using ImageJ software (as described in section 2.6.3.1.).

Table 2.10. Picrosirius Red staining protocol for staining collagen in cardiac tissue sections.

Step	Solution	Time
1	Distilled H_2O	5 seconds
2	Tap H_2O	5 minutes
3	Tap H_2O	5 minutes
4	Picrosirius Red	30 minutes
5	1% Acetic acid	3 minutes
6	1% Acetic acid	3 minutes
7	1% Acetic acid	3 minutes
8	100% Ethanol	3 minutes
9	100% Ethanol	3 minutes
10	100% Ethanol	3 minutes
11	Histoclear	3 minutes
12	Histoclear	3 minutes

2.6.2.1. Quantification of collagen deposition

To quantify collagen deposition in picrosirius stained tissues, blinded images were opened in ImageJ, and an outline of each heart section drawn freehand. The image was then converted to a HSB stack followed by adjustment of the threshold to highlight the stained collagen. The percentage area of collagen staining within the whole heart was then quantified by selecting 'area', 'area fraction', and 'limit to threshold' within the 'set measurements' feature in ImageJ and subsequently selecting 'measure'. Initial analysis involved thresholds of varying levels (3-6), however, once all of the blinded samples had been analysed the threshold levels were averaged, with a resultant mean threshold level of 5. The blinded images were then re-analysed with the threshold level being set to 5 for all images.

2.6.2.2. Measurement of left ventricular wall thickness

To measure left ventricular wall thickness, heart sections were cut and mounted as described in section 2.6.1. and stained and imaged as described in section 2.6.2. Left ventricular wall thickness was measured using ImageJ and measurements obtained in pixels converted to mm using a conversion factor calculated from the image of a haemocytometer taken at the same magnification. In brief, the image of the haemocytometer was opened in ImageJ, a line drawn along the bottom of the green box (see Figure 2.4.) and the length measured in pixels. The length of the line was 196.041 pixels which equates to the known length of the bottom of the green box i.e. 0.25mm. Once the conversion factor was calculated (i.e. 784.164pixels/mm), three measurements were taken for each image by drawing three lines from the septum to the edge of the left ventricular wall and these measurements converted to mm.

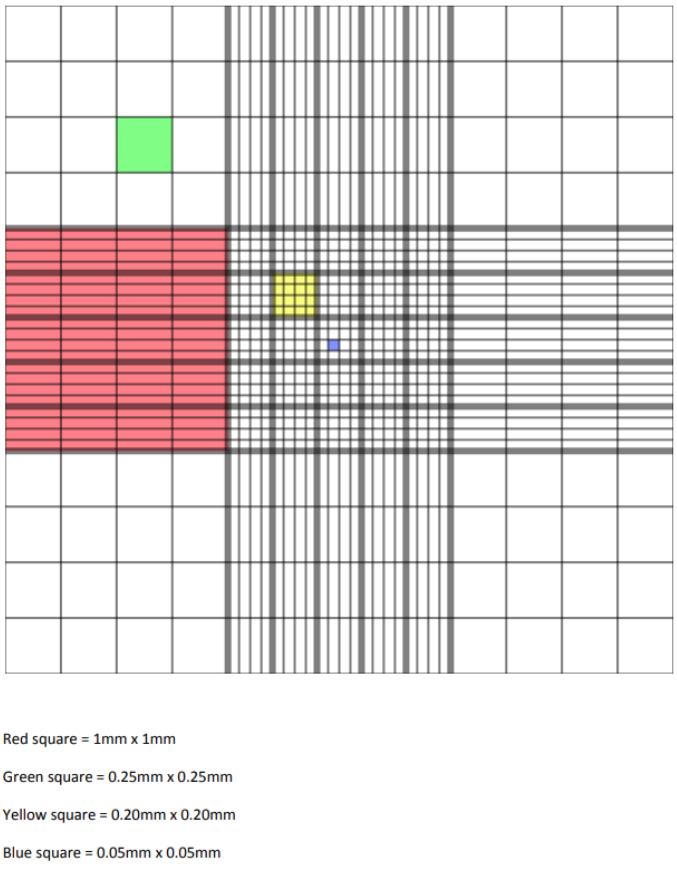

Figure 2.4. Haemocytometer with known areas used to convert pixels to mm in ImageJ to measure left ventricular wall size.

2.7. Statistical Analysis

All statistical analysis was conducted using GraphPad Prism 8 software and any differences between results were deemed significant when $P<0.05$. Data was plotted as mean ± standard error of the mean (SEM). In cell experiments, each n relates to cells from a single passage number, whereas in the animal experiments each n relates to an individual animal. The statistical test used for each set of data is detailed in its accompanying figure legend throughout the thesis. To test for normality within the data and to ensure values follow a Gaussian distribution, normality tests were conducted within GraphPad prior to further statistical analysis. Finally, individual data points were excluded if they were out with the mean ± (2x standard deviation).

Chapter 3: Optimisation of an *in vitro* model of cardiomyocyte hypertrophy

3.1. Introduction

3.1.1. Cardiac hypertrophy

One of the hallmark features associated with HFpEF is cardiac hypertrophy which involves numerous changes within cardiomyocytes including an increase in their size, increase in the number of sarcomeres, and enhanced protein synthesis (Frey *et al*. 2004). Cardiomyocytes commonly exit the cell cycle after birth resulting in the majority of cardiomyocytes being terminally differentiated in adults, therefore they do not proliferate under physiological conditions. However, recent research has suggested that the adult heart is capable of cardiomyocyte turnover initiated by cardiac stem cells/cardiac progenitor cells to replenish cardiomyocyte loss after injury (Le and Chong 2016). Cardiac tissue does exhibit plasticity which allows the heart to respond to environmental demands, resulting in cells either enlarging, shrinking, or entering apoptosis (Lazar *et al*. 2017). Initially cardiac hypertrophy acts as a compensatory mechanism in an attempt to try and normalise increased biochemical stress on the heart and improve cardiac pump function, however prolonged hypertrophy can lead to the development of HF due to impaired relaxation of the LV and an increase in metabolic demand. Cardiac hypertrophy can be split into two types known as physiological and pathological hypertrophy. Physiological hypertrophy is characterised by a 10-20% increase in cardiac mass and an increase in both the length and width of individual cardiomyocytes. The trigger for physiological hypertrophy is commonly normal postnatal growth, pregnancy, or exercise and contractile function is either preserved or increased with no evidence of interstitial fibrosis or cell death. Generally, physiological hypertrophy is reversible and will not progress to HF. On the other hand, pathological hypertrophy, initially induced as a compensatory mechanism with concentric growth of the ventricle, frequently progresses to ventricular chamber dilatation characterised by ventricular wall thinning due to the lengthening of cardiomyocytes and resultant contractile dysfunction. Interstitial and perivascular fibrosis are also commonly associated with pathological hypertrophy and are characterised by an increase in the expression of Col1 and myofibroblast activation (Nakamura and Sadoshima 2018).

3.1.2. Hypertrophic Agents

In *in vitro* experiments, agents such as ET-1 (Bupha-Intr *et al*. 2012; Archer *et al*. 2017), phenylephrine (Prasad *et al*. 2007; Peng *et al*. 2017) and AngII (Watkins *et al*. 2012; Chen *et al*. 2017) have all been shown to induce cardiomyocyte hypertrophy and there is also evidence that ET-1 and AngII are endogenous contributors to pathological cardiac hypertrophy *in vivo* (Huggins *et al*. 2003; Correa *et al*. 2014). ET-1 exerts its hypertrophic effects by binding to the endothelin A (ET_A) receptor (Hilal-Dundan and Brunton 2012), phenylephrine by binding to the

alpha 1 adrenoceptor (Papay *et al*. 2013), and AngII to the AT_1R (Kagiyama *et al*. 2002), all of which are coupled to the G_{q11} g protein. Binding to these receptors subsequently activates PLC which hydrolyses phosphatidylinositol 4,5-biphosphate to produce diacylglycerol (DAG) and inositol triphosphate (IP_3). DAG is a potent activator of PKC and is catalysed by diglycerol kinase (DGK). Research by Arimoto et al. (2006) has shown that cardiac specific overexpression of DGK prevents AngII induced cardiac hypertrophy in transgenic mice. IP_3 induces the release of intracellular Ca^{2+} from the sarcoplasmic and endoplasmic reticulum through IP_3 receptors, which then initiates the Ca^{2+}-calmodulin complex and CaN. Once the Ca^{2+}-calmodulin pathway is activated it also induces the activation of PKCα. PKCs are important enzymes that regulate cell growth and hypertrophy, as well as having an important role in signal transduction in the heart (reviewed by Singh *et al*. 2017). Multiple PKC isoforms are co-expressed in cardiomyocytes, however PKCα is of particular interest as a therapeutic target as research has indicated that its expression and/or activity increases in models of hypertrophy, HF and cardiac injury (Braz *et al*. 2002; Braz *et al*. 2004). There is increasing evidence indicating a link between PKC activation and cardiac hypertrophy (Bowling *et al*. 1999; Wang *et al*. 2003; Braz *et al*. 2004; Steinberg 2012); activation of PKCα has been shown to induce cardiomyocyte hypertrophy in cultured neonatal cardiomyocytes (Braz *et al*. 2002), while in a transgenic mouse model genetic deletion of PKCα protected mice against HF induced by pressure overload (Hambleton *et al*. 2007).

Activation of the RAAS is a central feature of HFpEF and thus is therapeutically targeted with ACE inhibitors and ARBs in an attempt to try to reverse cardiac hypertrophy. AngII, a peptide hormone and a key mediator of RAAS, influences the differentiation and proliferation of cells within the heart contributing to cardiomyocyte hypertrophy and cardiac fibrosis (Nehme *et al*. 2019). In particular, AngII has been shown to play a role in cardiovascular disease pathophysiology by enhancing inflammation, fibrosis, cardiomyocyte hypertrophy, and oxidative stress (Zablocki and Sadoshima 2013). AngII is routinely used in both cell models of cardiomyocyte hypertrophy (Prathapan *et al*. 2014; Wang *et al*. 2014a; Guan *et al*. 2017; Tian *et al*. 2018; Xu *et al*. 2019) and *in vivo* models of cardiac hypertrophy (Tsukamoto *et al*. 2013; Mathieu *et al*. 2018).

3.1.3. Hypertrophic Markers

Reactivation of the fetal gene programme occurs in cardiac hypertrophy and thus increases in the expression of these genes in the cardiomyocyte/heart are routinely used as positive indicators of hypertrophy in both *in vitro* and *in vivo* experimental models.

3.1.3.1. Myosin Heavy Chain 7 (Myh7)

Myosin filaments in the heart are composed of α and β subunits and can be used as biomarkers in cardiomyocyte hypertrophy. The Myh7 gene produces a protein known as beta myosin heavy chain (β-MHC) to form a larger protein myosin II that is involved in generating the mechanical force that is needed for muscle contraction. The expression of Myh7 is one of the most frequently affected in hypertrophic cardiomyopathy (Montag *et al*. 2018) and this gene has been shown to be expressed in the failing heart (Miyata *et al*. 2000). Research by Lopez et al. (2012) have also shown that protein expression of β-MHC increased significantly in the hearts of C57Bl/6J mice subjected to pressure overload. Furthermore, AngII has been shown to increase the Myh7 mRNA expression in both H9c2 cells (Gu *et al*. 2014) and neonatal rat ventricular myocytes (NRVMs; Pan *et al*. 2013; Wu *et al*. 2018).

3.1.3.2. Skeletal α-actin (ACTA1)

There are other non-myosin cytoskeletal proteins which are altered in cardiac hypertrophy and these include α-actin. ACTA1 and cardiac α actin are the main sarcomeric actin isoforms found in striated muscle, with increased ACTA1 expression being a well-known marker for cardiac hypertrophy (Driesen *et al*. 2009). In a rat model overexpressing AGT, the hearts of these animals were characterised by both high levels of AngII and increased expression of ACTA1. Moreover, in an *in vitro* model of cardiomyocyte hypertrophy AngII increased the expression of ACTA1 (Clement *et al*. 2001), while in a mouse model of pressure overload cardiac mRNA expression of ACTA1 was significantly increased (Wu *et al*. 2015). In a translational model of cardiomyocyte hypertrophy, the expression of ACTA1 was significantly increased in human induced pluripotent stem cell cardiomyocytes (hiPSC-CMs) treated with ET-1 (Aggarwal *et al*. 2014).

3.1.3.3. Natriuretic Peptides (NPs)

Another well-known marker belonging to the fetal gene programme are the NPs which are involved in the regulation of BP and fluid homeostasis. This family of peptides consists of ANP considered primarily a cardiac hormone, BNP produced by the heart as well as in the central nervous system, and C-type natriuretic peptide (CNP) located in both the central nervous system and vascular endothelium (Levin *et al*. 1998). ANP is produced mainly by atrial myocytes and is released when atrial wall tension increases. Ventricular myocytes also produce ANP although this production is mainly during prenatal development and declines as the heart matures, with a limited number of ventricular cells retaining the ability to produce ANP in the adult heart. The reactivation of fetal gene expression during cardiac hypertrophy is

controlled by both ubiquitous and cardiac-restricted transcriptions factor with GATA-4 in particular being responsible for controlling ANP expression in adult cardiac tissue (Kessler-Icekson *et al*. 2002). ANP protein expression has been shown to be upregulated in the hearts of mice after aortic banding (Li *et al*. 2017a), and ANP mRNA expression was shown to be elevated in the transverse aortic constriction (TAC) induced pressure overload mouse model of HF (De Jong *et al*. 2013; Jin *et al*. 2018). ANP has also been used extensively as a hypertrophic marker in H9c2 cell models treated with AngII (Yan *et al*. 2013; Wu *et al*. 2014; Zhou *et al*. 2014; Guan *et al*. 2017).

BNP was originally detected in the extracts of porcine brain and, while present in the human brain, is expressed at considerably higher levels in the ventricles of the heart (Chopra *et al*. 2013). BNP is initially synthesised as pre-proBNP, cleaved to proBNP, and then further cleaved to produce the biologically active BNP and the inactive NT-proBNP (Wettersten and Maisel 2016). In the human heart, both the expression (mRNA) and production of BNP protein is higher in atrial cardiomyocytes compared to ventricular cardiomyocytes, however a large amount of BNP secretion is expressed constitutively and, as the ventricles are larger, a greater proportion (60-80%) of plasma BNP originates from the ventricles (George and Struthers 2007). One of the main differences between BNP and ANP is that the former is not stored in the ventricles but is secreted into the peripheral circulation following production, whereas ANP protein can be stored within the atria (Nakagawa *et al*. 2019). Both BNP and NT-proBNP are established biomarkers for patients with various forms of HF including HFpEF (Nakagawa *et al*. 2019). BNP and NT-proBNP are more reliable biomarkers for clinical diagnosis due to their longer half-life (22 minutes and 70 minutes, respectively) when compared to ANP which only has a half-life of 2 minutes (Tanase *et al*. 2019).

The NPs exert their effects through receptors located on the surface of target cells. Three natriuretic peptide receptors known as Guanylyl cyclase-A (GC-A), Guanylyl cyclase-B (GC-B), and natriuretic peptide receptor 3 (NPR-C) have been identified in mammalian cells. Binding of NPs to either GC-A or GC-B receptors activates the cGMP-dependent signalling cascade which mediates many of their renal and cardiovascular effects (Nakagawa *et al*. 2019). Receptors GC-A and GC-B are structurally very similar and can bind ANP, BNP, and CNP, GC-A and NPR-C preferentially bind ANP, and CNP is the main ligand that binds to GC-B. The GC-A receptor is located mainly in large blood vessels along with a small portion of GC-B receptors, with the latter predominantly expressed in the brain (Pandy 2011). NPR-C is the receptor primarily responsible for the clearance of NPs from the circulation. Once peptides

are bound to NPR-C the receptor undergoes internalisation, the peptides are enzymatically degraded, and the receptor subsequently returned to the cell surface once degradation has occurred (receptor re-cycling). Throughout the development of HF NPs are released to induce a decrease in vascular tone and exert antifibrotic and antihypertrophic effects in the heart in an attempt to mitigate RAAS activation (Nishikimi *et al*. 2006); while initially successful, with time this compensatory mechanism fails and HF worsens (Lee and Daniels 2016).

3.1.4. Comparison of *in vitro* cardiomyocyte models

There are several cell models described in the literature that are used for cardiovascular research including NRVMs, adult mouse/rat ventricular cardiomyocytes (AMVM/ARVMs), mouse HL-1 cardiomyocytes, rat H9c2 cells, and both mouse and human induced pluripotent stem cell cardiomyocytes (miPSC-CMs and hiPSC-CMs). For each cell model there are advantages and disadvantages, and these should be considered in conjunction with the planned experimental endpoints when choosing a cell type. NRVMs are advantageous in that they beat in culture, a key phenotypic feature of cardiomyocytes and can be used for non-viral gene transfer. Neonatal cardiomyocytes are also easier to isolate than adult cardiomyocytes as cell harvesting does not require the difficult procedure of aortic cannulation and perfusion and they can be isolated by a simple two-step procedure consisting of enzyme digestion and mechanical agitation of ventricular tissue, followed by the purification of cells (Louch *et al*. 2011). However, these cells are phenotypically immature, do not proliferate and, from a 3Rs perspective where one of the main priorities is to reduce the number of animals used wherever possible, would use large numbers of rat neonates to obtain the required numbers of cells. Although there are some disadvantages to using NRVMs there are numerous cardiomyocyte hypertrophy studies using this cell type (Rusconi *et al*. 2013; Giguere *et al*. 2018; Zhao *et al*. 2018; Zhao *et al*. 2020). Primary cardiomyocytes isolated from the hearts of either adult rats or mice are routinely used for both short-term (same day) contractility and Ca^{2+} imaging studies (Guatimosim *et al*. 2011; Sprenger *et al*. 2016; Nollet *et al*. 2020) as they possess all of the contractile machinery and electrophysiological properties of mature cardiomyocytes. However, their utility in a wider range of studies is hampered by the fact that they are very challenging to isolate and cannot be cultured long-term for use in chronic intervention studies (reviewed by Peter *et al*. 2016). Notwithstanding this, both AMVMs (Sowah *et al*. 2014; Wu *et al*. 2017) and ARVMs (Huang *et al*. 2011; Fields *et al*. 2016; Gesmundo *et al*. 2017) have been used in a limited number of studies investigating cardiomyocyte hypertrophy.

HL-1 cardiomyocytes are a cardiac muscle cell line derived from the AT-1 mouse atrial cardiomyocyte tumour lineage (Claycomb *et al*. 1998). They are an immortalised homogenous cell line which are easily manipulated with rapid expansion. However, as they are derived from an atrial tumour lineage they do not recapitulate ventricular cells in culture, and in order to maintain a differentiated cardiac phenotype they need to be cultured with RA, norepinephrine, insulin, and essential lipids (White *et al*. 2004). The development of induced pluripotent stem cells (iPSCs) by Takahashi et al. in 2007 resulted in a novel field of medicine since the ability of hiPSCs and miPSCs to differentiate into many cell types has facilitated precise disease modelling, *in vitro* drug testing, and clinical regenerative medicine approaches (Machiraju and Greenway 2019). Both hiPSCs and miPSCs can be differentiated into cardiomyocytes with ventricular origin which can rapidly expand and contract spontaneously in culture. The limitation of these cells is that they are technically challenging and highly expensive with numerous protocols for differentiation (Peter *et al*. 2016). Cardiac hypertrophy can be induced *in vitro* by neurohormonal stimulation and physical stretching, with hiPSC-CMs having the ability to be genetically modified to mimic cardiac hypertrophy when differentiated into cardiomyocytes (Xie *et al*. 2019). Studies have used hiPSC-CMs to investigate cardiac hypertrophy (Ojala et al. 2014; Johansson *et al*. 2020), however due to them being highly expensive and non-proliferative other cells models are more often chosen. As previously stated, miPSCs can also be differentiated into cardiomyocytes (So *et al*. 2011; Fatima *et al*. 2016), however it appears from the literature that hiPSC-CMs are a more robust *in vitro* model for modelling cardiovascular diseases (Parrotta *et al*. 2020; Sacchetto *et al*. 2020).

3.1.5. H9c2 cells as a cardiomyocyte model

H9c2 rat embryonic ventricular myoblast cells (Kimes and Brandt 1976) are an immortalised, homogenous cell line that possess a proliferative capacity, can be easily manipulated (i.e. transfected) and, alongside NRVMs, are the most frequently used cell type in cardiomyocyte hypertrophy studies. A study by Watkins et al. (2011) directly compared H9c2 cells and primary neonatal rat cardiomyocytes following stimulation with hypertrophic agents (AngII and ET-1) and concluded that H9c2 cells displayed an almost identical hypertrophic response to those identified in the primary cardiomyocytes. While H9c2 cells are routinely used as *in vitro* models of cardiovascular cells in their undifferentiated/myoblast state, they can be differentiated into a more cardiomyocyte-like phenotype by culturing in medium containing low serum and RA, producing multinucleated cells with a low proliferative capacity (Fukushima *et al*. 2018; Liu *et al*. 2018; Qian *et al*. 2018; Iqbal *et al*. 2020). Further confirmation of successful differentiation of H9c2 cells has been determined via the detection of one or more cardiomyocyte specific markers (described in Table 3.1.) in these cells. While several studies have demonstrated

successful differentiation of H9c2 cells into 'cardiomyocyte-like' cells (Pereira *et al*. 2011; Kankeu *et al*. 2018), others have failed to do so (Patten *et al*. 2017), demonstrating the inconsistent nature of the differentiation process. Furthermore, while undifferentiated myoblast-type H9c2 cells have been routinely shown to respond to pro-hypertrophic agents, only a limited number of studies examining the response of differentiated H9c2 cells to pro-hypertrophic agents have been undertaken with some studies demonstrating successful induction of hypertrophy (Fukushima *et al*. 2018; Liu *et al*. 2018; Qian *et al*. 2018; Igbal *et al*. 2020), while others have resistance to hypertrophic stimuli (Zhou *et al*. 1995; Palm-Leis *et al*. 2004).

3.1.6. AngII treated H9c2 cells as a model of cardiomyocyte hypertrophy

Throughout the literature there are numerous reports of undifferentiated H9c2 cells being used as an *in vitro* model of cardiomyocyte hypertrophy, with all stipulating a range of different concentrations of the pro-hypertrophic AngII and incubation times. In particular, AngII concentrations used ranges from 0.1µM (Liu *et al*. 2015) to 10µM (Frank *et al*. 2007) with incubation times ranging from as little as 6 hours (Du *et al*. 2013) up to 96 hours (Flores-Munoz *et al*. 2011). Furthermore, there is also a lack of experimental information regarding whether serum is reintroduced to the media with the addition of AngII following serum starvation of H9c2 cells (Hernandez *et al*. 2014; Liu *et al*. 2015; Dong *et al*. 2017; Wu *et al*. 2020). The variation in methods throughout the literature illustrates the crucial importance of optimising the AngII induced model of cardiomyocyte hypertrophy in H9c2 cells for use in individual labs.

3.1.7. Aim

The principle aims of this study were to 1) examine the appropriateness of different cells types i.e. miPSC-CMs and H9c2 cells (undifferentiated compared with differentiated) for use as a model of cardiomyocytes by characterising their cardiomyocyte-like features, and 2) determine the optimum experimental conditions for the induction of cardiomyocyte hypertrophy with AngII.

Table 3.1. Cardiac specific markers shown to be present in mature cardiac cells.

Cardiac Marker	Description
Cardiac troponin T (cTnT) and Cardiac troponin I (cTnI)	Cardiac regulatory proteins which control the Ca^{2+} mediated effects between actin and myosin (Katrukha 2013).
Myosin light chain (Myl2)	A sarcomeric protein that belongs to the EF-hand Ca^{2+} binding protein superfamily that encodes three distinct genes in striated muscle. Myl2 plays an important role in embryonic heart muscle structure and function with phosphorylation of this gene regulating cardiac myosin cycling kinetics, torsion, and function (Sheikh *et al.* 2015).
Myosin heavy chain 6 (Myh6)	An isoform of myosin heavy chain which is predominantly expressed in cardiac atria. It is a major protein that makes up the cardiac muscle thick filament and functions in cardiac muscle contraction (England and Loughna 2013).
Nkx2.5	Encodes a homeobox-containing transcription factor which is involved in commitment to and/or differentiation of the myocardial lineage (Lien *et al*. 1999).

3.2. Methods

All necessary methodological detail is either described in section 3.3 Experimental Protocols, or in Chapter 2 as indicated.

3.3. Experimental Protocols

3.3.1. Investigation of the effect of culture duration on the expression of fetal genes (ANP and BNP) in miPSC-CMs

The objective of investigating different culture periods of miPSC-CMs was to identify a time point at which fetal gene expression in these cells was similar to that present in an adult mouse heart, thus indicating maturation. Ivashchenko et al. (2013), who investigated hiPSC-CM maturation, found that expression levels of ANP and BNP were high at 37 days of culture then decreased as duration in culture increased. Therefore, culture duration was investigated in miPSC-CMs to identify if fetal gene expression was similarly altered with culture duration. miPSC-CMs (Cor.At® cells; NCardia; Germany) are non-proliferative cells derived from fibroblasts (taken from the tail tip of an adult mouse) reprogrammed to produce iPSCs, which are subsequently differentiated into cardiomyocytes. miPSC-CMs were seeded at a density of approximately 175,000 cells per well in a gelatin (0.1% w/v, made up in Dulbecco's phosphate buffer solution (DPBS) with Ca^{2+} and Mg^{2+}) coated 24 well plate and cultured in Cor.At® complete culture media (supplied by Ncardia) in a humidified atmosphere at 37ºC with 5% CO_2. Cor.At® media containing puromycin (used as a selecting agent) was added for the first 24 hours of culture then replaced with Cor.At® media without puromycin and media was changed every 48 hours thereafter. Cells were cultured for 3, 7 and 14 days to investigate at which point fetal gene expression was similar to that of an adult mouse heart. The cardiac tissue used for comparison was obtained from five 12-week-old male C57Bl/6J mice killed via CO_2 asphyxiation and cervical dislocation and RNA extracted as described in Chapter 2, section 2.3.1. At the end of the different culture periods, media was removed from the wells and the cells were washed with 1ml of PBS twice. To lyse the cells, 100µl of Tri-reagent was added to each well and cells lifted using a cell scraper. The cell solution was then transferred to a RNase/DNase free microcentrifuge tube and RNA extracted as described in Chapter 2, section 2.3.1. Once miPSC-CM RNA was isolated, cDNA was prepared as described in Chapter 2, section 2.3.3. Mouse ANP and BNP QuantiTect primers (purchased from Qiagen, Manchester, UK) were optimised and validated as per Chapter 2, section 2.3.5.1. To quantify fetal gene expression in the cells, qPCR was used as described in Chapter 2, section 2.3.5. To measure changes in gene expression between the culture periods, the relative abundance

of the genes of interest (ANP and BNP) to the housekeeping gene Gapdh, were expressed using the following equation (Ang *et al*. 2017):

Equation 10: $\Delta Ct = Ct_{GOI} - Ct_{HKG}$

After normalisation of the target gene, the Ct value for the control sample is deducted from the test sample resulting in ΔΔCt shown in the equation below:

Equation 11: $\Delta\Delta Ct = Ct_{\text{Treated sample}} - Ct_{\text{Untreated Sample}}$

The resulting ΔΔCt is then used in the final calculation detailed below:

Equation 12: **Fold expression relative to control sample = $2^{-\Delta\Delta Ct}$**

3.3.2. Differentiation of H9c2 cells from a myoblast to a cardiomyocyte phenotype

H9c2 cells are myoblasts (the undifferentiated precursor to myocytes) which can be differentiated into either skeletal muscle cells or cardiomyocytes. Previous work has shown that H9c2 cells can be differentiated into either skeletal muscle cells by reducing the serum (FBS) content of the growth media (DMEM) from 10% to 1% (di Giacomo *et al*. 2010; Masilamani *et al*. 2014,) or into cardiomyocytes via the addition of RA to DMEM with 1% FBS (Branco *et al*. 2015; Suhaeri *et al*. 2015; Patten *et al*. 2017). Differentiating the cells changes their phenotype, switching them to a multinucleated, microtubular shape with a reduced proliferative capacity. Undifferentiated (myoblast) H9c2 cells were cultured in DMEM with 10% FBS as described in Chapter 2, section 2.2.1. For differentiation experiments, H9c2 cells were seeded at a density of 250,000 cells in T25 flasks and cultured overnight to allow attachment. Media was then removed from the T25 flasks and replaced with DMEM supplemented with 1% FBS (differentiation media) with either 0.1% DMSO (vehicle control) or RA (100nM or 1μM). RA was first diluted in DMSO then further diluted in DMEM (1% FBS) with all dilutions prepared in the dark as RA is light sensitive. H9c2 cells were then cultured in differentiation media for 5 days, which was replaced either on day 3 (differentiation media plus 0.1% DMSO) or daily (differentiation media plus RA). At the end of the differentiation protocol, the media was removed from the T25 flasks and the cells were washed with 4ml HBSS. To lift the cells, 2ml of Trypsin 0.25% was added to the flask and once the cells had detached they were transferred to a clean 15ml centrifuge tube. The flasks were then rinsed with 4ml of DMEM (1% FBS) and transferred to the appropriate centrifuge tube and centrifuged for 5 minutes at 200xg. The supernatant was poured off and the cells were resuspended in 1ml Tri-reagent and transferred to RNase/DNase free microcentrifuge tubes. RNA was extracted from the cells (undifferentiated and differentiated H9c2 cells), converted to cDNA, PCR performed for the

detection of a number of cardiac specific markers (Table 3.2.) and PCR products detected via gel electrophoresis as described in Chapter 2 sections 2.3.1 to 2.3.4. For comparison, the expression of cardiac specific markers in both rat ventricular and atrial tissue obtained from one male (12 weeks old) Sprague Dawley rat (killed via CO_2 asphyxiation and cervical dislocation) was also examined (see Chapter 2, sections 2.3.1. to 2.3.4.).

Table 3.2. Product sizes of fetal genes and cardiac specific markers examined in both H9c2 cells and rat cardiac tissue purchased from Qiagen.

Cardiac Specific Marker	Catalogue Number	Product Size
ANP	QT00366170	107bp
BNP	QT00183225	94bp
Gapdh	QT00199633	149bp
Cardiac troponin T (cTnT)	QT01081332	65bp
Cardiac troponin I (cTnI)	QT00192717	81bp
Myosin light chain (Myl2)	QT00405804	386bp
Myosin heavy chain 6 (Myh6)	QT00190267	127bp
Nkx2.5	QT00180859	113bp

3.3.3. Induction of hypertrophy in differentiated H9c2 cells

H9c2 cells were differentiated as per section 3.3.2, then serum starved for 24 hours before 1µM AngII was added in serum free media for 48 hours. Cells were lifted as described in Chapter 2, section 2.2.1.4 and RNA was extracted (Chapter 2, section 2.3.1), then converted to cDNA (Chapter 2, section 2.3.3). To measure the expression of fetal genes (ANP and BNP, primer information indicated in Table 3.2) qPCR was conducted as per Chapter 2, section 2.3.5. To calculate the effect of treatments on gene expression the mathematical model of relative expression ratio described in Chapter 2, section 2.3.5.2. was used.

3.3.4. Assessment of the potential cytotoxicity of AngII in undifferentiated H9c2 cells

Previous research has indicated that AngII ranging from 100nM to 1µM can decrease the viability of H9c2 cells (Yong *et al.* 2016; Wang *et al.* 2018), therefore a 3-[4,5-dimethylthiazol-2-yl]-2,5-diphenyl-tetrazolium bromide (MTT) assay was used to determine whether AngII altered cell viability over the concentration range tested (10nM – 10µM). The MTT assay is a colorimetric assay which measures cell metabolic activity (Riss *et al.* 2004). H9c2 cells were plated in a 96 well plate at a seeding density of 10,000 cells per well and left overnight to

attach. The media was removed from each well and replaced with 100µl of serum free DMEM for 24 hours to induce cell-cycle synchronisation. After the cells were serum starved for 24 hours they were treated with AngII for increasing periods of time (4hrs to 72hrs) with concentrations ranging from (0nM to 10µM). To prepare the MTT (1mg/ml) solution 10mg of MTT was diluted in 10ml of DMEM (10% FBS), vortexed then filtered using a 0.22µM filter, and covered in tin foil to protect from light. After the desired incubation time with AngII, the media was removed from the wells and 100µl of sterile filtered MTT solution was added to each well. The plate was then covered in tin foil and placed in the incubator at 37°C for 4 hours. After 4 hours, the MTT solution was removed from each well and 200µl of DMSO was added. The plate was then re-covered in tin foil and placed on a plate shaker for 20 minutes at room temperature. The absorbance of the wells was then measured at 560nm using a microplate reader (BioTek MQX200 uQuant). To determine whether AngII altered cell viability the mean absorbance values for cells treated with AngII were expressed as % absorbance of control cells (cells that were treated with vehicle), with the control value equating to 100% cell viability.

3.3.5. Determining the optimum seeding density of undifferentiated H9c2 cells for subsequent hypertrophy studies

Guidance from the European Collection of Authenticated Cell Cultures (ECACC) website recommends growing H9c2 cells to 70-80% confluency, as myotubes are formed at higher levels of confluence, thus changing the phenotype of the cells. Therefore, a series of experiments were carried out to determine the optimum seeding density to avoid H9c2 cells becoming too confluent (i.e. optimum confluence is 60-70% by visual estimation) over the proposed treatment period (4-72 hours) to be used in subsequent experiments investigating AngII induced hypertrophy, and to also ensure sufficient RNA yields (above 20ng/µl) that could be used in qPCR studies. To investigate optimum seeding density in T25 flasks H9c2 cells were seeded at 100,000, 200,000 and 300,000 cells in 4ml of DMEM (10% FBS) and left overnight to attach. To mirror the planned hypertrophy induction protocol all flasks were serum starved for 24 hours and then PBS added (in place of AngII) for varying treatment durations (4, 24, 48, and 72 hours). At each time point, the degree of confluency of each of the flasks was recorded, the cells harvested (see Chapter 2, section 2.2.1.4.) and RNA extracted and the concentration recorded (see Chapter 2, section 2.3.1.).

3.3.6. Investigation into the impact of the duration of AngII treatment on the expression of fetal genes in undifferentiated H9c2 cells

The effects of increasing treatment times with AngII on fetal gene (ANP and Myh7; primer sequence shown in Table 3.3.) expression was investigated in undifferentiated H9c2 cells to determine the optimum treatment time. H9c2 cells were seeded at a density of 150,000 cells in T25 flasks with 4ml in DMEM (10% FBS) and left overnight to attach. The following day, the media was removed and 4ml of serum free DMEM was added for 24 hours. The media was then removed, replaced with fresh serum free DMEM containing 1µM of AngII, and the flasks incubated for 4, 12, 24, and 48 hours, with PBS being added to control flasks. At the end of each treatment cells were harvested (see Chapter 2, section 2.2.1.4.), RNA extracted (see Chapter 2, section 2.3.1.), and quantitative reverse transcription-polymerase chain reaction (qRT-PCR) to determine fetal gene expression conducted (see Chapter 2, sections 2.3.3. and 2.3.5.). To calculate the effect of treatments on gene expression the mathematical model of relative expression ratio described in Chapter 2, section 2.3.5.2. was used.

Table 3.3. Primer sequences for use in qPCR pre-designed and purchased from Sigma Aldrich.

Gene	Ref Sequence	Forward 5'-3'	Reverse 5'-3'	Amplicon Length
Myh7	NM_017240.2	GGAGAAAGAGAAGAGCGAGTTC	GGCACATCTTCTCCAGGTTAG	97bp

3.3.7. Determination of the optimum serum concentration in the cell media for the induction of hypertrophy in undifferentiated H9c2 cells

To determine whether the amount of serum in cell media affects AngII induced changes in fetal gene (ANP and BNP) expression in cells, different serum concentrations were investigated. Undifferentiated H9c2 cells were seeded at a density of 150,000 cells in T25 flasks with 4ml of DMEM (10% FBS) and left overnight to attach. The following day, the cells were serum starved with 4ml of serum free DMEM for 24 hours. Once the cells had been serum starved either PBS (control) or 1µM AngII was added in DMEM with FBS concentrations of 1, 5, and 10% to the T25 flasks. Two different treatment times (24 and 48 hours) were also tested to determine if duration of treatment influenced AngII induced changes in fetal gene expression within the varying concentrations of FBS. At the end of each treatment, cells were harvested (see Chapter 2, section 2.2.1.4.), RNA extracted (see Chapter 2, section 2.3.1.), and qRT-PCR to determine fetal expression conducted (see Chapter 2, sections 2.3.3. to 2.3.5.). To calculate

the effect of treatments on gene expression the mathematical model of relative expression ratio described in Chapter 2, section 2.3.5.2. was used.

3.3.8. Statistical Analysis

All statistical analysis was conducted using GraphPad Prism 8 software and any differences between results were deemed significant when $P<0.05$. Data was plotted as mean ± SEM. In cell experiments, each n relates to cells from a single passage number. The statistical test used for each set of data is detailed in its accompanying figure legend throughout this chapter. Individual data points were excluded if they were out with the mean ± (2x standard deviation).

3.4. Results

3.4.1. The effect of culture period duration on the expression of fetal genes ANP and BNP in miPSC-CMs

To measure the expression of fetal genes over the different culture periods, qRT-PCR was used. To assess primer efficiency, average Ct values were calculated for a series of cDNA concentrations and a semi-logarithmic analysis plot was created using linear regression for each primer. Gradients between -3.1 and -3.6 and an R^2 value of ≥0.98 indicate a primer efficiency between 90-110%, which was the range considered acceptable for subsequent studies examining gene expression. The primers for both ANP and Gapdh had gradients between -3.1 and -3.6 (Figure 3.1A. & 3.1C.) with BNP being slightly out with the range with a gradient of -3.69 (Figure 3.1B.), however the latter still had a R^2 value of 0.9942. ANP and Gapdh primers had percentage efficiencies of 93% and 90%, respectively, while the BNP primer had a slightly lower efficiency of 86.6%. All three primers were deemed to have acceptable efficiency for subsequent use. The purpose of investigating different culture periods was to identify the time point at which the level of fetal gene expression in the miPSC-CMs was comparable to that in an adult mouse heart, as the former are immature/fetal-like cells. The level of expression of ANP in miPSC-CMs was significantly lower than that of an adult mouse heart following 3 and 7 days of culture (10±1 (3 days) and 56±14 (7 days) vs. 100±9 (adult mouse heart) relative expression (arbitrary units; AU); both $P<0.05$; Figure 3.2A.). However, prolonging the culture period to 14 days resulted in an increase in the level of ANP expression in miPSC-CMs similar to that observed in the adult mouse heart (Figure 3.2A.). BNP expression was approximately three-fold lower than that of ANP in both the mouse heart and miPSC-CMs following 3, 7, and 14 days of culture (4±1 (3 days), 2±0.6 (7 days) and 1±0.4 (14 days) vs. 26±8 (adult mouse heart) relative expression (AU; Figure 3.2A. & 3.2B.). In

contrast to ANP, BNP expression appeared to decrease with increasing culture duration and remained lower than that observed in the adult mouse heart throughout (P<0.05 at all time points; Figure 3.2B.). Although the expression of both ANP and BNP in miPSC-CMs at 3 days was lower than that in the mouse heart (Figure 3.2A. & 3.2B.), the ratio of the expression of ANP to BNP (3±0.5 (3 days), 28±7 (7 days) and 82±22 (14 days) measured in AU was most similar to that of the adult mouse heart (4±1) after 3 days in culture (Figure 3.2C.). However, due to the limitations associated with the use of miPSC-CMs described in the section 3.5.1. of the discussion, all subsequent studies investigating cardiomyocyte hypertrophy were conducted using rat H9c2 myoblast cells.

3.4.2. Examination of cardiac specific markers in differentiated and undifferentiated H9c2 cells

Following differentiation H9c2 cells change from a rhomboid shape in undifferentiated state (Figure 3.3A.) to a more spindle-like shape (Figure 3.3B.). To examine if there were differences between the expression of specific cardiac markers in differentiated and undifferentiated H9c2 cells, reverse transcription-polymerase chain reaction (RT-PCR) was performed using five specific cardiac markers. All cardiac markers (cTnT, cTnI, Nkx2.5, Myl2 and Myh6) tested were expressed in both rat atrial and ventricular tissue (Figures 3.4. – 3.8.). Undifferentiated H9c2 cells (i.e. H9c2 cells cultured in 10% FBS) expressed cTnT (Figure 3.4A.), cTnI (Figure 3.5A.), and Nkx.2.5 (Figure 3.6A.). In contrast, only faint bands for Myl2 were detected in 1 sample of an n=3 of undifferentiated H9c2 cells (Figure 3.7A.) and these bands were undetectable following a repeat gel electrophoresis experiment (gel not shown). Differentiated H9c2 cells (i.e. H9c2 cells cultured in 1% FBS) expressed cTnT (Figure 3.4A. & 3.4B.), cTnI (Figure 3.5A. & 3.5B.), Nkx2.5 (Figure 3.6A. & 3.6B.), and Myl2 (Figure 3.7A. & 3.7B.), and the inclusion of RA in the low serum culture media did not appear to have any influence on the expression of these cardiac markers. Myh6 was present in both rat atrial and ventricular tissue but was not detected in H9c2 cells under any of the culture conditions tested (Figure 3.8.). Table 3.4. summarises the expression of cardiac markers in both undifferentiated and differentiated H9c2 cells and rat cardiac (atrial and ventricular) tissue.

A

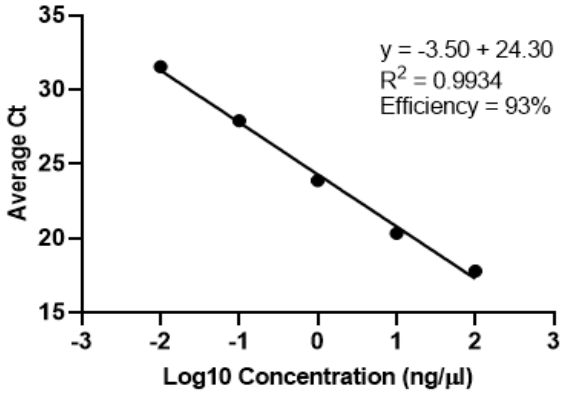

B

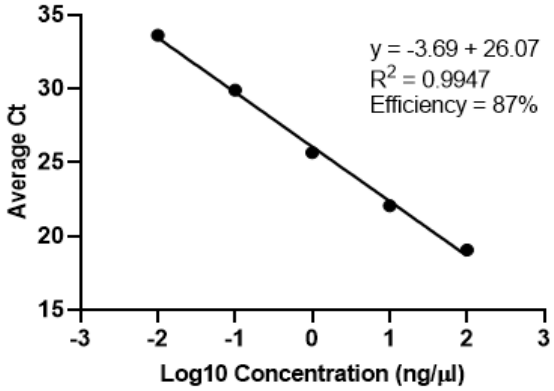

C

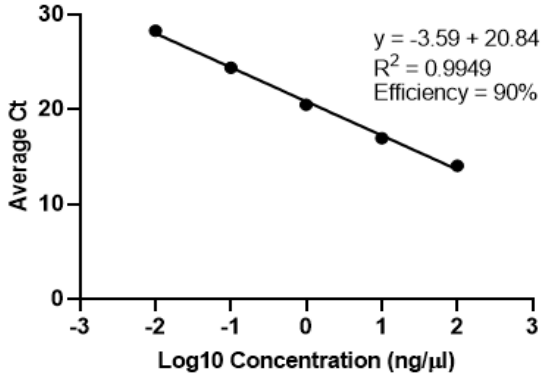

Figure 3.1. Standard curve of average Ct vs. Log10 cDNA concentration for the validation of mouse primers ANP (A), BNP (B), and Gapdh (C).

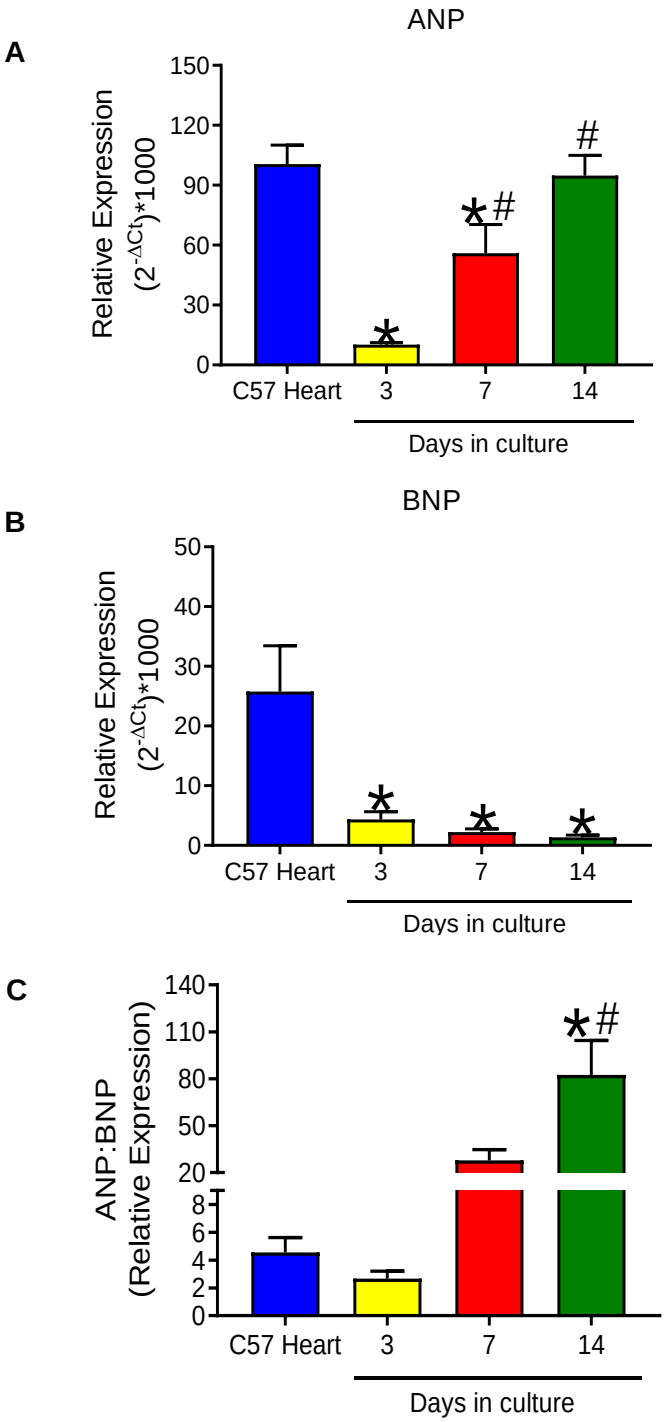

Figure 3.2. Time course of fetal gene expression in miPSC-CMs. Relative gene expression of both ANP (A) and BNP (B) and ANP:BNP ratio (C) in C57Bl/6J mouse ventricular tissue (n=5) and miPSC-CMs (n=3; RNA was extracted from cells from three separate vials of cells and the qRT-PCR experiment ran on three separate occasions) cultured for different durations. Data is expressed as mean ± SEM and analysed using a one way ANOVA test with a Dunnett's post hoc test. **P*<0.05 vs. C57 heart; #*P*<0.05 vs. 3 days.

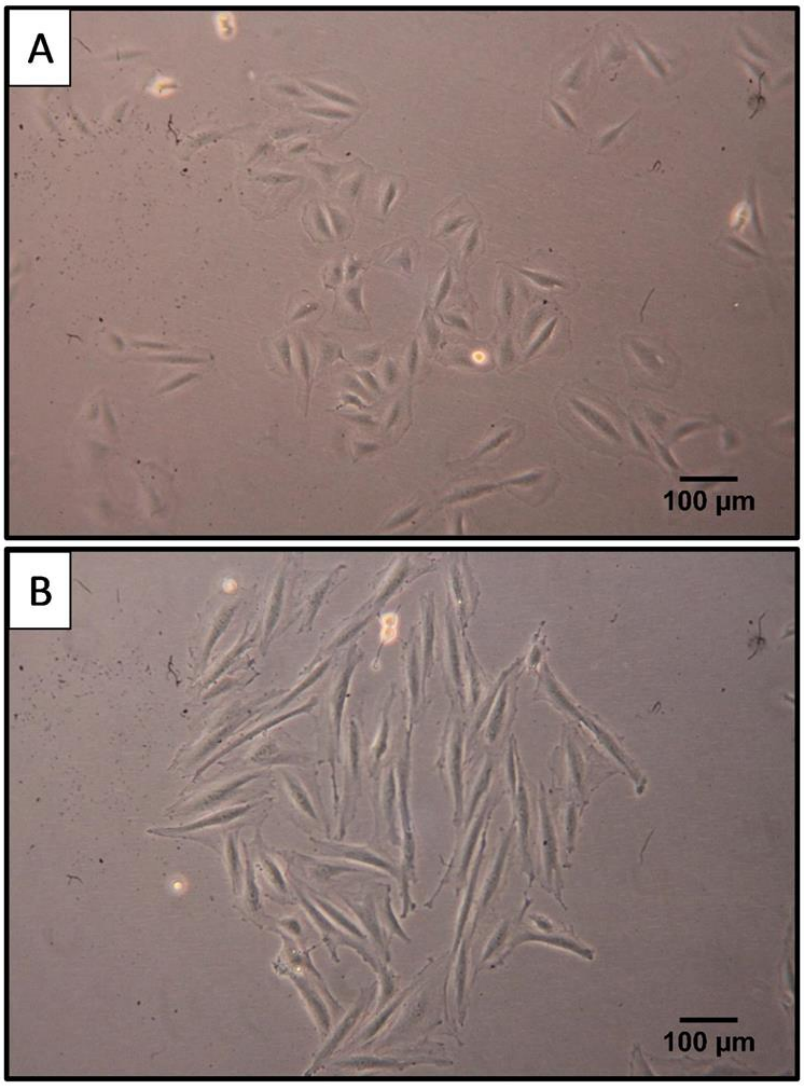

Figure 3.3. Photomicrographs illustrating the morphological changes associated with the differentiation of H9c2 cells following the reduction of serum concentration of media (from 10% to 1% FBS). Undifferentiated H9c2 cells cultured in DMEM with 10% FBS are rhomboid in shape and possess a proliferative capacity (A). In contrast, differentiated H9c2 cells (i.e. those cultured in DMEM low serum (1% FBS) media) are spindle shaped and possess limited proliferative ability (B). Images were taken at x100 magnification.Scale bar = 50µm.

A

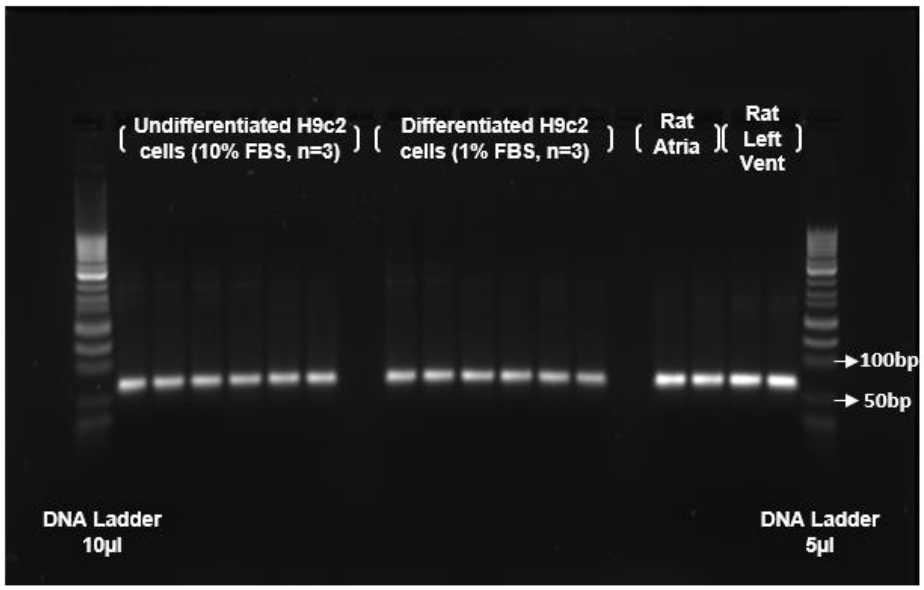

B

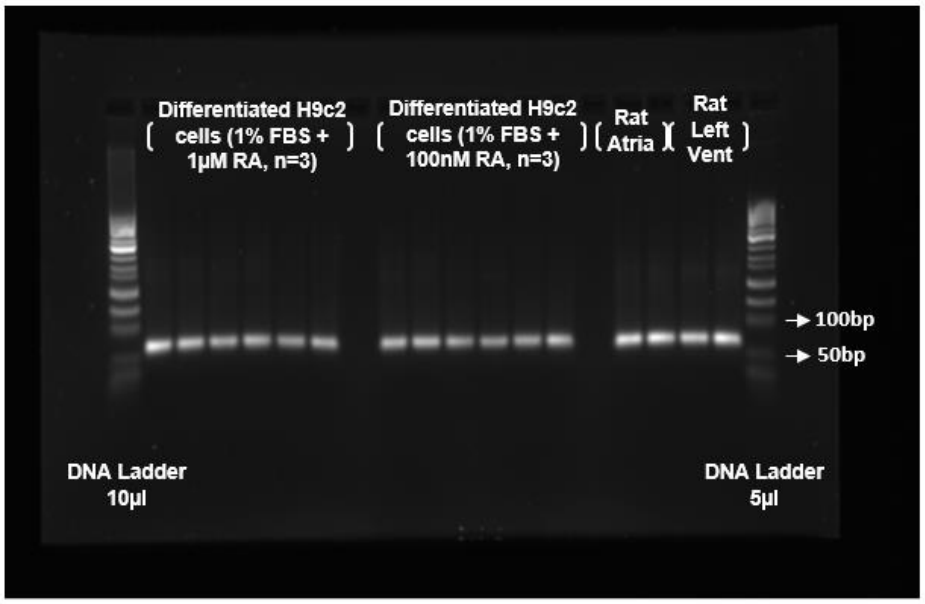

Figure 3.4. mRNA expression of the cardiac specific marker cardiac troponin T (cTnT) in H9c2 cells and rat cardiac tissue. cTnT (product size 65bp) was expressed in both undifferentiated H9c2 cells and differentiated H9c2 cells with (A) or without RA (B). Rat atrial and ventricular tissue both highly expressed cTnT (A & B). n=3 with each sample ran in duplicate. Rat atrial and ventricular tissue both highly expressed cTnT (A & B). n=1 with each sample ran in duplicate.

A

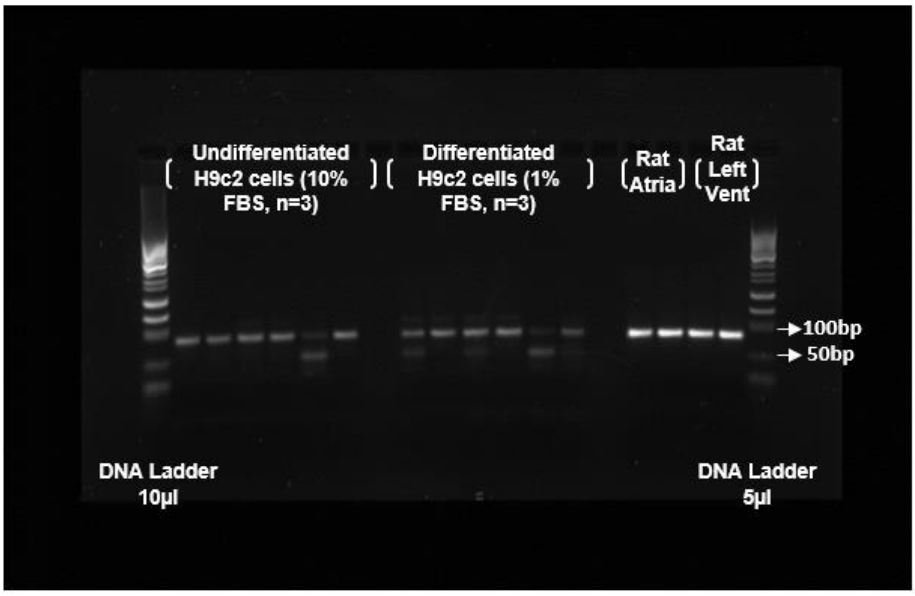

B

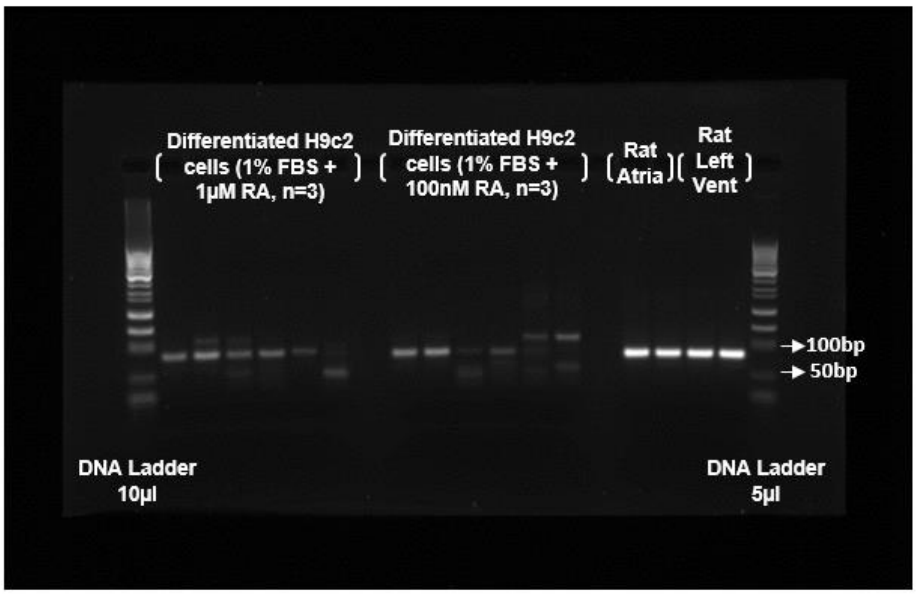

Figure 3.5. mRNA expression of the cardiac specific marker cardiac troponin I (cTnI) in H9c2 cells and rat cardiac tissue. cTnI (product size 81bp) is highly expressed in both rat ventricular tissue and in rat atria (A & B). In H9c2 cells, cTnI is expressed in all cells cultured in media containing either 1% or 10% FBS (A & B) and does not appear to be influenced by the inclusion of RA (B). n=3 with each sample ran in duplicate. Rat atrial and ventricular tissue both highly expressed cTnI (A & B). n=1 with each sample ran in duplicate.

A

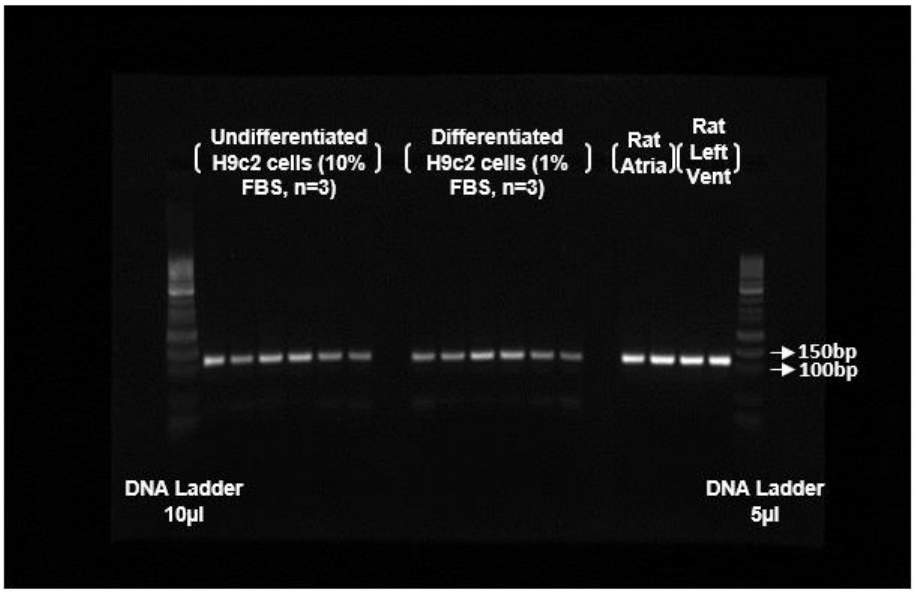

B

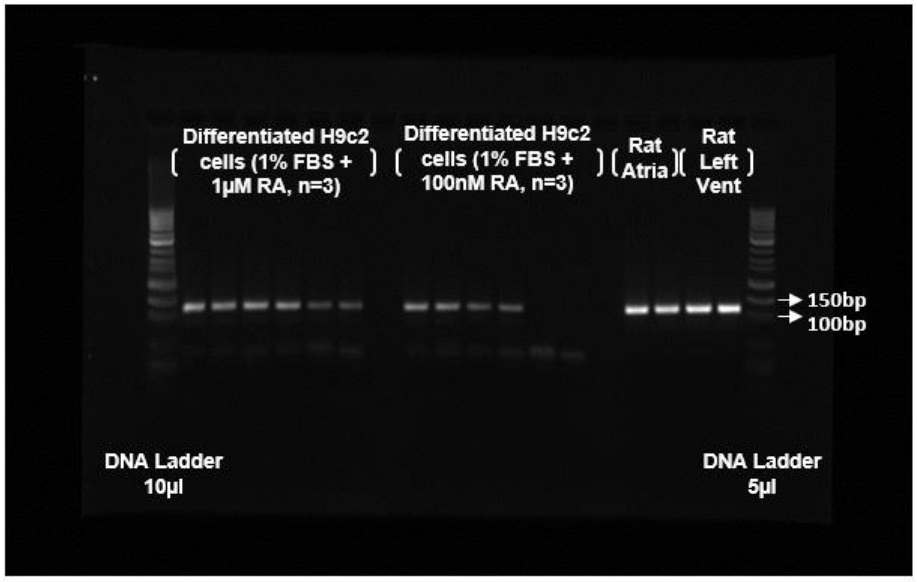

Figure 3.6. mRNA expression of the cardiac specific marker Nkx2.5 in H9c2 cells and rat cardiac tissue. Nkx2.5 (product size 113bp) is highly expressed in both rat ventricular tissue and in rat atria (A & B). In H9c2 cells, Nkx2.5 is expressed in all cells cultured in media containing either 1% or 10 % FBS (A & B) and does not appear to be influenced by the inclusion of RA (B). n=3 with each sample ran in duplicate. Rat atrial and ventricular tissue both highly expressed NKx2.5 (A & B). n=1 with each sample ran in duplicate.

A

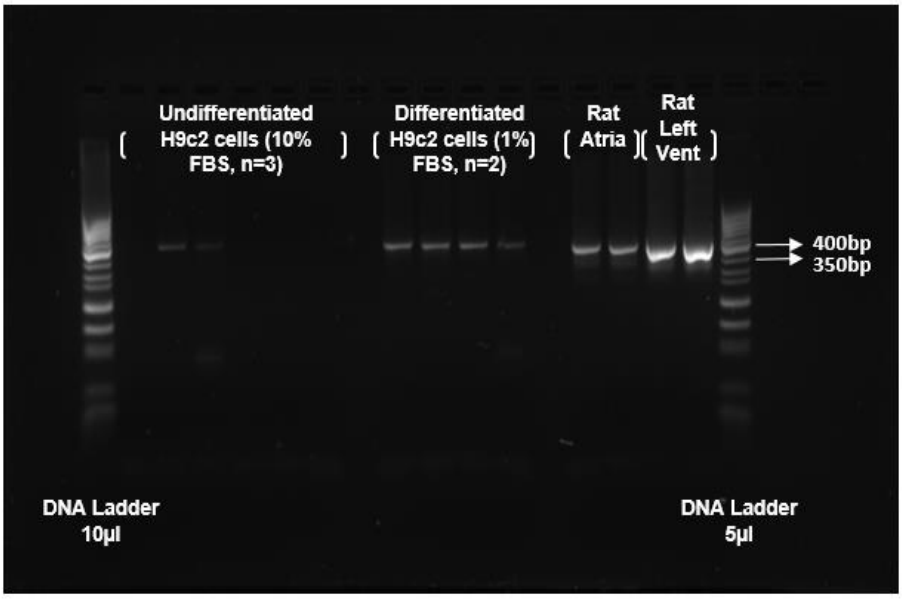

B

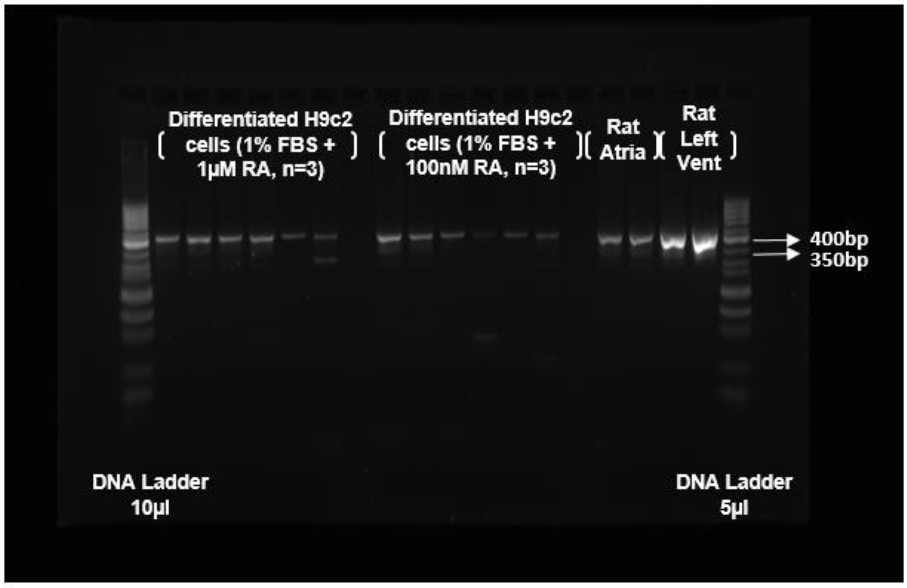

Figure 3.7. mRNA expression of the cardiac specific marker myosin light chain 2 (Myl2) in H9c2 cells and rat cardiac tissue. Myl2 (product size 386bp) is highly expressed in rat ventricular tissue and to a lesser extent in rat atria (A & B). In H9c2 cells, Myl2 appears to be most absent in undifferentiated cells but is expressed in all cells cultured in media containing 1% FBS (A & B) and does not appear to be influenced by the inclusion of RA (B). n=2-3 with each sample ran in duplicate. Rat atrial and ventricular tissue both highly expressed Myl2 (A & B). n=1 with each sample ran in duplicate.

A

B

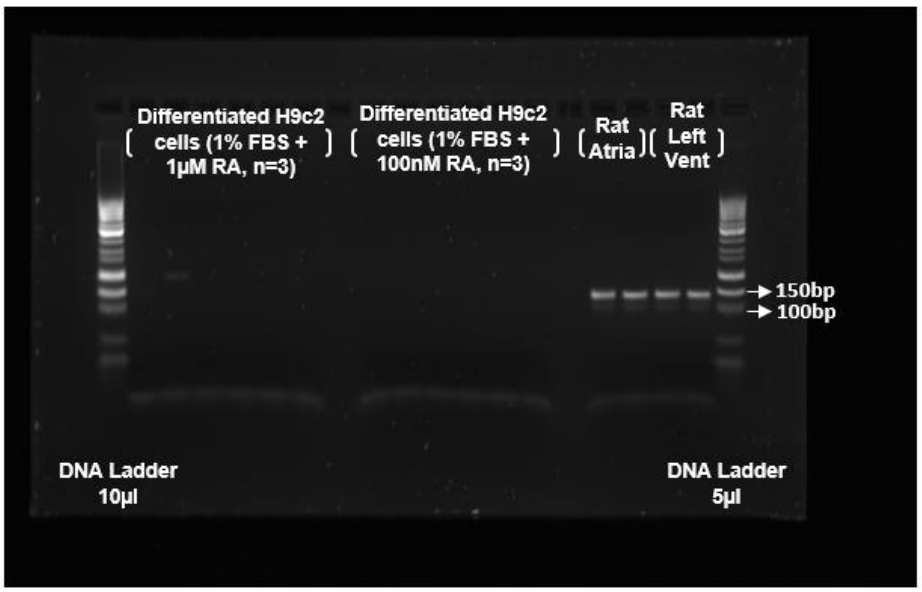

Figure 3.8. mRNA expression of the cardiac specific marker myosin heavy chain 6 (Myh6) in H9c2 cells and rat cardiac tissue. Myh6 (product size 127bp) was not detectable in H9c2 cell and but was highly expressed in both rat atrial and ventricular tissue (A & B). n=1 with each sample ran in duplicate.

Table 3.4. Summary of cardiac markers expressed in undifferentiated and differentiated H9c2 cells, as well as atrial and ventricular tissue from a Sprague Dawley rat. ✓ refers to present and x refers to absent. Values refer to the number of samples expressing the marker out of the total n number tested.

	cTnT	cTnI	Myl2	Myh6	Nkx2.5
H9c2 cells in 10% FBS	✓ 3/3	✓ 3/3	✓ 1/3	x 0/3	✓ 3/3
H9c2 cells in 1% FBS	✓ 3/3	✓ 3/3	✓ 2/2	x 0/3	✓ 3/3
H9c2 cells in 1% FBS + 100nM RA	✓ 3/3	✓ 2/3	✓ 3/3	x 0/3	✓ 2/3
H9c2 cells in 1% FBS + 1µM RA	✓ 3/3	✓ 3/3	✓ 3/3	x 0/3	✓ 3/3
Rat ventricular tissue	✓ 1/1	✓ 1/1	✓ 1/1	✓ 1/1	✓ 1/1
Rat atrial tissue	✓ 1/1	✓ 1/1	✓ 1/1	✓ 1/1	✓ 1/1

3.4.3. Impact of AngII on the expression of fetal genes in differentiated H9c2 cells

The ability of AngII (1µM; 48-hour incubation) to induce hypertrophy (indicated by an upregulation of ANP and/or BNP) in differentiated H9c2 cells was examined via qRT-PCR. Primer efficiencies were previously calculated for ANP (101.8%) and BNP (102.3%). Treatment with AngII did not induce a statistically significant increase in either ANP or BNP expression in H9c2 cells differentiated in low serum (1% FBS) alone (skeletal myocyte-like cells) (Figure 3.9A. & 3.9B.). Furthermore, treatment of H9c2 cells differentiated in low serum containing RA (cardiomyocyte-like cells) with AngII did not alter the expression of either ANP or BNP in comparison to controls (Figure 3.9A. & 3.9B.).

3.4.4. Investigation into the potential cytotoxicity of AngII in undifferentiated H9c2 cells

A series of cell viability (MTT assay) experiments were carried out to determine if suggested pro-hypertrophic concentrations of AngII were cytotoxic in undifferentiated H9c2 cells. Concentrations of AngII ranging from 10nm up to 10µM were tested over 4, 24, 48, and 72 hours. None of the concentrations of AngII tested significantly altered cell viability over the 4 to 72 hour treatment period, indicating that over this concentration range AngII is not cytotoxic in H9c2 cells (Figure 3.10.).

3.4.5. Optimum seeding density of undifferentiated H9c2 cells for subsequent hypertrophy studies

Seeding densities of H9c2 cells were investigated to ensure that flasks did not become too confluent (>70%) during the hypertrophy induction protocol but still yielded sufficient RNA (above 20ng/µl) for further downstream experiments. Seeding densities ranging from 100,000 cells to 300,000 cells per T25 flask were chosen to investigate over four time periods (4, 24, 48, and 72 hours). At a seeding density of 100,000 cells, H9c2 cells cultured up to 48 hours produced RNA yields that were too low for subsequent qRT-PCR experiments, however cells cultured for 72 hours provided sufficient RNA (Table 3.5.) and at no time point did the flasks become too confluent (Table 3.6.). A seeding density of 200,000 cells produced sufficient RNA yield for downstream experiments and did not become too confluent following 4 and 24 hours in culture (Tables 3.5. & 3.6.). However, after 48 or 72 hours in culture flasks were too confluent to use (Table 3.6.). Although a seeding density of 300,000 cells gave a high concentration of RNA, the flasks were too confluent at all time periods (Tables 3.5. & 3.6.). Therefore, a seeding density of 150,000 cells seeded in a T25 flask was chosen for subsequent hypertrophy experiments, which would give a high enough yield of RNA but would not become too confluent over the time periods examined.

A

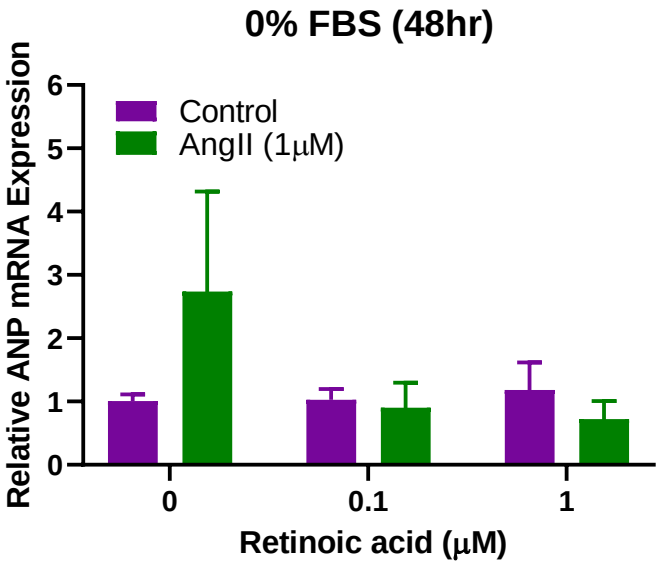

B

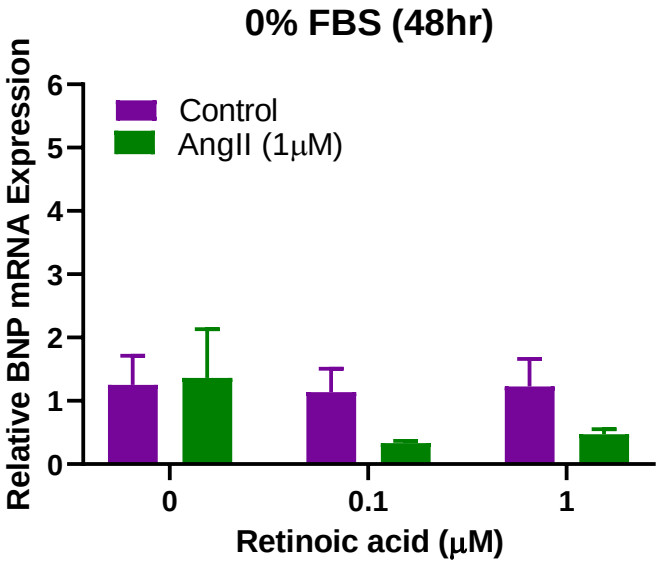

Figure 3.9. Effect of AngII on fetal gene expression in differentiated H9c2 cells. Differentiated H9c2 cells were treated with AngII (1μM) for 48hr and both ANP (A) and BNP (B) mRNA expression measured via qRT-PCR. Data is expressed as mean ± SEM and analysed using a two-way ANOVA with a Tukey's post hoc test. n=3.

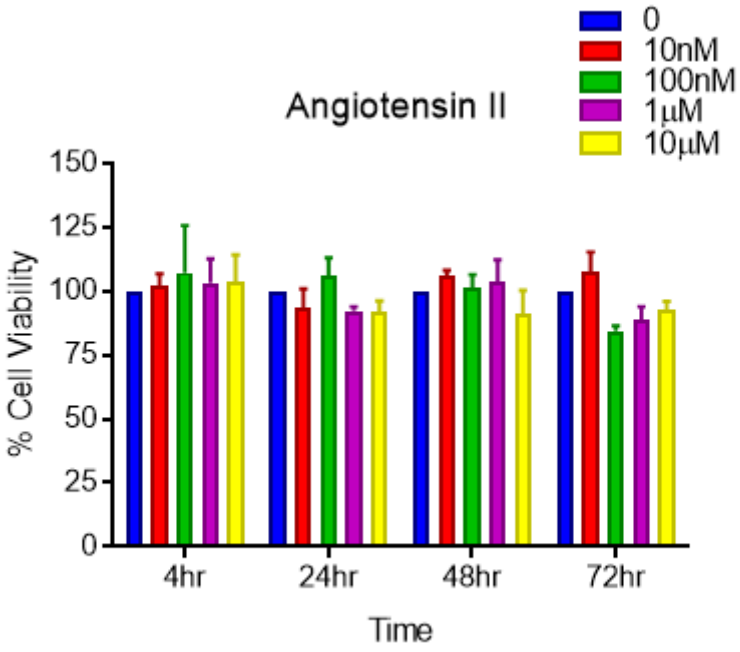

Figure 3.10. Effect of AngII on cell viability in undifferentiated H9c2 cells. Cells were treated with concentrations of AngII ranging from 10nM to 10μM and compared to control cells treated with vehicle (PBS). Cell viability was assessed using an MTT assay. Data is expressed as mean ± SEM and analysed using a Mixed model ANOVA with a Dunnett's post hoc test. n=3.

Table 3.5. RNA concentrations from different seeding densities of undifferentiated H9c2 cells over 4 different time periods. As experiments were conducted as part of the optimisation process and not subjected to statistical analysis only n=2 were conducted.

	Average RNA Concentration (ng/µl)		
Time Period (Hrs)	100,000 cells	200,000 cells	300,000 cells
4	24	46	86
24	24	44	68
48	28	56	86
72	44	44	68

Table 3.6. Estimated percentage confluence of differing seeding densities of undifferentiated H9c2 cells cultured over 4 different time periods. As experiments were conducted as part of the optimisation process and not subjected to statistical analysis only n=2 were conducted.

	Estimated Percentage of Confluence (%)		
Time Period (Hrs)	100,000 cells	200,000 cells	300,000 cells
4	40-60%	30-50%	60-100%
24	40-50%	70-90%	80-100%
48	40-50%	60-90%	80-100%
72	50-70%	85-95%	90-100%

3.4.6. Impact of duration of AngII treatment on the expression of fetal genes in undifferentiated H9c2 cells

Treatment duration was investigated to identify if time had an effect on the expression of ANP and Myh7 after AngII (1µM) had been added to the cells in serum free media. Four time points were investigated (4, 12, 24, and 48 hours) and gene expression was measured via qRT-PCR. The primer for ANP had an efficiency of 101.8% and the primer for Myh7 80.7%. Incubation of cells with AngII (1µM) in serum free medium for 4, 12, 24, or 48 hours did not significantly alter either ANP (Figure 3.11A.) or Myh7 (Figure 3.11B.) expression compared to vehicle treated control cells.

3.4.7. Influence of serum concentration on the ability of AngII to induce hypertrophy in undifferentiated H9c2 cells

The impact of FBS concentration in the cell medium on AngII induced changes in fetal gene expression in H9c2 cells was investigated over the most commonly reported incubation times for AngII induced hypertrophy i.e. 24 and 48 hours. Three different concentrations of FBS were tested in the culture media (1%, 5% and 10%) over two time points (24hrs and 48hrs). Following 24 hours of treatment with 1µM AngII, ANP (Figure 3.12A.) and BNP (Figure 3.12B.) expression was not altered compared to controls in cells cultured in 1% FBS. In H9c2 cells cultured in DMEM with 5% FBS and treated with AngII for 24 hours BNP expression was significantly increased (P<0.05; Figure 3.12B.) and although upregulated, ANP expression was not significantly increased (P=0.08; Figure 3.12A.). Furthermore, when the FBS concentration of DMEM was increased to 10%, the expression of ANP (Figure 3.12A.) and BNP (Figure 3.12B.) expression in H9c2 cells remained unchanged compared to controls. Following 48 hours of treatment with 1µM AngII, neither ANP (Figure 3.13A.) nor BNP (Figure 3.13B.) expression was significantly altered when compared to controls regardless of the FBS concentrations (1%, 5% and 10%) in the medium. On the basis of these findings, AngII was administered in DMEM with 5% FBS for 24 hours in all subsequent cardiomyocyte hypertrophy studies.

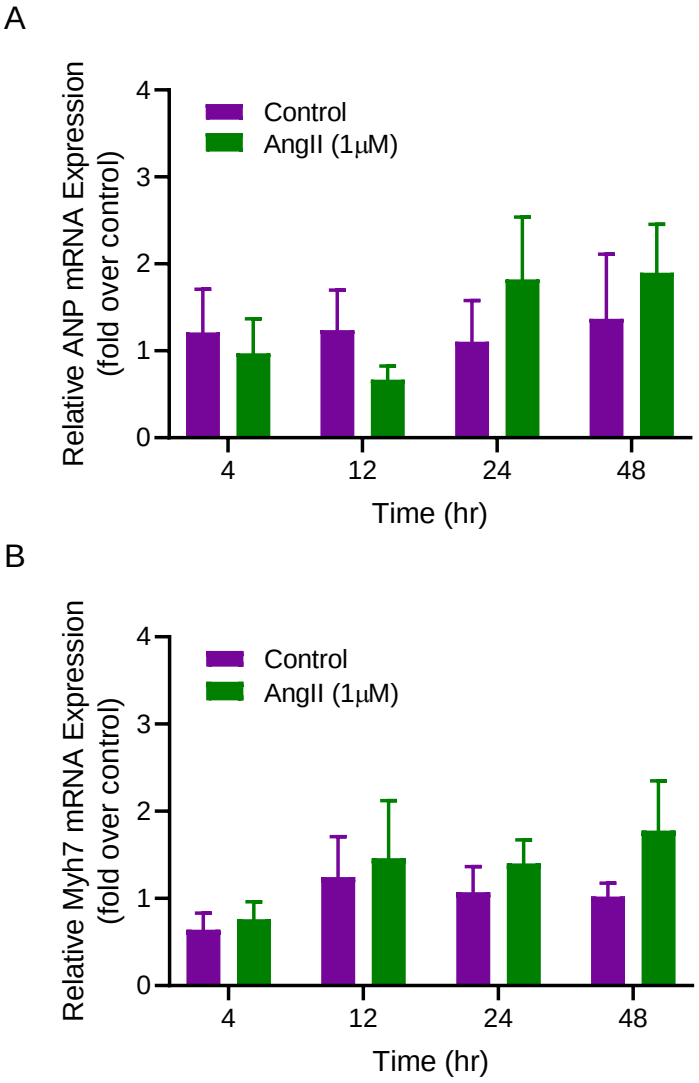

Figure 3.11. The expression of ANP and Myh7 in undifferentiated H9c2 cells after the addition of AngII (1μM) for different time periods measured via qRT-PCR. Data is expressed as mean ± SEM and analysed using a two-way ANOVA with a Bonferroni post hoc test. n=2-4 (Data points relating to experiment 1 in the ANP 24hr data set were removed as ANP expression was 21 fold in the control group and 35 fold in the AngII group).

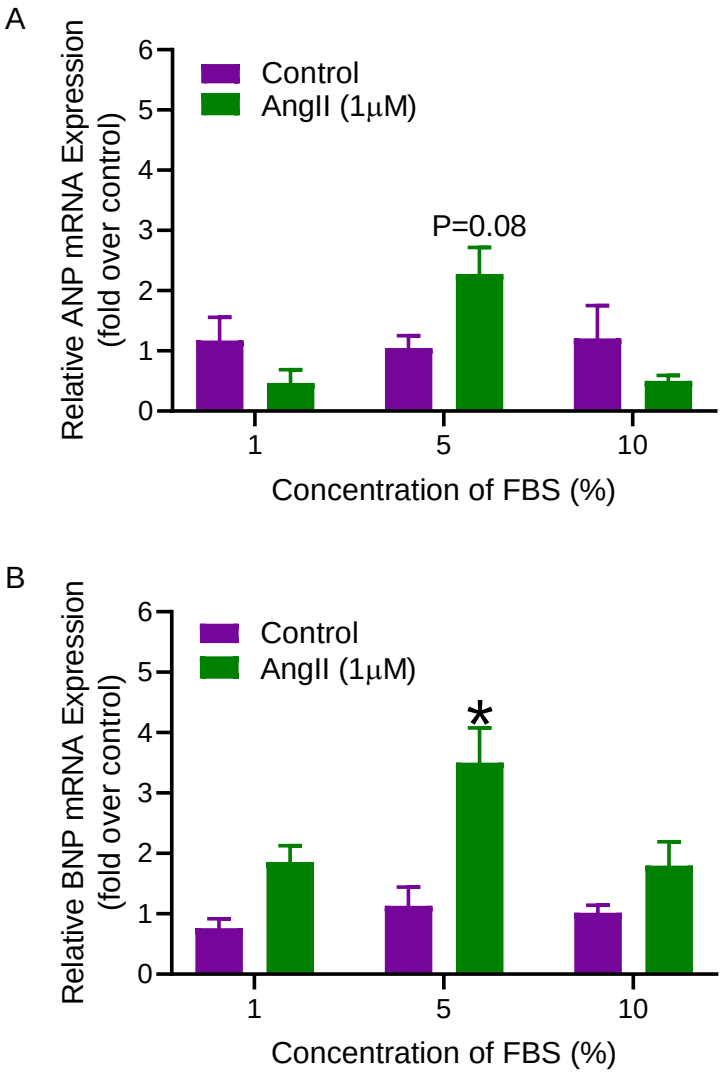

Figure 3.12. Gene expression of ANP and BNP in H9c2 cells cultured in media containing different percentages of serum over 24 hours. Data is expressed as mean ± SEM and analysed using a two-way ANOVA with a Bonferroni post hoc test. P=0.08 vs. control (5% FBS); **P*<0.01 vs. control (5% FBS); n=2-4. (BNP expression was only detectable in two out of three experiments in which H9c2 cells were cultured in DMEM with 1% FBS).

.

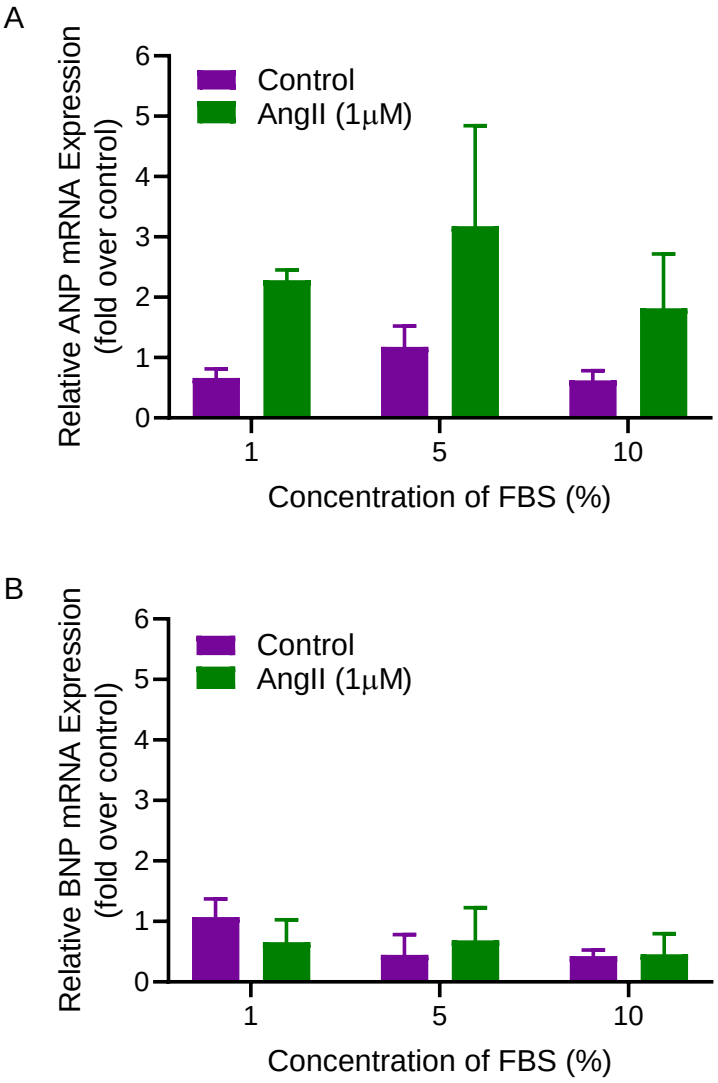

Figure 3.13. Gene expression of ANP and BNP in H9c2 cells cultured in media containing different percentages of serum over 48 hours. Data is expressed as mean ± SEM and analysed using a two-way ANOVA with a Bonferroni post hoc test. n=2-4. (ANP and BNP expression were only detectable in two out of three experiments in which H9c2 cells were cultured in DMEM with 10% FBS. Data points relating to experiment 3 in the BNP 5% FBS data set were removed as BNP expression was 11 fold in the control group and 9 fold in the AngII group).

3.5. Discussion

The principle aim of this study was to optimise an *in vitro* model of cardiomyocyte hypertrophy for use in subsequent experiments investigating the contribution of Wnt signalling to pathological cardiomyocyte hypertrophy. Initial studies explored the utility of miPSC-CMs as a potential model, on the basis that this would allow a more direct comparison of findings between the latter and the mouse model of cardiac hypertrophy used as part of this project. Due to the limitations associated with the use of miPSC-CMs described below, subsequent studies involving rat H9c2 myoblast cells were then undertaken to determine the optimum conditions for the differentiation (from myoblast to cardiomyocyte) and/or induction of hypertrophy in these cells.

3.5.1. The effect of culture duration on the expression of fetal genes (ANP and BNP) in miPSC-CMs

Research by Takahashi and Yamanaka (2006) confirmed that both mouse embryonic and adult fibroblasts can be reprogrammed into pluripotent stem cells through retroviral transfection of four transcription factors (OCT4, SOX2, KLF4 and MYC). Induced pluripotent stem cells (iPSCs) are functionally similar to embryonic stem cells and can subsequently be differentiated into cardiomyocytes (Skalova *et al*. 2015). The miPSC-CMs used in this study (obtained from NCardia) were non-proliferative cells derived from fibroblasts taken from the tail tip of an adult mouse reprogrammed to produce iPSCs, then differentiated into cardiomyocytes. Previous research by Ivashchenko et al. (2013) demonstrated that prolonged culturing of hiPSC-CMs resulted in cell maturation and a reduction in fetal gene expression to levels comparable to those in adult ventricular tissue. Thus, in the present study the effects of culture periods of differing durations on miPSC-CMs (immature fetal cells) was examined to identify the time point at which the level of fetal gene expression was comparable to that in an adult mouse heart. Surprisingly, the expression of both ANP and BNP were not only lower in miPSC-CMs compared with an adult mouse heart initially, but while ANP expression increased with time in culture to levels comparable to the mouse heart, BNP expression continued to decrease in the fetal cells over the same period. In a recent study investigating hiPSC-CM maturation, expression levels of ANP and BNP were highest at the earliest time point examined (37 days in culture) then decreased as time in culture increased, plateauing at 45 days (Ivashchenko *et al*. 2013). The hiPSC-CMs used in Ivashchenko's study had been cultured for 30 days before they were purchased, therefore the culture periods used in this study are comparable to those used in the previous study i.e. 7 days (this study)/37 days (study by Ivaschenko) and 14 days (this study)/45 days (study by Ivaschenko). Although a similar trend was observed in terms of the change in BNP expression in both studies, the profile of ANP expression with increasing

time in culture was conflicting. In contrast, results from Carlson et al. (2013), who investigated BNP expression in hiPSC-CMs over 14 days, reported a BNP expression trend similar to that observed in this study, as BNP levels were elevated at 4-5 days in culture but then decreased to almost undetectable levels following 10 days in culture. Carlson et al. (2013) also investigated different culture media, comparing normal maintenance medium supplemented with serum and serum free media supplemented with fatty acids, and found that hiPSC-CMs matured quicker in the media supplemented with fatty acids with BNP returning to baseline within 4 days of culture compared to 14 days with the maintenance media. This is due to mature cardiomyocytes changing their energy source from glucose to fatty acids to promote fatty acid oxidation. Previous research by Carlson et al. (2013) has also identified that cryopreserved iPS cardiomyocytes can express stress markers post thaw, and that prolonged time in culture can decrease the expression of stress related genes, which could potentially explain the results seen in Ivashchenko's research. A further study using hiPSC-CMs demonstrated somewhat similar findings to the present study in that ANP expression was increased 4-fold following 14 days of culture, however BNP expression (which was expressed at a lower level) also increased from day 2 in culture culminating at an overall 1.75-fold increase after 14 days in culture (Puppala *et al*. 2013). The reasons for the disparities in the impact of culture duration on ANP expression in hiPSC-CMs in the aforementioned published studies is unclear.

Based on the data from the present study, 3 days in culture appeared to be the optimum time point at which to potentially induce hypertrophy in miPSC-CMs, as although the expression of both ANP and BNP was considerably lower than that seen in the adult mouse heart, the ratio of the expression of ANP to BNP was similar between both. This may therefore suggest that at this time point (i.e. 3 days in culture) expression of the fetal gene programme in miPSC-CMs is being regulated in a similar pattern to that in mature cardiomyocytes which undergo hypertrophy in HFpEF. Furthermore, as ANP expression significantly increases with time in culture, it is possible that in miPSC-CMs cultured for more than 3 days ANP expression may have already reached its peak and thus may not increase further following the addition of the pro-hypertrophic AngII. Despite these initial successful experiments, further progress regarding the optimisation of a model of cardiomyocyte hypertrophy using miPSC-CM cells was significantly complicated by extremely low or undetectable RNA yields following extraction. It is unclear why such low concentrations of RNA were extracted from these samples, but one possible explanation may be reduced adherence of cells due to the poor plating efficiency of miPSC-CMs. Information from the supplier stated that the plating efficiency for these cells was 55% in fibronectin (Fn1) coated wells, however Fn1 could not be used as

a coating agent in this project, as research demonstrates that Fn1 can induce hypertrophy on its own (Ogawa *et al*. 2000; Chen *et al*. 2004; Konstandin *et al*. 2013). Therefore, a 0.1% gelatin solution was used as an alternative coating agent based on the recommendation of the miPSC-CM supplier, NCardia. However, previous research has demonstrated that Fn1 is one of the key ECM proteins responsible for the adhesion of cardiomyocytes (Wu *et al*. 2010) and in the case of endothelial cells (from explanted carotid arteries) produced a higher rate of cell adhesion compared to gelatin coated plates (Cornelissen *et al*. 2013). Furthermore, Patra et al. (2012) investigated nephronectin as a potential attachment factor for 3-day old post-natal rat cardiomyocytes comparing it with Fn1, which acted as a positive control, and gelatin which acted as a negative control due its poor adhesive properties. They reported that at 6 and 18 hours a significantly higher number of cardiomyocytes had attached to both nephronectin and Fn1 compared to gelatin. Therefore, the plating efficiency for miPSC-CMs plated on gelatin coated plates may have been even lower than the 55% level of adhesion expected with Fn1, thus resulting in minimal numbers of viable cells from which to extract RNA at the end of experiments. It is also possible that the RNA integrity may have been compromised during extraction and/or prolonged storage (Vermeulen *et al*. 2011). A 260nm/280nm ratio of >1.7 is generally accepted as an indication of 'pure' RNA and deemed acceptable for use for further studies. Due to the very small amount of RNA obtained from the miPSC-CMs it was not possible to calculate the 260nm/280nm ratio and thus the integrity of the RNA extracted was questionable. The frequent low concentrations of RNA obtained from the miPSC-CMs was therefore the basis for changing to a cell line that is proliferative in the first instance (to enable generation of sufficient cell numbers) but can be terminally differentiated into a more cardiomyocyte-like cell i.e. H9c2 cells. The issues encountered in the current project may explain why miPSC-CMs are not as widely used as an *in vitro* model of CVD when compared to both rat H9c2 myoblasts (Watkins *et al*. 2011; Gu *et al*. 2014; Liu *et al*. 2015; Peng *et al*. 2016) and hiPSC-CMs (Ivashchenko *et al*. 2013; Aggarwal *et al*. 2014; Duan *et al*. 2015; Jen *at el.* 2017).

3.5.2. Differentiation of H9c2 cells from a myoblast to a cardiomyocyte phenotype

H9c2 cells are a proliferative cell line originally derived from embryonic BDIX rat ventricular tissue (Kimes and Brandt 1976) and used extensively as an *in vitro* experimental model in cardiomyocyte hypertrophy studies (Watkins *et al.* 2011; Song *et al*. 2015; Li *et al*. 2017b; Wang *et al*. 2018; Cheng *et al*. 2019), cytotoxicity studies (Mojarrab *et al*. 2013; Tsai *et al*. 2015; Liu *et al*. 2016; Witek *et al*. 2016; Zhang *et al*. 2018a) and oxidative stress studies (Jun *et al*. 2011; Li *et al*. 2015; Zhang *et al*. 2018b; Davargaon *et al*. 2019). Although H9c2 cells have numerous advantages and are routinely used in cardiovascular research, they also have

their limitations as a cardiomyocyte model. For example, they are immature cells which proliferate and do not spontaneously beat in culture (a key characteristic of mature cardiomyocytes), therefore leading to the question of how well they replicate a cardiomyocyte model (reviewed by Peter *et al*. 2016). However, an important feature of H9c2 cells is their ability to differentiate from proliferative rhomboid shaped mono-nucleated myoblasts to elongated spindle shaped multi-nucleated myotubes with significantly reduced proliferative capacity by culturing the cells in media containing a low concentration (≤1%) of serum. During this differentiation process the cells acquire a skeletal muscle phenotype as indicated by an increase in the expression of the skeletal muscle specific gene, myogenin (Pagano *et al*. 2004). In addition, H9c2 cells can be further differentiated into a more cardiomyocyte-like phenotype with the addition of all-trans RA to media containing low concentrations of serum as confirmed by both the increased expression of the cardiac (α_{1C}) L-type Ca^{2+} channel and decreased expression of the skeletal (α_{1S}) L-type Ca^{2+} channel (Menard *et al*. 1999).

To determine whether undifferentiated or differentiated H9c2 cells were most appropriate for use as a cardiomyocyte model, a series of RT-PCR studies were carried out to characterise their individual phenotypes in terms of their expression of cardiac specific markers. The present study confirmed that the cardiac markers cTnT (Suhaeri *et al*. 2015), cTnI (Kankeu *et al*. 2018), and Nkx2.5 (Behrens *et al*. 2013) were all expressed in both undifferentiated H9c2 cells and those which had been differentiated for 5 days in 1% serum media, with or without the addition of RA (100nM or 1µM). Nkx2.5 is a gene that encodes a homeobox-containing transcription factor which plays an essential role in early cardiac development and is expressed in the human and murine heart (Funke-Kaiser *et al*. 2003). Furthermore, Nkx2.5 is an important transcription factor involved in cardiomyocyte differentiation and is a marker frequently reported in the characterisation and differentiation of both human embryonic stem cells (hESCs; Xu *et al*. 2002; Mehta *et al*. 2014) and murine iPSCs (Kuzmenkin *et al*. 2009) to functional cardiomyocytes. While Nkx2.5 has previously been demonstrated to be present in undifferentiated H9c2 cells (Funke-Kaiser *et al*. 2003), the present study is the first to demonstrate the expression of Nkx2.5 in differentiated H9c2 cells. Recent studies have also demonstrated the expression of both cTnT and cTnI protein in both undifferentiated (cultured in 10% FBS) and differentiated (cultured in 1% FBS supplemented with RA) H9c2 cells, with expression of both troponins highest in differentiated cells (Pereira *et al*. 2011; Branco *et al*. 2015). Although the level of expression of either troponin was not quantified in the present study their mRNA expression did not appear to differ between undifferentiated and differentiated cells.

In contrast to the cardiac troponins Myl2, which is predominantly expressed in the ventricle (England and Loughna 2013), was only detectable in H9c2 cells cultured in 1% serum media with or without the addition of RA, indicating successful differentiation from myoblast to cardiomyocyte type cells. In support of this, several studies have demonstrated that the mRNA expression of Myl2 (Karagiannis *et al*. 2010) and protein expression of Myl2 (Pereira *et al*. 2011) are both increased in RA differentiated cells compared to those differentiated in low serum media alone. In the present study, mRNA expression of Myl2 was only detected in differentiated cells, however the level of expression was not quantified following the different culture treatments and thus it is unknown whether the addition of RA enhanced the expression of Myl2 beyond that induced by low serum alone. In contrast to the present findings, studies by both Pereira et al. (2011) and Liu et al. (2015) demonstrated that both mRNA and protein expression of Myl2 was detected in both undifferentiated and differentiated (1% media on its own and with the addition of 10nM RA) H9c2 cells, with the level of expression of Myl2 being lower in undifferentiated cells compared to those differentiated with RA. Despite the effectiveness of low serum (+/- RA) induced H9c2 differentiation, there still remains a degree of inconsistency relating to the presence or absence of certain markers in supposedly differentiated cells. This is particularly illustrated by the findings of Patten et al. (2017) in which two separate labs attempted to induce differentiation of H9c2 cells, with one lab reporting an increase in the expression of cTnT and Myl2 in differentiated cells, while the other lab failed to detect the expression of either marker despite using several different concentrations of RA to induce differentiation. One explanation for the inconsistencies could be differences in the passage numbers of H9c2 cells used, which has been shown to alter the responsiveness of these cells to pharmacological agents. In particular, Witek et al. (2016) demonstrated that successive passaging of H9c2 cells leads to hypersensitivity to stress conditions resulting in increased variability in their responses to a cytotoxic agent and suggested that for consistency cells should be used within the first five passages in toxicology tests. It is unclear whether H9c2 cells cultured beyond five passages respond differently to low serum (+/- RA) induced differentiation, however as multiple passage numbers (passage 7-11) were used in all of the studies previously discussed it is a possible source of variability. Another explanation for the inconsistency could be the confluency of the cells, as the ECACC website state that H9c2 cells should only be cultured to 70-80-% confluency as the myoblastic population will rapidly deplete as cells undergo differentiation and fuse to form multinucleated myotubes if cultures are allowed to become too confluent. It is therefore possible that, in some instances, what were considered to be undifferentiated H9c2 cells may have become too confluent in culture and differentiated into myotubes consequently expressing myocyte markers i.e. Myl2, although this requires further investigation.

3.5.3. Induction of hypertrophy in differentiated H9c2 cells

Although variability persists between groups as to the success of inducing the differentiation of H9c2 myoblast cells, differentiated H9c2 cells have been used as models of cardiomyocyte hypertrophy in a limited number of studies. In particular, Qian et al. (2018) differentiated H9c2 cells in DMEM with 1% FBS and 1μM RA for 5 days and induced hypertrophy via the addition of 10μM isoprenaline for 24 hours as evidenced by both an increase in ANP and BNP expression as well as an increase in cell size. In a separate study, Fukushima et al. (2018) differentiated H9c2 cells in medium containing 1% FBS and 1μM RA over a longer period of time (7-10 days) and induced hypertrophy with 100nM phenylephrine (added for 48 hours) reporting an increase in ANP expression. In more recent studies, H9c2 cells differentiated in low serum medium containing 10nM RA for 6 days were characterised by an increase in the expression of the hypertrophic markers Myh7 in response to 24hr treatment with 500nM Adriamycin (Iqbal *et al*. 2020) and both ANP and BNP in response to 24hr treatment with 1μM AngII (Liu *et al*. 2018), demonstrating that hypertrophy can be successfully induced in differentiated H9c2 cells. In contrast, several studies have reported that RA can exert anti-hypertrophic effects in cardiomyocytes. In NRVMs, micromolar concentrations of RA reduced both ET-1 induced increases in ANP, BNP, and ACTA1 expression (Wu *et al*. 1996) and phenylephrine induced increases in ANP expression and cell size (Zhou *et al*. 1995). Furthermore, treatment with RA (5μM) for 24 hours has been shown to significantly inhibit AngII induced (0.1μM for 24 hours) cardiac hypertrophic features which included increased total protein content, cell size, and myofibrillar reorganisation in NRVMs (Palm-Leis *et al*. 2004). In addition, Wang et al. (2002) also demonstrated that RA (1μM for 5 days) inhibited the AngII (100nM) induced increase in total protein content in NRVMs. In a rat model of MI, chronic treatment with RA (0.3mg/kg/day) for 6 months prevented ventricular fibrosis and improved impaired systolic function (Paiva *et al*. 2005). However, contrasting research by Silva et al. (2017) has indicated that cardiac remodelling can be induced by RA in a dose dependent manner. One explanation as to why RA prevents the development of cardiac remodelling in aortic banded rats is through the inhibition of the RAAS (Choudhary *et al.* 2008). In pressure overload models, AngII production is increased, subsequently binds to AT_1R inducing ROS generation which then leads to the activation of the MAP kinase cascade resulting in cardiac remodelling. RA prevents cardiac remodelling by binding to the retinoic acid receptor/retinoid X receptor (RAR/RXR) which induces the upregulation of MAPK phosphatases (MKPs) consequently dephosphorylating and inactivating MAPK. In addition, RA also combats cardiac remodelling by inhibiting oxidative stress via increasing the expression of members of the antioxidant defence system (i.e. SOD-1 and SOD-2). In related studies, RA (2μM) was also shown to protect against doxorubicin induced cardiotoxicity in H9c2 cells via an antioxidant mechanism (Yang *et al*. 2016). Finally, AngII production is also thought to be supressed by RA

via the inhibition of RAAS components and through an increase in ACE2 which converts AngII to Ang1-7 (Choudary *et al*. 2008).

In the present study, hypertrophy (confirmed via an upregulation of ANP and/or BNP) was not successfully induced in H9c2 cells differentiated in 1% FBS with and without the addition of RA (100nM and 1μM) in response to 1μM AngII treatment for 48 hours. A potential reason for this result could have been a reduction in the expression of AT_1Rs in H9c2 cells following differentiation with RA, however this seems unlikely as Gerena et al. (2017) demonstrated that AT_1R expression is actually increased in 1μM RA differentiated H9c2 cells. Another possible explanation for this result could be attributed to both the direct and indirect antioxidant effects of RA, particularly as AngII induced oxidative stress is a key contributor to the development of cardiomyocyte hypertrophy. As described in the previous section RA attenuates oxidative stress via an upregulation of antioxidant defence mechanisms which may in part explain why AngII did not induce hypertrophy in H9c2 cells differentiated with RA. However, in the present study, RA was replaced daily during the differentiation process as it is rapidly broken down and was not present during the 48hr treatment with AngII so it is unclear whether any residual RA mediated antioxidant actions are likely to have contributed to an anti-hypertrophic effect. However, as the presence and/or anti-hypertrophic potential of RA cannot be ruled out, subsequent studies focused on optimising an AngII induced model of hypertrophy in undifferentiated H9c2 cells.

3.5.4. Induction of hypertrophy in undifferentiated H9c2 cells

Undifferentiated H9c2 cells treated with either phenylephrine (Anestopoulos *et al*. 2013; Hahn *et al*. 2014; Xu *et al*. 2014), ET-1 (Liou *et al*. 2015; Barta *et al*. 2018), isoprenaline (Han *et al*. 2016; Qian *et al*. 2018; Liu *et al*. 2020), or AngII (Peng *et al*. 2016; Zhu *et al*. 2016; Chen *et al*. 2017; Guan *et al*. 2017; Liu *et al*. 2018; Zhao *et al*. 2018) are routinely used in cardiovascular research as a model of cardiomyocyte hypertrophy. As AngII has previously been shown to mediate its hypertrophic effects in part via activation of Wnt signalling (Zhao *et al*. 2018), this peptide was used to induce hypertrophy in undifferentiated H9c2 cells in the present study. Searching through the literature, undifferentiated H9c2 cells have been treated with a variety of AngII concentrations ranging from 0.1μM (Qin *et al*. 2006) to 200μM (Yan *et al*. 2013) over several different time periods ranging from 15 minutes (Peng *et al*. 2016) to 96 hours (Flores-Munoz *et al*. 2011) to induce hypertrophy. To further complicate matters, AngII has also been shown to be cytotoxic to H9c2 cells at 'pro-hypertrophic' concentrations i.e. 100nM to 1μM (Gu *et al*. 2014; Yong *et al*. 2016; Wang *et al*. 2018), which could therefore potentially impact final

viable cell numbers and resultant RNA concentrations obtained in the present study. The most frequently used concentration of AngII in the literature is 1µM over an incubation period of 24-48hrs (Sheng *et al*. 2008; Pan *et al*. 2013; Huang *et al*. 2014; Peng *et al*. 2016; Wu *et al*. 2018). Due to the inconsistencies in the experimental conditions reported for AngII induced hypertrophy in undifferentiated H9c2 cells, a series of studies were carried out to determine the optimum conditions for the present study. Furthermore, a series of cell viability (MTT assay) experiments were also conducted to investigate the potential cytotoxicity of AngII in undifferentiated H9c2 cells. The findings from this study demonstrated that none of the concentrations (10nM up to 10µM) of AngII tested significantly altered cell viability over the time periods (4 to 72 hours) investigated, indicating that this range of concentrations of AngII was not toxic to undifferentiated H9c2 cells. In contrast, Gu et al. (2014) reported a decrease of 40% in cell viability when undifferentiated H9c2 cells were treated with AngII (1µM) for 24hrs, while data from Yong et al. (2016) demonstrated a 20% decrease in the viability of H9c2 cells using a similar concentration of AngII over a 24hr period. Moreover, 48 hour treatment of H9c2 cells with 100nM AngII was reported to lead to a 40% decrease in cell viability (Wang *et al*. 2018). Paradoxically, at a concentration of 1µM, AngII has been shown to exert both the greatest reduction in H9c2 cell viability and the most significant hypertrophic response i.e. the largest increase in cell surface area (Gu *et al*. 2014; Yong *et al*. 2016). Therefore, on the basis of both the findings from the published literature and the results from the cytotoxicity experiments conducted as part of this study, a concentration of 1µM AngII was chosen for the induction of hypertrophy in undifferentiated H9c2 cells in subsequent experiments.

Prior to undertaking experiments involving the induction of hypertrophy in undifferentiated H9c2 cells, the optimum cell seeding density was investigated to ensure that flasks did not become too confluent (subsequently undergoing differentiation to skeletal-type myocytes) throughout the proposed hypertrophy induction protocol, while still providing sufficient cell numbers/RNA concentrations for subsequent qRT-PCR experiments investigating fetal gene expression. These experiments determined that 150,000 H9c2 cells seeded in a T25 flask was the optimum seeding density to enable extraction of adequate amounts of RNA while keeping the confluency lower than 70% over the proposed incubation periods (4-72 hours) being tested. Subsequent studies were then undertaken to investigate the optimum treatment time (4,12, 24, or 48 hours) with AngII (1µM) for the induction of hypertrophy (as indicated by an increase in the level of expression of either of the hypertrophic markers, ANP or Myh7) in undifferentiated H9c2 cells. Following AngII treatment, neither the expression of ANP nor Myh7 was significantly altered in undifferentiated H9c2 cells at any of the time points investigated. These findings appear to conflict with those published in the literature as several studies have

reported that at 24-48 hours following the addition of AngII (concentrations ranging from 100nM to 5µM) to cells the expression of either ANP (Du *et al*. 2013; Wu *et al*. 2014; Zhou *et al*. 2014; Lu *et al*. 2018; Singh *et al*. 2020) and/or Myh7 (Du *et al*. 2013; Lu *et al*. 2018; Prathapan *et al*. 2018; Jiang *et al*. 2021) was significantly increased. However, a possible explanation for the lack of response of H9c2 cells to AngII in the experiments described above may have been the lack of serum in the medium during the 24-48 hour treatment period with AngII.

In the present study, undifferentiated H9c2 cells were subjected to serum starvation to synchronise all cells at the same stage of the cell cycle prior to the addition of AngII as a means of reducing variability in experimental conditions from one experiment to another (Pirkmajer and Chibalin 2011). Serum starving of cells is such a common practice that many papers do not report it, or only report that cells were serum starved with no other experimental details such as duration of starvation period included (Chen *et al*. 2017; Liu *et al*. 2018). In addition to this, published studies often fail to mention whether or not serum was re-introduced to the culture media with the addition of the hypertrophic agent, which is an important factor as several studies have demonstrated that serum can both exert hypertrophic effects on its own and also influence the ability of pro-hypertrophic agents. In particular, Dambrot et al. (2014) demonstrated that treatment of NRVMs with either 5% or 20% fetal calf serum (FCS) for 36 hours induced a significant increase in cell size compared to those cultured in serum free media. Furthermore, while phenylephrine induced hypertrophy in cells cultured in media containing 5% FCS, this effect was lost in those cultured in 20% FCS (Dambrot *et al*. 2014). To determine whether serum concentration influenced the ability of AngII to induce cell hypertrophy, H9c2 cells were exposed to AngII (1µM) for 24 and 48 hours in the presence of increasing concentrations of FBS (1%, 5%, and 10%). The results demonstrated that administration of AngII (1µM) in media containing 5% FBS for 24hrs was the optimum experimental conditions to induce an increase in the gene expression of ANP and BNP (which are known markers of hypertrophy) in undifferentiated H9c2 cells in the present study. A time duration of 48hrs was not chosen due to only one of the fetal gene markers being significantly increased in 1% FBS, with nether fetal genes being increased when cultured in 5% or 10% FBS.

3.6. Conclusion

In conclusion, the results demonstrate that culturing H9c2 cells in medium containing low serum (without the addition of RA) was sufficient to differentiate the cells into a more

cardiomyocyte-like phenotype characterised by a spindle-shaped morphology, a switch to a non-proliferative state, and expression of Myl2. Furthermore, AngII did not induce any changes in the hypertrophic markers ANP and BNP in differentiated H9c2 cells, however treatment of undifferentiated H9c2 cells (cultured in medium containing 5% FBS) with AngII (1µM) for 24 hours successfully induced an increase in the expression of fetal genes ANP and BNP (which are known markers of hypertrophy) and this experimental model was subsequently used to explore the role of Wnt signalling in cardiomyocyte hypertrophy.

Chapter 4: Investigating the role of Wnt3a in Cardiomyocyte Hypertrophy

4.1. Introduction

4.1.1. RAAS induced activation of canonical Wnt signalling contributes to cardiomyocyte hypertrophy

While the role of the RAAS in mediating cardiomyocyte hypertrophy appears to be well established, more recent findings suggest that RAAS induced activation of canonical Wnt signalling contributes to its hypertrophic effects. In particular, chronic infusion of AngII in rats resulted in the increased expression of multiple Wnt ligands (Wnt1, Wnt2, Wnt2b, Wnt3, Wnt3a, Wnt5a, Wnt5b, and Wnt9a) in the hypertrophic hearts of these animals, while co-administration of ICG-001, a known inhibitor of β-catenin dependent Wnt signalling, prevented the development of AngII-induced cardiac hypertrophy (Zhao *et al*. 2018). In NRVMs, treatment with hypertrophic agents such as phenylephrine and ET-1 induced β-catenin accumulation which is indicative of activation of canonical Wnt signalling (Haq *et al*. 2003) and treatment with AngII stabilised β-catenin and triggered its translocation to the nucleus (Li *et al*. 2015). Furthermore, recent work has demonstrated that an increase in β-catenin levels in endothelial cells of genetically modified mice leads to an upregulation in the expression of the fetal genes (ANP and BNP) in cardiomyocytes (Nakagawa *et al*. 2016). The same study also demonstrated that β-catenin signalling in endothelial cells resulted in a decrease in the neuregulin expression which activates anti-hypertrophic ErbB signalling in cardiomyocytes (Liu *et al.* 2006; Hedhli *et al*. 2011).

Elevated β-catenin levels have also been detected in cardiomyocytes exposed to hypertrophic stimuli (Zelarayan *et al*. 2007). These findings are further supported by an *in vivo* study, which demonstrated that mice with cardiomyocyte-specific depletion of β-catenin had substantially reduced hypertrophy and improved cardiac function in comparison with mice with preserved β-catenin levels (Chen *et al*. 2006). Research has also shown that stabilisation of β-catenin in both *in vitro* and *in vivo* experiments induces hypertrophic growth (Haq *et al*. 2003), and that TAC-induced hypertrophy is reduced following the depletion of β-catenin (Qu *et al*. 2007). Furthermore, experimental studies carried out *in vivo* have demonstrated both increased protein expression of β-catenin in the hypertrophic hearts of rats subjected to pressure overload (Haq *et al*. 2003) and evidence of hypertrophy (i.e. increased heart weight to BW ratio and upregulated expression of ANP) in the hearts of mice with cardiac-specific overexpression of the canonical Wnt signalling mediator, Dvl-1 (Malekar *et al*. 2010). The role of Dvl1 was further explored in research by van de Schans et al. (2007) who reported that mice lacking the Dvl1 gene had both reduced wall thickness and decreased expression of ANP and BNP after 7 days of pressure overload. They also reported that β-catenin protein was reduced in mice

lacking the Dvl1 gene demonstrating that Dvl1 is required for canonical Wnt signalling. Taken together, these data suggest a prominent role for canonical Wnt signalling in the progression of cardiomyocyte hypertrophy, a key feature of HFpEF.

4.1.2. Wnt3a as an activator of canonical Wnt signalling

Research has identified Wnt3a as a chief mediator of canonical Wnt signalling, with different cell types exhibiting increased expression of β-catenin and its target genes (CCND1 and c-Myc) following exposure to Wnt3a (Liu *et al.* 2012; Xu and Gotlieb 2013; Reischmann *et al.* 2015). Throughout the literature there is accumulating evidence demonstrating that Wnt3a is upregulated in hearts in a variety of different experimental models of cardiac hypertrophy. In particular, Wnt3a expression is upregulated in the hypertrophic hearts of animals infused with AngII (Zhao *et al.* 2018), administered isoprenaline (He *et al.* 2015), and those subjected to TAC induced pressure overload (Zhang *et al.* 2019; Zhao *et al.* 2019a; Zhao *et al.* 2020). Furthermore, both direct and indirect roles for Wnt3a in mediating cardiomyocyte hypertrophy have recently been described in the literature. In these studies, Wnt3a was shown to directly induce hypertrophy in NRVMs (Zhao *et al.* 2018) and to play a role in mediating TGF-β1 induced cardiac hypertrophy, as Wnt3a overexpression in NRVMs was shown to induce the expression of TGF-β1 (Li *et al.* 2021). Wnt3a has been shown to activate the canonical/β-catenin dependent Wnt signalling pathway and has also been reported to bind to both FZD_1 and FZD_2 receptors (reviewed by Dawson *et al.* 2013), the latter of which is highly expressed in heart tissue (Dong *et al.* 2015). Recent data has demonstrated that the myocardial expression of both FZD_2 and target genes of canonical Wnt signalling (i.e. CCND1 and c-Myc) are increased in the TAC induced pressure overload model in mice (Jiang *et al.* 2018), which may suggest FZD_2 as the primary mediator of Wnt3a induced hypertrophy although this remains to be established. An insight into the signalling pathway involved in Wnt induced cardiomyocyte hypertrophy was explored by Hagenmuller et al. (2013) who demonstrated that cardiac-restricted overexpression of Dapper 1 (Dpr1) activated canonical Wnt signalling, while inhibition of Dpr1 results in smaller cardiomyocyte surface area and the inhibition of Wnt3a-induced protein synthesis. However, research by Zhang et al. (2019) highlighted that inhibition of ACE by captopril caused a reduction in protein expression of Wnt3a and β-catenin in a mouse TAC induced pressure overload model, potentially highlighting a link between the RAAS and Wnt signalling. Although Wnt3a is frequently shown to be upregulated in hearts which have undergone hypertrophy, there are only a limited number of studies demonstrating a causal role for Wnt3a in terms of inducing cardiomyocyte hypertrophy. The present study therefore investigated the role of Wnt3a in cardiomyocyte hypertrophy and the possible involvement of the RAAS in Wnt signalling induced hypertrophy.

4.1.3. Aim:

The principle aims of this study were 1) to determine biologically active concentrations of Wnt ligands in H9c2 cells assessed via changes in DMR activity, and 2) to determine whether activation of Wnt signalling either directly (via Wnt3a) or indirectly (via AngII), induces an increase in fetal gene expression which is indicative of cardiomyocyte hypertrophy.

4.2. Methods

All necessary methodological detail is either described in the following Experimental Protocols section or in Chapter 2 as indicated.

4.3. Experimental Protocols

4.3.1. Determination of the optimum H9c2 cell seeding density for the detection of DMR activity

A range of different H9c2 cell seeding densities was investigated to identify which seeding density produced the most substantial change in DMR activity in response to adenosine 5′-triphosphate (ATP; used as a positive control). Initially, H9c2 cells were cultured in T175 flasks until they reached 60-70% confluence, cells were then harvested and seeded at a density of 5,000, 7,500, 10,000, 15,000, or 20,000 cells per well in a 384 well microplate (Epic® 384 well Fn1 coated cell assay microplate) using a Multi-drop Combi cell dispenser. Cells were cultured overnight in a humidified atmosphere at 37°C under 5% CO_2 to allow attachment, prior to the addition of ATP (100µM) and the measurement of DMR activity as described in Chapter 2, section 2.4.2.

4.3.2. Determination of biologically active concentrations of Wnt3a, Wnt5a, and sFRP1 in H9c2 cells

Due to a lack of information in the literature regarding biologically active concentrations of Wnt3a, Wnt5a, and sFRP1 in H9c2 cells, a series of experiments were conducted to determine active concentrations for subsequent use in cardiomyocyte hypertrophy studies. H9c2 cells were seeded in a 384 well microplate and Wnt3a, Wnt5a, and sFRP1 (10, 50, and 100ng/ml) induced changes in DMR activity measured as described in Chapter 2, section 2.4.2.

4.3.3. Examination of the potential hypertrophic role for Wnt3a in H9c2 cells

Previous research (Zhao *et al.* 2018) has shown that AngII can upregulate the expression of Wnt3a in NRVMs and that Wnt3a on its own can induce hypertrophy (indicated by an increase in mRNA expression of ANP and BNP). Therefore, to investigate whether Wnt3a induces hypertrophy in H9c2 cells a series of experiments were conducted in which H9c2 cells were treated with Wnt3a (10 and 100ng/ml) for 24 hours and BNP mRNA expression subsequently measured via qRT-PCR as described in Chapter 2, sections 2.3.1. to 2.3.3. and 2.3.5. To determine whether Wnt3a induced BNP secretion from H9c2 cells, 1ml of cell medium was taken from each T25 flask and BNP concentration measured via ELISA (described in detail in Chapter 2, section 2.4.3.).

4.3.4. Investigation of the effect of sFRP1 on Wnt3a induced cardiomyocyte hypertrophy

sFRP1 (endogenous Wnt signalling antagonist) is expressed in several different human tissues, with the highest expression observed in the heart and is reported to exert cardioprotective effects via the inhibition of canonical Wnt signalling (Pan *et al.* 2018). Therefore, to investigate whether sFRP1 alters Wnt3a induced cardiomyocyte hypertrophy (indicated by an increase in BNP mRNA expression) , H9c2 cells were seeded and serum starved as described in Chapter 2, section 2.4.1.1. Cells were then pre-treated with sFRP1 (10 and 100ng/ml) 30 minutes prior to the addition of Wnt3a (100ng/ml) for 24 hours. BNP mRNA expression was then measured in cell lysates as described in Chapter 2, sections 2.3.1. to 2.3.3. and 2.3.5.

4.3.5. Exploration of the role of Wnt signalling in AngII mediated cardiomyocyte hypertrophy

Firstly, to investigate whether or not AngII induces the expression of Wnt3a in H9c2 cells, the cells were treated with AngII (1µM) for 24 hours as described in Chapter 2, section 2.4.1.1. Wnt3a mRNA expression was then measured in cell lysates as described in Chapter 2, sections 2.3.1. to 2.3.3. and 2.3.5. In separate experiments, the role of Wnt signalling in AngII mediated hypertrophy was investigated via the co-administration of AngII with Wnt-c59. Wnt-c59 is a PORCN inhibitor which abrogates Wnt signalling (both canonical and non-canonical) via the prevention of Wnt palmitoylation and subsequent secretion of active Wnt ligands. H9c2 cells were seeded and serum starved as described in Chapter 2, section 2.4.1.1. and then pre-treated with Wnt-c59 (10nM and 1µM) 30 minutes prior to the addition of AngII (1µM) for 24 hours. BNP mRNA expression was then measured in cell lysates as described in Chapter 2, sections 2.3.1. to 2.3.3. and 2.3.5.

4.3.6. Investigation into the potential hypertrophic effects of AngII and/or Wnt3a in HCMs

To determine if AngII and/or Wnt3a exert similar hypertrophic effects in primary HCMs to those observed in rodent H9c2 cells, a series of experiments were conducted in which HCMs were seeded in T25 flasks as described in Chapter 2, section 2.4.1.2. After 48 hours, the medium was discarded from the flasks and either AngII (1µM) or Wnt3a (100ng/ml) added in MGM to cells for 24 hours. After 24 hours, cells were harvested as per Chapter 2, section 2.2.2.3 and BNP mRNA expression measured via qRT-PCR as described in Chapter 2, sections 2.3.1. to 2.3.3. and 2.3.5.

4.3.7. Evaluation of the effect of Wnt-c59 on AngII induced hypertrophy in HCMs

To investigate whether AngII induced HCM hypertrophy was mediated via the activation of Wnt signalling, HCMs were cultured as described in Chapter 2, section 2.4.1.2. and subsequently treated with AngII (1µM) in the absence or presence of Wnt-c59 (10nM and 1µM; added 30 minutes prior to the addition of AngII) for 24 hours. After 24 hours, cells were harvested as per Chapter 2, section 2.2.2.3 and BNP mRNA expression measured via qRT-PCR as described in Chapter 2, sections 2.3.1. to 2.3.3. and 2.3.5.

4.3.8. Statistical Analysis

All statistical analysis was conducted using GraphPad Prism 8 software and any differences between results were deemed significant when $P<0.05$. Data was plotted as mean ± SEM. In cell experiments, each n relates to cells from a single passage number. The statistical test used for each set of data is detailed in its accompanying figure legend throughout this chapter. Individual data points were excluded if it was out with the mean ± (2x standard deviation).

4.4. Results

4.4.1 The optimum seeding density of H9c2 cells for the detection of changes in DMR activity

A range of seeding densities of H9c2 cells in a 384 well microplate was investigated to determine the optimum seeding density to detect the largest increase in DMR activity in response to ATP. The DMR changes within cells were measured as picometer (pm) wavelength shift of light reflection. At a seeding density of 5,000 cells per well, ATP produced an increase in DMR activity of approximately 13.8pm which increased to 20.8pm when the seeding density was increased to 7,500 cells per well (Figure 4.1.). Increasing the cell density

further to 10,000 cells resulted in an ATP induced increase in DMR activity of 27.4pm, which was not altered by increasing the cell density to either 15,000 (28pm) or 20,000 (25pm) cells per well (Figure 4.1.). On this basis, a seeding density of 10,000 cells per well was chosen for subsequent experiments. Figure 4.1 is an illustration of the profile of agonist (in this case ATP) induced change in DMR activity. In all subsequent experiments the area under the curve (AUC) of each agonist induced response was measured, then normalised to the AUC calculated for the vehicle (which represents 100%), and was reported in the form of bar graphs.

4.4.2. Biologically active concentrations of Wnt3a, Wnt5a, and sFRP1 in H9c2 cells

Due to a lack of published information regarding biologically active concentrations of Wnt3a, Wnt5a, and sFRP1 in H9c2 cells, varying concentrations of all three proteins were applied to these cells (10,000 cells per well in a 384 well microplate) and their effects on DMR activity assessed. Wnt3a, at concentrations of 10ng/ml and 50ng/ml, did not alter DMR activity (calculated as AUC) when compared to the vehicle response, however increasing the concentration to 100ng/ml produced an increase in DMR activity that exceeded that observed with the vehicle (145% vs. 100%; $P<0.05$; Figure 4.2.). Wnt5a, at all concentrations (10, 50 and 100ng/ml) tested, did not alter DMR activity in comparison to the vehicle response (Figure 4.3.). Conversely, sFRP1 induced an increase in DMR activity that exceeded that observed with the vehicle (100%) at all concentrations tested 10ng/ml (153%), 50ng/ml (190%), and 100ng/ml (198%) (all $P<0.05$; Figure 4.4.).

4.4.3. Wnt3a induces expression of hypertrophic markers in H9c2 cells

Based on the findings from section 4.4.2, concentrations of 10ng/ml and 100ng/ml were used to investigate the potential pro-hypertrophic effect of Wnt3a. Following 24 hours of treatment with 10ng/ml Wnt3a, ANP mRNA expression was not altered in H9c2 cells, however increasing the concentration of Wnt3a to 100ng/ml produced a significant increase in ANP mRNA expression in comparison to the control ($P<0.05$; Figure 4.5A.). In contrast, Wnt3a induced increases in BNP mRNA expression in H9c2 cells at both concentrations tested, with a 2.9-fold increase observed at 10ng/ml (not significant) and a 3.9-fold increase observed at 100ng/ml compared to the control ($P<0.05$; Figure 4.5B.). Furthermore, Wnt3a at concentrations of 10ng/ml and 100ng/ml produced a significant increase in the secretion of BNP into the cell media in comparison to control samples ($P<0.05$; Figure 4.6.).

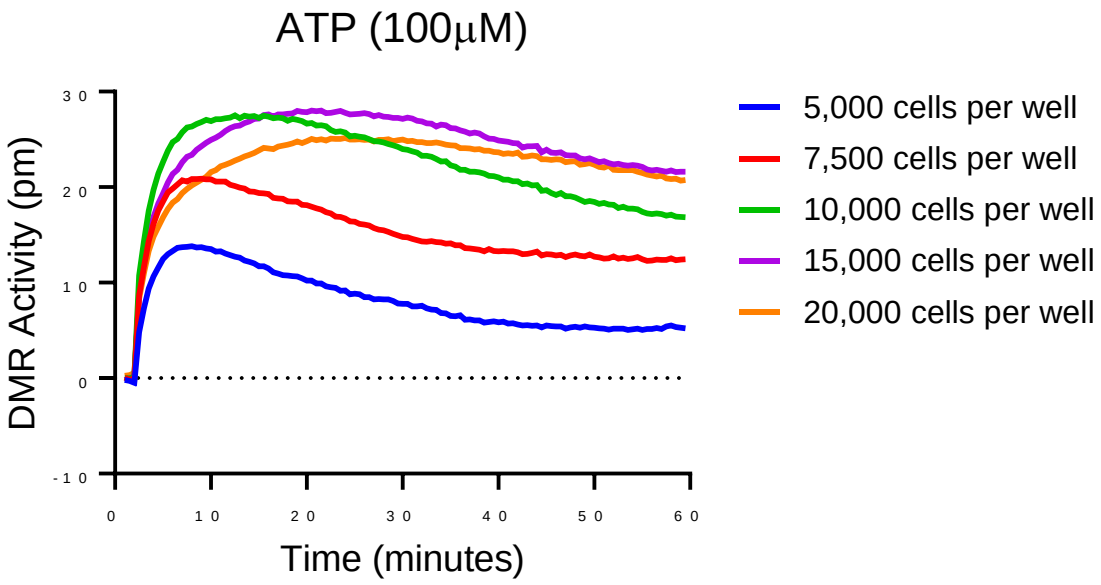

Figure 4.1. Influence of seeding density (cells per well) on ATP (100µM) induced changes in DMR activity in H9c2 cells. n=1.

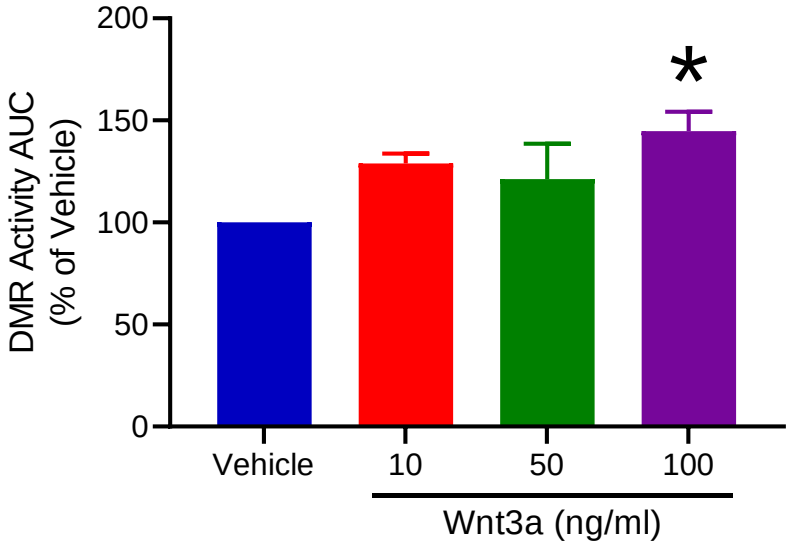

Figure 4.2. Wnt3a (10, 50, and 100ng/ml) induced changes in DMR activity (10,000 cells per well). Data is expressed as mean ± SEM and analysed using a Mixed model ANOVA with a Dunnett's post hoc test. *P<0.05 vs. Vehicle; n=4.

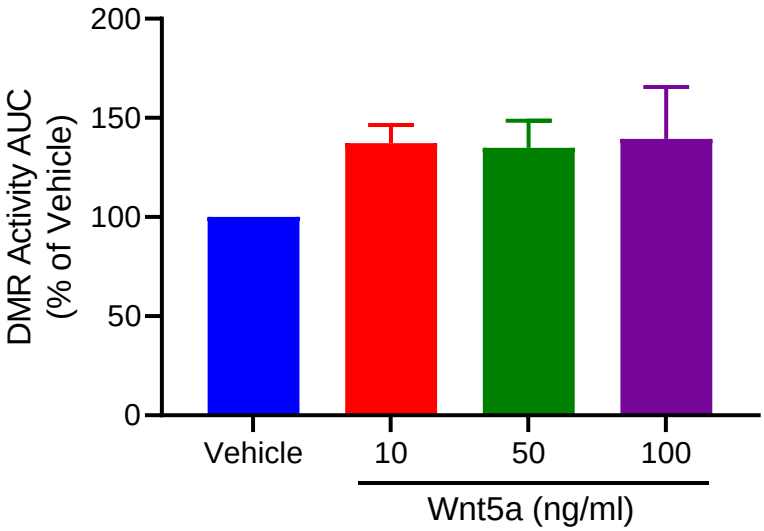

Figure 4.3. Wnt5a (10, 50, and 100ng/ml) induced changes in DMR activity (10,000 cells per well). Data is expressed as mean ± SEM and analysed using a Mixed model ANOVA with a Dunnett's post hoc test. n=4.

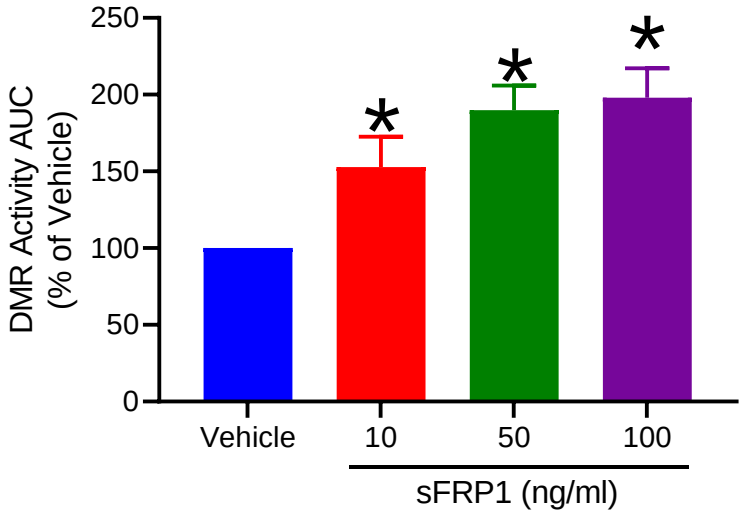

Figure 4.4. sFRP1 (10, 50, and 100ng/ml) induced changes in DMR activity (10,000 cells per well). Data is expressed as mean ± SEM and analysed using a Mixed model ANOVA with a Dunnett's post hoc test. **P*<0.05 vs. Vehicle; n=4.

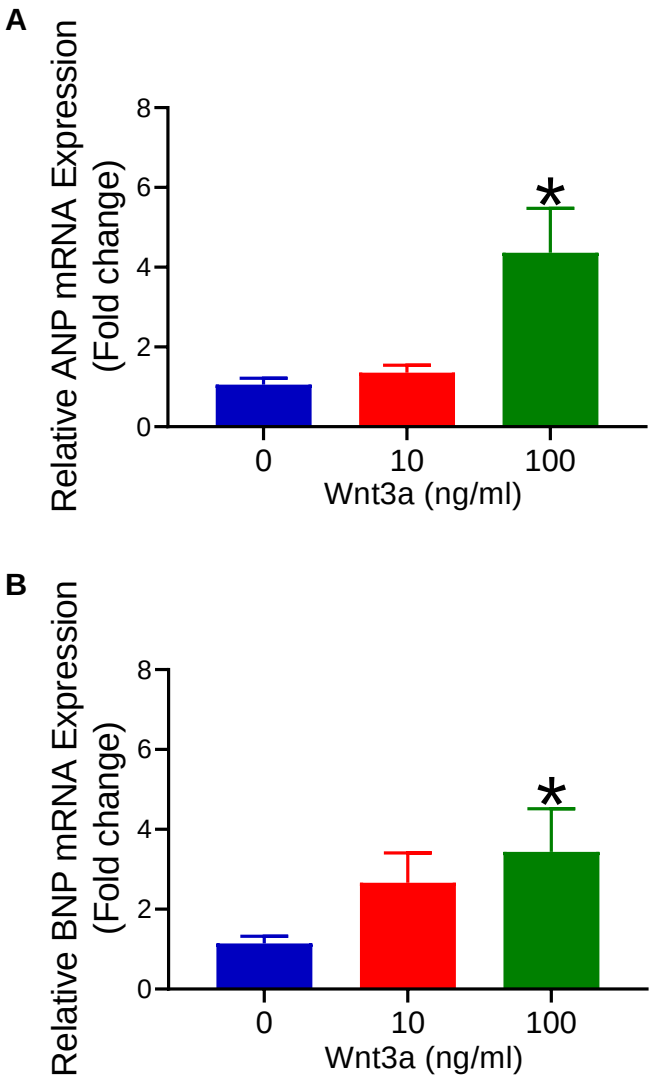

Figure 4.5. Effect of Wnt3a (10 and 100ng/ml) on the mRNA expression of ANP (A) and BNP (B) in H9c2 cells cultured in DMEM (with 5% FBS) for 24 hours. Data is expressed as mean ± SEM and analysed using a Mixed model ANOVA with a Dunnett's post hoc test. **P*<0.05 vs. 0ng/ml; n=4-5.

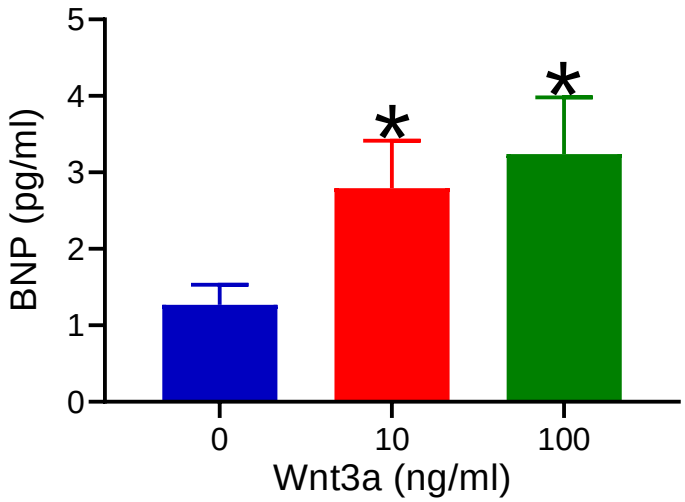

Figure 4.6. BNP secretion from H9c2 cells in response to Wnt3a (10ng/ml and 100ng/ml). Wnt3a, at both concentrations tested, produced a statistically significant increase in the secretion of BNP from H9c2 cells into the cell medium. Data is expressed as mean ± SEM and analysed using a Mixed model ANOVA with a Dunnett's post hoc test. **P*<0.05 vs. 0ng/ml; n=3-7.

4.4.4. sFRP1 does not alter Wnt3a induced upregulation of BNP expression in H9c2 cells

The addition of Wnt3a (100ng/ml) to H9c2 cells produced a significant increase (2.2-fold) in BNP mRNA expression when compared to the control (P<0.05; Figure 4.7.). However, the pre-treatment of H9c2 cells with either concentration (10 and 100ng/ml) of sFRP1 did not significantly alter the Wnt3a induced increase in mRNA expression of BNP (Figure 4.7.).

4.4.5. AngII induced an increase in a hypertrophic marker in H9c2 cells via the induction of Wnt signalling

To determine whether AngII induced the expression of the canonical Wnt ligand, Wnt3a, H9c2 cells were treated with AngII for 24 hours and Wnt3a mRNA expression was measured. The addition of AngII (1µM) induced a significant 2.2-fold increase in the mRNA expression of Wnt3a in comparison to the control (P<0.05; Figure 4.8A.). To investigate whether the PORCN inhibitor, Wnt-c59, altered AngII induced hypertrophy, H9c2 cells were treated with AngII in the absence and presence of Wnt-c59. The addition of AngII (1µM) to H9c2 cells produced a significant (2.3-fold) increase in BNP mRNA expression in comparison to the control (P<0.05; Figure 4.8B.). At a concentration of 10nM, Wnt-c59 did not alter the AngII induced increase in BNP mRNA expression, however increasing the concentration of Wnt-c59 to 1µM abrogated the effect of AngII on BNP mRNA expression (P<0.05; Figure 4.8B.).

4.4.6. Wnt3a induces a marker of hypertrophy in primary human cardiomyocytes

Previous results obtained in this study and others have shown that Wnt3a can induce increases in both ANP and BNP gene expression (markers of hypertrophy) in rodent cardiomyocytes, however no studies to date have investigated whether Wnt3a can alter the expression of hypertrophic markers in HCMs. Wnt3a (100ng/ml) was added to HCMs for 24 hours and mRNA expression of BNP was measured. The addition of Wnt3a to HCMs induced a 1.9-fold increase in BNP mRNA expression in comparison to the control (P<0.05; Figure 4.9.).

4.4.7. AngII does not appear to induce hypertrophy in human cardiomyocytes via the activation of Wnt signalling

To investigate the role of Wnt signalling in AngII induced hypertrophy, HCMs were pre-treated with Wnt-c59 (10nM and 1µM) prior to the addition of AngII (1µM) for 24 hours. The addition of AngII to HCMs produced a 2-fold increase in BNP mRNA expression in comparison to the control (P=0.06; Figure 4.10.), however pre-treatment with either concentration of Wnt-c59 did not significantly alter the AngII induced increase in BNP mRNA expression (Figure 4.10.).

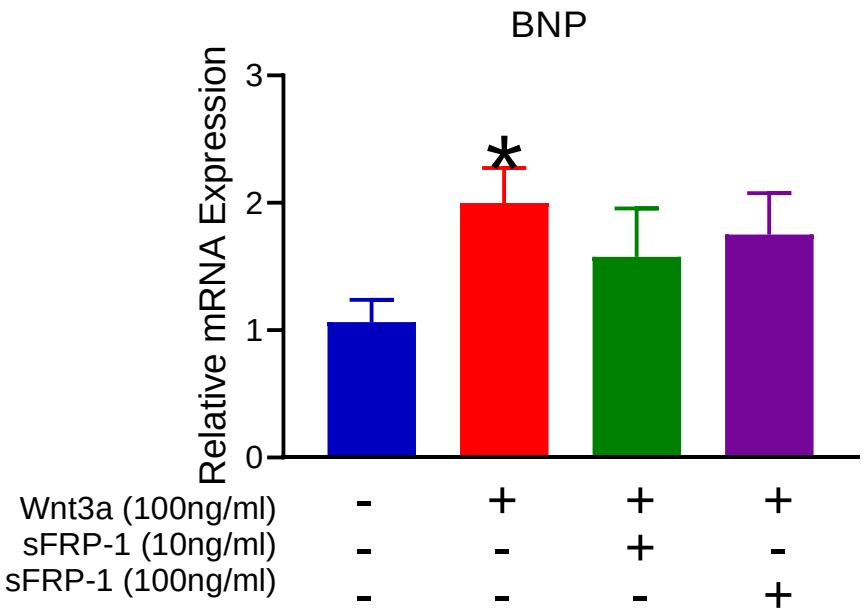

Figure 4.7. BNP mRNA expression in H9c2 cells in response to Wnt3a (100ng/ml) in the absence and presence of sFRP1 (10ng/ml and 100ng/ml). Data is expressed as mean ± SEM and analysed using a Mixed model ANOVA with a Dunnett's post hoc test. **P*<0.05 vs. Control; n=5-7.

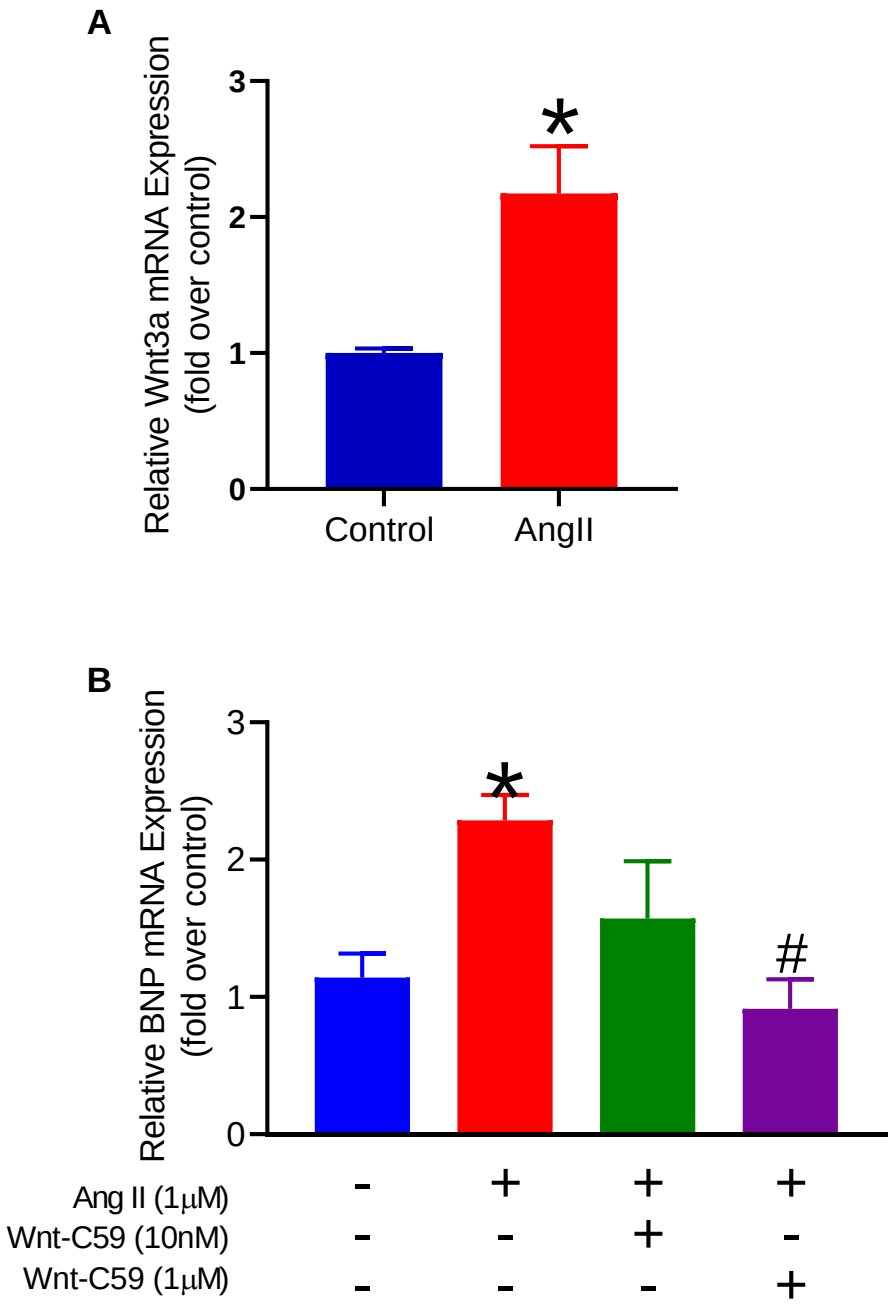

Figure 4.8. AngII upregulates Wnt3a mRNA expression in H9c2 cells, an effect which is attenuated via the co-administration with the PORCN inhibitor, Wnt-c59. (A) AngII (1μM) increases mRNA expression of Wnt3a in H9c2 cells. Data is expressed as mean ± SEM and analysed using a paired *t*-test. (B) BNP mRNA expression in H9c2 cells in response to AngII (1μM) alone or in the presence of Wnt-c59 (10nM and 1μM). Data is expressed as mean ± SEM and analysed using a Mixed model ANOVA with a Dunnett's post hoc test. **P*<0.05 vs. Control; #*P*<0.05 vs. AngII (1μM); n=5-9.

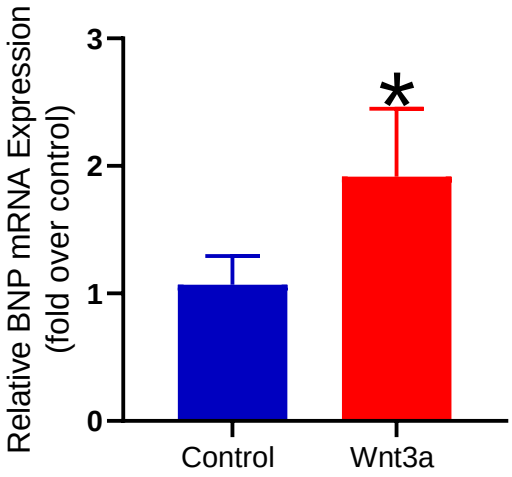

Figure 4.9. BNP mRNA expression in HCMs cells after the addition of Wnt3a (100ng/ml). Data is expressed as mean ± SEM and analysed using a paired *t*-test. **P*<0.05 vs. Control; n=4.

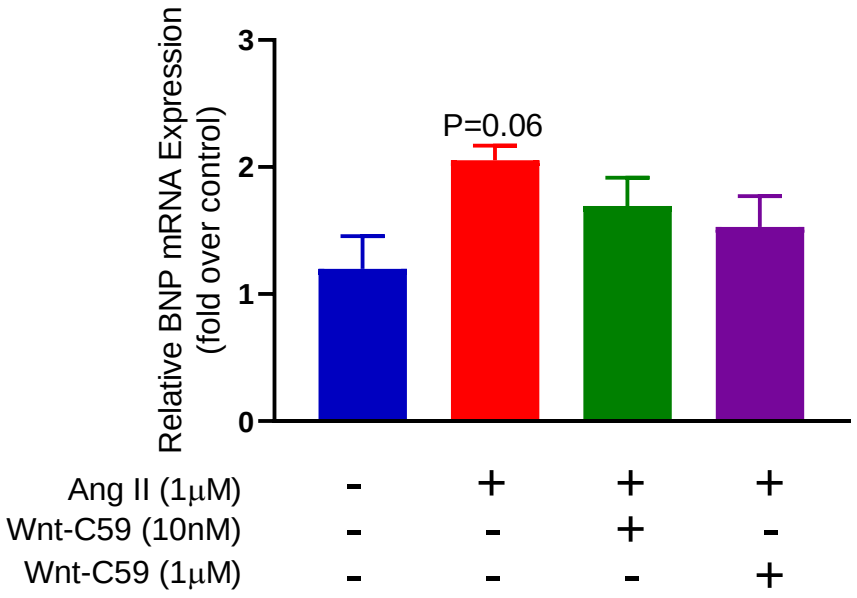

Figure 4.10. BNP mRNA expression in HCMs cells after the addition of AngII (1μM) alone or in the presence of Wnt-c59 (10nM and 1μM). Data is expressed as mean ± SEM and analysed using a Mixed model ANOVA with a Dunnett's post hoc test. n=3.

4.5. Discussion

Previous studies (Chapter 3) identified the optimal culture time (24 hours), concentration of pro-hypertrophic agent (i.e. AngII 1µM), and serum percentage (5% FBS) in cell media for the induction of hypertrophy in H9c2 cells and these experimental parameters were used for the studies detailed in this chapter. The principal aim of this study was to determine whether activation of Wnt signalling either directly (via Wnt3a) or indirectly (AngII) induced a reactivation of the fetal gene programme (i.e. upregulation of the expression of ANP and/or BNP) as an indicator of the presence of cardiomyocyte hypertrophy. The first objective was to identify biologically active concentrations of Wnt3a, Wnt5a, and sFRP1 in H9c2 cells for use in subsequent experiments using *in vitro* models of AngII induced cardiomyocyte hypertrophy (i.e. H9c2 cells and HCMs). The second objective was to explore Wnt signalling in cardiomyocyte hypertrophy using two different antagonists (sFRP1 and Wnt-c59) acting at different points of the Wnt signalling cascade and determine whether they alter the hypertrophic effects induced by AngII and/or Wnt3a.

4.5.1. Use of label free technology for determining biologically active concentrations of Wnt ligands

High throughput screening has become a widely used tool to rapidly and efficiently test a vast number of compounds to identify biological activity and as a consequence is a process essential for successful drug discovery (Szymanski *et al.* 2012). In the present study, the high throughput Corning Epic® System was used for the label-free detection of compound induced biological activity (indicated by changes in DMR activity) in H9c2 cells. This system has been used in a variety of pharmacological studies to date with a range of different seeding densities being used. In particular, neonatal rat cardiac fibroblasts were seeded at 10,000-25,000 cells per well (Carter *et al.* 2014), NRVMs at 20,000 cells per well (Tilley *et al.* 2015), Chinese Hamster Ovary (CHO) cells at 12,500 cells per well (Kebig *et al.* 2009; Schroder *et al.* 2011), HEK293 cells at 15,000 cells per well (Schroder *et al.* 2011), IMR cells at 15,000 cells per well (Klein *et al.* 2016), and most recently H9c2 cells at 25,000 cells per well (Song *et al.* 2017). The present study investigated a range of seeding densities for H9c2 cells (5,000-20,000 cells per well) and determined that the peak response to the positive control, ATP, was achieved when cells were seeded at a density of 10,000 cells per well, and this seeding density was used for the subsequent studies. Throughout the literature there is a lack of information regarding biologically active concentrations of Wnt proteins and inhibitors in mammalian cells and in particular H9c2 cells. Consequently, the Corning Epic® System was used to assess a range of concentrations of Wnt ligands (Wnt3a, Wnt5a, and sFRP1) to rapidly and effectively

detect biologically active concentrations of each ligand in H9c2 cells, while keeping the cost low and reducing the number of cells needed.

Previous research has reported biological activity of Wnt3a in a variety of different cell types over the concentration range (10-100ng/ml) tested in the present study. In particular, Wnt3a, at a concentration of 100ng/ml, was shown to induce differentiation of hESCs into cardiomyocytes as evidenced by their ability to beat in culture and also their expression of several genes characteristic of cardiac cells i.e. ANP, alpha myosin heavy chain (α-MHC)/Mhy6, β-MHC/Myh7, Myl2v, cTnT, and Nkx2.5 (Tran *et al.* 2009; Paige *et al.* 2010). In HEK293T cells, Wnt3a has been shown to be biologically active over a concentration range of 10-200ng/ml, inducing cell proliferation via a β-catenin dependent pathway involving the targeting of CCND1 and c-Myc (Reichmann *et al.* 2015). Moreover, research by Tebroke et al. (2019) reported that at a concentration of 100ng/ml, Wnt3a activated canonical (i.e. β-catenin dependent) Wnt signalling in mature human mast cells leading to the upregulation of interleukin-8 (IL-8) and chemokine ligand 8 mRNA expression. Similar to the published studies, Wnt3a induced a biological response in H9c2 cells at 100ng/ml in the present study, indicating this to be the optimum Wnt3a concentration for use in the subsequent cardiomyocyte hypertrophy studies.

Wnt5a is also a member of the Wnt family but, unlike Wnt3a, is mainly thought to activate non-canonical (i.e. β-catenin independent) signalling through the FZD receptors FZD_2, FZD_4, FZD_5, and FZD_7 (reviewed by Dawson *et al.* 2013). Throughout the literature there are a limited number of studies reporting concentrations of Wnt5a that have been used in a variety of different cell types, though as yet no studies have reported using H9c2 cells. Addition of 1nM (equates to approximately 40ng/ml) recombinant Wnt5a to both mouse and human cardiac fibroblasts has been shown to increase the expression of both IL-6 and TIMP-1, while the same concentration of Wnt5a induced both the activation of NFAT and the release of sFRP3 from neonatal mouse cardiomyocytes (Abraityte *et al.* 2017a). In VSMCs, Wnt5a, at both 200ng/ml and 400ng/ml, induced β-catenin dependent survival signalling in these cells (Mill *et al.* 2014). Furthermore, research by Brown et al. (2019) reported that at a concentration of 400ng/ml Wnt5a significantly decreased H_2O_2-induced apoptosis and increased WISP-1 mRNA in VSMCs from young (2 months old) but not old (18-20 months old) mice. Contrasting results by Yu et al. (2013) demonstrated that Wnt5a at 200ng/ml exerted antiproliferative effects in an experimental model of hypoxia-induced proliferation of human pulmonary artery derived VSMCs by reducing the expression of both β-catenin and its target gene CCND1. In the

present study, Wnt5a did not appear to be biologically active in H9c2 cells (at the concentrations tested) and therefore was not subsequently explored further in this project.

Similar to both Wnt3a and Wnt5a, the action of sFRP1 in H9c2 cells has not previously been explored based on current literature. However, rat VSMCs treated with 10nM (equates to approximately 320ng/ml) sFRP1 exhibited a delay both within the G1 phase and subsequent entry into the S-phase, as well as a decrease in the expression of both the cyclins and cyclin-dependent kinases that control the cell cycle (Ezan *et al.* 2004). At lower concentrations (25-100ng/ml) and within the range examined in the present study, sFRP1 decreased dexamethasone induced osteogenesis in primary mesenchymal cells (Wang *et al.* 2005) and increased the expression of MMP9 in small airway epithelial cells (Foronjy *et al.* 2010). At considerably higher concentrations (400ng/ml-10µg/ml), sFRP1 induced the differentiation of human TH17 cells (Lee *et al.* 2012) and reduced the migration of human MDA-MB-231 breast cancer cells (Klemm *et al.* 2011). As the literature demonstrates, a range of different concentrations of sFRP1 are active in a variety of different cells types, however the present study is the first to demonstrate that over a concentration range of 10-100ng/ml sFRP1 is biologically active in H9c2 cells.

4.5.2. The addition of Wnt3a induced changes in hypertrophic markers in H9c2 cells, an effect which was not altered by pre-treatment of sFRP1

Recent research by Zhao et al. (2018) demonstrated that AngII increases the expression of Wnt3a in NRVMs and that the addition of Wnt3a (100ng/ml) to NRVMs induces hypertrophy as indicated by the increased expression of ACTA1 and β-MHC which are known hypertrophic markers. Findings from the present study agree with those of the latter demonstrating for the first time that Wnt3a (100ng/ml) induces hypertrophy in rat H9c2 cells. While neither study investigated whether this pro-hypertrophic effect of Wnt3a involved activation of canonical Wnt signalling it seems likely as Wnt3a has previously been shown to increase the expression of the Wnt target genes Axin2 and Lef1 in NRVMs (Liang *et al.* 2015) and β-catenin expression has frequently been shown to be upregulated in hypertrophic cardiomyocytes (Zelarayan *et al*. 2007).

Research has shown that both sFRP1 and sFRP2 inhibit Wnt3a-induced accumulation of β-catenin in enteroendocrine L cells, whereas sFRP3 does not (Galli *et al.* 2006). Furthermore, the addition of AngII to NRVMs downregulated the protein expression of sFRP2, while treatment with 15nM (approximately equating to 470ng/ml) sFRP2 attenuated AngII induced cardiomyocyte hypertrophy (Wei *et al*. 2019). In a TAC mouse model, a recombinant adeno-

associated virus 9 vector was used to deliver sFRP1 into the myocardium which resulted in improved systolic and diastolic cardiac function, as well as a reduction in the protein expression of β-catenin (Pan *et al*. 2018). In the present study, pre-treatment with sFRP1 (10 and 100ng/ml) did not alter Wnt3a induced hypertrophy in H9c2 cells, despite both concentrations of sFRP1 previously demonstrating biological activity (as indicated by the change in DMR activity) in these cells. A possible explanation for this lack of inhibitory effect of sFRP1 could be that the concentrations used in this study although biologically active were insufficient to antagonise Wnt3a mediated signalling as the latter appears to be both concentration and cell type dependent. A study by Xavier et al. (2014) investigated the influence of both concentration and cell type on the ability of sFRP1 to alter Wnt3a mediated activity. They reported that, while nanomolar concentrations of sFRP1 (32.6ng/ml-326ng/ml) increased the luciferase reporter activity of Wnt3a, higher concentrations (3.26µg/ml and 9.78µg/ml) inhibited the luciferase activity of Wnt3a in HEK293 cells. In C57MG cells, low concentrations of sFRP1 (97.8ng/ml and 326ng/ml) enhanced Wnt3a luciferase activity signalling, however at a higher concentration (i.e. 9.78 µg/ml) sFRP1 decreased the luciferase activity of Wnt3a. Furthermore, all concentrations of sFRP1 (97.8ng/ml, 326ng/ml, and 9.78µg/ml) tested antagonised Wnt3a mediated effects in L929 fibroblasts. Finally, the expression of sFRP1 also increased luciferase reporter activity in L cells that were engineered to express FZD_5, though not FZD_2 suggesting that FZD expression pattern could also determine the effect of sFRP1 (Xavier *et al.* 2014). The mechanisms via which sFRP1 regulates Wnt3a activity is also varied, as both sFRP1 and sFRP2 have been shown to directly bind to Wnt3a and inhibit its activity (Wawrzak *et al.* 2007). However, a more recent study demonstrated that sFRP1 can negatively regulate β-catenin signalling by binding to β-catenin in the nucleus without interacting with Wnt3a extracellularly (Liang *et al.* 2019), demonstrating that the regulation of Wnt3a signalling by sFRP1 has yet to be fully elucidated.

4.5.3. Wnt-c59 inhibited AngII induced changes in hypertrophic markers in H9c2 cells

In the present study, AngII increased the mRNA expression of Wnt3a in H9c2 cells, which agrees with previous research demonstrating that both a 4 week infusion of AngII in rats and treatment of NRVMs with AngII lead to the increased expression of a number of Wnts including Wnt3a (Zhao *et al.* 2018). Due to the findings that AngII upregulates the expression of both Wnt3a and BNP, the latter being indicative of the presence of cardiomyocyte hypertrophy, in H9c2 cells, the role of Wnt signalling in AngII induced cardiomyocyte hypertrophy was examined with the use of a pharmacological inhibitor of Wnt signalling i.e. the PORCN inhibitor Wnt-c59. As Wnt-c59 had not been previously used to inhibit PORCN in H9c2 cells, the literature was consulted to determine appropriate concentrations for use in this study. Dey et

al. (2013) reported that at a concentration of 10nM Wnt-c59 inhibited integrin-directed migration and invasion of MDA-MB-231 cells providing evidence that Wnt signalling is upregulated in triple negative breast cancer. At a concentration of 10nM, Wnt-c59 reduced the Super8xTopFlash luciferase activity of nine canonical Wnt ligands and four non-canonical Wnt ligands in HT1080 cells (Proffitt *et al.,* 2012) and decreased Wnt signalling in HEK293T cells as evidenced by a reduction in the cytosolic expression of β-catenin protein and phosphorylated Dvl (Rios-Esteves and Resh 2013). The highest concentration of Wnt-c59 identified in the literature was 1μM in hCMEC/D3 cells which reduced β-catenin protein expression by 40% compared to control cells and reduced Axin2 gene expression by 80%, indicating reduced canonical Wnt signalling (Laksitorini *et al.* 2019). Based on the literature, two concentrations of Wnt-c59 (10nM and 1μM) were used in an attempt to inhibit PORCN and prevent any AngII mediated Wnt signalling. Data from the present study is the first study to demonstrate that Wnt-c59 reduced AngII induced hypertrophy in H9c2 cells in a concentration dependent manner, indicating that activation of Wnt signalling contributes to AngII induced cardiomyocyte hypertrophy. These findings agree with a recently published study in which Wnt-c59 attenuated AngII induced hypertrophy in NRVMs (as demonstrated by both decreased cell size and reduced expression of ANP, BNP, and β-MHC), however in the present study the effect was achieved at the lower concentration of 10nM (Zhao *et al.* 2020).

A growing body of research suggests that cross-talk exists between the Wnt signalling system and the RAAS (Yun *et al.* 2005; Zhou *et al.* 2015; Zhou and Liu 2016; Jeong *et al.* 2018), which may potentially explain how a Wnt signalling inhibitor (Wnt-c59) can inhibit cardiomyocyte hypertrophy induced by AngII. RAAS comprises of five distinct components which include renin, AGT, ACE, and the AT_1 and AT_2 receptors. In HKC-8 cells (a human-derived renal proximal tubular epithelial cell line), the ectopic expression of numerous Wnt ligands (Wnt1, Wnt2, Wnt3a, Wnt5a, Wnt5b, Wnt6, Wnt7b, and Wnt9a) significantly increased AGT mRNA expression and the overexpression of β-catenin significantly increased the mRNA expression of AGT, renin, ACE, AT_1R, and Ang II type 2 receptor (AT_2R). Furthermore, treatment of HKC-8 cells with ICG-001 (Wnt signalling inhibitor) resulted in a reduction in both the mRNA and protein expression of a number of RAAS mediators including AGT, renin, ACE, and AT_1R (Zhou *et al.* 2015). Work by Cuevas et al. (2015) also demonstrated that treatment of M-1 cells (a mouse-derived cortical collecting duct epithelial cell line) with AngII increased mRNA and protein levels of Col1 and Fn1, as well as an induction of the β-catenin target genes CCND1 and c-Myc, which was then subsequently prevented by treatment with the AT_1R blocker, Candesartan. More recently, a study by Zhao et al. (2019a) investigated the role of Wnt signalling in both the heart and kidney in a TAC mouse model of pressure overload. In this

study mice subjected to TAC surgery were characterised by cardiac hypertrophy and fibrosis, as well as left ventricular systolic and diastolic dysfunction. It was also shown that TAC surgery induced increased mRNA expression of multiple Wnt ligands (Wnt1, Wnt3a, Wnt7a, Wnt8b, Wnt10b), as well as an increase in the protein expression of Wnt1, Wnt3a, and β-catenin in the hearts of these animals. Furthermore, treatment with ICG-001 reduced the protein levels of β-catenin, Col1, Fn1, and TNF-α in the hearts of TAC mice. The study also reported that Wnt3a upregulated multiple RAAS components including protein expression of ACE, AGT, AT_1R, and renin in primary cardiomyocytes and increased protein expression of ACE, AGT and AT_1R in primary cardiac fibroblasts, with the expression reduced by ICG-001. In this model, canonical Wnt signalling also appeared to be activated in the renal system as the expression of β-catenin was increased and the expression of Klotho (an endogenous inhibitor of Wnt signalling) decreased in the kidneys of mice subjected to TAC surgery. In an *in vitro* model using Madin-Darby canine kidney cells the addition of AngII (1nM) decreased the gene expression of Klotho which was reversed by the addition of losartan. Furthermore, a decrease in gene and protein expression of Klotho in a 5/6 nephrectomy rat model resulted in an increase in gene expression of Wnt3 and Wnt7a, which was subsequently decreased via the addition of the ARB, Losartan (Maquigussa *et al*. 2018). Furthermore, in a mouse model of TAC induced pressure overload Captopril (ACE inhibitor) reduced the protein expression of both Wnt3a and β-catenin in the heart (Zhang *et al*. 2019). Based on the literature and the novel findings from this study it is possible that Wnt3a induced activation of canonical Wnt signalling leads to an increase in β-catenin accumulation in cardiomyocytes/renal cells, which then subsequently activates downstream mediators of RAAS (including AngII) leading to further exacerbation of cardiomyocyte hypertrophy via a detrimental feedback loop.

4.5.4. The role of Wnt signalling in AngII induced hypertrophy in HCMs

Throughout the literature there are several lines of evidence to suggest that Wnt signalling is upregulated in patients with various cardiac diseases. Abraityte et al. (2017b) demonstrated that systemic and myocardial Wnt5a was elevated in HF patients, supporting a role for non-canonical Wnt signalling activation in HF. Plasma levels of sFRP1 have been shown to be increased in patients with CAD (Guo *et al.* 2017), while sFRP3 was shown to be elevated in the circulation of patients with clinical HF (Askevold *et al.* 2014). Sklepkiewicz et al. (2015) demonstrated that the gene expression of sFRP1 was decreased while Wisp1, a Wnt target gene, was increased in ventricular tissue from patients with DCM indicating activation of canonical Wnt signalling in these patients. Furthermore, the activity of GSK-3β, an enzyme essential for the negative regulation of canonical Wnt signalling via the phosphorylation of β-catenin, was significantly reduced in cardiac tissue from patients with idiopathic DCM (Haq *et*

al. 2001). Taken together, these observations suggest a potential detrimental role for Wnt signalling in CVD.

The majority of studies exploring the role of Wnt signalling in HCMs have either focused on the role of this system in the differentiation of hiPSCs into mature HCMs (Lian *et al.* 2012; Mazzotta *et al.* 2016; Zhao *et al.* 2019b) or the ability of Wnt signalling to reactivate the proliferative capacity of mature HCMs (Fan *et al.* 2018). In contrast, there is very limited research to date investigating a causal role for Wnt signalling in pathophysiological mechanisms involved in CVD using HCMs, and in particular studies examining cardiomyocyte hypertrophy. Consequently, the present study investigated the role of Wnt signalling in AngII induced HCM hypertrophy. Similar to the experiments conducted in H9c2 cells, HCMs were treated with AngII in both the absence and presence of Wnt-c59 and the presence of hypertrophy assessed via BNP mRNA expression. The results demonstrated that AngII induced a 2-fold increase in BNP mRNA expression and, following the addition of the higher concentration of Wnt-c59 this increased BNP mRNA expression was reduced by approximately 50%, although neither effect was found to be statistically significant. However, caution must be exercised when concluding whether or not Wnt signalling mediates AngII induced hypertrophy in HCMs as only one measure of hypertrophy was assessed i.e. BNP expression. In support of this, a recent study that investigated I/R injury in AC16 human cardiomyocytes (proliferating cell line formed via the fusion of primary cardiomyocytes with SV40 transformed, uridine auxotroph human fibroblasts, devoid of mitochondrial DNA) detected an increase in the gene expression of Myh7 following I/R, while BNP expression was not altered (Khan *et al*. 2019). Therefore, it would have been of interest to determine Myh7 expression in HCMs in the present study. The present study is the first to demonstrate that Wnt3a induces hypertrophy in human cardiomyocytes demonstrated by the increased mRNA expression of BNP in response to this canonical Wnt ligand. Therefore, given the somewhat inhibitory (albeit not significant) effect of Wnt-c59 on AngII induced hypertrophy in HCMs it seems plausible to suggest that the findings in the rat H9c2 cells may translate to the human cardiomyocytes and AngII may induce hypertrophy in part via upregulation of Wnt3a. Taken together, this study is the first to implicate a potential causal role for AngII induced activation of Wnt signalling in human cardiomyocyte hypertrophy (shown by an increase in BNP gene expression).

4.6. Conclusion

In conclusion, the results demonstrate that Wnt3a, which primarily activates canonical Wnt signalling, induces hypertrophy in H9c2 cells characterised by both an increase in the mRNA expression of ANP and BNP, as well as an increase in the secretion of BNP protein, which as

of yet has not previously been shown in H9c2 cells. Furthermore, the pre-treatment of H9c2 cells with Wnt-c59 prior to the addition of AngII significantly reduced the mRNA expression of BNP, which has only been shown in NRVMs, demonstrating that AngII, at least in part, induces cardiomyocyte hypertrophy via the activation of Wnt signalling. This is the first study to identify that AngII appeared to induce the expression of a marker of hypertrophy in HCMs via the activation of Wnt signalling though this requires further investigation. Finally, Wnt3a induced an increase in the hypertrohic marker BNP in HCMs and as of yet no other studies have identified the potential of Wnt3a to increase hyperterophic markers in HCMs. Subsequent chapters have therefore investigated whether Wnt signalling is upregulated in an *in vivo* model of HFpEF and consequently whether administration of Wnt-c59 alters any observed adverse structural and/or functional effects present in this HFpEF model.

Chapter 5: Characterisation of a ‘two-hit’ experimental model of HFpEF

5.1. Introduction

Patients with HFpEF also tend to have a range of comorbidities, such as HTN, obesity, and T2DM, therefore therapeutic intervention is based largely on individual biological phenotypes and the treatment of those associated co-morbidities. One of the critical obstacles to therapeutic innovation in HFpEF is the lack of suitable animal models that encapsulate the complexity and comorbidities associated with this disease. Recently, Bai et al. (2019) suggested that an ideal experimental model of HFpEF should exhibit at least two or more of the following pathophysiological features i.e. concentric hypertrophy, diastolic dysfunction, and/or impaired exercise activity, while Valero-Munoz et al. (2017) suggested that the model should also exhibit pulmonary oedema in addition to a preserved EF. Furthermore, ideally an animal model of HFpEF should also be characterised by one or more of the most common co-morbidities (HTN, obesity, and/or T2DM). A recently published review by Withaar et al. (2021a) comprehensively details the characteristics/features of the most common experimental animal models used to study HFpEF and these findings are summarised in Table 5.1. Several of these animal models are described in more detail below.

5.1.1 Hypertensive models of HFpEF

HTN is one of the main comorbidities associated with HFpEF and an estimated 28% of adults in the UK have high BP, equating to around 15 million adults (BHF 2021). The latter occurs as a result of both endothelial dysfunction due to impaired activity of endothelial NO synthase (eNOS) (Konukoglu and Uzun 2017) and arterial stiffness (Safar *et al*. 2018). BP can be a major contributor to the induction of LV structural alterations with an increase in BP being correlated with LV hypertrophy in later life (Ghosh *et al*. 2014). Increased BP has also been shown to induce detrimental changes in cardiomyocytes and fibrotic changes resulting in adverse cardiac remodelling (Tomek and Bub 2017).

5.1.1.1. AngII infused mouse

The infusion of AngII in mice has been shown to lead to cardiac hypertrophy and remodelling, both in the presence (Becher *et al*. 2012; Glenn *et al*. 2015; Shen *et al*. 2016; Cambier *et al*. 2018) and absence (Matsumoto *et al*. 2013; Regan *et al*. 2015) of HTN. It seems possible that changes in BP are likely dependent upon both the dose and duration of AngII infusion as studies have used doses ranging from 0.2mg/kg/day to 1.4mg/kg/day (Regan *et al*. 2015; Li *et al*. 2019) over time periods of 2 to 4 weeks. The induction of cardiac hypertrophy by AngII infusion also appears to be influenced by the strain of mouse used, since C57Bl/6J mice exhibit compensatory concentric hypertrophy in response to AngII (Essick *et al*. 2013), while

Table 5.1. Key features present in currently used animal models of HFpEF. Table is adapted from Withaar et al. (2021a) and references used to create the table are documented in the original review. pEF, preserved ejection fraction; HTN, hypertension; T2DM, type 2 diabetes mellitus; LA, left atrial; LV left ventricle; HFD, high fat diet; AngII, angiotensin II; SAMP, accelerated senescence model; DOCA, deoxycorticosterone acetate; L-NAME, N_{ω}-Nitro-L-arginine methyl ester hydrochloride; DOCP, desoxycorticosterone pivalate.

Model	pEF	Sex	Age (months)	Lung congestion	↓ exercise capacity	HTN	Obesity	T2DM	Renal dysfunction	Diastolic dysfunction	↑ LA	↑ LV mass	↑ LV wall thickness	Concentric hypertrophy	↑ natriuretic peptides
Aldosterone uninephrectomy mouse	Yes	M	3	Yes	Yes	Yes	Yes	Yes	N/A	Yes	N/A	Yes	Yes	Yes	Yes
HFD	Yes	M/F	3-16	Yes	Yes	Yes	Yes	Yes	No	Yes	N/A	Yes	Yes	Yes	No
Aged mice	Yes	M	24-30	Yes	No	No	No	No	No	Yes	N/A	Yes	Yes	Yes	Yes
AngII infused model	Yes	M/F	3	Yes	Yes	Yes	No	No	No	Yes	N/A	Yes	Yes	Yes	Yes
SAMP model	Yes	F	3-12	No	Yes	Yes	No	No	N/A	Yes	Yes	Yes	Yes	Yes	Yes
db/db model	Yes	M/F	3	No	Yes	Yes	Yes	Yes	No	Yes	Yes	Yes	Yes	Yes	No
ob/ob model	Yes	M/F	3	No	Yes	No	Yes	Yes	No	Yes	No	Yes	Yes	Yes	No
DOCA model	Yes	M	3	No	No	Yes	No	No	No	Yes	N/A	Yes	Yes	Yes	Yes
HFD+AngII Infused model	Yes	M	3	No	No	Yes	Yes	Yes	N/A	Yes	N/A	Yes	Yes	Yes	Yes
HFD+L-NAME	Yes	M/F	3	Yes	Yes	Yes	Yes	Yes	N/A	Yes	Yes	Yes	Yes	Yes	Yes
Aging, HFD and AngII	Yes	F	22	Yes	Yes	Yes	Yes	Yes	Yes	Yes	Yes	Yes	Yes	Yes	Yes
Aging, HFD and DOCP	Yes	M/F	18	Yes	Yes	Yes	Yes	Yes	N/A	Yes	Yes	Yes	Yes	Yes	Yes

Balb/c mice exhibit severe LV chamber dilatation which is considered more of a feature of DCM (Peng *et al.* 2011). Furthermore, while several studies have demonstrated that the AngII infused mouse model is characterised by diastolic dysfunction (Xu *et al*. 2008; Jia *et al.* 2012; Misaka *et al.* 2013; Fan *et al.* 2014; Choi *et al.* 2016; Kamiya *et al*. 2021), numerous studies have also demonstrated that this diastolic dysfunction is often accompanied by systolic dysfunction (Becher *et al*. 2012; Westermann *et al.* 2012; Divorty *et al.* 2018; Wu *et al.* 2018). Exercise intolerance related to both mitochondrial dysfunction and skeletal muscle atrophy has also been shown in AngII infused mice (Kadoguchi *et al*. 2015), however evidence of pulmonary congestion appears to be controversial (Barhoumi *et al*. 2017; Withaar *et al*. 2021b). Another common feature associated with HFpEF that does not appear to be present in AngII infused mouse models is obesity, with studies demonstrating either no change or a reduction in BW in AngII infused mice compared to controls (Peng *et al.* 2011; Regan *et al*. 2015). However, studies are now combining AngII infusion in mice with the co-administration of a HFD in order to induce both diastolic dysfunction and obesity in the same animals (Withaar *et al*. 2021b). Moreover, high fat feeding has been shown to disrupt glucose homeostasis via an increase in RAAS activity (Chodavarapu *et al*. 2016), which suggests that this co-treatment (AngII infusion and high fat feeding) model may also be characterised by T2DM.

5.1.1.2. Aldosterone infused and unilateral nephrectomised mouse model

Previous studies have shown that the combination of uninephrectomy (i.e. surgical excision of one kidney), aldosterone infusion, and 1% sodium chloride administration in rats and mice resulted in increased BP, in addition to cardiac hypertrophy and fibrosis (Blasi *et al*. 2003; Sawada *et al*. 2015; Shuai *et al*. 2020). Animals subjected to this model develop HTN, concentric LV hypertrophy, pulmonary congestion, echocardiographic evidence of diastolic dysfunction, a preserved EF, and exercise impairment (Wilson *et al*. 2009). At the molecular level, these animals exhibit an increase in the expression of natriuretic peptides (ANP and BNP) and an increase in the titin transcript variants N2BA and N2B, which play an important role in regulating diastolic stiffness (Valero-Munoz *et al*. 2016). Although this model contains many features of HFpEF, with the exception of HTN, it doesn't exhibit any of the other commonly associated co-morbidities.

5.1.1.3. Deoxycorticosterone acetate (DOCA) salt rodent model

The administration of DOCA to rodents leads to an imbalance in renal sodium handling by the kidneys, which leads to greater amounts of water and sodium being reabsorbed resulting in hypervolemia. Furthermore, in addition to DOCA administration animals are also often

subjected to both a high-salt diet (0.6-1% sodium chloride in drinking water) and uninephrectomy, with the combination resulting in chronically high BP levels (Bae *et al*. 2012; Baumann *et al*. 2020). This experimental model is characterised by HTN, cardiac hypertrophy, and perivascular fibrosis (Grobe *et al*. 2006). Regarding its suitability as a HFpEF model, it has been shown that uninephrectomised rats exhibit concentric hypertrophy with severe restrictive diastolic dysfunction in the presence of a preserved EF following 28 days of DOCA administration (Allan *et al.* 2005). Moreover, Connelly et al. (2019) showed that rats administered DOCA with 1% sodium chloride displayed increased cardiac overload, increased LV mass, cardiomyocyte hypertrophy, interstitial cardiac fibrosis, and diastolic dysfunction. However, unlike rats, the induction of HTN in DOCA treated mice is somewhat inconsistent (Lovelock *et al.* 2012). In a comparison study, separate groups of mice were either 1) administered DOCA alone; 2) subjected to TAC induced pressure overload; or 3) administered DOCA in the presence of TAC. Mice administered DOCA alone exhibited mild cardiac hypertrophy without fibrosis and no changes in either diastolic function or BP. Conversely, mice subjected to TAC alone displayed cardiac hypertrophy and diastolic stiffness, while those subjected to both TAC and DOCA administration were characterised by more pronounced cardiac hypertrophy and exhibited cardiac fibrosis, diastolic dysfunction, and increased lung weights all of which is consistent with HFpEF (Mohammed *et al.* 2010). Although some studies have shown that the DOCA mouse model displays diastolic dysfunction, preserved systolic function, and exercise intolerance (Silberman *et al*. 2010; Jeong *et al*. 2013), they have been unable to demonstrate pulmonary congestion in this model nor is it characterised by either of the comorbidities of T2DM or obesity.

5.1.2. Obese and/or diabetic mouse models of HFpEF

Obesity is a major risk factor for the development of HFpEF and approximately 28% of all adults in the UK are classed as obese while 36% have a BMI categorised as overweight (BHF 2021). There are various mechanisms in which obesity could contribute to HFpEF, with increased adiposity inducing inflammation, insulin resistance, dyslipidaemia, endothelial dysfunction and vascular changes (Ebong *et al*. 2014). T2DM is also one of the main comorbidities associated with HFpEF and more than 4 million people in the UK are currently diagnosed with T2DM (BHF 2021), which is likely to be an underestimate due to many cases of T2DM being undiagnosed. Some of the key pathophysiological mechanisms evident in diabetic patients include systemic insulin resistance and hyperglycaemia, which can induce cardiac insulin resistance and neurohormonal, sympathetic, and cytokine imbalances in the heart (Rosano *et al*. 2017). Furthermore, pathophysiological features common to both obesity and T2DM (i.e. insulin resistance, inflammation, endothelial dysfunction etc.) have all been

shown to contribute to adverse cardiac remodelling, as evidenced by the presence of cardiac hypertrophy and/or cardiac fibrosis in experimental models of these conditions (Russo and Frangogiannis 2016). Finally, as high fat feeding to induce obesity and hyperglycaemia in mice does not necessarily induce cardiac dysfunction, many researchers use genetic obesity/diabetic mouse models to understand cardiac defects related to risk factors (Brainard *et al*. 2013).

5.1.2.1. db/db mouse model

The *db/db* mouse model is a leptin receptor deficient (created via a point mutation in the gene encoding the leptin receptor) mouse, which is characterised by increased adiposity and severe hyperglycaemia. In addition to being both obese and diabetic, at 6 months of age these animals exhibit decreased vascular compliance, increased LV stiffness (Reil *et al*. 2013), and evidence of both enlarged cardiomyocytes and cardiac fibrosis (Alex *et al*. 2018). However, these mice do not initially display cardiac hypertrophy, as research by Reil et al. (2013) demonstrated that 11 week old *db/db* mice did not exhibit any changes in heart weight (normalised to tibia length (TL)) or show any signs of myocardial hypertrophy or fibrosis. *db/db* mice have also been shown to display diastolic dysfunction with preserved EF (Alex *et al*. 2018) and pulmonary congestion (shown by an increase in lung weight; Papinska *et al*. 2016), however some studies have demonstrated that myocardial expression of markers of hypertrophy (ANP, BNP, and Myh6) are reduced in this model compared to control animals (Gutkowska *et al*. 2009; Broderick *et al*. 2012).

5.1.2.2. ob/ob mouse model

The *ob/ob* leptin deficient mouse is characterised by both obesity and T2DM (Lindstrom 2007). These mice have also been shown to develop concentric hypertrophy coupled with diastolic dysfunction, while systolic function does not appear to be altered (Christoffersen *et al*. 2003). BP measurements have been shown to be variable, with either hypotension or no changes in BP being reported in these mice (Barouch *et al*. 2003; Christoffersen *et al*. 2003; Dong *et al*. 2006; Silvani *et al*. 2009; Simonds *et al*. 2014). Data indicates that EF is preserved in this model however, and like the *db/db* mouse myocardial expression of BNP is either unchanged or slightly reduced in comparison to control mice (Broderick *et al*. 2014; Manolescu *et al*. 2014). One of the main limitations of this experimental model is that leptin deficiency is rarely seen in obese patients with HFpEF (reviewed by Clement 2006).

5.1.3. 'Two-hit' experimental model of HFpEF

Due to the complex comorbidities associated with HFpEF and clinical data suggesting that an imbalance of NO levels in the vasculature is crucial for the development of HFpEF (Chirinos and Zamani 2016), a new 'two-hit' (metabolic and mechanical stress) experimental model of the condition has been developed (Schiattarella *et al.* 2019). In this experimental model, metabolic stress is induced by subjecting mice to a HFD while mechanical stress is induced via the simultaneous administration of N_{ω}-Nitro-L-arginine methyl ester (L-NAME) to suppress all NOS isoforms (i.e. inducible NOS (iNOS), neuronal NOS (nNOS), and eNOS), and induce HTN. Following 5 or 15 weeks of co-administration of L-NAME and a HFD diet to male mice, these animals are characterised by elevated SBP and DBP, increased BW/adiposity, glucose intolerance, cardiac hypertrophy and fibrosis, and evidence of pulmonary congestion (Schiattarella *et al.* 2019). At a functional level, echocardiographic data showed that these animals had a preserved EF and elevated filling LV pressures, in addition to increases in both the E/A and E/e' ratios, demonstrating the presence of diastolic dysfunction. Finally, this study also demonstrated that the mice were characterised by both pulmonary congestion and impaired exercise performance (Schiattarella *et al*. 2019). Interestingly, this study also demonstrated that on their own, neither high fat feeding nor L-NAME administration, were sufficient to induce the HFpEF phenotype which agrees with other published studies (Okazaki *et al.* 2006; Martins *et al.* 2015; Matias *et al*. 2020). Other studies have utilised this HFpEF model with one such study concluding that the diastolic dysfunction observed in these animals is associated with endothelial dysfunction (Cornuault *et al*. 2021). Furthermore, although cardiac function was not measured, two studies by Cordero-Herrera et al. (2019 & 2020) demonstrated that HFD+L-NAME treated mice exhibit HTN, endothelial dysfunction, and insulin resistance. While more recent studies by Kitakata et al. (2021) and Huang et al. (2021), which did assess cardiac function, demonstrated that this HFpEF model is characterised by obesity, impaired glucose tolerance, cardiac hypertrophy and fibrosis, as well as diastolic dysfunction, demonstrating the reproducibility of this experimental model in the hands of other researchers. Finally, sex-dependent effects have also been investigated in this model, where it was shown that female mice were more resistant to the effects of the HFD and L-NAME intervention and only develop some (diastolic dysfunction and impaired exercise performance), but not all (cardiac hypertrophy and pulmonary congestion) of the key features of HFpEF (Tong *et al*. 2019). Furthermore, ovariectomised female mice exhibited a similar muted response to the HFD and L-NAME intervention as regards to developing HFpEF, indicating that the latter is not due to the potential cardioprotective effects of oestrogen (Tong *et al*. 2019). Therefore the 'two-hit' experimental model first presented by Schiattarella et al. (2019) encapsulates many of the key structural and functional features of HFpEF making it a promising preclinical model for HFpEF based research.

5.1.4. Aim

Previous chapters have shown that Wnt3a can induce hypertrophy (a key feature of HFpEF) in H9c2 cells and the addition of Wnt-c59 (an inhibitor of Wnt signalling) reduced AngII induced hypertrophy. Wnt signalling has been investigated in both AngII and TAC induced pressure overload models, however as of yet has not been investigated in an experimental model of HFpEF. The aim of the present study was to establish the 'two-hit' experimental model of HFpEF in our lab and subsequently investigate whether there was any evidence of the activation of Wnt signalling in this model prior to the investigation of the role of this pathway in HFpEF via an intervention study.

5.2. Methods

All necessary methodological detail is either described in the following section 5.3. Experimental Protocols or in Chapter 2 as indicated.

5.3. Experimental Protocols

A pilot study was initially carried out to investigate whether high fat feeding and L-NAME administration in mice induced activation of Wnt signalling prior to conducting a larger intervention study investigating the role of this signalling system in HFpEF (see Chapter 6). The pilot study design is described below in section 5.3.1.

5.3.1. Pilot Study Design

Fourteen (9-19 weeks old) C57Bl/6J male mice were obtained from the Medical Research Facility, University of Aberdeen and allowed to acclimatise in the BSU at RGU for one week before dietary intervention was commenced. To induce metabolic stress (obesity and metabolic syndrome) in animals, 7 mice were randomly assigned to receive a HFD (D12492 Research Diet) while the other 7 animals were given a matched control diet (D12450J Research Diet) for a period of 5 weeks. Full nutritional details/composition of each diet is included in Table 5.2. To induce mechanical stress, L-NAME (0.5g/L) was given in drinking water (bottles covered to protect light sensitive L-NAME) to the HFD fed group and changed every 2-3 days. The preparation of L-NAME is described in Chapter 2, section 2.12. Food intake, water intake, and BW were all measured weekly. A schematic of the pilot study design is shown in Figure 5.1.

5.3.2. Measurement of arterial BP for the detection of hypertension

After 5 weeks of dietary intervention arterial BP was measured (as described in Chapter 2, section 2.5.2.2.) to determine if mice were hypertensive. Once BP measurements had been obtained, the catheter was gently removed, and the carotid artery securely tied off to prevent blood loss. Blood was then collected via cardiac puncture under terminal anaesthesia and tissues were taken post-mortem from all mice for subsequent molecular analysis. A total of six readings for both SBP and DBP were taken from the LabChart recording and averaged. To calculate MABP the equation below was used:

Equation 13: **MABP = ((SBP – DBP) x 0.33) + DBP**

5.3.3. Investigation of the presence of markers of hypertrophy, fibrosis, and/or Wnt signalling via gene expression studies

To determine the effects of co-administration of a HFD and L-NAME on markers of cardiac hypertrophy, fibrosis, and/or Wnt signalling a series of gene expression studies were conducted. Approximately 30mg of both cardiac and adipose tissues were placed in microcentrifuge tubes containing 1ml of Tri-reagent and RNA extracted as described in Chapter 2, section 2.3.1. RNA concentration was measured (Chapter 2, section 2.3.2) and converted to cDNA using the method stated in Chapter 2, section 2.3.3. To measure gene expression, qPCR was conducted (Chapter 2, section 2.3.5.) with Sigma Aldrich primer sequences shown below in Table 5.3. Primers bought from Sigma Aldrich were designed using the NCBI primer blast tool https://www.ncbi.nlm.nih.gov/tools/primer-blast/ with a product size of between 70-200bp and the primer spanning an exon-exon junction. Furthermore, primers were also selected on the basis that they contained either a C or G residue at the 3' end, had a GC content of approximately 40-60% to ensure product stability, and the lowest self-complementarity to reduce the chance of primer-dimer formation. QuantiTect primers bought from Qiagen do not have primer sequences available, however catalogue numbers are listed in Table 5.4. Prior to being used in gene expression studies, primer product sizes were confirmed as described in Chapter 2, section 2.3.4. and primer efficiencies calculated as per section Chapter 2, section 2.3.5.1. Primer efficiencies for both Sigma and Qiagen primers ranged from 86-141%.

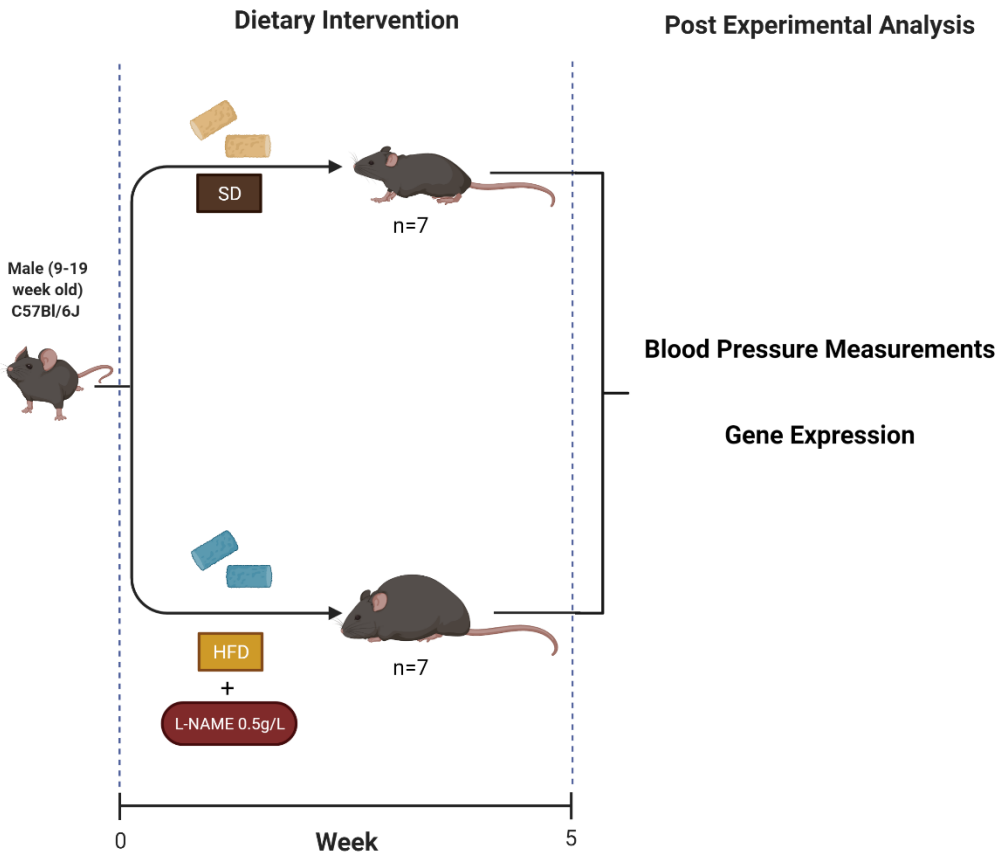

Figure 5.1. Schematic of experimental groups for dietary intervention pilot study. Separate groups (n=7) of male C57Bl/6J mice were subjected to either a standard diet (SD) or a high fat diet (HFD) with L-NAME.

Table 5.2. Composition and nutritional information for both the SD (D12450J) and the HFD (D12492).

Composition of SD (D12450J).

Protein	**19.2gm%**
Fat	**4.3gm%**
Carbohydrate	**67.3gm%**
Energy Density	**3.85 kcal/gm**

Nutritional information for SD (D12450J).

Class Description	Ingredients	Grams (gm)
Protein	Casein, Lactic, 30 Mesh	200
Protein	Cystine, L	3
Carbohydrate	Starch, Corn	506.2
Carbohydrate	Lodex 10	125
Carbohydrate	Sucrose, Fine Granulated	72.8
Fibre	Solka Floc, FCC200	50
Fat	Lard	20
Fat	Soybean Oil, USP	25
Mineral	S10026B (Mineral Mix)	50
Vitamin	Choline Bitartrate	2
Vitamin	V10001C (Vitamin Mix)	1

Composition of HFD (D12492).

Protein	**26gm%**
Fat	**35gm%**
Carbohydrate	**26gm%**
Energy Density	**5.24 kcal/gm**

Nutritional information for HFD (D12492).

Class Description	Ingredients	Grams (gm)
Protein	Casein, Lactic, 30 Mesh	200
Protein	Cystine, L	3
Carbohydrate	Starch, Corn	0
Carbohydrate	Lodex 10	125
Carbohydrate	Sucrose, Fine Granulated	72.8
Fibre	Solka Floc, FCC200	50
Fat	Lard	245
Fat	Soybean Oil, USP	25
Mineral	S10026B (Mineral Mix)	50
Vitamin	Choline Bitartrate	2
Vitamin	V10001C (Vitamin Mix)	1

Table 5.3. Mouse primer sequences designed and purchased from Sigma Aldrich and used in qRT-PCR studies.

Gene	Ref Sequence	Forward 5'-3'	Reverse 5'-3'	Product Size
sFRP1	NM_013834.3	CAAGCGAGTTTGCACTGAGG	AGTTGTGGCTGAGGTTGTCC	192bp
sFRP5	NM_018780.3	CTCCAGTGACTTTGTGGTCAAG	TGTCTAACTGTGGGCAAGGG	185bp
Axin2	NM_015732.4	TCAGTAACAGCCCAAGAACCG	CCTCCTCTCTTTTACAGCAAAGC	122bp
CCND1	NM_001379248.1	TCAAGTGTGACCCGGACTGC	CCTTGGGGTCGACGTTCTG	99bp
c-Myc	NM_001177352.1	CCCATTACAAAGCCGCCGAC	CACTTTCGTCAGCGTGTCCA	86bp
Fn1	NM_001276408.1	GAAGACAGATGAGCTTCCCCA	GGTTGGTGATGAAGGGGGTC	110bp
MMP2	NM_008610.3	AACGGTCGGGAATACAGCAG	GTAAACAAGGCTTCATGGGGG	125bp
Col1	NM_007742.4	CCCTGGTCCCTCTGGAAATG	GGACCTTTGCCCCCTTCTTT	72bp
Col3	NM_009930.2	TGACTGTCCCACGTAAGCAC	GAGGGCCATAGCTGAACTGA	105bp

Table 5.4. QuantiTect mouse primer catalogue numbers purchased from Qiagen and used in qRT-PCR studies.

Primer	Catalogue Number	Product Size
ANP	QT00250922	132bp
BNP	QT00107541	115bp
Gapdh	QT01658692	144bp
Wnt3a	QT00250439	94bp
Wnt5a	QT00164500	130bp

5.3.4. Exclusion criteria

BP measurements: The pilot study was conducted in two stages over two different time periods due to the COVID-19 pandemic induced lockdown. In the first part of the study, group sizes consisted of n=3 for both the control group and HFD+L-NAME group and BP measurements were conducted in all mice. In the second part of the study, group sizes consisted of n=4 for both the control group and HFD+L-NAME group, however due to a temporary lack of a NACWO regulated procedures could not be conducted at RGU during this period and so BP measurements were not carried out in these animals.

5.3.5. Statistical Analysis

All statistical analysis was conducted using GraphPad Prism 8 software and any differences between results were deemed significant with a $P<0.05$. Data was plotted as mean ± SEM. Each n number refers to an individual mouse. The statistical test used for each set of data is detailed in its accompanying figure legend throughout this chapter. Individual data was excluded if it was out with the mean ± (2x standard deviation).

5.4. Results

5.4.1. Mice fed a HFD and administered L-NAME exhibited increased adiposity and lung weight, cardiac hypertrophy, and cardiac fibrosis

On average mice on the standard diet (SD) ate 3.3g/mouse/day, while those on a HFD ate 2.5g/mouse/day. Daily water intake did not differ between groups and was approximately 5.1ml/mouse/day. Mice fed a HFD with L-NAME for 5 weeks were characterised by increases in both BW (31±0.86 vs. 28.6±0.61g; $P<0.05$; Figure 5.2A.) and adiposity (0.025±0.004 vs. 0.015±0.001g/g; $P<0.05$; Figure 5.2B.). Following normalisation to TL, both heart weight (7.1±0.46 vs. 5.9±0.33mg/mm; $P<0.05$; Figure 5.3A.) and lung weight (7.4±0.36 vs. 6.5±0.27mg/mm; $P<0.05$; Figure 5.3B.) were significantly increased in the HFD+L-NAME group compared to the control group, while neither liver nor kidney weights (normalised to BW) differed between the two experimental groups. At a molecular level, mRNA expression of the hypertrophic marker BNP was significantly increased (2.2-fold) in the hearts of HFD+L-NAME mice compared to the control mice ($P<0.05$; Figure 5.4A.), however there was no change in ANP mRNA expression between the two groups (Figure 5.4B.). Assessment of fibrotic mediators/markers demonstrated that mRNA expression of Col1 was increased by 3.6-fold ($P<0.05$; Figure 5.5A.), Col3 increased by 1.9-fold ($P<0.05$; Figure 5.5B.), matrix

metalloproteinase 2 (MMP2) increased by 1.5-fold (P<0.05; Figure 5.5C.), and Fn1 increased by 1.5-fold (P=0.05; Figure 5.5D.) in the hearts of HFD+L-NAME mice compared to controls.

5.4.2. Mice fed a HFD and administered L-NAME were characterised by HTN

Arterial BP measured by a conductance catheter revealed that both SBP (145±2.1 vs. 116±4.5mmHg; P<0.05; Figure 5.6A.) and MABP (121±11.7 vs. 94±0.33mmHg; P<0.05; Figure 5.6C.) were significantly increased in mice fed a HFD and administered L-NAME compared to control animals. Furthermore, although DBP appeared to be elevated in the HFD+L-NAME experimental group compared to control mice (109±16.5 vs. 84±2.1mmHg; Figure 5.6B.) this increase was not statistically significant.

5.4.3. Wnt signalling was upregulated in mice fed an HFD+L-NAME

Cardiac mRNA expression of Wnt3a, one of the chief canonical Wnt signalling ligands, was significantly increased (2.8-fold) in the HFD+L-NAME group compared to controls (P<0.05; Figure 5.7A.), while mRNA expression of the non-canonical ligand Wnt5a was not altered between the two groups (Figure 5.7B.). Furthermore, expression of the endogenous Wnt inhibitor, sFRP1, was also significantly increased (1.7-fold) in the hearts of mice fed a HFD+L-NAME compared to control mice (P<0.05; Figure 5.7C.), while cardiac expression of sFRP5 was not altered between the two groups (Figure 5.7D.). Conversely, in WAT from HFD+L-NAME mice, Wnt3a gene expression appeared to decrease slightly compared to controls (0.5-fold; Figure 5.8A.), while mRNA expression of Wnt5a was not altered between experimental groups (Figure 5.8B.). In contrast to the findings in cardiac tissue, mRNA expression of sFRP1 in WAT did not differ between experimental groups (Figure 5.8C.), however sFRP5 gene expression was increased 4.6-fold in WAT from HFD+L-NAME mice (P<0.05; Figure 5.8D.). The mRNA expression of Axin2, a negative regulator of canonical Wnt signalling, was significantly decreased in the WAT from the HFD+L-NAME group compared to controls (P<0.05; Figure 5.9A.), however the expression of target genes (c-Myc & CCND1; Figure 5.9B. & Figure 5.9C.) of canonical Wnt signalling were not altered between the two experimental groups.

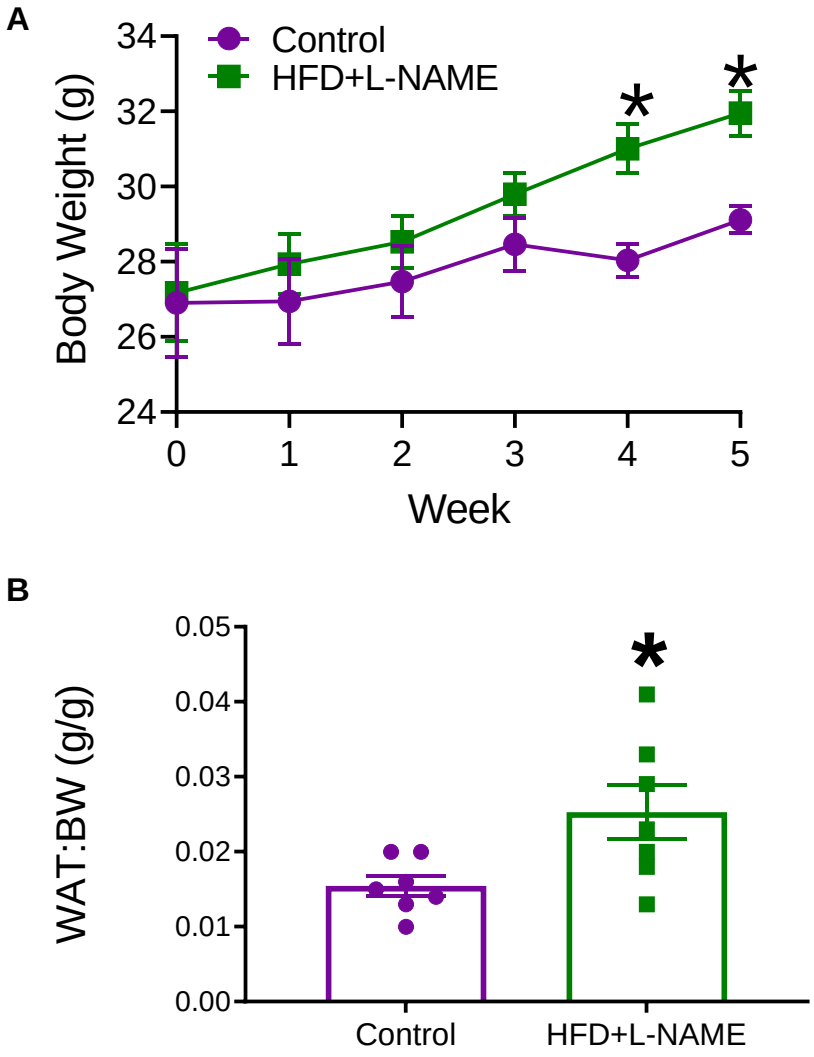

Figure 5.2. Weekly body weights (A) and WAT:BW (B) for control and HFD+L-NAME mice. Data is expressed as mean ± SEM and analysed using either a two-way ANOVA with Bonferroni post hoc test (A) or an unpaired *t*-test (B). **P*<0.05; n=6-7.

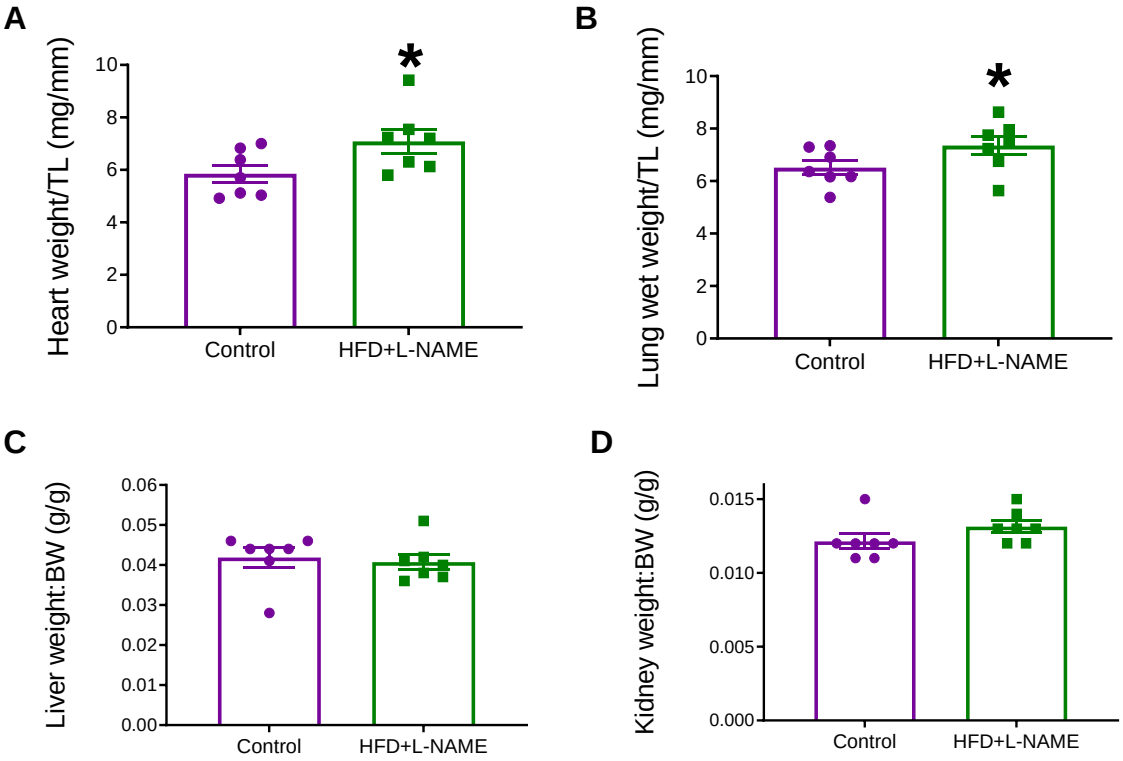

Figure 5.3. Heart weight (A) and lung weight (B) normalised to TL and liver weight (C) and kidney weight (D) normalised to BW. Data is expressed as mean ± SEM and analysed using an unpaired *t*-test. **P*<0.05; n=7.

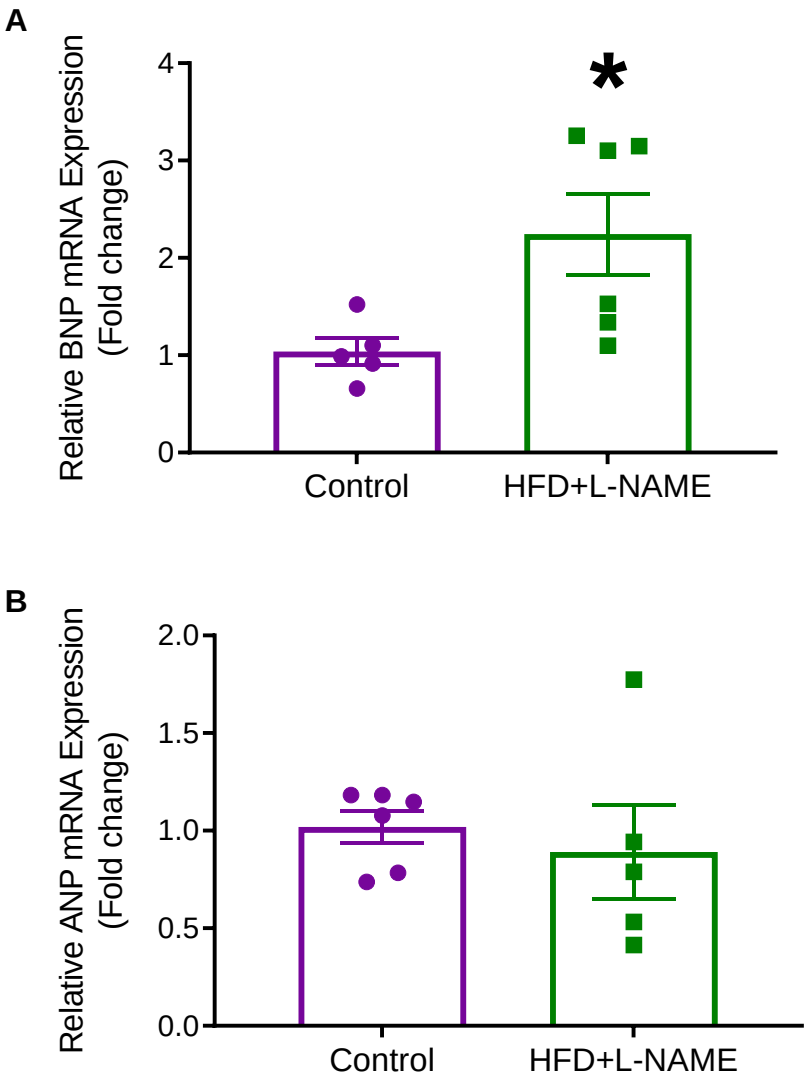

Figure 5.4. mRNA expression of BNP (A) and ANP (B) in murine ventricular tissue. Data is expressed as mean ± SEM and analysed using an unpaired *t*-test. **P* <0.05; n=5-6.

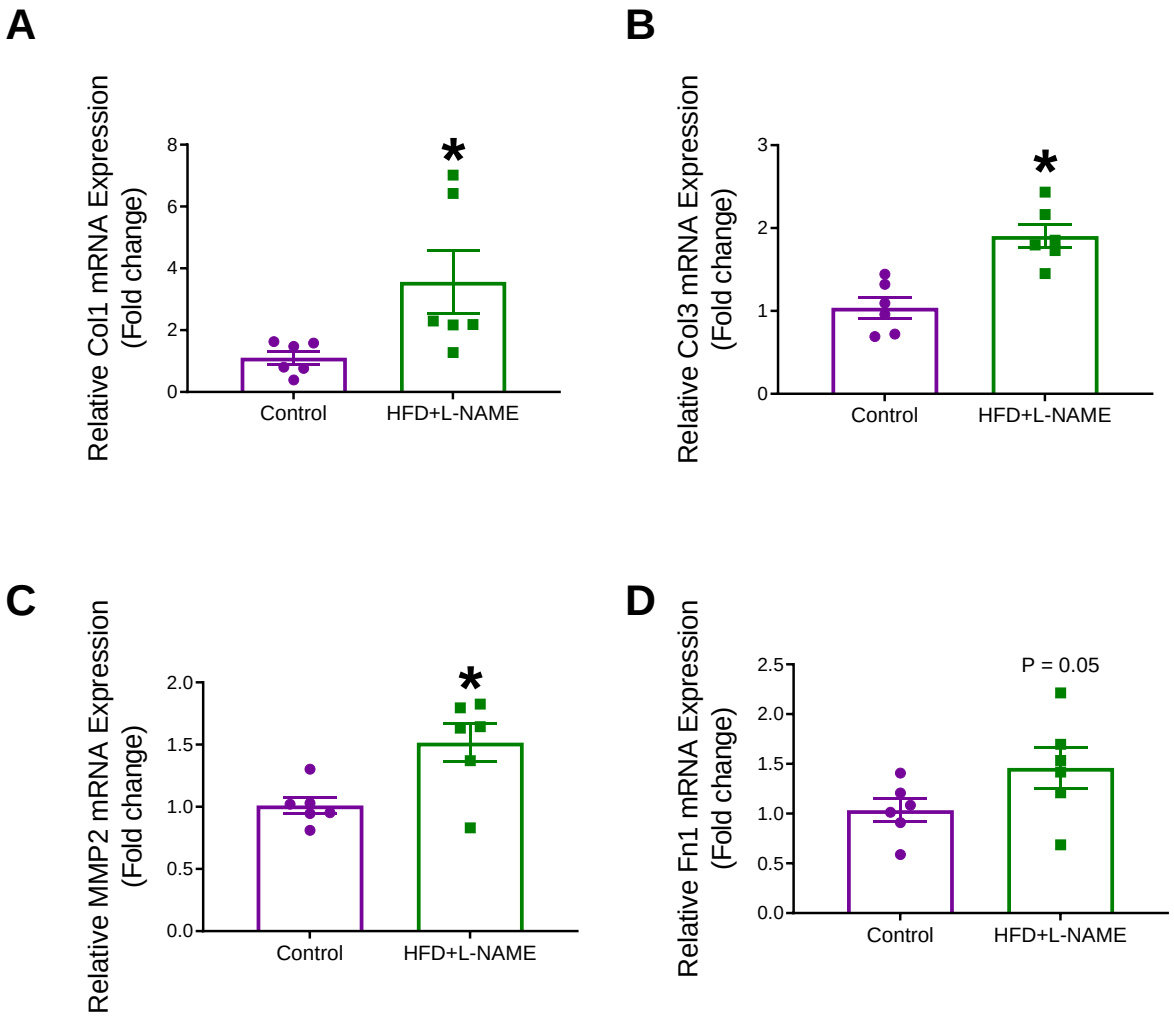

Figure 5.5. mRNA expression of Col1 (A), Col3 (B), MMP2 (C), and Fn1 (D) in murine ventricular tissue. Data is expressed as mean ± SEM and analysed using an unpaired *t*-test. **P*<0.05; n=6.

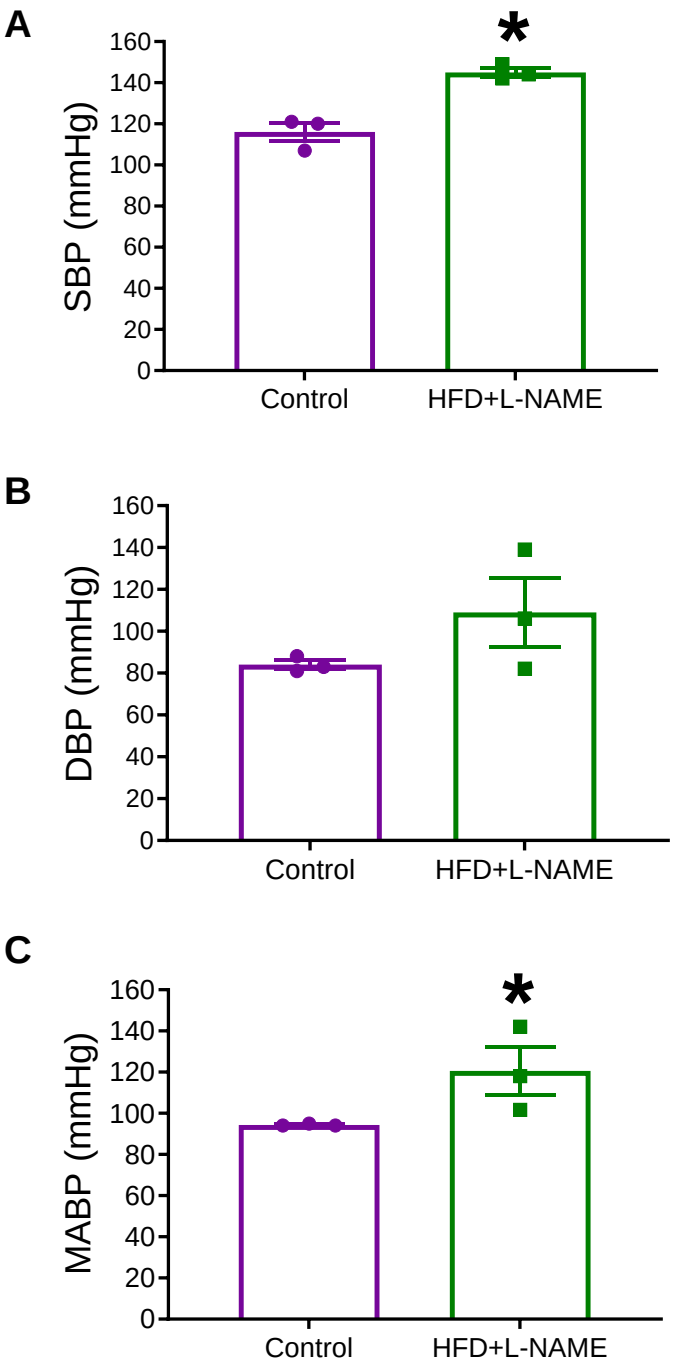

Figure 5.6. SBP (A), DBP (B), and MABP (C). Data is expressed as mean ± SEM and analysed using an unpaired *t*-test. **P*<0.05; n=3.

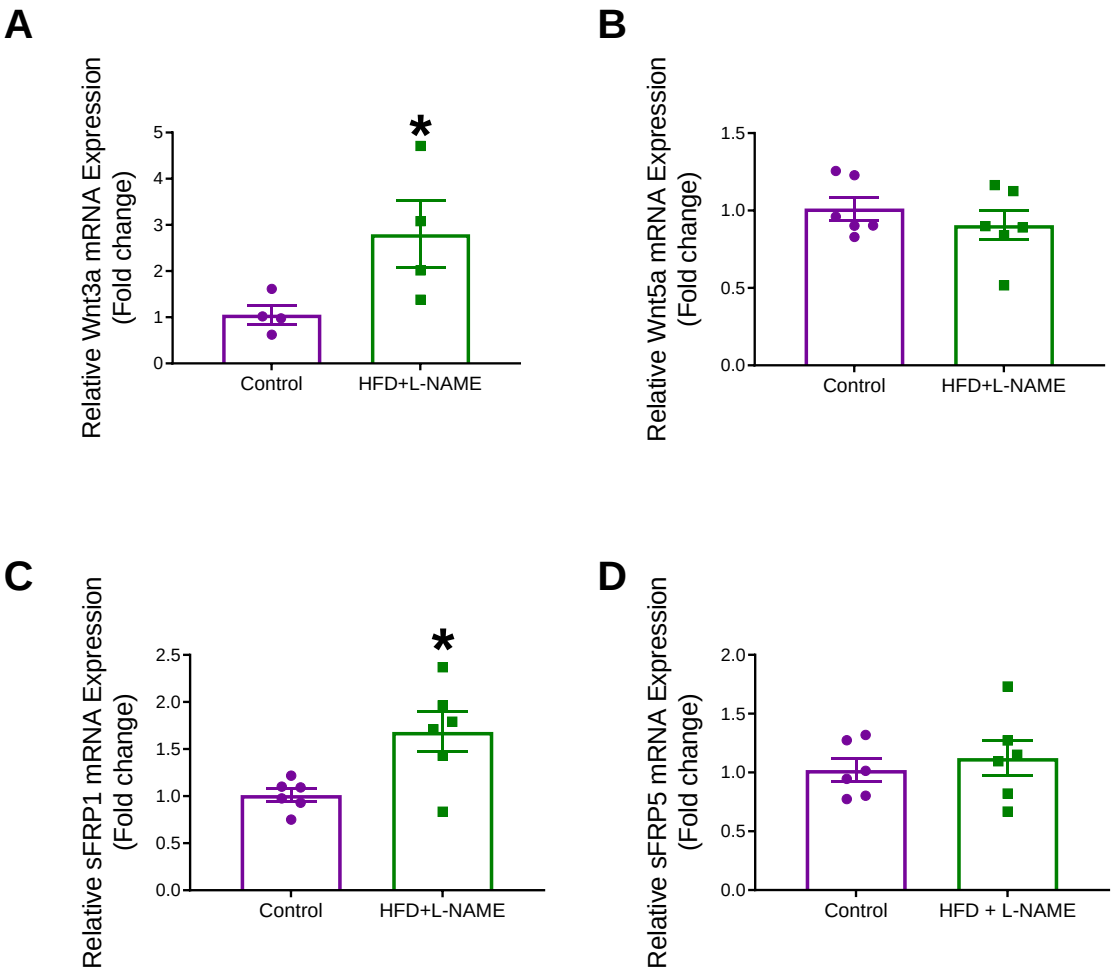

Figure 5.7. mRNA expression of Wnt3a (A), Wnt5a (B), sFRP1 (C), and sFRP5 (D) in murine ventricular tissue. Data is expressed as mean ± SEM and analysed using an unpaired *t*-test. **P*<0.05; n=4-6.

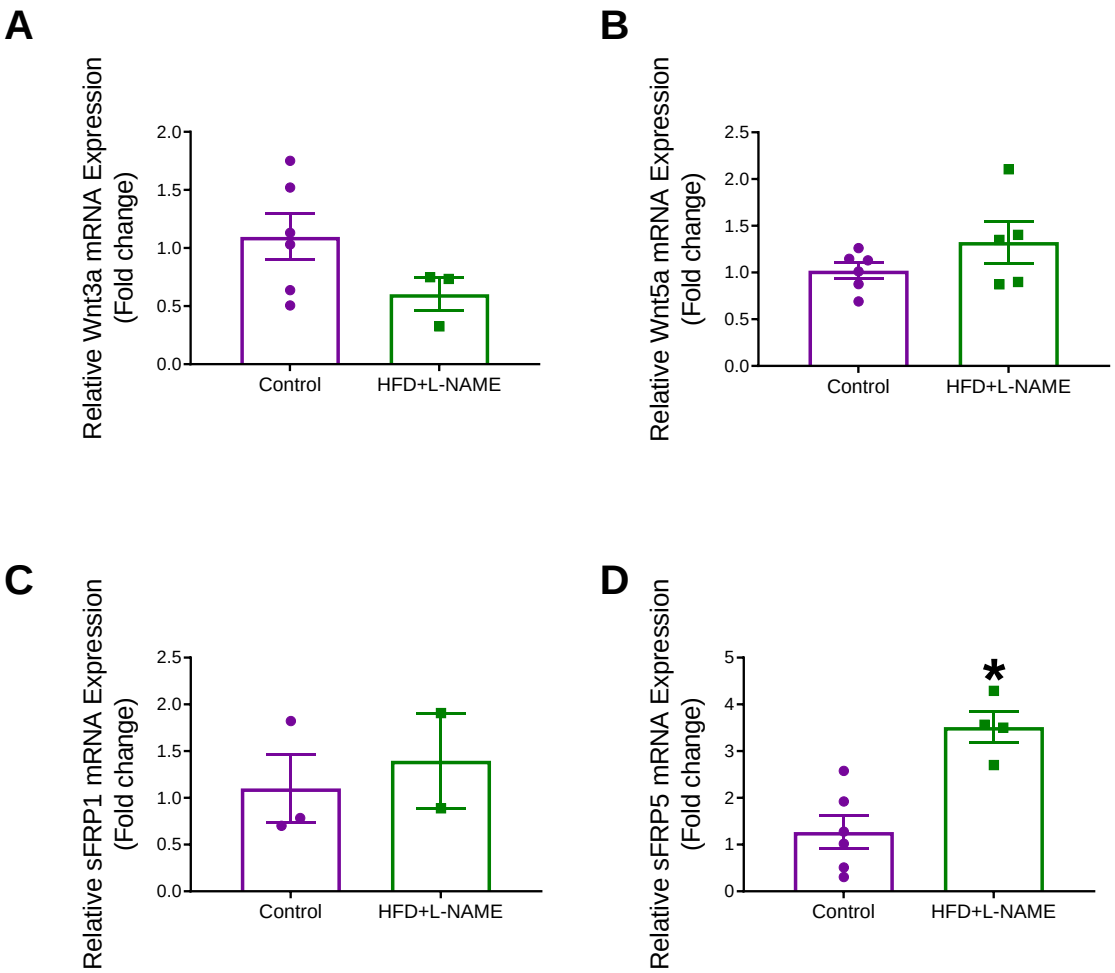

Figure 5.8. mRNA expression of Wnt3a (A), Wnt5a (B), sFRP1 (C), and sFRP5 (D) in murine WAT.
Data is expressed as mean ± SEM and analysed using an unpaired *t*-test. **P*<0.05; n=2-6.

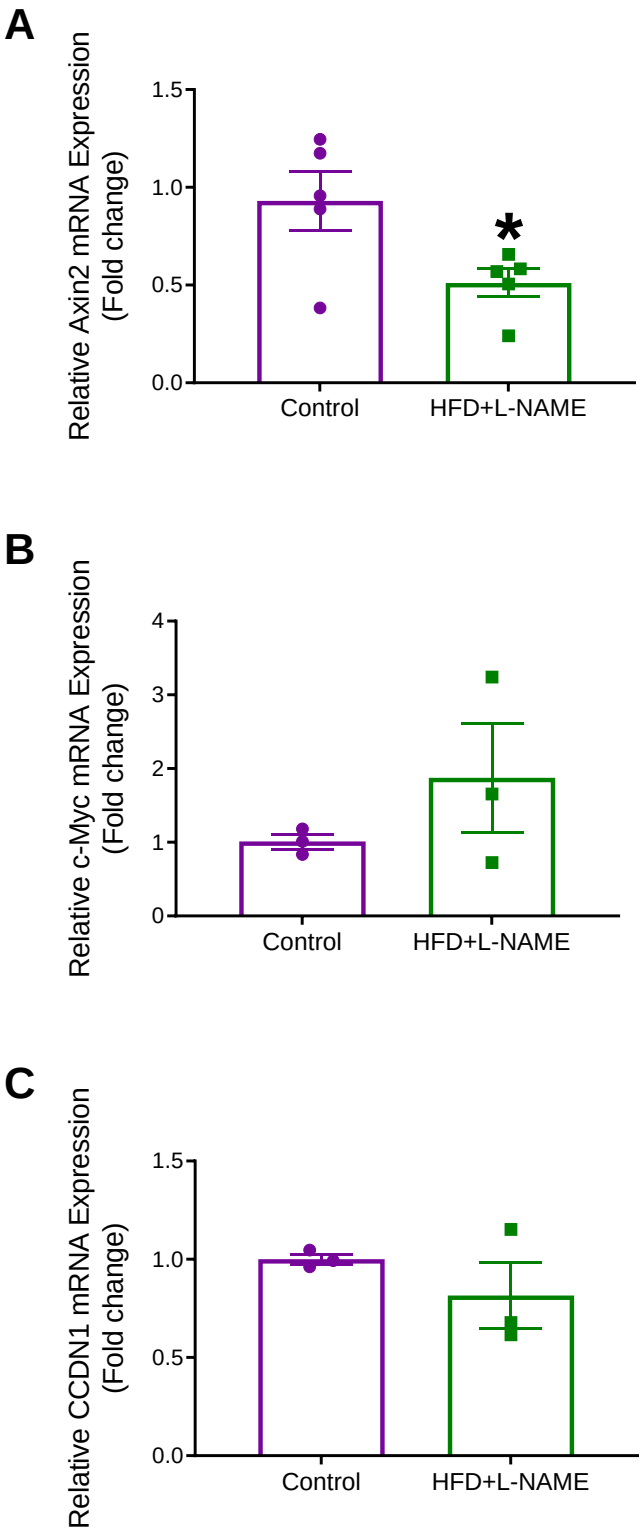

Figure 5.9. mRNA expression of Axin2 (A), c-Myc (B) and CCND1 (C) in murine ventricular tissue.
Data is expressed as mean ± SEM and analysed using an unpaired *t*-test. **P*<0.05; n=3-6.

5.5. Discussion

Previous studies in Chapter 4 have demonstrated that Wnt3a can induce hypertrophy in H9c2 cells characterised by both an increase in the mRNA expression of ANP and BNP, as well as an increase in the secretion of BNP protein. Furthermore, the pre-treatment of H9c2 cells with Wnt-c59 prior to the addition of AngII significantly reduced the gene expression of BNP, indicating that AngII, at least in part, induces reactivation of the fetal gene programme (a key feature of cardiomyocyte hypertrophy) via activation of Wnt signalling. There are various animal models that encapsulate features of HFpEF as discussed in section 5.1., however Wnt signalling has only been investigated in AngII and TAC induced pressure overload models to date. Recently, a 'two-hit' model of HFpEF was shown to exhibit several of the key features associated of the condition, however Wnt signalling has not been investigated in this model or any other model of HFpEF. The principle aim of this study was to determine whether Wnt signalling is activated in a 'two-hit' *in vivo* model of HFpEF.

5.5.1. High fat feeding (with L-NAME) induced an increase in body weight (BW) and adiposity in 5 weeks

Research by Schiattarella et al. (2019) was the first to characterise the 'two-hit' *in vivo* model of HFpEF, in which mice were subjected simultaneously to both mechanical stress (HTN) and metabolic stress (obesity/metabolic syndrome) in order to encapsulate key pathophysiological features of HFpEF. The original study compared 5 and 15 weeks of high fat feeding (with L-NAME administered in drinking water) in mice and found that many of the hallmarks of HFpEF were established following 5 weeks of dietary/pharmacological intervention. Ideally development of this model of HFpEF in female mice would potentially be more beneficial, as it is now more common for women to be diagnosed with HFpEF than men, however a study by Tong et al. (2019) demonstrated that female sex was protective in this particular HFpEF model. They reported that female mice had minimal changes in E/e' ratio and no change in HW:TL. Furthermore, the degree of tissue fibrosis and cardiomyocyte hypertrophy were significantly attenuated compared to male mice (Tong *et al.* 2019). Therefore, based on these results male mice were chosen for this model.

In the present study, following 5 weeks of HFD+L-NAME, mice were characterised by both increased BW and increased adiposity, which agrees with that previously reported by Schiattarella et al. (2019). In other studies that have used the HFD+L-NAME model, body weights were significantly higher than the controls after 7 weeks (Cordero-Herrera *et al.* 2019) and 12 weeks (Kitakata *et al*. 2021). Furthermore, in studies where C57Bl/6J mice were only

subjected to a HFD to induce obesity, body weights of these mice were greater than that of the normal diet fed group after 12 weeks, and this increase in BW was detectable as early as 5 weeks into the dietary intervention period (Lang *et al*. 2019). Another study demonstrated that a HFD resulted in a significant increase in BW after 8 weeks, with differences starting to appear between HFD and normal-fed controls after 2 weeks (Withaar *et al*. 2021b). Finally, experimental studies in which rodents were administered L-NAME alone showed no differences in BW compared to controls (Nagano *et al*. 2013; Pechanova *et al*. 2020), demonstrating that high fat feeding is necessary to induce obesity in this model.

5.5.2. A HFD+L-NAME intervention induced hypertension in mice after 5 weeks

Under physiological conditions, endothelium-derived NO diffuses to VSMCs where it binds to sGC and produces cGMP, a key regulator of vascular tone. A rise in intracellular cGMP in VSMCs initiates activation of PKG which in turn decreases intracellular Ca^{2+} levels, induces membrane hyperpolarisation, and inhibits myosin light chain phosphorylation, all of which contributes to vasorelaxation (Thoonen *et al*. 2013). In HTN, NO is reduced due to decreased eNOS levels, which results in a reduction of cGMP production by sGC and decreased PKG activity in the underlying vascular smooth muscle. In an experimental setting, rodents are administered L-NAME to induce HTN and this *in vivo* model is one of the most widely used in cardiovascular research for studies investigating endothelial dysfunction, vascular wall remodelling, and pressure induced cardiac remodelling (reviewed by Kopincova *et al.* 2012). As a non-selective NOS inhibitor, L-NAME, reduces the production of NO (a powerful endogenous vasodilator) from L-arginine consequently increasing vascular resistance and BP. HFD+L-NAME mice were characterised by elevated BP with an increase in SBP (145mmHg) and DBP (109mmHg) indicating that HTN, the most common co-morbidity in patients with HFpEF, was present in these animals. These results are in agreement with studies by both Schiattarella et al. (2019) and Tong et al. (2019) which reported that both SBP and DBP were increased following 5 weeks of high fat feeding and L-NAME administration in male mice. Furthermore, in separate studies L-NAME induced increases in BP have been demonstrated as early as 5 days following commencement of L-NAME (1g/L in drinking water) administration in male Institute of Cancer Research (ICR) mice (Nagano *et al.* 2013), and 7 days following daily i.p. injection of L-NAME (400µg/g body weight) in male Swiss Webster mice (Peotta *et al.* 2001).

5.5.3. Key features of HFpEF such as cardiac hypertrophy and pulmonary congestion were present in HFD+L-NAME mice

Mice fed a HFD+L-NAME were characterised by cardiac hypertrophy as evidenced by both an increase in the ratio of heart weight to tibia length (HW:TL) and an increase in BNP mRNA expression in ventricular tissue. TL was used to normalise both heart and lung weights as BW fluctuates in response to dietary intervention while the former remains constant after maturity and has been shown to more accurately quantify cardiac hypertrophy in rodents (Yin *et al*. 1982). An increase in HW:TL has previously been reported in male mice after 5 weeks of high fat feeding and L-NAME administration (Schiattarella *et al*. 2019; Tong *et al*. 2019). Increasing the duration of high fat feeding and L-NAME to 8 and 10 weeks in mice also caused an increase in HW:TL (Huang *et al*. 2021; Kitakata *et al*. 2021). An increase in HW:TL has been demonstrated to be a key indicator of cardiac hypertrophy in pressure overload models induced by TAC (Richards *et al*. 2019), suprarenal aortic constriction (Nicks *et al*. 2020), and L-NAME administration (Bienvenu *et al*. 2017), while other studies have used HW:BW as a means to detect cardiac hypertrophy following L-NAME administration (Sung *et al*. 2013; Soliman *et al*. 2019; Pechanova *et al*. 2020). In AngII infusion models of HFpEF, HW:TL was shown to be increased in response to combined high fat feeding (12 weeks) and AngII infusion (1.25mg/kg/day for 4 weeks) and with AngII infusion alone (Peng *et al*. 2011). Conversely, van Bilson et al. (2014) reported that mice infused with AngII (1mg/kg/day) for 4 weeks were characterised by increased left ventricular weight, however this measurement was not normalised to TL.

In this study, the presence of cardiac hypertrophy was further confirmed via an upregulation in the expression of the hypertrophic marker BNP in the ventricular tissue of mice fed a HFD and administered L-NAME. This finding is in agreement with data from studies by Schiattarella et al. (2019) and Tong et al. (2019) which also demonstrated an increase in BNP mRNA expression in the hearts of male mice subjected to the same dietary/pharmacological intervention for 5 weeks. An increase in the gene expression of ANP and BNP was also recorded in mice fed a HFD+L-NAME for 10 and 15 weeks (Huang *et al*. 2021; Liao *et al*. 2021). Although BNP increased in this study, ANP was more variable and did not significantly increase. A possible explanation for this is that ANP is predominantly expressed in the atria (reviewed by da Silva *et al*. 2021) and so what little expression there is in the ventricles may fluctuate in response to stressors i.e. HFD+L-NAME. Furthermore, in a previous study in which mice were administered L-NAME alone (i.e. without a HFD) for 4 weeks gene expression of ANP was not altered in these animals (Ren *et al*. 2015), while in rats administration of L-NAME (20mg/kg/day) for 8 weeks was shown to increase the mRNA expression of both ANP and

BNP in the hearts of these animals (Suo *et al*. 2002). In a separate study, administration of 40mg/kg/day L-NAME to rats for 2 weeks induced HTN but did not alter cardiac ANP mRNA expression and the latter was only increased when L-NAME was co-administered with AngII (0.26mg/kg/day) delivered via osmotic minipump (Hou *et al.* 1995). Furthermore, AngII infusion alone has been shown to increase mRNA expression of both ANP and BNP in the hearts of rodents over a range of both concentrations (1.1mg/kg/day to 1.8mg/kg/day) and treatment durations (1 to 4 weeks) (Becher *et al.* 2012; Duerrschmid *et al.* 2013; Choi *et al.* 2016; Luo *et al.* 2016; Li *et al.* 2019). Finally, the administration of a HFD on its own has been shown to increase gene expression of ANP and BNP in mice after 24 weeks of feeding (Zhang *et al*., 2020).

Another key marker of diastolic dysfunction/HFpEF is increased lung weight, which can be indicative of pulmonary congestion (Guazzi 2014). In this study, lung weight normalised to TL increased in the HFD+L-NAME mice, which agrees with results reported by both Schiattarella et al. (2019) and Huang et al. (2021). In a previous study Hubert et al. (2014) demonstrated that lung weight:TL was increased in response to L-NAME administration, while Schiatterella et al. (2019) reported that lung weight (wet weight:dry weight) was increased in mice that had been subjected to both a HFD with L-NAME administration, but not in those mice that had only been administered L-NAME. Conversely, mice infused with AngII (1.25mg/kg/day) for 4 weeks with or without a HFD for 12 weeks displayed an increase in lung weight normalised to TL (Withaar *et al*. 2021b). However, in another mouse model infused with AngII (1000ng/kg/min for 2 weeks) lung weight normalised to TL was not altered (Barhoumi *et al*. 2017). Taken together, this demonstrates that increased lung weight is not a feature that is consistently observed across experimental models of HFpEF.

5.5.4. A HFD+L-NAME intervention induced cardiac fibrosis in mice after 5 weeks

One of the main structural proteins of the ECM is collagen, which is distributed extracellularly in most tissues, with Col1 and Col3 being the most common types. Col1 and Col3 are both predominantly secreted by fibroblasts and smooth muscle cells. Col1 fibrils are notably stiffer and provide structural rigidity and strength resulting in reduced tissue compliance, whereas Col3 fibrils are thinner and more elastic providing more tissue distensibility and resilience (reviewed by Witteg and Szulcek 2021). Furthermore, both Col1 and Col3 have been suggested as biomarkers of fibrosis (reviewed by Gibb *et al*. 2020). A systematic review has highlighted that MMP2 may have a role as a biomarker for cardiovascular remodelling in HTN (Marchesi *et al*. 2012). MMP2 is a member of a superfamily of zinc-dependent endopeptidases

which are involved in ECM remodelling through Fn1, elastin and collagen degradation. Fn1 is a glycoprotein secreted as a soluble protein from cardiac fibroblasts, myofibroblasts, and endothelial cells and has been shown to play a potential role in cardiac fibrosis (Valiente-Alandi *et al*. 2018).

In this pilot study, HFD+L-NAME mice also presented with cardiac fibrosis, as shown by increases in the mRNA expression of Col1, Col3, Fn1, and MMP2. These results correlate with previous results recorded by Huang et al. (2021), where they reported an increase in the mRNA levels of Col1 and Col3 and an increase in the protein expression of MMP2. In other studies in which mice were subjected to a HFD with L-NAME both the cardiac expression of Col1 (Cai *et al*. 2021) and percentage area of fibrosis in hearts (Schiattarella *et al*. 2019; Tong *et al.* 2019; Kitakata *et al*. 2021) were increased. In contrast, the percentage area of collagen deposition was not altered in the hearts of mice given L-NAME for 5 weeks and only increased when L-NAME was administered in combination with AngII (Hamilton *et al.* 2016). However, in a separate study, administration of L-NAME to both male and female mice for 8 weeks increased interstitial fibrosis and the gene expression of Col1 (to a greater extent in female compared to male mice), while the expression of Col3 was not altered in either sex (Bienvenu *et al*. 2017). On its own, the administration of a HFD to mice has been shown to induce cardiac fibrosis after both 6 and 11 months of dietary intervention (Wang *et al*. 2015; Zhang *et al*. 2019), with some studies indicating that collagen accumulation/fibrosis occurs as early as 14 weeks (Li *et al*. 2017c). However, Schiattarella et al. (2019) demonstrated that high fat feeding alone for 5 weeks did not induce cardiac fibrosis in mice potentially suggesting that fibrosis induced by a HFD is time dependent. In other models of HFpEF, the expression of Col1 and Col3 were both increased in the hearts of AngII (3µg/g/day for 7 days or 1.4mg/kg/day for 4 weeks) infused mice (Li *et al*. 2019; Ock *et al*. 2021), while the protein levels of Col1 and Fn1 were increased in the hearts of rats infused with AngII (450ng/min/kg) for 4 weeks (Zhao *et al.* 2018). While in other models of pressure overload (i.e. TAC model), the cardiac expression of Col1, Col3, MMP2, and Fn1 mRNA were all increased demonstrating the presence of cardiac fibrosis in this model (Klein *et al*. 2005; Matsusaka *et al*. 2006; Methatham *et al*. 2021). Finally, previous studies have also demonstrated that protein levels of both MMP2 and Fn1 are increased in the cardiovascular system of rodents administered L-NAME (Pessanha *et al*. 1999; Bouvet *et al*. 2005), which agrees with the findings from the present study.

5.5.5. Co-administration of L-NAME with high fat feeding induced an upregulation of Wnt signalling related mediators

Following 5 weeks of dietary (HFD) and pharmacological (L-NAME) intervention, mice were characterised by an increase in the mRNA expression of Wnt3a in the heart, while Wnt5a mRNA expression was not altered, indicating potential activation of canonical Wnt signalling. So far Wnt signalling does not appear to have been investigated in any experimental model of HFpEF including the 'two-hit' experimental model of this condition. In experimental studies using a surgically induced pressure overload model (i.e. TAC), the protein expression of Wnt1 and Wnt3a (both activators of canonical Wnt signalling) and β-catenin were all increased in the hearts of mice subjected to TAC compared to controls (Zhao *et al*. 2020; Methatham *et al*. 2021), which may suggest that Wnt signalling is activated in response to pressure/stretch. Alternatively, activation of canonical signalling may also be in response to activation of the RAAS which has been demonstrated in both L-NAME (Pollock *et al.* 1993) and TAC (Wang *et al.* 2018) induced models of pressure overload. In support of this, the mRNA expression of several Wnt ligands (including Wnt3a and Wnt5a) and the protein expression of β-catenin were all increased in the hearts of rats infused with AngII (Zhao *et al.* 2018). In the present study, mRNA expression of both c-Myc and CCND1 (canonical Wnt signalling gene targets) were unaltered in the hearts of HFD+L-NAME mice, which conflicts with reports demonstrating that both the mRNA and protein expression of c-Myc and CCND1 are increased in the hypertrophic hearts of several different experimental models of pressure overload (Jiang *et al*. 2018; Pan *et al*. 2018; Zhao *et al*. 2020). In particular, protein levels of active β-catenin and c-Myc were increased in the hearts of rats infused with AngII (450ng/kg/min) for 4 weeks (Zhao *et al*. 2018). While in other studies, the protein expression of CCND1 and the mRNA expression of Axin2 and CCND1 were increased in the cardiovascular system of rodents after only a week-long infusion with AngII (Diep *et al*. 2001; Sumida *et al*. 2015). Furthermore, studies using the TAC pressure overload mouse model demonstrated that both the mRNA and protein expression of c-Myc, CCND1, and β-catenin were all increased 4 weeks post-surgery (Jiang *et al.* 2018; Zhao *et al*. 2020). However, in one such study although β-catenin mRNA expression was increased in hearts of mice subjected to TAC, the expression of c-Myc mRNA was decreased in comparison to control mice (Pan *et al*. 2018). It is therefore possible that the lack of an increase in the expression of c-Myc and/or CCND1 in the present study may be due to their expression at mRNA level being more transient than other genes. In particular the half-life of mRNA produced by regulatory genes, such as transcription factors is relatively short, in some cases less than an hour, therefore this requires further investigation potentially looking at protein levels of c-Myc and CCND1.

Another marker of canonical Wnt signalling that was investigated in this pilot study was Axin2 (also known as conductin or axil). Axin2 is an axin paralog which functions as a scaffold protein in the β-catenin destruction complex, however it is also a β-catenin target gene (Leung *et al.* 2002; Lustig *et al.* 2002) that can act in a negative feedback loop to limit Wnt signalling. Once activated, canonical Wnt signalling can induce the transcription of the Axin2 gene (controlled by the TCF/LEF factors) in the nucleus, which subsequently initiates a negative feedback loop to regulate β-catenin levels/canonical Wnt signalling (Jho *et al*. 2002). In the present study mRNA expression of Axin2 was decreased in the hearts of the HFD+L-NAME mice, which given its negative regulatory role regarding canonical Wnt signalling may suggest the latter goes unchecked.

sFRPs act as endogenous regulators of Wnt activity and have been shown to be altered in both obesity and CVD. In the present study, mRNA expression of sFRP1, but not sFRP5, was increased in the hearts of mice fed a HFD with L-NAME, while the opposite occurred (i.e. sFRP1 expression was unchanged and sFRP5 expression increased) in the adipose tissue of these animals. sFRP1 has been suggested to exert cardioprotective effects having previously been shown to improve both systolic and diastolic function in mice subjected to TAC pressure overload when administered via a viral vector to the myocardium of these animals (Pan *et al*., 2018). Furthermore, research has also shown that a loss of sFRP1 in mice resulted in cardiac hypertrophy and fibrosis, deterioration of cardiac function, and an increase in LVEDP (Sklepkiewicz *et al.* 2015). Therefore, the increase in cardiac expression of sFRP1 in the HFD+L-NAME mice could be an adaptive response to attempt to exert cardioprotective effects in these mice, however further investigation is needed. In humans, sFRP1 expression in adipose tissue increases in response to increasing BW, however the level of expression peaks in individuals with a BMI of between 30-35 and decreases in the setting of extreme obesity (i.e. BMI >40) (Lagathu *et al.* 2010). In experimental animals subjected to high fat feeding, WAT expression of sFRP1 mRNA was increased after 3 days, unchanged after 4 weeks (which is comparable to the findings from the present study), and reduced following 6 months of dietary intervention when compared to control animals (Lagathu *et al.* 2010). Conversely, mRNA expression of sFRP5 has been shown to be upregulated in WAT from both obese mice and obese individuals (Wang *et al.* 2014b), which agrees with the findings from the present study. However, conflicting reports have also demonstrated that circulating levels of sFRP5 are decreased in overweight/obese patients (Hu *et al*. 2013) and the expression of sFRP5 in WAT is transiently increased after 12 weeks but reduced after 24 weeks of administration of a high fat/high sugar diet to mice (Ouchi *et al.* 2010).

5.6. Conclusion

The findings from this pilot study demonstrate that mice subjected to metabolic (HFD) and mechanical (L-NAME) stress for 5 weeks are characterised by increased adiposity, HTN, and cardiomyocyte hypertrophy and fibrosis, all of which are key features of HFpEF. Furthermore, this is the first study to show evidence of both activation of canonical Wnt signalling and an upregulation of cardioprotective negative regulators of Wnt signalling in this model. Taken together, this is the first study to provide evidence for a role for canonical Wnt signalling in this HFpEF model. The next chapter thus investigated whether the administration of Wnt-c59 (Wnt inhibitor) could reverse the adverse structural and/or functional effects characteristic of this HFpEF model.

Chapter 6: Investigating the effect of inhibition of Wnt signalling in a ‘two-hit’ experimental model of HFpEF

6.1. Introduction

6.1.1. Wnt signalling and cardiomyocyte hypertrophy

Accumulating evidence has suggested that activation of Wnt signalling plays a significant role in both the initiation and progression of cardiac hypertrophy. In particular, research to date has demonstrated the activation/upregulation of canonical (β-catenin dependent) Wnt signalling as a key contributor to both cardiomyocyte hypertrophy and subsequent cardiac dysfunction. In NRVMs the addition of hypertrophic stimuli (phenylephrine and ET-1) induced an increase in cytosolic β-catenin thought to be due to the inhibition of GSK-3β via the recruitment of protein kinase B (PKB) (Haq *et al*. 2003). In mice exposed to TAC, protein levels of total β-catenin were increased in comparison to controls, with immunostaining confirming that β-catenin was induced in hypertrophic cardiomyocytes (Zhao *et al*. 2019a). Furthermore, deletion of β-catenin has also been shown to inhibit cardiac hypertrophy in cardiomyocytes from mice after TAC (Qu *et al*. 2007). In other studies using pressure overload models, the overexpression of the Wnt agonist, Dvl-1, was shown to enhance cardiac hypertrophy (as indicated by increased HW:BW, cardiomyocyte size, and ANP mRNA expression) in rats (Malekar *et al*. 2010), while depletion of Dvl-1 attenuated cardiac hypertrophy (as indicated by an LV wall thickness similar to control mice and a reduction in the mRNA expression of ANP and BNP) in mice (van de Schans *et al*. 2007).

More recently, a link between AngII and the activation of canonical Wnt signalling in the heart has been reported. In particular, chronic infusion of AngII in rats resulted in the increased expression of multiple Wnt ligands in the hypertrophic hearts of these animals, while co-administration of ICG-001, a known inhibitor of β-catenin dependent Wnt signalling, prevented the development of AngII-induced cardiac hypertrophy (Zhao *et al*. 2018). Furthermore, in a recent publication by Methatham et al. (2021) the administration of ICG-001 to mice subjected to TAC reduced cardiac hypertrophy as shown by a decrease in cardiomyocyte size as well as a reduction in BNP mRNA expression. Research has also shown that upregulation of DKK1, a canonical Wnt signalling inhibitor, reduced cardiac hypertrophy after TAC was induced in mice (Fang *et al*. 2020). Wnt signalling can initiate cardiac hypertrophy by inducing an upregulation of several hypertrophy associated target genes including c-Myc (Zhong *et al.* 2006) and CCND1 (Tamamori-Adachi *et al*. 2002). As c-Myc is important for cellular growth and proliferation it is also likely to mediate hypertrophic cardiac growth. A study identified that c-Myc alone can induce hypertrophic growth in the ventricles of adult mice as evidenced by an upregulation in genes such as ANP, ACTA1, and β-MHC (Xiao *et al*. 2001). Finally, the

overexpression of CCND1 in NRVMs using adenovirus gene transfer resulted in hypertrophic growth of these cells (Tamamori-Adachi *et al*. 2002).

6.1.2. Wnt signalling and cardiac fibrosis

Cardiac fibrosis, in particular, is associated with increased collagen accumulation/deposition which results in a stiffening of the heart and impaired relaxation (Park *et al*. 2020). Recently, it has emerged that Wnt signalling could have a role in the development of cardiac fibrosis. In a murine TAC model of pressure overload, a loss of β-catenin function in myocardial fibroblasts significantly reduced cardiac fibrosis and improved cardiac function (Xiang *et al*. 2017). In a separate study, a pro-fibrotic role for Wnt1 was demonstrated as the latter was shown to both promote fibroblast proliferation and induce the expression of pro-fibrotic genes in murine hearts (Duan *et al*. 2012). In neonatal mouse hearts subjected to cryoinjury, the expression of Wnt2b, Wnt5a, and Wnt9a were all increased and associated with the formation of fibrotic tissue (Mizutani *et al.* 2016), while Wnt3a induced activation of FZD_2 increased α-SMA, Col1, and Fn1 expression in cardiac fibroblasts (Carthy *et al*. 2011). Finally, the addition of Wnt3a (250ng/ml) was shown to promote the formation of a myofibroblast phenotype in cultured mouse fibroblasts with the upregulation of TGF-β signalling though Smad2 (Carthy *et al.* 2011). Conversely, Wnt inhibitors have been shown to be protective against fibrosis with sFRP2 attenuating MI induced Col1 accumulation and significantly reducing LV fibrosis in rats (He *et al*. 2010b). Furthermore, Blyszczuk et al. (2017) reported that sFRP2 prevented the TGF-β induced differentiation of cardiac fibroblasts into myofibroblasts, while sFRP1 decreased post infarction scar formation via the modulation of pro-inflammatory mediators (Barandon *et al*. 2011). In an AngII infused mouse model, ICG-001, an inhibitor of canonical Wnt signalling, reduced the accumulation and extracellular deposition of Fn1 in the heart (Zhao *et al*. 2018), while in a TAC mouse model, administration of ICG-001 reduced both interstitial fibrosis and the mRNA expression of connective tissue growth factor, Col1, and Fn1 in the hearts of these animals (Methatham *et al*. 2021).

6.1.3. Inhibition of Wnt signalling by Porcupine Inhibitors

As Wnt signalling appears to be reactivated in both cardiac hypertrophy and fibrosis, research has focused on Wnt inhibitors as potential therapeutic interventions for this adverse cardiac remodelling. Recently, novel inhibitors of Wnt signalling known as Porcupine (PORCN) inhibitors have been developed, which have produced promising results in experimental models of cancer (Liu *et al.* 2013; Proffitt *et al.* 2013; Jiang *et al.* 2018) and HFrEF (Moon *et al.* 2017; Zhao *et al.* 2020). PORCN inhibitors prevent the palmitoylation of both canonical and

non-canonical Wnt proteins, consequently preventing their secretion and the subsequent activation of the three Wnt signalling pathways. Furthermore, PORCN activity is specific to Wnt ligands as it does not appear to affect other similar lipid modified signalling proteins, thus making it a promising therapeutic target for Wnt mediated diseases i.e. various types of cancer and/or CVD. In a recent study by Goldsberry et al. (2020), the PORCN inhibitor, CGX1321, was shown to reduce tumour size (assessed via omentum weight and H&E staining) in a murine model of ovarian cancer. The same study also reported that decreasing Wnt ligand production resulted in an elevation of T cells, macrophage and dendritic cell functions, as well as a reduced tumour burden and an overall improvement in survival rate. At present, CGX1321 has entered Phase I clinical trials (NCT02675946) to determine safety, pharmacokinetics, and clinical activity in treating several types of solid tumours with results expected in 2022. Not only has CGX1321 proven to be effective in treating cancerous cells, there has also been research to suggest it can have anti-hypertrophic effects as well. Jiang et al. (2018) reported that CGX1321 improved cardiac function and significantly decreased cardiomyocyte hypertrophy and fibrosis in mice subjected to TAC. Moreover, CGX1321 also inhibited the pressure overload induced increases in the cardiac expression of β-catenin, CCND1, c-Myc, and FZD_2, indicating an inhibition of canonical Wnt signalling.

Another recently described PORCN inhibitor, Wnt-c59, has been shown to inhibit PORCN activity at nanomolar concentrations, displayed good bioavailability in mice (i.e. plasma concentrations maintained well above the IC_{50} for the drug following oral administration), and also an ability to attenuate the progression of mammary tumours in mice via the downregulation of Wnt target genes (Proffitt *et al.* 2013). Furthermore, mice did not exhibit any toxicity in response to the drug (as indicated by a lack of detrimental changes in the gut and/or other tissues) offering pre-clinical proof that administration of Wnt-c59 is safe *in vivo* (Proffitt *et al.* 2013). In a separate study, Cheng et al. (2015) demonstrated that Wnt-c59 suppressed Wnt-driven undifferentiated cell growth in nasopharyngeal carcinoma, further supporting its potential as an anti-cancer agent. In the cardiovascular system, evidence is emerging to indicate a protective role for Wnt-c59 in experimental models of HFrEF. In particular, Wnt-c59 significantly improved cardiac function and increased survival of mice that were exposed to TAC surgery (Zhao *et al.* 2020). Furthermore, Wnt-c59 reduced the TAC-induced increase in heart mass, cardiomyocyte cross-sectional area, cardiac fibrosis, as well as the expression of hypertrophic markers ANP, BNP, and β-MHC. The cardioprotective effects of Wnt-c59 were mediated via an attenuation of canonical Wnt signalling as indicated by Wnt-c59 induced reduction in protein expression of Wnt3a, β-catenin, CCND1, and c-Myc (Zhao *et al.* 2020). To date Wnt-c59, and PORCN inhibitors in general, have been shown to exert therapeutic effects

in experimental models of both cancer and HFrEF, however their potential as a therapeutic intervention in HFpEF has yet to be investigated.

6.1.4. Aim

Previous data presented in this thesis (Chapter 4) identified that Wnt3a, which primarily activates canonical Wnt signalling, can induce hypertrophy in H9c2 cells characterised by both an increase in the gene and protein expression of hypertrophic markers. Furthermore, data from the pilot studies described in Chapter 5 provided evidence that Wnt signalling was upregulated in the 'two-hit' mouse model of HFpEF. Therefore, the aim of this study was to investigate the effect of Wnt-c59 administration in the same *in vivo* model of HFpEF to determine whether inhibition of Wnt signalling alters adverse structural/functional changes associated in HFpEF.

6.2. Methods

All necessary methodological detail is either described in the following section 6.3. Experimental Protocols or in Chapter 2 as indicated.

6.3. Experimental Protocols

A pilot study was previously completed which indicated that Wnt signalling was upregulated in the high fat feeding/L-NAME administration induced model of HFpEF (results described in Chapter 5). Subsequently, an intervention study was then conducted to examine the effect of administration of a Wnt signalling inhibitor (Wnt-c59) to mice with HFpEF (i.e. those treated with a HFD (35gm%)/L-NAME (0.5g/L) and compare any observed effects with a more standard clinical therapy i.e. the angiotensin receptor blocker (ARB), Candesartan. A schematic of the study design is shown in Figure 6.1. To identify if there was any reversal of the features of HFpEF with the addition of the treatments, measurement of cardiac function (section 6.3.3), gene expression (section 6.3.4), and histological staining (section 6.3.5) were all measured.

6.3.1. Study Design

Male C57Bl/6J mice aged 8 weeks were purchased from Charles River, Edinburgh and acclimatised for one week before dietary/pharmacological intervention was started. Mice were split into four groups of 11-12 mice (4 mice per cage) consisting of 1) a control group; 2) a

HFD+L-NAME group plus vehicle (0.1% DMSO); 3) a HFD+L-NAME plus Wnt-c59 (5mg/kg/day); and 4) a HFD+L-NAME plus Candesartan (5mg/kg/day). Commencement of animals on dietary/pharmacological intervention was staggered over a 9 week period and the four experimental groups were fed either a SD or HFD (the composition of both diets is described in Chapter 5) with the addition of L-NAME (bottles were covered to protect the solution from the light and changed ever 2-3 days) for 7 weeks. Both the inhibitors (Wnt-c59 and Candesartan; both 5mg/kg/day) and vehicle (0.1% DMSO) were administered in drinking water containing L-NAME (0.5g/L) and 2% sucrose (added to increase palatability to ensure the mice were not deterred by the taste of the vehicle/drugs) for the final 2 weeks (weeks 6 & 7) of the dietary/pharmacological intervention period. Wnt-c59 and Candesartan were prepared as described in Chapter 2, section 2.1.1 and changed daily. Previous studies have shown that Wnt-c59 (5mg/kg/day) is biologically active in mice and was sufficient to maintain plasma concentrations well above the IC_{50} for this drug (Proffitt *et al.* 2013; Zhao *et al.* 2020). Candesartan was used at a concentration of 5mg/kg/day based on results shown by Callera et al. (2016) demonstrating that this concentration in mice was sufficient to reduce BP, while at a lower concentration (1mg/kg/day) it was not.

6.3.2. Measurement of BP and cardiac function in anaesthetised animals

Following completion of the dietary/pharmacological intervention study mice were anaesthetised and BP measurements and/or PVL analysis conducted as described in Chapter 2, section 2.5.2. Descriptions and definitions of cardiac measurements that were taken in this study are stated in Table 6.1. Post completion of the *in vivo* protocol, blood was collected via cardiac puncture to conduct a blood volume calibration of the conductance catheter (Chapter 2, section 2.5.2.4.) and to obtain plasma samples. Once the blood had been collected, the heart was immediately removed by cutting the connecting blood vessels to ensure that circulation had stopped and to confirm death of the animal before removing other tissues. Further details on tissue and plasma harvesting are stated in Chapter 2, section 2.5.3.

6.3.3. Investigation of the effects of Wnt-c59 and Candesartan administration on circulating levels of AngII in mice

Blood was obtained pre-mortem via cardiac puncture from mice and plasma was obtained as outlined in Chapter 2, section 2.5.3. and circulating levels of AngII were determined with an AngII EIA kit (details of the ELISA protocol are described in Chapter 2, section 2.5.4.).

6.3.4. Investigation of the effects of Wnt-c59 and Candesartan administration on the expression of genes related to cardiac hypertrophy, fibrosis, and Wnt signalling

To determine the effects of HFD+L-NAME alone and in combination with Wnt-c59 or Candesartan on markers of cardiac hypertrophy, fibrosis, and Wnt signalling a series of gene expression studies were conducted. Approximately 30mg of ventricular tissue from each mouse was placed in a microcentrifuge tube containing 1ml of Tri-reagent and RNA extracted as described in Chapter 2, section 2.3.1. RNA concentration was measured (Chapter 2, section 2.3.2.) and converted to cDNA using the method stated in Chapter 2, section 2.3.3. To measure gene expression, qPCR was conducted (Chapter 2, section 2.3.5.) with primers from both Sigma Aldrich (primer sequences detailed in Chapter 5, Table 5.3.) and Qiagen (primer catalogue numbers detailed in Chapter 5, Table 5.4.).

6.3.5. Determination of the impact of Wnt-c59 and Candesartan administration on the cardiac expression of Wnt3a protein

To further investigate if Wnt3a was increased in HFD+L-NAME mice and if there was any effect of the treatment with Wnt-c59 or Candesartan, protein expression of Wnt3a was measured in heart tissue using an ELISA. Approximately 25-30mg of ventricular tissue was weighed out and placed in homogenisation buffer (1ml per 100mg of tissue; composition described in Table 2.8. in Chapter 2). Once protein was extracted from the heart tissue it was quantified using the Bradford Assay (outlined in Chapter 2, section 2.5.4.2.) and then diluted to 10mg/ml using the sample diluent provided by the Wnt3a DuoSet ELISA kit. The cardiac expression of Wnt3a protein was then measured in all experimental groups as per the method described in Chapter 2, section 2.5.4.3.

6.3.6. Investigation of the effects of Wnt-c59 and Candesartan administration on total β-catenin protein expression in the heart

To identify if canonical Wnt signalling was upregulated in HFD+L-NAME mice and if Wnt-c59 or Candesartan inhibited this signalling pathway, total β-catenin protein expression was measured in the heart tissue. Hearts were harvested (Chapter 2, section 2.5.3) and protein was extracted (Chapter 2, section 2.5.5.1.) and quantified (Chapter 2, section 2.5.5.2.). All protein samples concentrations were adjusted to 5mg/ml using the sample diluent provided by the ELISA kit. Details of the ELISA protocol is described in Chapter 2, section 2.5.5.4.

6.3.7. Examination of the effects of Wnt-c59 and Candesartan administration on cardiac hypertrophy and fibrosis via histological staining

To investigate whether HFD+L-NAME mice displayed cardiac fibrosis, Picrosirius red staining was conducted to measure collagen deposition in the heart. Ventricular tissue sections were cut as described in Chapter 2, section 2.6.1 and Picrosirius red staining was carried out as outlined in Chapter 2, section 2.6.2. To quantify collagen deposition the method outlined in Chapter 2, section 2.6.2.1 was used. To detect if cardiac hypertrophy was altered via the administration of Wnt-c59 or Candesartan, left ventricular wall thickness was measured in cardiac tissue sections stained with Picrosirius red as per Chapter 2, section 2.6.2.2.

6.3.8. Exclusion Criteria

Three mice administered Candesartan exhibited both a rapid decrease in BW and signs of ill-health and so were culled early in the study and not included in any of the subsequent data analysis. PVL analysis: Cardiac function was not assessed in the remaining (8) Candesartan treated mice as at the dose tested (5mg/kg/day) this ARB produced a profound hypotensive effect (reduction of ~60mmHg and ~35mmHg in SBP and DBP, respectively) which was likely to confound any changes in cardiac function that may have been due to Candesartan induced structural changes in the heart. In the remaining three experimental groups (i.e. control, vehicle (HFD+L-NAME), and Wnt-c59 (HFD+L-NAME)) initial experiments (n=4 per group) were conducted using CC PVL analysis however due to technical challenges (i.e. inability to correctly place the catheter in the LV or tearing of the carotid artery) this experimental approach was changed to OC PVL analysis for the remaining n=7-8 animals in each of the three experimental groups. OC PVL analysis was successfully conducted in all remaining mice except for one animal which had an adverse reaction to the anaesthetic and died before surgery and a second animal in which insertion of the catheter into the heart led to excessive blood loss and the experiment was terminated (both mice were from the control group). Furthermore, due to differences in baseline data (i.e. HR tended to be higher and SV smaller in PVL analysis obtained from CC vs OC surgery) any data obtained from successful CC experiments was not combined with that from open chest experiments. Finally, some IVC occlusions (to obtain load independent data) were excluded on the basis of technical issues i.e. an inability to carry out the occlusion of the IVC smoothly. BP measurements: To minimise the duration of the surgical procedure and reduce the risk of technical errors BP measurements were only attempted in experimental group sizes of 5-7 and all BP data obtained was included in the subsequent analysis. Detailed below are the exact number of animals from which data was obtained.

	Number of animals included (n)			
	Control	**Vehicle**	**Wnt-c59**	**Candesartan**
Dietary Intervention	12	12	11	11
PVL - CC	4	4	4	0
PVL- OC	8	8	7	0
Load Dependent	6	8	7	0
Load Independent	5	5	4	0
BP	5	7	6	7

6.3.9. Statistical Analysis

All statistical analysis was conducted using GraphPad Prism 8 software and any differences between results were deemed significant when $P<0.05$. Data was plotted as mean ± SEM. Each n number refers to an individual mouse. The statistical test used for each set of data is detailed in its accompanying figure legend throughout this chapter. Individual data was excluded if it was out with the mean ± (2x standard deviation).

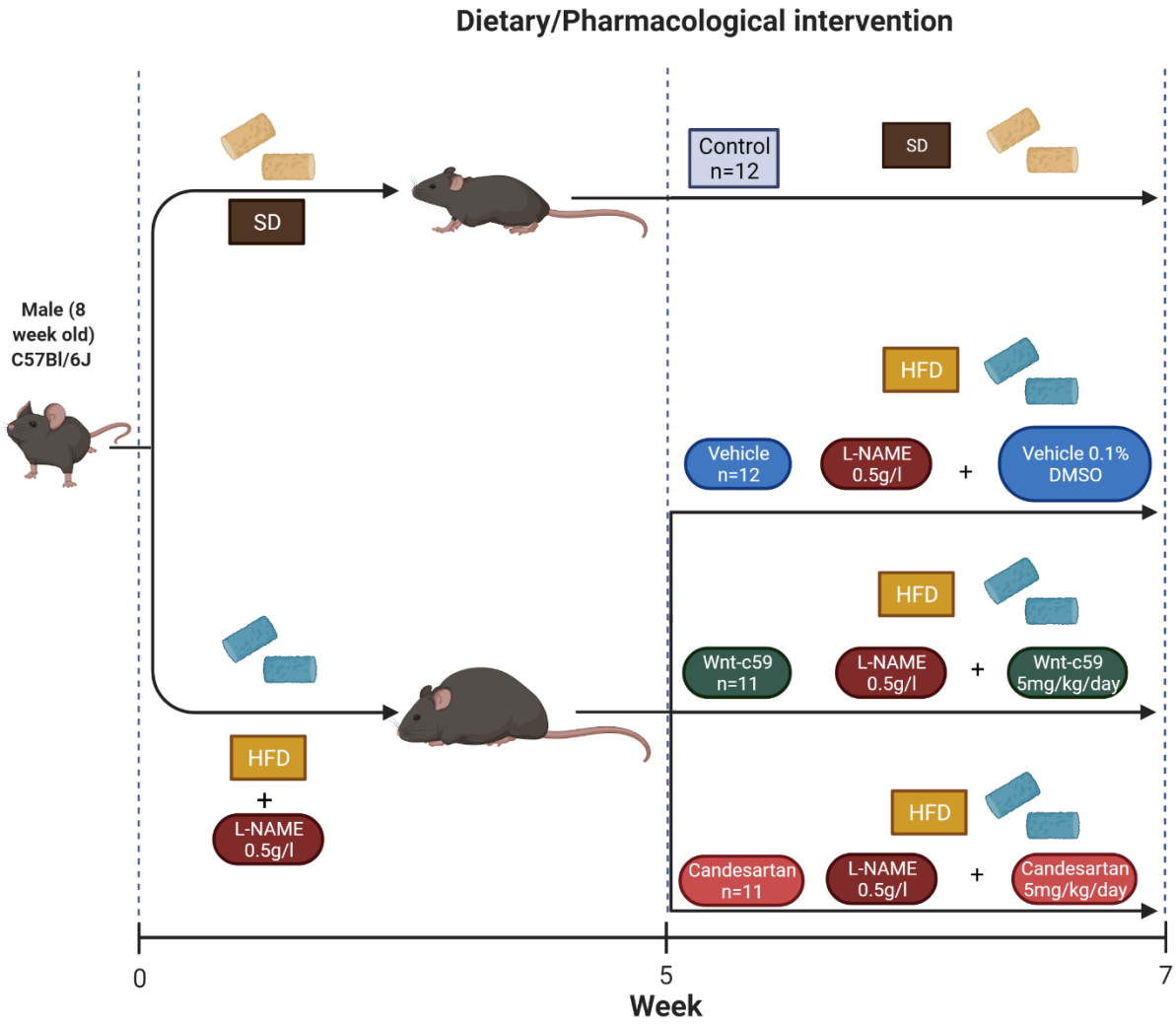

Figure 6.1. Schematic of experimental groups for dietary/pharmacological intervention study. Separate groups (n=11-12) of male C57Bl/6J mice were subjected to one of the four different dietary/pharmacological interventions. SD; Standard diet. HFD; High fat diet.

Table 6.1. Description of cardiac function parameters measured via PVL analysis in this study.

Description	Abbreviation	Definition	Units	Systolic or Diastolic measurement
Heart Rate	HR	The number of heart beats per unit of time, usually per minute.	Beats per min (bpm)	N/A
Cardiac Output	CO	Volume of blood ejected from the heart in one minute (SV x HR).	µl/min	Systolic
Stroke Volume	SV	The volume of blood pumped out of the LV during each systolic cardiac contraction (EDV-ESV).	µl	Systolic
End-Systolic Volume	ESV	The volume of blood in a ventricle at the end of contraction (systole).	µl	Systolic
End-Systolic Pressure	ESP	The pressure in the ventricle at the end of systole.	mmHg	Systolic
Ejection Fraction	EF	Percentage of blood ejected from the ventricle in each contraction ((SV/EDV) x 100).	%	Systolic
dP/dt_{max}	-	Maximal rate of rise of left ventricular pressure determined by contractility.	mmHg/s	Systolic
dP/dt_{min}	-	Minimum rate of change of ventricular pressure to asses ventricular relaxation	mmHg/s	Diastolic
End-Diastolic Volume	EDV	Volume of blood in ventricle at the end of diastole.	µl	Diastolic
End-Diastolic Pressure	EDP	Pressure in the ventricle at the end of diastole.	mmHg	Diastolic
Arterial Elastance	E_a	Measurement of arterial compliance (ESP/SV).	mmHg/µl	Systolic
End-Systolic Pressure Volume Relationship	ESPVR	The maximum pressure that can be developed by the ventricle at any given LV volume. Measurement of contractility.	mmHg/µl	Systolic
End-Diastolic Pressure Volume Relationship	EDPVR	A measurement of ventricular compliance.	mmHg/µl	Diastolic

6.4. Results

6.4.1. Wnt-c59 did not affect body weight (BW), adiposity, or tissue weights compared to the vehicle treated group

As shown in Figure 6.2A., mice in all experimental groups had a similar starting BW. After 7 weeks of dietary and pharmacological intervention, mice in the vehicle group exhibited significantly increased BW (36.3±1.4 vs. 29.7±0.3g; $P<0.05$; Figure 6.2B.) and adiposity i.e. WAT:BW (0.04±0.004 vs. 0.02±0.001g/g; $P<0.05$; Figure 6.3A.) when compared to control animals. Administration of Candesartan to HFD+L-NAME mice significantly decreased BW (28.5±1.7 vs. 36.3±1.4g; $P<0.05$; Figure 6.2B.) after the two-week intervention period, however it did not appear to affect the WAT:BW ratio (Figure 6.3A.). Conversely, administration of Wnt-c59 for 2 weeks did not have any effect on BW (Figure 6.2B.) or adiposity (Figure 6.3A.) when compared to the vehicle group. In the vehicle treated HFD+L-NAME group, liver weight normalised to BW was significantly decreased compared to the control group (0.036±0.001 vs. 0.043±0.001g/g; $P<0.05$; Figure 6.3B.), however neither Wnt-c59 nor Candesartan had any effect on liver weight compared to the vehicle group (Figure 6.3B.). There were no detectable differences in the kidney weight:BW ratio in the control, vehicle, or Wnt-c59 experimental groups, however there was a significant increase in kidney weight:BW in the Candesartan group compared to the vehicle group (0.013±0.0006 vs. 0.011±0.0006g/g; $P<0.05$; Figure 6.3C.). Lastly lung weight normalised to TL did not differ between any of the experimental groups (Figure 6.3D.).

6.4.2. Wnt-c59, unlike Candesartan, did not affect the HFD+L-NAME induced HTN in mice

High fat feeding and L-NAME administration induced a significant increase in SBP (144±8.3 vs. 114±4.0mmHg; $P<0.05$; Figure 6.4A.), DBP (105±4.5 vs. 88±5.9mmHg; $P<0.05$; Figure 6.4B.), and MABP (118±5.2 vs. 97±5.2mmHg; $P<0.05$; Figure 6.4C.) in the vehicle group compared to control mice. The administration of Wnt-c59 to HFD+L-NAME treated mice did not significantly affect SBP, DBP, or MABP when compared to the vehicle group (Figure 6.4A-C.). However, in contrast, Candesartan induced a significant decrease in SBP (85±2.1 vs. 144±8.3mmHg; $P<0.05$, Figure 6.4A.), DBP (69±2.2 vs. 105±4.5mmHg; $P<0.05$; Figure 6.4B.) and MABP (75±2.0 vs. 118±5.2mmHg; $P<0.05$; Figure 6.4C.) compared to vehicle treated HFD+L-NAME mice.

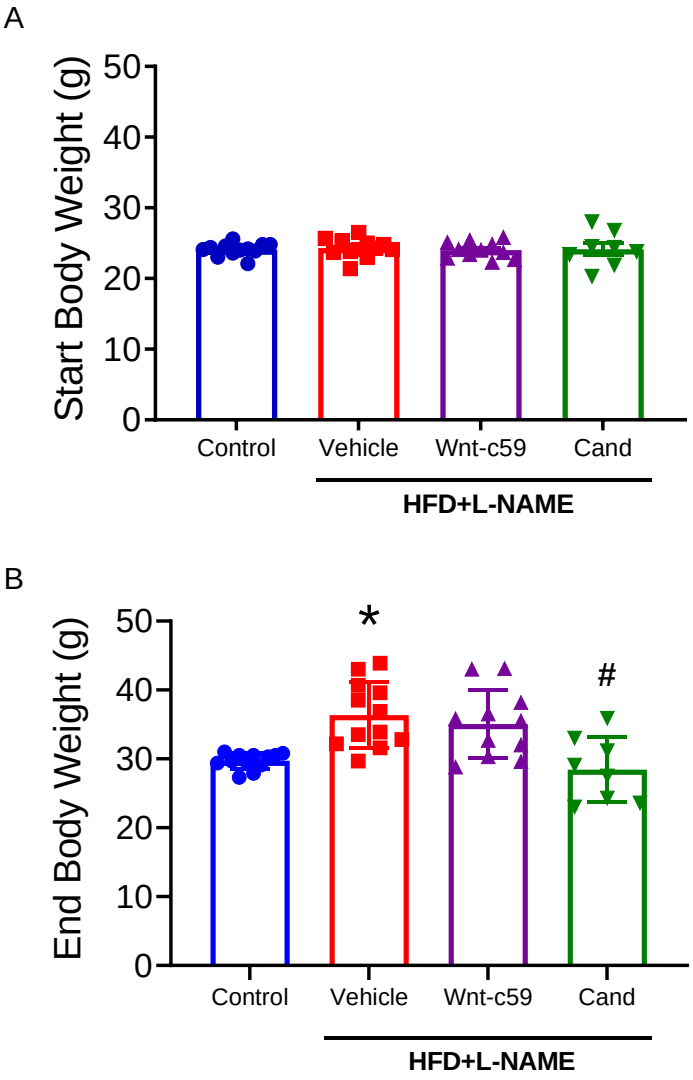

Figure 6.2. Body weight at the beginning of the dietary intervention (A) and at the end of the 7-week dietary and pharmacological intervention (B). Data is expressed as mean ± SEM and analysed using a one-way ANOVA with a Bonferroni post hoc test *P<0.05 vs. Control; #P<0.05 vs. Vehicle; n=8-12.

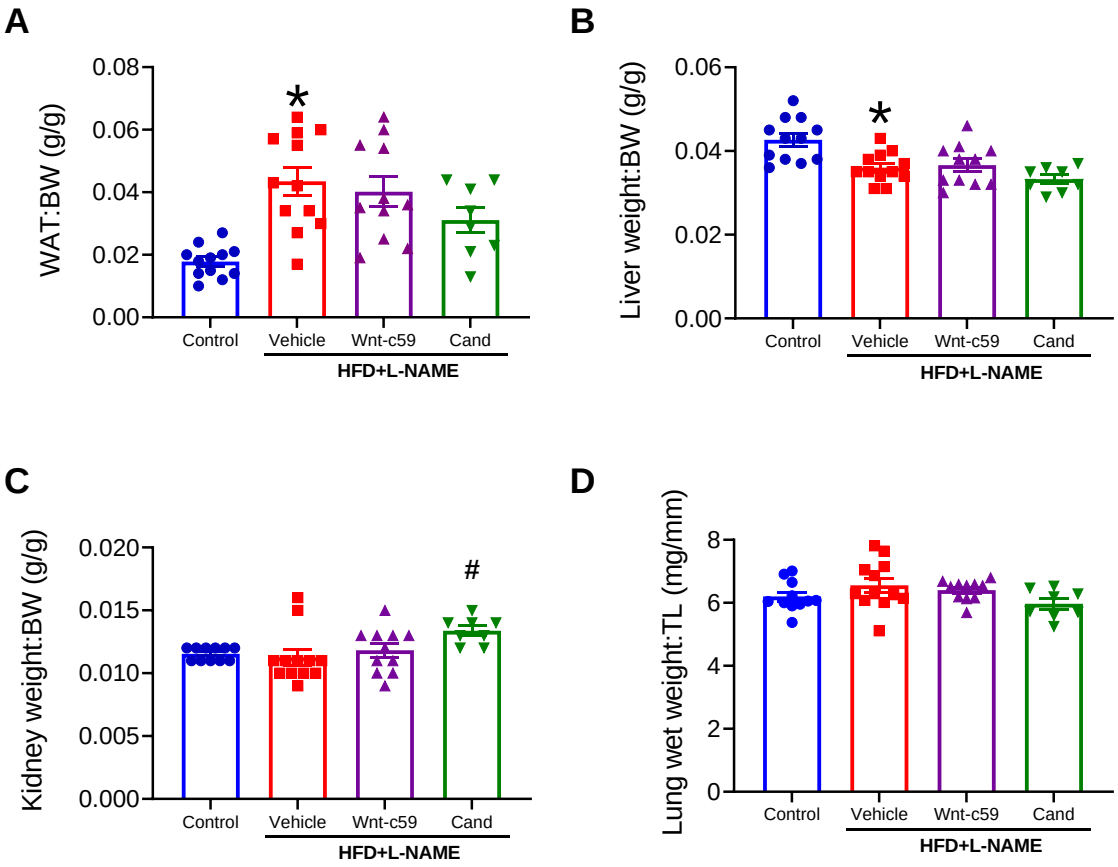

Figure 6.3. WAT normalised to BW (A), liver weight normalised to BW (B), kidney weight normalised to BW (C), and lung weight normalised to TL (D). Data is expressed as mean ± SEM and analysed using a one-way ANOVA with a Bonferroni post hoc test. **P*<0.05 vs. Control; #*P*<0.05 vs. Vehicle; n=8-12.

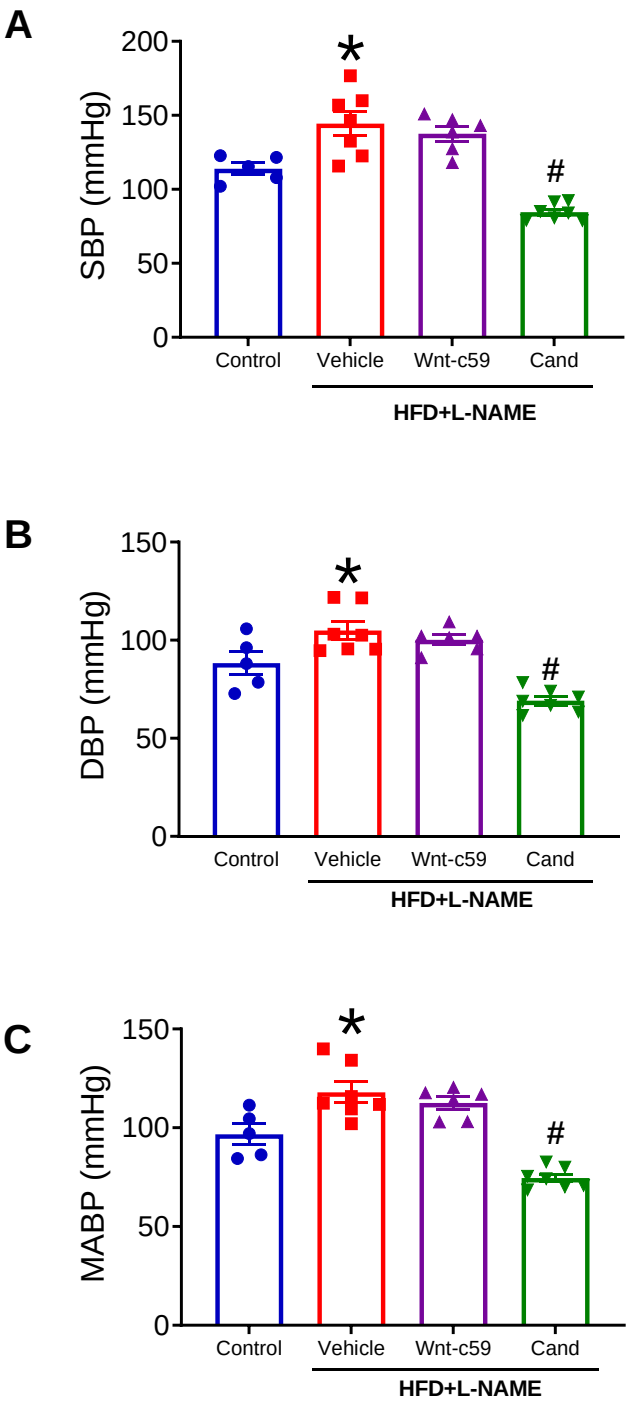

Figure 6.4. SBP (A), DBP (B), and MABP (C). Data is expressed as mean ± SEM and analysed using a one-way ANOVA with a Bonferroni post hoc test *P<0.05 vs. Control; #P<0.05 vs. Vehicle; n=5-7.

6.4.3. Both Wnt-c59 and Candesartan reduced circulating levels of AngII to a similar level

Circulating (plasma) levels of AngII were increased in response to high fat feeding and L-NAME administration (4.3±1.3 vs. 2.4±0.4pg/ml; P=0.06; Figure 6.5.). Furthermore, treatment of HFD+L-NAME mice with Wnt-c59 significantly reduced plasma AngII levels (1.5±0.2 vs. 4.3±1.3pg/ml; *P*<0.05; Figure 6.5.), and a similar effect was demonstrated following Candesartan administration (1.7±0.2 vs. 4.3±1.3pg/ml; *P*<0.05; Figure 6.5.).

6.4.4. Wnt-c59, unlike Candesartan, did not affect the HFD+L-NAME induced cardiac hypertrophy in mice

To assess the effects of Wnt-c59 and Candesartan administration on HFD+L-NAME induced cardiac hypertrophy, the following parameters were measured: heart weight normalised to tibia length (HW:TL), BNP mRNA expression, and left ventricular wall size. In the vehicle group there was a significant increase in HW:TL compared to control animals (6.8±0.23 vs. 5.9±0.15mg/mm; *P*<0.05; Figure 6.6A.) and this hypertrophic effect was significantly attenuated by Candesartan (5.1±0.14 vs. 6.8±0.23mg/mm; *P*<0.05; Figure 6.6A.) but not Wnt-c59 (Figure 6.6A.). In the vehicle group, left ventricular wall thickness was significantly increased in comparison to the control group (2.4±0.09 vs. 2±0.07mm; *P*<0.05; Figure 6.6B.), and was reduced in response to treatment with Candesartan (1.9±0.08 vs. 2.4±0.09mm; *P*<0.05; Figure 6.6B.) but not Wnt-c59 (Figure 6.6B.). Finally, cardiac BNP mRNA expression appeared to be slightly increased (1.5-fold) in the vehicle treated HFD+L-NAME group compared to the control group (Figure 6.6C.), while in the hearts of Candesartan treated mice BNP mRNA expression was reduced by approximately 80% compared to the vehicle group (*P*<0.05; Figure 6.6C.). Conversely, administration of Wnt-c59 induced a significant increase in cardiac BNP mRNA expression when compared to the vehicle group (3.5-fold vs. 1.5-fold; *P*<0.05; Figure 6.6C.).

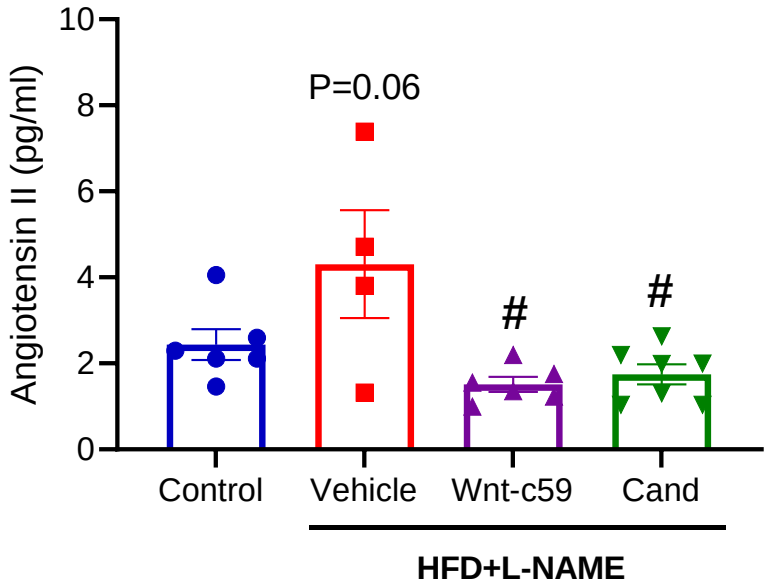

Figure 6.5. Plasma concentration of AngII in experimental animals. Data is expressed as mean ± SEM and analysed using a one-way ANOVA with a Bonferroni post hoc test. n=4-7.

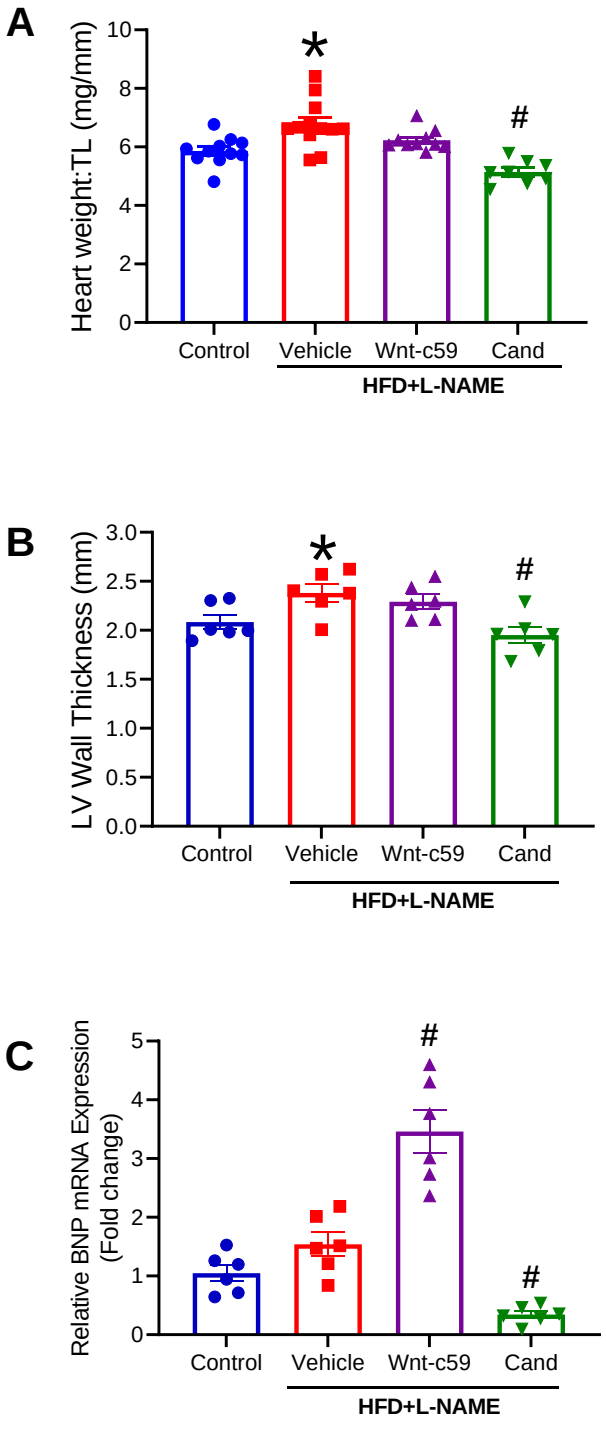

Figure 6.6. Heart weight normalised to TL (A), left ventricular wall thickness (B), and ventricular expression of BNP mRNA (C). Data is expressed as mean ± SEM and analysed using a one-way ANOVA with a Bonferroni post hoc test. **P*<0.05 vs. Control; #*P*<0.05 vs. Vehicle; n=6-12.

6.4.5. Wnt-c59 treatment modulated HFD+L-NAME induced cardiac fibrosis in mice

To detect the presence of cardiac fibrosis, the mRNA expression of both Col1 and Col3 was examined in hearts in addition to the quantification of collagen deposition via Picrosirius red staining. In the vehicle group, mRNA expression of both Col1 (Figure 6.7A.) and Col3 (Figure 6.7B.) were significantly increased (1.95-fold and 1.74-fold, respectively) compared to the control group. Furthermore, this HFD+L-NAME induced increase in Col1 (Figure 6.7A.) and Col3 (Figure 6.7B.) mRNA expression was reduced by approximately 78% and 65%, respectively following treatment with Candesartan (P<0.05 vs. vehicle group for both). In contrast, Wnt-c59 did not significantly alter the mRNA expression of Col1 compared to the vehicle group (1.66-fold vs. 1.95-fold; Figure 6.7A.), but did significantly increase the expression of Col3 compared to the latter (2.2-fold vs. 1.75-fold; P<0.05; Figure 6.7B.). The Col3:Col1 ratio did not differ between either the control, vehicle or Candesartan groups, however Wnt-c59 produced a significant increase in the Col3:Col1 ratio when compared to the vehicle group (P<0.05; Figure 6.7C.). Histological staining demonstrated that collagen deposition was significantly increased in ventricular tissue from the vehicle group compared to the control group (1.42±0.24 vs. 0.63±0.06%; P<0.05; Figure 6.8C.). Furthermore, collagen deposition in ventricles from both Wnt-c59 and Candesartan treated mice appeart to be reduced (1.04±0.08% and 1.26±0.12%, respectively) compared to vehicle treated HFD+L-NAME mice, however neither reduction was statistically significant (Figure 6.8C.).

6.4.5. Wnt-c59 attenuated diastolic dysfunction in HFD+L-NAME treated mice

PVL analysis was conducted to assess the effects of HFD+L-NAME alone and in combination with Wnt-c59 on cardiac function. As previously described in section 6.3.8. cardiac function was not assessed in Candesartan treated mice due to its profound hypotensive effect in these animals. As expected for a model of HFpEF, the dietary/pharmacological intervention (HFD+L-NAME) did not significantly affect the majority of indices of systolic function (ESV; Figure 6.9A.), SV (Figure 6.9B.), CO (Figure 6.9C.), EF (Figure 6.9D.), and dP/dt_{max} (Figure 6.9E.)) recorded in these animals. In all experimental groups, HR values recorded were considerably lower than physiological levels (<400bpm) and are likely due to the choice of anaesthetic (i.e. mixture of ketamine and xylazine) used, which represents a limitation of this study. Nothwithstanding this, HR was not affected by either dietary or pharmacological intervention (Figure 6.9F.). However, there was a significant increase in end-sytolic pressure (ESP) in the vehicle treated HFD+L-NAME group compared to control mice (122±8.7 vs. 94±3.4mmHg; P<0.05; Figure 6.10A.); while arterial elastance (E_a) also appeared to be increased in the former this effect was not statistically significant (8.3±0.9 vs 5.9±0.9mmHg/µl; P=0.15; Figure 6.10B.). Administration of Wnt-c59 to mice did not significantly affect any of the systolic parameters measured when compared to the vehicle group (Figures 6.9A-F. and 6.10A-B.).

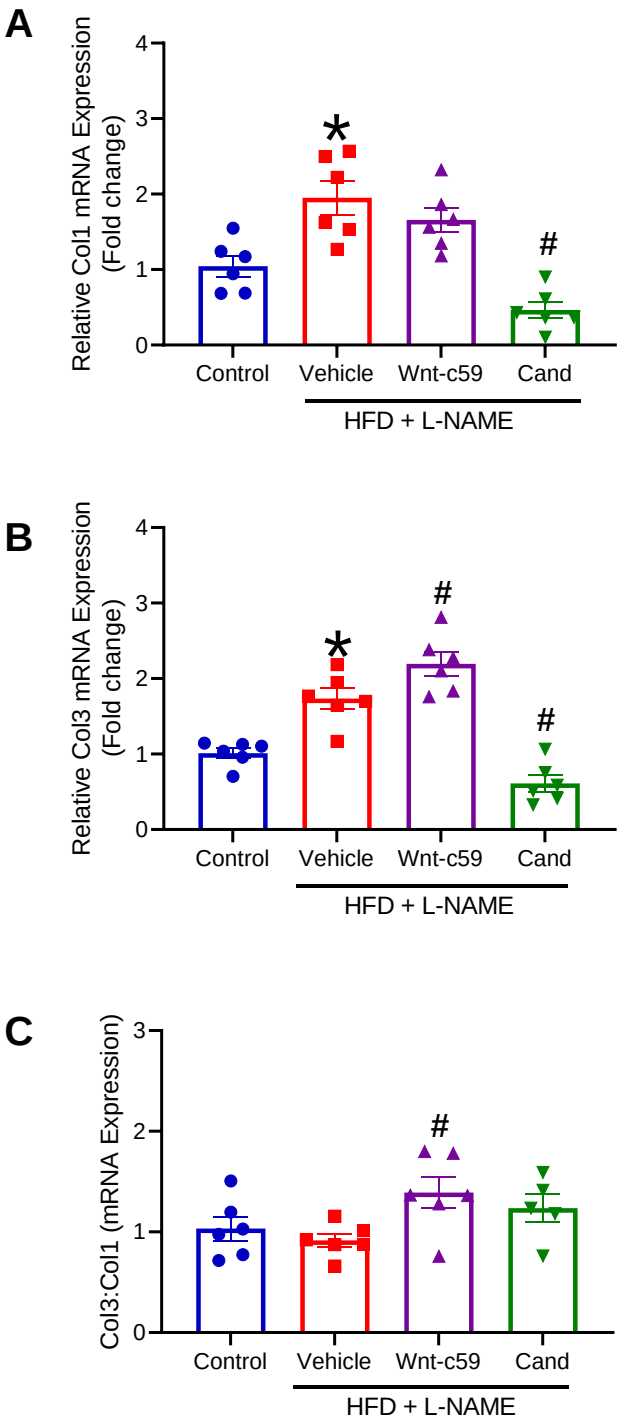

Figure 6.7. mRNA expression Col1 (A) and Col3 (B) and Col3:Col1 ratio (C). Data is expressed as mean ± SEM and analysed using a one-way ANOVA with a Bonferroni post hoc test. **P*<0.05 vs. Control; #*P*<0.05 vs. Vehicle; n=5-6.

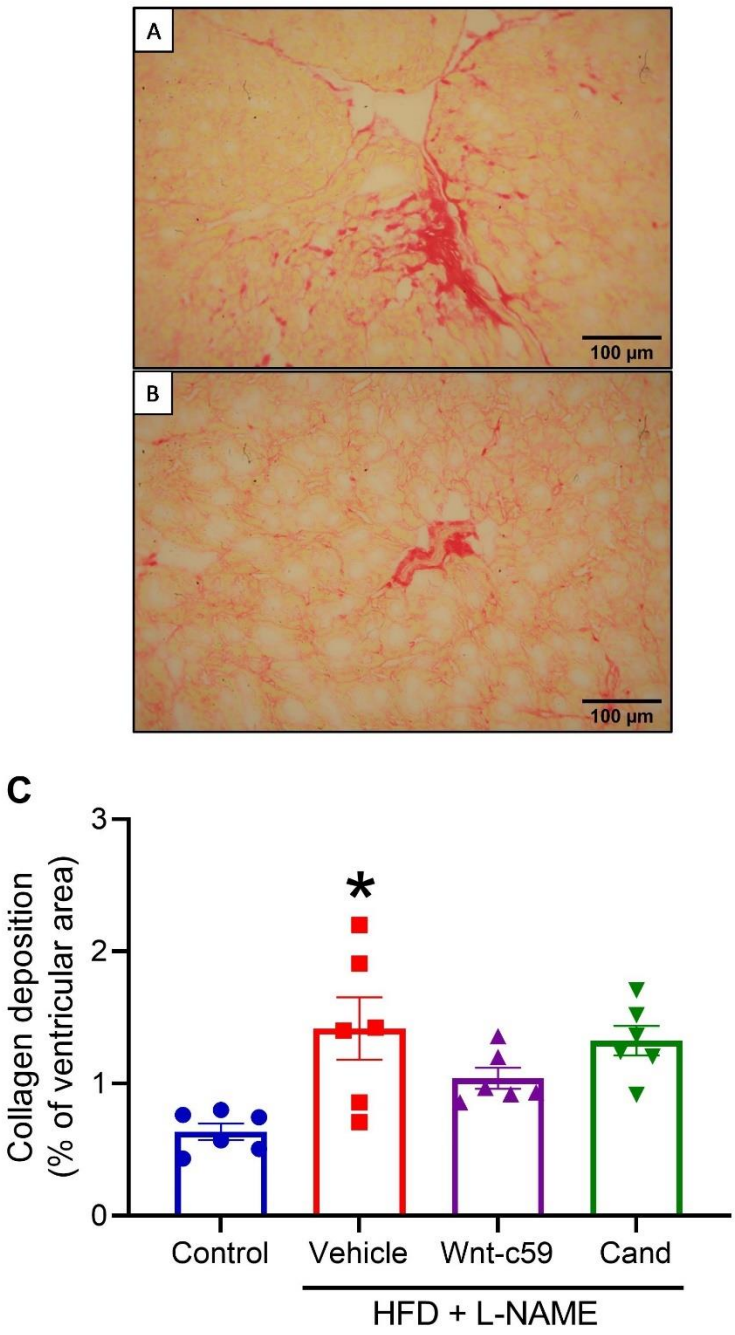

Figure 6.8. Collagen deposition in murine ventricular tissue. Representative images of picrosirius stained ventricular tissue (to detect collagen) demonstrating both interstitial fibrosis (A) and perivascular fibrosis (B) in hearts from control mice. Images were taken at x200 magnification. Scale bar = 100µm. Quantification of collagen deposition in ventricular tissue (C). Data is expressed as mean ± SEM and analysed using a one-way ANOVA with a Bonferroni post hoc test. **P*<0.05 vs. Control; n=6.

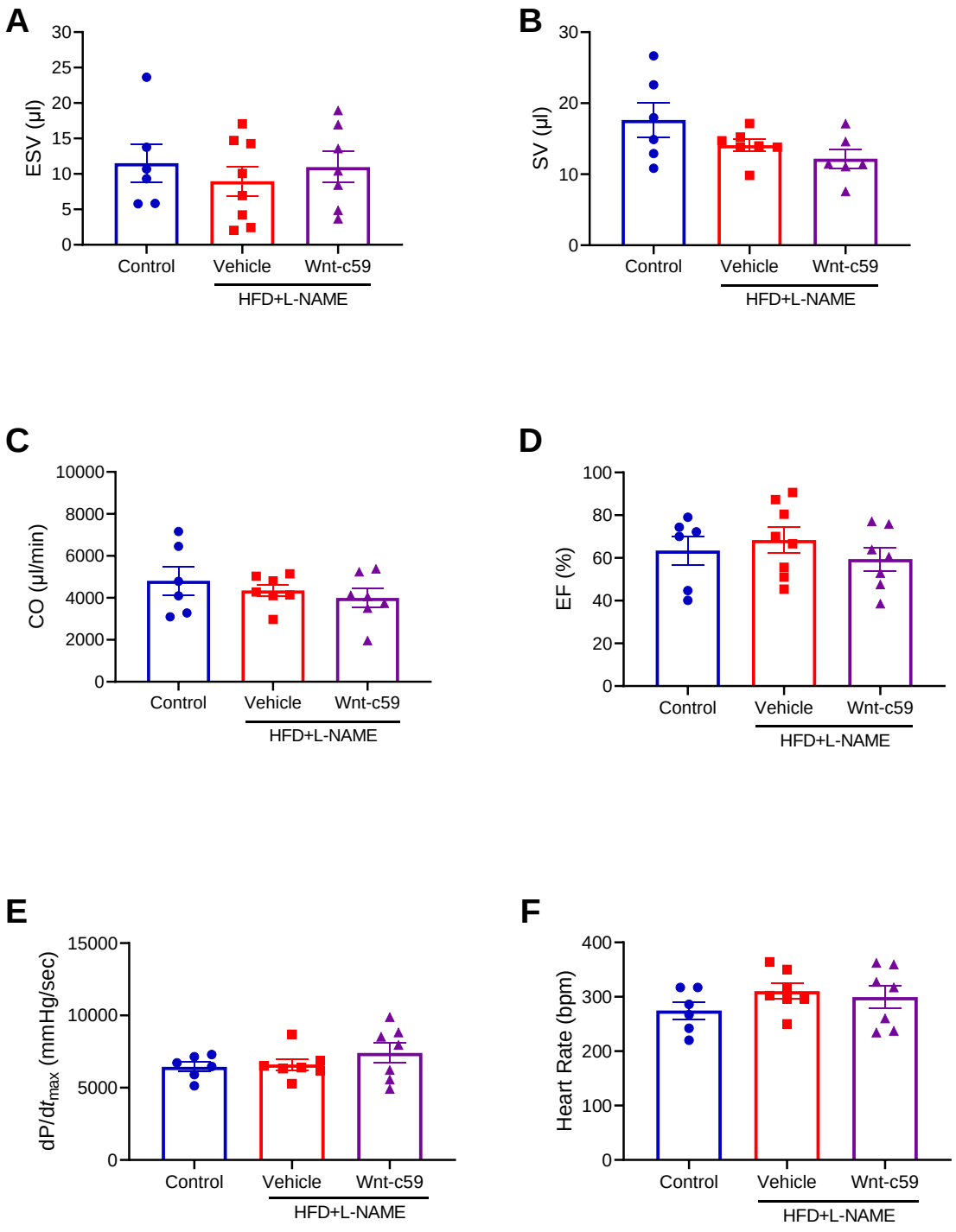

Figure 6.9. Load dependent indices of systolic function; ESV (A), SV (B), CO (C), EF (D), dP/dt_{max} (E), and HR (F). Data is expressed as mean ± SEM and analysed using a one-way ANOVA with a Bonferroni post hoc test. n=6-8.

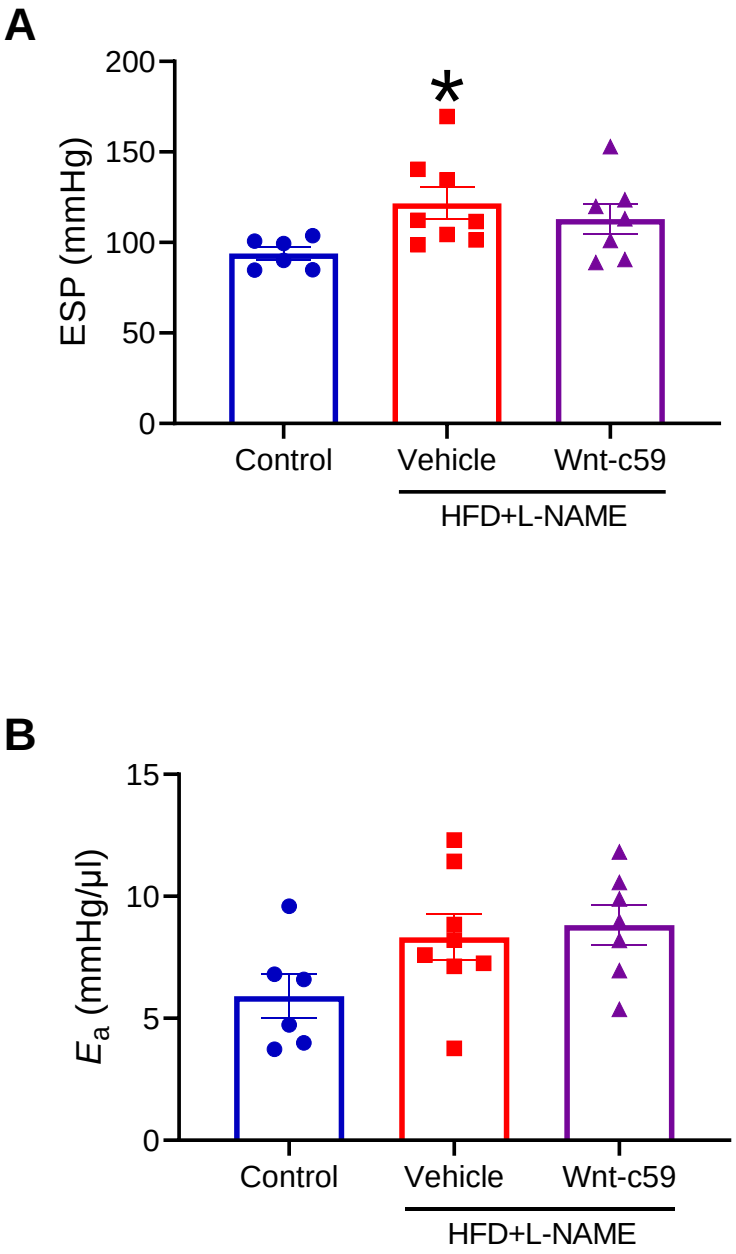

Figure 6.10. Load dependent indices of systolic function; ESP (A), and E_a (B). Data is expressed as mean ± SEM and analysed using a one-way ANOVA with a Bonferroni post hoc test. *P<0.05 vs. Control; n=6-8.

In terms of diastolic measurements of cardiac function, the vehicle group displayed a decrease in EDV compared to the controls (20.1±2.3 vs. 27.5±3.1µl; P=0.18; Figure 6.11A.), which, although pronounced, did not achieve statistical significance. However, end-diastolic pressure (EDP) was significantly increased in the vehicle treated HFD+L-NAME group compared to control mice (7.1±0.7 vs. 4.2±0.3mmHg; *P*<0.05; Figure 6.11B.). Moreover, administration of Wnt-c59 for two weeks significantly reduced the HFD+L-NAME induced increase in EDP (4.1±0.8 vs. 7.1±0.7mmHg; *P*<0.05; Figure 6.10B.). Finally, dP/dt_{min} was not altered in either the vehicle and Wnt-c59 treated HFD+L-NAME groups (Figure 6.11C.). In terms of load independent indices of cardiac function, the value for the ESPVR was unaltered in response to either high fat feeding and L-NAME alone or when co-administered with Wnt-c59 group (Figure 6.12A.). In contrast, the EDPVR value appeared to be increased in the vehicle group compared to the control group but didn't reach statistical significance (0.31±0.03 vs. 0.22±0.03mmHg/µl; P=0.09; Figure 6.12B.). Following 2 weeks of administration of Wnt-c59, the EDPVR value in this experimental groups was similar to that observed in the control group and reduced compared to the vehicle treated HFD+L-NAME mice (0.19±0.03 vs. 0.31±0.03mmHg/µl; P=0.06; Figure 6.12B.).

6.4.6. Canonical Wnt signalling was not activated in the hearts of HFD+L-NAME mice but Wnt signalling markers were reduced by both Wnt-c59 and Candesartan

To investigate whether Wnt signalling was activated in the hearts of HFD+L-NAME mice, the mRNA expression of both Wnt3a (canonical Wnt ligand) and Wnt5a (non-canonical Wnt ligand) was measured. In contrast to the findings from the pilot study, cardiac expression of Wnt3a mRNA was not altered in vehicle treated HFD+L-NAME mice compared to control animals (Figure 6.13A.). However, treatment of HFD+L-NAME mice with either Wnt-c59 or Candesartan decreased the cardiac expression of Wnt3a mRNA by approximately 85% and 92%, respectively, compared to vehicle treated animals (*P*<0.05; Figure 6.13A.). Furthermore, cardiac expression of Wnt3a protein (measured via ELISA) did not differ between any of the experimental groups (229±9pg/mg (control); 233±10pg/mg (vehicle); 218±9pg/mg (Wnt-c59); 241±10pg/mg (Candesartan); Figure 6.13B.). Cardiac expression of Wnt5a mRNA also did not differ significantly between the vehicle and control experimental groups, however, unlike Wnt3a, Wnt5a expression was not altered following treatment with either Wnt-c59 or Candesartan (Figure 6.13C.). In further support of a lack of activation of canonical Wnt signalling, the expression of β-catenin (non-phosphorylated and phosphorylated) protein (measured via ELISA) did not differ in the hearts of animals from any of the experimental groups (2832±215.5pg/mg (control); 2739±150pg/mg (vehicle); 2774±256.9pg/mg (Wnt-c59); 2760±254pg/mg (Candesartan); Figure 6.14.). mRNA expression of target genes (c-Myc,

CCND1, and Axin2) of canonical Wnt signalling were also examined in the hearts of all animals. The results demonstrated that expression of c-Myc mRNA was not significantly altered in response to high fat feeding and L-NAME, however administration of Candesartan to mice reduced the cardiac expression of this gene compared to vehicle treated animals ($P<0.05$; Figure 6.15A.). Similarly, the expression of CCND1 mRNA was not significantly altered in the vehicle group compared to the control group, however both Wnt-c59 and Candesartan produced a significant decrease in the cardiac expression of CCND1 compared to the vehicle group ($P<0.05$; Figure 6.15B). Lastly, the mRNA expression of Axin2 was also unchanged in the vehicle group compared to the control group, however treatment with both Wnt-c59 and Candesartan reduced Axin2 expression by approximately 40% and 30%, respectively, compared to the vehicle group ($P<0.05$; Figure 6.15C.).

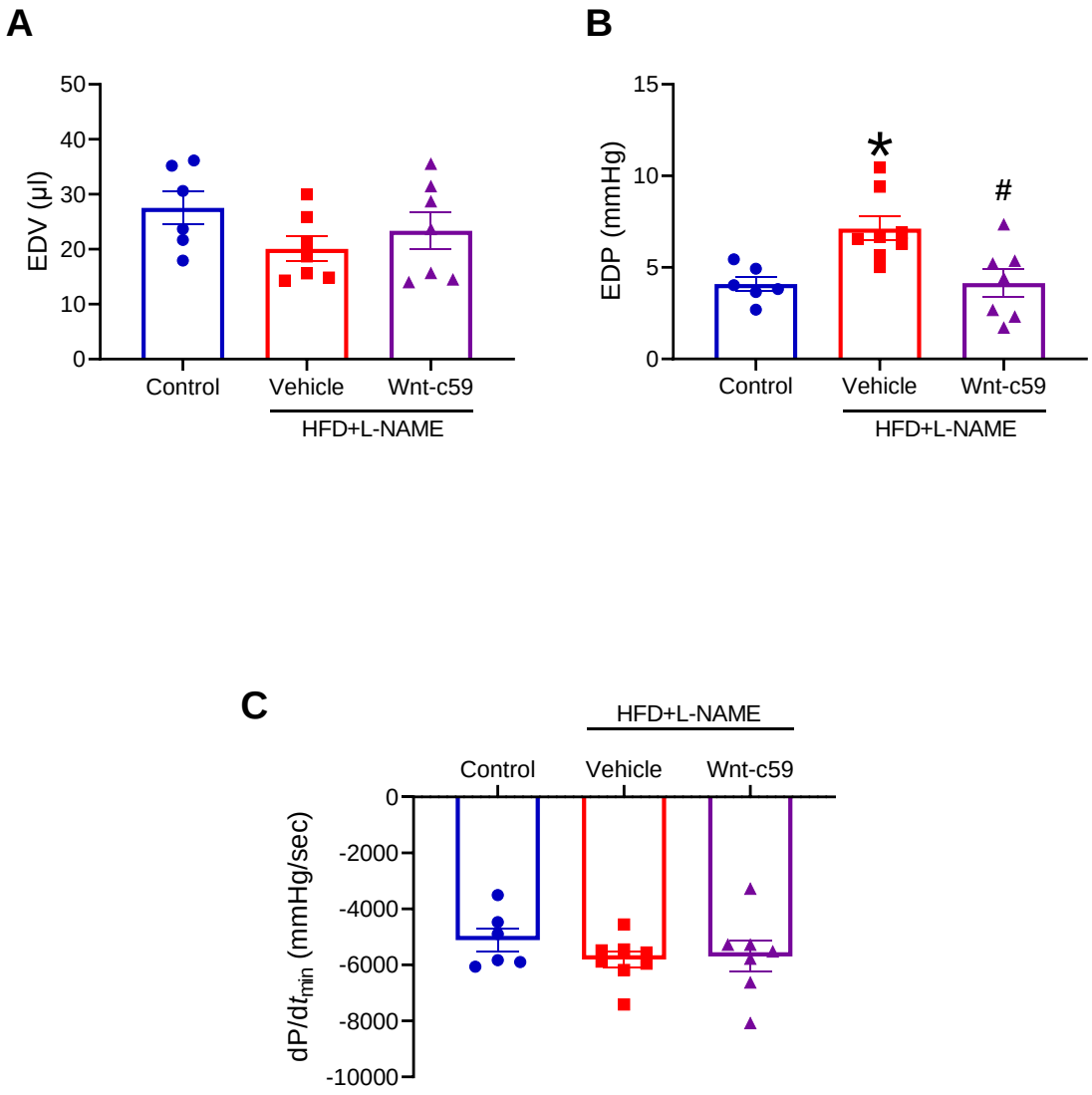

Figure 6.11. Load dependent indices of diastolic function; EDV (A), EDP (B), and dP/dt_{min} (C). Data is expressed as mean ± SEM and analysed using a one-way ANOVA with a Bonferroni post hoc test. **P*<0.05 vs. Control; #*P*<0.05 vs. Vehicle; n=6-8.

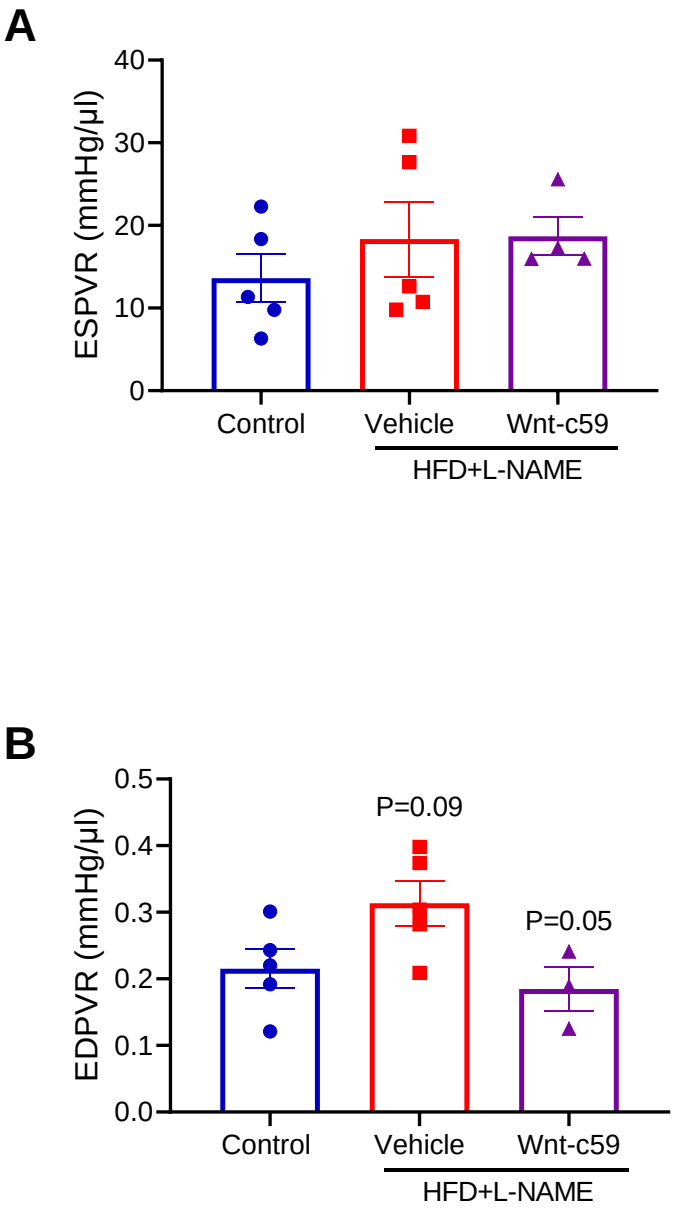

Figure 6.12. Load independent indices of both systolic (ESPVR; (A)) and diastolic (EDPVR; (B)) function. Data is expressed as mean ± SEM and analysed using a one-way ANOVA with a Bonferroni post hoc test. n=3-5.

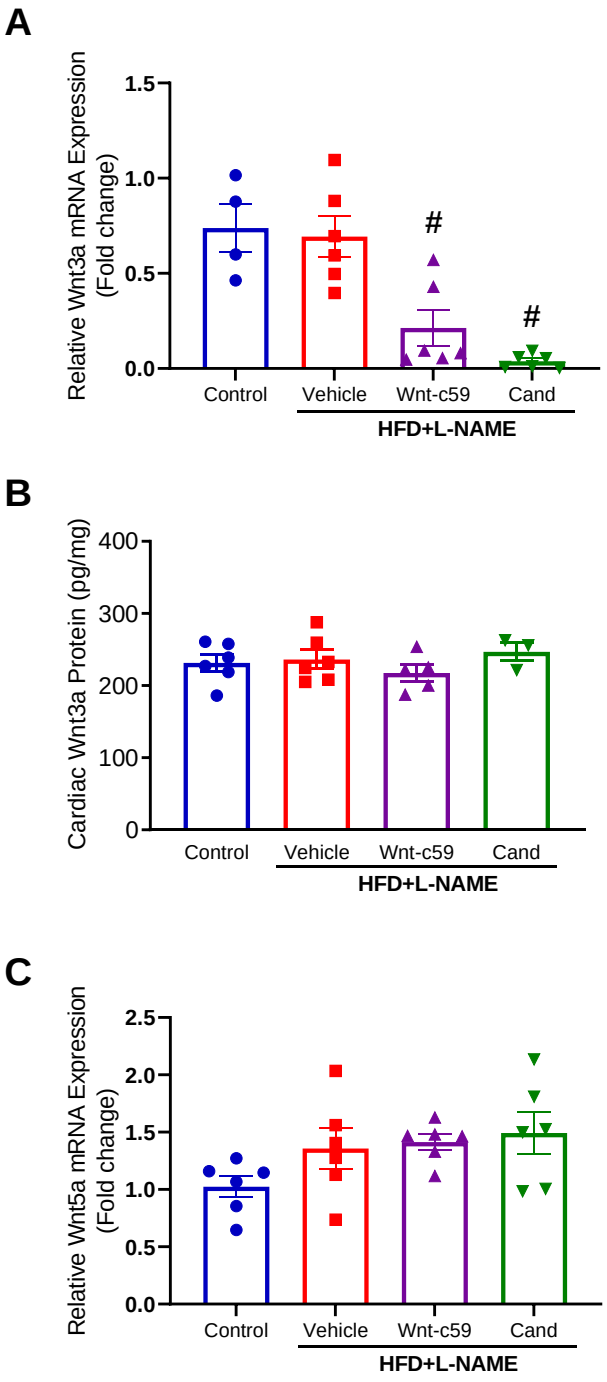

Figure 6.13. mRNA expression (A) and protein expression (B) of Wnt3a and mRNA expression of Wnt5a (C) in murine ventricular tissue. Data is expressed as mean ± SEM and analysed using a one-way ANOVA with a Bonferroni post hoc test. #*P*<0.05 vs. Vehicle; n=4-6.

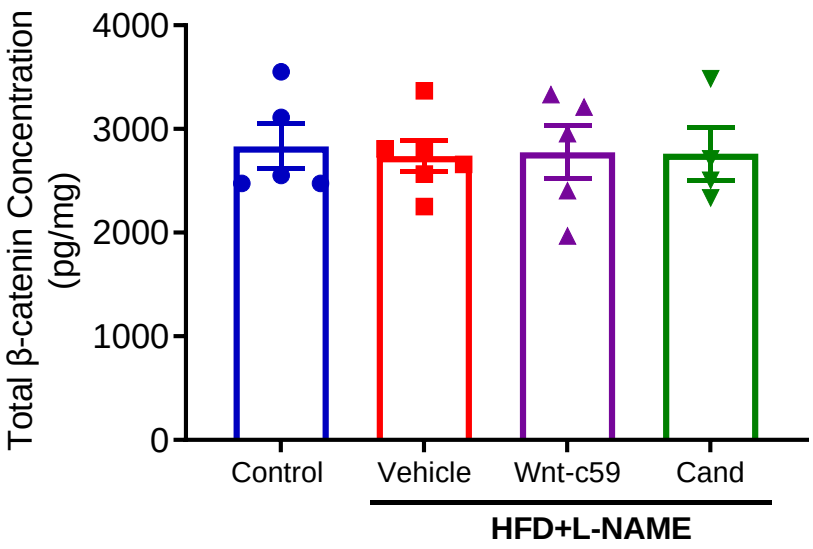

Figure 6.14. Expression of total (non-phosphorylated and phosphorylated) β-catenin protein in murine ventricular tissue. Data is expressed as mean ± SEM and analysed using a one-way ANOVA with a Bonferroni post hoc test; n=4-6.

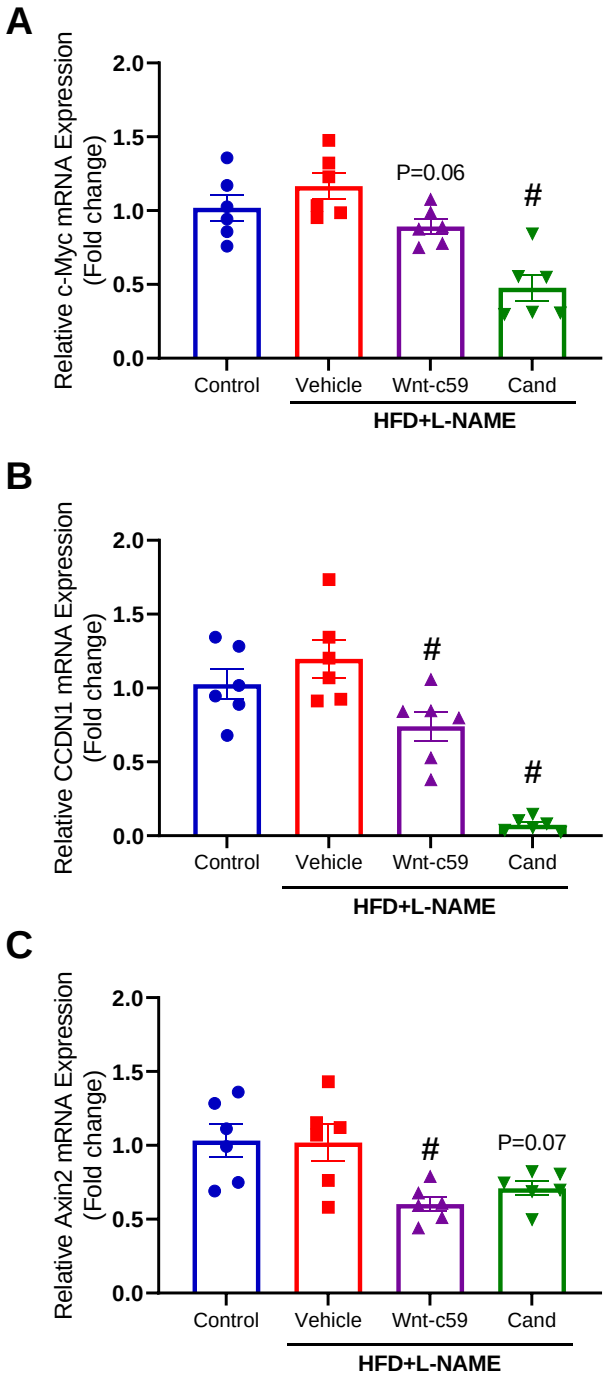

Figure 6.15. mRNA expression of c-Myc (A), CCND1 (B), and Axin2 (C) in murine ventricular tissue. Data is expressed as mean ± SEM and analysed using a one-way ANOVA with a Bonferroni post hoc test. #*P*<0.05 vs. Vehicle; n=6.

6.5. Discussion

The principle aim of this study was to investigate whether Wnt-c59 influences the functional and/or structural effects induced by a 'two-hit' (i.e. metabolic and mechanical stress) *in vivo* model of HFpEF and compare any observed effects with a more standard clinical therapy i.e. Candesartan. In this study, the vehicle treated HFD+L-NAME mice (experimental model of HFpEF) were characterised by HTN, increased BW and adiposity, cardiac hypertrophy and fibrosis, and diastolic dysfunction as shown by reduced ventricular compliance. Canonical Wnt signalling did not appear to activated in this model of HFpEF as none of the markers of Wnt signalling (Wnt3a, β-catenin, CCND1, c-Myc, and Axin2) assessed were altered in the hearts of these animals. Notwithstanding this, administration of the Wnt signalling inhibitor, Wnt-c59, did ameliorate diastolic dysfunction (i.e. reduced EDP and EDPVR), but did not alter HTN, cardiac hypertrophy or fibrosis, in HFpEF mice.

6.5.1. Wnt-c59 did not alter the phenotypic changes associated with the dietary/pharmacological induction of HFpEF

This is the first study to report the effects of Wnt-c59 on BW and adiposity in mice subjected to a HFD. In this study, the vehicle treated HFD+L-NAME mice displayed a significant increase in both BW and adiposity, which is due to the HFD (discussed previously in Chapter 5, section 5.1.1.) as L-NAME administration has previously been shown to reduce BW (Sung *et al*. 2013; Berenyiova *et al*. 2018). Administration of Wnt-c59 did not alter BW or degree of adiposity which correlated with results shown by Proffitt et al. (2013), where BW was not altered in mice after 21 days of administration of Wnt-c59. In female mice, a higher concentration of Wnt-c59 (10mg/kg/day) also did not induce any changes in BW over a period of 21 days (Funck-Bretano *et al*. 2018). In contrast, BW was reduced in mice in response to treatment with the ARB, Candesartan, which agrees with previous reports demonstrating that antagonism of the RAAS (either via ACE inhibitors or ARBs) can induce weight loss in rodents (de Kloet *et al*. 2009; He *et al*. 2010b; Mul *et al*. 2013). However, this effect appears to be dose dependent, at least in terms of ARBs, since a study investigating the effects of Candesartan (2, 6, and 16mg/kg/day) on BW in spontaneously hypertensive rats found that only the highest dose tested (i.e. 16mg/kg/day) reduced BW following 4 weeks of treatment, and that this effect was due to a decrease in daily food intake (Müller-Fielitz *et al.* 2011). In contrast, daily administration of Candesartan (up to a dose of 75mg/kg/day) for 4 weeks did not affect BW in *db/db* mice (Callera *et al.* 2016), while Saegusa et al. (2007) reported that treatment of virally (encephalomyocarditis virus) infected mice with Candesartan (10mg/kg/day) for 7 days led to weight gain compared to vehicle treated mice. In the present study, a dose of 5mg/kg/day Candesartan was chosen on the basis of previously observed hypotensive effects at this

concentration (Wang *et al.* 2012; Callera *et al.* 2016) rather than on its ability to alter BW. The Candesartan-induced reduction in the BW of mice in the present study did not appear to be due to increased lipolysis, since the ratio of WAT:BW was not altered in this group compared to vehicle treated mice. However, only epididymal fat was used in the determination of WAT:BW and so a reduction in the accumulation of WAT in other areas of the body cannot be ruled out.

In the present study, daily food intake decreased in response to Candesartan treatment and likely explains the reduction in BW in this group. A possible explanation for this is the ability of ARBs to alter the secretion of hormones that regulate hunger/food intake. The administration of Candesartan (2mg/kg/day) to rats produced a significant decrease in the plasma concentration of ghrelin, a hormone which stimulates appetite (Hamada *et al*. 2012). Furthermore, the administration of the ARB, Telmisartan, to mice for 6 weeks decreased agouti-related protein, a neuropeptide that is co-expressed with neuro peptide Y to increase appetite (Aubert *et al*. 2010). The vehicle treated HFD+L-NAME group also displayed a decrease in liver weight normalised to BW, which is likely due to higher BW as individual liver weights did not vary. It has previously been reported that a HFD can increase liver weights in mice following dietary intervention periods of between 12 and 16 weeks (Eccleston *et al*. 2011; Woo *et al.* 2014) and thus the lack of change in individual liver weights in this study is likely to the relatively short dietary intervention period of 7 weeks. However, in a separate study that compared liver weights in mice subjected to a HFD alone or in combination with L-NAME for 12 weeks, the authors found that L-NAME treatment appeared to mitigate the HFD induced increase in liver weight (Tsuchiya *et al*. 2007) and thus it is possible that a similar effect may have occurred in the present study. Finally, neither Wnt-c59 nor Candesartan had any effect on liver weight normalised to BW. The ratio of kidney weight to BW was also not altered in either vehicle or Wnt-c59 treated HFD+L-NAME mice, however it was increased in response to Candesartan treatment. It seems likely that this effect is due to the lower BWs of the mice in the Candesartan experimental group, as combined (right and left) kidney weights alone did not differ between experimental groups.

6.5.2. Wnt-c59 reduced circulating AngII, but did not alter HTN in this mouse model HFpEF

The combination of high fat feeding and administration of L-NAME for 7 weeks induced HTN (a SBP of 144mmHg, a DBP of 105mmHg, and a MABP of 118mmHg) in male mice. These results agree with those from previously published studies and those from the pilot study

(discussed in Chapter 5), which demonstrated that following 5-7 weeks of dietary/pharmacological intervention SBP, DBP, and MABP were all elevated in male mice (Cordero-Herrera *et al.* 2019; Schiattarella *et al.* 2019; Tong *et al.* 2019; Cordero-Herrera *et al.* 2020). Studies have shown that on its own high fat feeding is not sufficient to induce HTN (Schiattarella *et al*. 2019) even when the dietary intervention period is extended to 16 months (Calligaris *et al.* 2013) and thus co-administration of a hypertensive agent such as AngII or L-NAME is necessary. To induce HTN, L-NAME is added to the drinking water of rodents and has been shown to elevate BP in both rats (Sung *et al.* 2013; Li *et al.* 2020; Pechanova *et al.* 2020) and mice (Nagano *et al.* 2013; Schiattarella *et al*. 2019; Wang *et al*. 2020). L-NAME is a potent NOS inhibitor which subsequently reduces the availability of NO, a vasorelaxant released by vascular endothelial cells. Mice treated with L-NAME are characterised by both HTN and endothelial dysfunction (as indicated by both an upregulation in the pro-inflammatory genes vascular cell adhesion protein 1 and plasminogen activator inhibitor-1, and a reduction in the expression of eNOS) (Nagano *et al*. 2013).

It has also been demonstrated that L-NAME can increase the activity of the RAAS, thus further contributing to HTN. In an L-NAME induced rat model of HTN, both the serum concentration of aldosterone and the aldosterone/AngII ratio were enhanced (Simko *et al*. 2018). Furthermore, both renal AngII and AGT have been shown to be significantly elevated in mice treated with L-NAME as measured by radioimmunoassay (Giani *et al*. 2014). Studies have shown that administration of L-NAME increases the circulating level of renin (Ishiguro *et al*. 2007), the renal expression of renin, ACE, and AT_1Rs (Lee *et al*. 2002), and the expression of ACE (converts AngI to AngII) in both plasma and tissue (Sharifi *et al*. 2005). AngII plays an important role in HTN as it is a potent vasoconstrictor and can activate sympathetic nerve function. In the present study, circulating AngII was increased in vehicle treated HFD+L-NAME mice and thus is likely to contribute to the HTN observed in these animals. This finding agrees with others that demonstrated an increase in the circulating level of AngII in rats treated with L-NAME for either 3 weeks (Ishiguro *et al*. 2007) or 5 weeks (Mannesai *et al*. 2016). Conversely, administration of L-NAME to rats has also been shown to reduce serum levels of AngII (Simko *et al*. 2018), while high fat feeding has been shown to increase plasma AngII (Kim 2017; Santos *et al*. 2020; Xue *et al*. 2021). Therefore, in the present study the elevated circulating AngII in the vehicle treated HFD+L-NAME mice is likely due to the combination of both dietary and pharmacological intervention.

Results from this study demonstrated that administration of Wnt-c59 to HFD+L-NAME mice for 2 weeks reduced plasma levels of AngII to a similar extent achieved by Candesartan treatment. This study is the first to demonstrate that a PORCN inhibitor i.e. Wnt-c59 reduces circulating levels of AngII and consequently the mechanism via which it does this has yet to be fully elucidated. However, one possible explanation may involve the NPs which acts as negative regulator of AngII secretion (reviewed by Fu *et al*. 2018). In particular, ANP has been shown to exert an anti-hypertrophic role via inhibiton of RAAS signalling (reviewed by Volpe *et al*. 2016), thus as Wnt-c59 increased BNP mRNA expression in the hearts of these mice it is possible that it also increased ANP which may explain its AngII lowering effect, however this requires further investigation. Conversely, Candesartan induced reductions in plasma AngII levels is well reported with experimental studies demonstrating that when administered at doses between 0.2-10mg/kg/day for 7-28 days this ARB reduced circulating AngII in both mice (Zhao and Wang 2018) and rats (Luo *et al*. 2021). However, in a conflicting study administration of Candesartan (3mg/kg/day) for 8 weeks did not alter plasma AngII levels in mice with DCM (Odagiri *et al*. 2014). Candesartan is an AT_1R blocker and therefore prevents the binding of AngII and subsequent vasoconstriction. A possible explanation as to how Candesartan reduces plasma AngII levels in this study could be through enhancing ACE2 activity, which converts AngII to Ang1-7, which produces vasodilatory and hypotensive effects (reviewed by Touyz and Montezano 2018). In a rat model of DCM, the administration of Candesartan for 4 weeks increased expression of ACE2 and Ang1-7 in the myocardium (Arumugam *et al*. 2012). Furthermore, Takeda et al. (2007) also reported that ACE2 mRNA levels in the hearts of Dahl sat-sensitive hypertensive rats were increased following treatment with Candesartan.

In addition to reducing circulating AngII, Candesartan also exerted a profound hypotensive effect in HFD+L-NAME mice, providing further support for a role for RAAS activation in L-NAME induced HTN. This finding agrees with previous studies demonstrating a BP lowering effect of AT_1R antagonism in L-NAME induced HTN. In particular, administration of Candesartan (3mg/kg/day) for 2 weeks to L-NAME treated connexin 40 deficient ($Cx40^{-/-}$) mice reduced MABP from 133mmHg to 107mmHg (Krattinger *et al*. 2009). While in rat models of L-NAME induced HTN, administration of Candesartan at a dose of 3mg/kg/day for 3 weeks or 10mg/kg/day for 10 days significantly reduced BP (Casellas *et al*. 2001; Mohammed and Hussein 2020). Similar to Candesartan, Wnt-c59 also reduced circulating AngII, however this PORCN inhibitor did not affect BP. To date, there are no reports documenting the impact of PORCN inhibition on BP for comparison, however the current findings seem surprising in light of the reduced circulating AngII and the seemingly significant contribution AT_1R activation

makes towards the regulation of BP in this model. One possible explanation may be the suggested AngII hypersensitivity, which has been reported to occur as a consequence of increased AT_1R expression in L-NAME induced hypertensive rodents (Lee *et al.* 2002; Rivera-Jardon *et al*. 2009; Mannesai *et al*. 2016). Thus, in the current model (i.e. HFD+L-NAME treated mice), Candesartan would antagonise this increased abundance of AT_1Rs thus reducing BP, while Wnt-c59, which thus far has not been reported to act at AT_1Rs, would not. Finally, it may also be surprising that in the face of the Wnt-c59 induced increase in cardiac BNP mRNA expression, BP remains elevated in these animals despite the previously described hypotensive effect of NPs. However, it has frequently been reported that ANP, rather than BNP, is the NP that regulates BP (reviewed by Volpe *et al*. 2016). Futhermore, in incidences in which BNP was shown to exert a hypotensive effect this was via a NO-dependent mechanism (Edvinsson *et al*. 2014), which would be abrogated in the current model. Taken together, both suggestions may explain why Wnt-c59 did not alter BP in mice.

6.5.3. Wnt-c59 did not alter the hypertrophic response of HFpEF mice

In L-NAME treated animals, increased AngII in addition to reduced levels of NO, leads to adverse vascular remodelling, cardiac fibrosis, cardiac hypertrophy, and inflammation (Campbell 2006). In this study, the vehicle treated HFD+L-NAME mice were characterised by cardiac hypertrophy as shown by an increase in the ratio of heart weight to TL, increased left ventricular wall thickness, and a slight increase in ventricular BNP mRNA expression. These findings replicate those of the pilot study which is described in Chapter 5 and discusses the role of L-NAME in the induction of cardiac hypertrophy in rodents in detail.

Treatment with Candesartan reduced cardiac hypertrophy in mice as demonstrated by reductions in the ratio of heart weight to TL, LV wall thickness, and BNP gene expression compared to vehicle treated mice. These results correlate with previous reports demonstrating an anti-hypertrophic effect of Candesartan in both patients with hypertensive heart disease (Isobe *et al*. 2002) and rodents with L-NAME induced HTN (Casellas *et al*. 2001; Okazaki *et al*. 2006). Furthemore, in a mouse model of DCM, Candesartan administration (3mg/kg/day) for 2 months reduced the rato of heart weight to TL and decreased BNP mRNA expression (Odagiri *et al*., 2014). Given the direct pro-hypertrophic effect of AngII (see Chapter 4) it seems likely that Candesartan exerts its anti-hypertrophic effect via antagonism of AT_1Rs expressed on cardiomyocytes in the hearts of these animals. In support of this, several other studies have also demonstrated the pro-hypertrophic role of AngII in mice (Matsumoto *et al*. 2013; Tsuruda *et al*. 2016; Zhang *et al*. 2020). These results together with the results shown in this study

provide evidence the RAAS contributes to the development of cardiac hypertrophy in this model.

Treatment of HFD+L-NAME mice with Wnt-c59 did not alter cardiac hypertrophy in these animals which conflicts with previous reports demonstrating an anti-hypertrophic effect of PORCN inhibitors in TAC models of pressure overload (Jiang *et al.* 2018; Zhao *et al.* 2020). In the latter studies which used a model of systolic dysfunction, cardiac hypertrophy was associated with the induction of canonical Wnt signalling and the subsequent attenuation of hypertrophy due to inhibition of this signalling pathway by Wnt-c59. Previous studies have reported that Wnt signalling can contribute to cardiac hypertrophy as discussed in section 6.1.1, and *in vitro* experiments in this project have confirmed the hypertrophic potential of canonical Wnt, Wnt3a, in H9c2 cells. This is the first study to investigate if Wnt signalling is upregulated in a model of HFpEF, therefore there is no literature available to directly compare the results of this study with. In this intervention study, mice fed a HFD+L-NAME did not display any changes in cardiac Wnt3a gene expression, which is in contrast to the pilot study, where Wnt3a expression was upregulated in the heart after 5 weeks of a HFD+L-NAME (discussed in full in Chapter 5, section 5.5.5.). Given the transient nature of gene expression both circulating levels of secreted Wnt3a and cardiac expression of Wnt3a protein were also measured in this study. However, Wnt3a was not detectable in the plasma from any of the mice and there were no differences in the cardiac expression of Wnt3a protein between any of the experimental groups. These results disagree with results reported by Zhao et al. (2018) and Zhao et al. (2020), where both protein and gene expression of Wnt3a were increased in hypertrophic rodent hearts from both a TAC pressure overload model and an AngII infusion model, although the latter are more representative of HFrEF. As it is possible that a canonical Wnt other than Wnt3a may mediate cardiac hypertrophy, the expression of total (non-phosphorylated and phosphorylated) β-catenin protein was measured via ELISA in the heart tissue, as the latter is modulated in response to activation of canonical Wnt signalling regardless of the particular canonical Wnt ligand. However, there were no differences in the expression of total β-catenin in the hearts of mice from any of the experimental groups, which further supports a lack of activated canonical Wnt signalling in this model of HFpEF. Some caution should be exercised when interpreting this result though as the ELISA used quantifies total β-catenin and does not distinguish between unphosphorylated and phosphorylated β-catenin. In the setting of canonical Wnt signalling activation, unphosphorylated β-catenin accumulates in the cytosol prior to translocation to the nucleus, while in the presence of inactive canonical Wnt signalling β-catenin undergoes phosphorylation, therefore, it would be useful in future studies to quantify the amount of both total and phosphorylated β-catenin with the use of Western blotting.

In addition to the absence of an increase in β-catenin accumulation, the expression of target genes of this protein (i.e. c-Myc, CCND1, and Axin2) were also unaltered in the hearts of vehicle treated HFD+L-NAME mice. However, gene expression can be transient and expressed for a short period of time and protein expression of these markers was not measured. Protein expression of β-catenin, c-Myc, and CCND1 have all been shown to be elevated in a TAC pressure overload model (Zhao *et al*. 2020), with an increase in the protein expression of β-catenin also reported in an AngII infused rat model (Zhao *et al*. 2018). The vehicle group appeared to show a slight increase in non-canonical Wnt5a gene expression; however, this was not significant in comparison to controls. Although canonical Wnt signalling does not appear to be upregulated in this model, the possibility that non-canonical Wnt signalling is activated remains, as only one non-canonical gene was assessed, however further investigation is needed. Despite the absence of alterations in the expression of Wnt signalling markers in the vehicle group (compared to the control) treatment with Wnt-c59 decreased Wnt3a gene expression which correlates with results reported by Zhao et al. (2020), however had no effect on the expression of the Wnt5a gene. A study has identified, that in mice, PORCN affects the processing of Wnt1, Wnt3a, Wnt4, Wnt6, and Wnt7b, however does not affect the processing of Wnt5a (Tanaka *et al*. 2000). Therefore, this may explain why Wnt-c59 had no effect on Wnt5a gene expression in this study. Treatment with Wnt-c59 also reduced the gene expression of canonical signalling markers c-Myc, CCND1, and Axin2, which agrees with findings in a TAC pressure overload model, in which Wnt-c59 reduced the protein expression of c-Myc, CCND1, and β-catenin levels in the heart (Zhao *et al*. 2020). Finally, Wnt-c59 has also been shown to reduce gene expression of Axin2 in a mammary cancer mouse model (Proffitt *et al*. 2013).

Mice treated with Candesartan also had a decrease in the gene expression of Wnt3a, c-Myc, and CCND1, indicating that there is a link between RAAS and Wnt signalling. However, it did not have any effect on the gene expression of Wnt5a, suggesting that it mainly targets canonical Wnt signalling. The current findings are supported by those from other studies. In mice subjected to unilateral ureteral obstruction and folic acid–induced renal fibrosis treatment with Candesartan (30mg/kg/day) for 7 days, reduced the surgical/dietary induced increase in the expression of c-Myc protein (Shen *et al*. 2017). Conversely, contrasting results have been reported in a recent study which demonstrated that the gene expression of Wnt3a and CCND1 were reduced in the hippocampus of hypertensive rats, but subsequently increased in reponse to administration of Candesartan (2mg/kg/day) for 35 days (Bhat *et al*. 2018). There is limited data providing evidence that Candesartan reduces Wnt signalling in the heart, however it has been shown to reduce the gene expression of CCND1 in a mouse model of colorectal cancer

(Tabatabai *et al*. 2021). Finally, activation of canonical Wnt signalling does not appear to mediate the cardiac hypertrophy observed in the experimental model of HFpEF used in the present study. In contrast, it seems likely that cardiac hypertrophy was induced in response to the L-NAME induced pressure overload, as the BP lowering effect of Candesartan was associated with an anti-hypertrophic effect, while Wnt-c59 did not alter either BP or cardiac hypertrophy.

6.5.4. Wnt-c59 did not alter cardiac fibrosis in HFpEF mice

Vehicle treated HFD+L-NAME mice were characterised by cardiac fibrosis as shown by an increase in the gene expression of both Col1 and Col3, as well as an increase in collagen deposition in the heart. These findings replicate those of the pilot study described in Chapter 5, where the role of L-NAME in the induction of cardiac fibrosis in rodents is discussed in detail. Wnt-c59 did not affect the expression of Col1, but did increase the expression of Col3 in the hearts of HFD+L-NAME mice. It has been reported that the ratio of Col1 to Col3 within cardiac interstitial tissue can influence both cardiac systolic and diastolic function and as adverse LV remodelling progresses Col3 expression is decreased and supplemented with Col1. Col1 is the more tensile collagen and contributes to rigidity, whereas Col3 promotes vascular elasticity (Pfeffer and Braunwald 1990). Furthermore, it has been shown that increased myocardial levels of Col1 lead to a deterioration of cardiac function, whereas increased levels of Col3 can lead to improved cardiac function (Ravichandran and Puvanakrishnan 1991). In a *db/db* mouse model of diastolic dysfunction, the Col1:Col3 ratio is increased in the heart (Plante *et al*. 2015), while excess dietary linoleic acid increased Col1:Col3 ratio in the hearts of mice fed a HFD resulting in cardiac stiffening characterised by impaired transmitral flow (Beam *et al*. 2015). Furthermore, in a hypercholesterolemic rabbit model of diastolic dysfunction, the ratio of Col1:Col3 was shown to be significantly increased compared to controls (Nacher *et al*. 2019). In addition, the overexpression of Col3 attenuated systolic dysfunction in a rat model of ischaemic cardiomyopathy by altering the balance of collagen type distribution (Uchinaka *et al*. 2018).

As the administration of Wnt-c59 to mice increased the cardiac expression of Col3 mRNA the ratio of Col3 to Col1 was calculated to determine whether the observed improvement in diastolic function may be attributable, at least in part, to a greater abundance of Col3 compared to Col1. This study is therefore the first to demonstrate that both Col3 mRNA expression and the ratio of Col3:Col1 is increased in the hearts of mice following the administration of Wnt-c59. In terms of overall collagen deposition, Wnt-c59 slightly reduced the percentage of

collagen within ventricular tissue, however this was not significant in comparison to the vehicle group. Conversely, in a TAC induced pressure overload model, Wnt-c59 reduced collagen deposition (% fibrosis) in the heart as measured by Masson trichrome staining (Zhao *et al.* 2020). In that study and the present one, Wnt-c59 was administered to mice at a concentration of 5mg/kg/day, however in the study by Zhao et al. (2020), Wnt-c59 was given for 4 weeks as opposed to the 2 week pharmacological intervention period used in the present study, this may explain the disparity in results. In comparison, Candesartan reduced the gene expression of both Col1 and Col3, but did not affect collagen deposition in the heart. The effects of Candesartan on the gene expression of collagen subtypes agrees with a previous study in which administration of this ARB (0.1mg/kg/day) for 2 weeks reduced the L-NAME induced increase in Col1 mRNA expression in rats (Okazaki *et al*. 2006). Furthermore, administration of Candesartan (3mg/kg/day) to mice for 2 months reduced the degree of fibrosis in the hearts of these animals (Odagiri *et al*. 2014), while treatment of rats for 4 weeks with Candesartan (2mg/kg/day) reduced myocardial collagen deposition as measured by picrosirius red staining (Brown *et al*. 2001). Thus, it is possible that although the 2 week treatment period used in the present study was sufficient for Candesartan to reduce the gene expression of the collagen subtypes, it was not sufficient to significantly alter collagen deposition.

6.5.5. Wnt-c59 ameliorated diastolic dysfunction in HFpEF mice

As anticipated, systolic function (including EF) was not altered in this model of HFpEF, however both high fat feeding and L-NAME administration induced diastolic dysfunction. In particular, vehicle treated HFD+L-NAME mice were characterised by a slight reduction in EDV, and increased EDP and EDPVR, all of which suggest increased ventricular stiffness and impaired relaxation. These results agree with those findings reported by Schiattarella et al. (2019) which demonstrated that mice subjected to a HFD with L-NAME for either 5 or 15 weeks exhibit diastolic dysfunction (increased E/A and E/e' ratios at 5 and 15 weeks and also increased EDP and EDPVR at 15 weeks) while systolic function (EF and dP/dt_{max}) was not altered. Separate studies by Tong et al. (2019) and Kitakata et al. (2021) also confirmed the presence of diastolic dysfunction (increased E/e' ratio as measured by echocardiography) and the absence of systolic dysfunction (EF was unaltered) in the HFD+L-NAME induced model of HFpEF. In contrast, Huang et al. (2021) reported that mice subjected to the same HFD and L-NAME concentration (0.5g/L) for 10 weeks not only exhibited diastolic dysfunction characterised by a loss of LV compliance (decreased dP/dt_{min}) and increased LV pressure (increased EDP) but also some evidence of systolic dysfunction (decreased dP/dt_{max} although EF was unaltered). The reason for the reduced dP/dt_{max} reported by Huang et al. (2021) is unclear however, they also reported a reduction in E/A ratio in their HFpEF mice which conflicts with the previously

dicussed studies (Schiattarella *et al.* 2019; Tong *et al.* 2019; Kitakata *et al.* 2021) which all reported increases in E/A ratio. In mild (Grade I) diastolic dysfunction E/A ratio is decreased while in severe (Grade III) diastolic dysfunction E/A ratio is increased compared to healthy controls (Mitter *et al.* 2017) and thus the model reported by Huang et al. (2021) is more likely to reflect the former. Therefore, it is possible that in the early stages of diastolic dysfunction the force of contraction (dP/dt_{max}) of the LV is reduced potentially as some form of adaptive reponse in an attempt to reduce the strain on the heart but this requires further investigation. Taken together, these studies demonstrate the suitability and usefulness of the HFD+L-NAME induced experimental model of HFpEF.

The administration of Wnt-c59 to mice reduced the HFD+L-NAME-induced increase in both EDP and EDPVR, the latter of which returned to that observed in control animals. These Wnt-c59 induced changes suggest increased ventricular compliance and consequently improved diastolic function in HFpEF mice. As previously discussed (section 6.5.4.), it seems likely that the Wnt-c59 induced increase in Col3 expression is, at least in part, responsible for the increased ventricular compliance in these animals, however another possible explanation may involve the phosphorylation of titin. In the present study, Wnt-c59 increased the cardiac expression of BNP, which has been shown elsewhere to signal via cGMP to induce the activation of PKG and subsequent phosphorylation of titin promoting increased ventricular compliance (discussed in detail in Chapter 1, section 1.4.3.). A reduction in PKG-mediated phosphorylation of the myofilament protein titin leads to an increase in cardiomyocyte passive tension and reduced LV capacitance, and thus hypophosphorylation of titin has been suggested as a key contributor to diastolic dysfunction in HFpEF (Kruger *et al*. 2008; Borbely *et al*. 2009). In support of this, both cGMP and PKG activity have been shown to be reduced in myocardial biopsies from patients with HFpEF (van Heerebeek *et al*. 2012). Furthermore, administration of BNP to dogs was shown to increase both plasma cGMP and cardiac titin phosphorylation resulting in a reduction in titin-based cardiomyocyte stiffness and an increase in LV diastolic capacitance (Bishu *et al*. 2011). In patients and animal models of HFpEF, a reduction in NO bioavailability contributed to decreased cGMP and PKG activity (Franssen *et al*. 2016), therefore it is possible that the HFpEF model used in this study is also characterised by decreased cGMP and PKG activity due to the L-NAME induced reduction in NO. If the latter is true then Wnt-c59 could potentially increase cGMP and PKG activity via the upregulation of BNP expression, resulting in phosphorylation of titin and a reduction in ventricular stiffness. The present study is the first to demonstrate the induction of BNP expression by a PORCN inhibitor and so the exact mechanism via which Wnt-c59 exerts this effect has yet to be investigated. In previous years, cGMP-enhancing drugs, in particular PDE5 inhibitors have

been tested as a therapeutic approach for HFpEF, however, despite some promising results initially, ultimately proved not to be effective (discussed in Chapter 1, section 1.5.2.).

BNP-based drugs enhance cGMP via a different mechanism to PDE5 inhibitors. One such drug, the vasodilator Nesiritide, exerts its effects by increasing vascular cGMP production. It was recommended for the treatment of acutely decompensated HF and was approved by the Food and Drug Administration (FDA) in 2001. Clinical studies reported that Nesiritide decreased pulmonary capillary wedge pressure (used to assess LV filling and LA pressure), systemic BP and systemic vascular resistance (Colucci *et al*. 2000; Burger *et al*., 2002; Michaels *et al*. 2003). However, two meta-analysis studies (Sackner-Bernstein *et al*. 2005a,b) reported that Nesiritide resulted in worsening renal function and higher short-term mortality, findings which were subsequently not supported by a large randomised trial conducted in 2011 (O'Connor *et al*. 2011). More recently, a meta-analysis by Gong et al. (2015) reported that Nesiritide was not associated with an increased risk of mortality, however it did increase the risk of adverse cardiovascular events. In 2018, the FDA reported that Janssen Pharmaceuticals were discontinuing the manufacture of Nesiritide, therefore currently there is a lack of BNP based drugs available for clinical use. Other pharmaceutical agents that increase the plasma levels of BNP include beta-blockers such as Metoprolol (Davis *et al*. 2006), and vasopeptidase inhibitors such as Omapatrilat (McClean *et al*. 2002), however further investigation is needed to confirm if Wnt-c59 can increase cGMP levels in the heart by increasing BNP levels and subsequently induce phosphorylation of titin.

6.6. Conclusion

In conclusion, this is the first study that has investigated the therapeutic potential of a PORCN inhibitor (Wnt-c59) in a model of HFpEF. The results demonstrated that in this 'two-hit' *in vivo* model systolic function is not altered, as expected, however there is evidence of diastolic dysfunction as consequence of increased ventricular stiffness. On the basis of this study, a role for canonical Wnt signalling in the development of HFpEF is not supported. Notwithstanding this, treatment of HFpEF mice with Wnt-c59 did ameliorate diastolic dysfunction via mechanisms that may contribute to increased ventricular compliance such as BNP induced phosphorylation of titin and/or favourable regulation of the ratio of collagen subtype expression, however this requires further investigation.

Chapter 7: General Discussion

7.1. Key Findings

The incidence of HFpEF is rising year on year and as yet there is no effective pharmacotherapy to directly treat this condition, only those directed at treating the associated co-morbidities. Taken together, this emphasises the clinical importance of investigating potential therapeutic interventions for HFpEF. Throughout the literature, it has been widely documented that there is a link between Wnt signalling and cardiovascular diseases (reviewed by Foulquier *et al*. 2018), with studies showing that Wnt signalling plays a key role in the development of both cardiomyocyte hypertrophy and cardiac fibrosis (Carthy *et al*. 2011; Malekar *et al*. 2010; Xiang *et al*. 2017; Zhao *et al*. 2019a), both of which are key features of HFpEF. However, targeting Wnt signalling as a potential therapeutic intervention in HFpEF has not been investigated thus far. In order to address this knowledge gap, the aims of this study were to 1) examine the role of Wnt signalling in cardiomyocyte hypertrophy; 2) investigate whether Wnt signalling contributes to the development of HFpEF using an *in vivo* model of the condition; and 3) determine whether the administration of a Wnt inhibitor (Wnt-c59) alters the maladaptive structural and/or functional changes associated with HFpEF.

7.1.1. Wnt3a exerts hypertrophic cellular effects and is increased after the addition of a pro-hypertrophic agent

Research has highlighted a link between RAAS and Wnt signalling in cardiac hypertrophy, with AngII (a key effector peptide in RAAS) being shown to induce the activation of Wnt signalling in rodent cardiomyocytes (i.e. NRVMs) (Zhao *et al.* 2018). The findings from this study support the latter by demonstrating that AngII increases the expression of the canonical Wnt ligand, Wnt3a, in rat H9c2 cells. However, the present study extends these findings by demonstrating for the first time that this effect is recapitulated in human cells with the observation that AngII induces the upregulation of Wnt3a mRNA expression in primary HCMs. Furthermore, the addition of Wnt-c59 (Wnt inhibitor) reduced AngII-induced BNP expression in H9c2 cells, further confirming a potential link between RAAS and Wnt signalling (illustrated in Figure 7.1.). Based on the literature and the findings from this study it is possible that Wnt3a induced activation of canonical Wnt signalling leads to an increase in β-catenin accumulation in cardiomyocytes, which then subsequently activates downstream mediators of RAAS (including AngII) further exacerbating cardiomyocyte hypertrophy via a detrimental feedback loop. However, further investigation is needed to demonstrate if any of the components of the RAAS are upregulated in H9c2 cells and/or HCMs in response to Wnt3a. Finally, this study and others have clearly demonstrated a pro-hypertrophic role for Wnt3a (shown by an increase in fetal gene expression) and thus the latter should be investigated further as a potential therapeutic target in conditions characterised by cardiac hypertrophy.

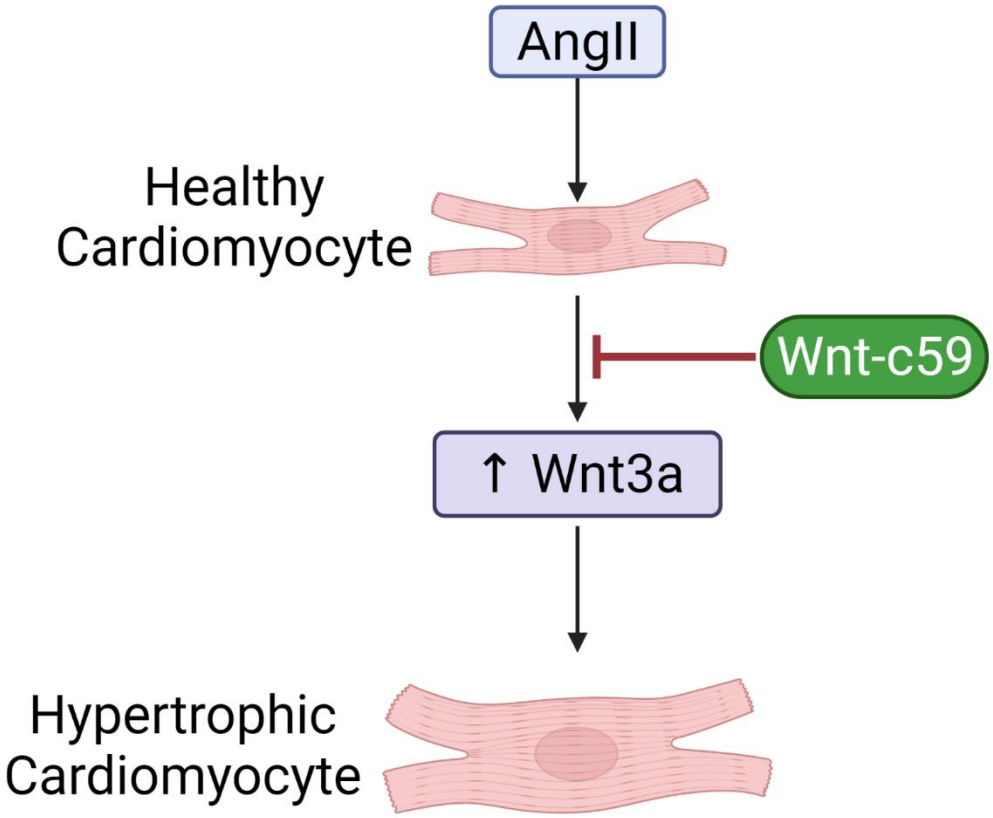

Figure 7.1. Graphical display of the proposed AngII/Wnt3a induced cardiomyocyte hypertrophy. *In vitro* experiments demonstrated that AngII induced cardiomyocyte hypertrophy is, in part, mediated via the activation of Wnt signalling (blocked by treatment with Wnt-c59). Furthermore, AngII increases the expression of the canonical Wnt ligand, Wnt3a, and the latter induces cardiomyocyte hypertrophy. Therefore, the proposed mechanism for AngII induced cardiomyocyte hypertrophy involves the secretion of Wnt3a and subsequent induction of cardiomyocyte hypertrophy (as illustrated above).

7.1.2. Wnt signalling is not increased in the 'two-hit' experimental model of HFpEF

This is the first study to investigate Wnt signalling in the 'two-hit' (i.e. metabolic and mechanical stress) experimental model of HFpEF. This experimental model of HFpEF was characterised by increased adiposity, HTN, cardiomyocyte hypertrophy/fibrosis, and diastolic dysfunction. Although there was evidence of activation of the Wnt signalling system (i.e. increased expression of Wnt3a and sFRP1 in the heart and sFRP5 in the WAT, and decreased cardiac expression of Axin2) in HFpEF animals from the pilot study, these findings were not replicated in HFpEF animals from the intervention study (i.e. cardiac expression of Wnt3a, Axin2, and β-catenin were not altered in HFpEF mice compared to control mice) and the reason for this is unclear. Previous studies reporting activation of canonical Wnt signalling in experimental models of CVD have used either the chronic AngII infusion rat model (Zhao *et al*. 2018) or the TAC pressure overload mouse model (Zhao *et al*. 2020). Although these experimental models share common features (i.e. cardiac hypertrophy and cardiac fibrosis) with the HFpEF mouse model used in the present study, both are characterised by systolic dysfunction and therefore are more representative of HFrEF than HFpEF. Therefore, it is possible that activation of canonical Wnt signalling only contributes to HFrEF and not HFpEF, further reinforcing the consensus that the pathophysiological mechanisms involved in the development of both forms of HF are likely to differ, which in turn may explain why treatments used to treat HFrEF have little or no therapeutic effect in patients with HFpEF. Alternatively, the age of the animals (2 months old) used may have also influenced whether or not canonical Wnt signalling was active in HFpEF, as previous work has provided evidence of a more prominent role for Wnt signalling in aged (2 years) vs young (2 months) mice (Naito *et al.* 2012); however, aged animals are not widely used in experimental studies due to the significant costs incurred. Finally, although the cardiac expression of Wnt5a was not altered in HFpEF animals, a potential role for non-canonical Wnt signalling in this condition is possible given the accumulating evidence demonstrating a detrimental role for Wnt5a in both obesity (Ouchi *et al.* 2010; Fuster *et al.* 2015; Tang *et al.* 2018; Akoumianakis *et al.* 2019) and endothelial dysfunction (Pereira *et al.* 2008; Breton-Romero *et al.* 2016; Cho *et al.* 2018). To conclude, on the basis of the findings from this study it does not appear that canonical Wnt signalling is activated in HFpEF (though additional studies in aged mice should be considered); however, a role for non-canonical Wnt signalling in the pathogenesis of HFpEF should not be ruled out.

7.1.3. Wnt-c59 exerts cardioprotective effects independently of inhibition of Wnt signalling

This is the first study to investigate the potential therapeutic effects of a PORCN inhibitor (Wnt-c59) in HFpEF. In the present study, the diastolic dysfunction evident in HFpEF mice was

ameliorated in response to Wnt-c59 treatment, and as canonical Wnt signalling was not activated in this model it seems unlikely that the cardioprotective effects of Wnt-c59 were induced via the inhibition of this signalling pathway. Alternatively, Wnt-c59 may have ameliorated diastolic dysfunction via mechanisms that contribute to increased ventricular compliance such as BNP induced phosphorylation of titin and/or favourable regulation of the ratio of expression of the different collagen subtypes (i.e. increasing Col3:Col1) (as illustrated in Figure 7.2.). HFpEF patients have been shown to have impaired cGMP/PKG signalling which leads to hypophosphorylation of titin and an associated increase in cardiomyocyte passive stiffness (van Heerebeek *et al*. 2012). It has been reported that the NP, BNP, increases the production of cGMP, which activates PKG, and subsequently induces the phosphorylation of titin reducing ventricular stress (reviewed by Hoffmann 2018). Therefore, it is possible that the Wnt-c59 induced increase in cardiac BNP in the HFpEF mice demonstrated in this study may lead to both increased cGMP-PKG signalling and titin phosphorylation and underlie the improved diastolic function observed in these animals, though this requires further investigation. In addition to enhanced cGMP-PKG signalling, Wnt-c59 may also improve diastolic function in HFpEF mice via BNP induced effects on both collagen subtype expression and total collagen deposition. BNP has been shown to exert anti-fibrotic effects in the heart (Ogawa *et al*. 2000) and cultured cardiac fibroblasts (Kapoun *et al.* 2004; Watson *et al.* 2012), which may in part explain the slight attenuation in collagen deposition in the hearts of Wnt-c59 treated mice. However, whether or not BNP differentially regulates the expression of the different collagen subtypes (i.e. increasing the expression of the more flexible Col3 and decreasing the expression of the more rigid Col1) leading to reduced ventricular stiffness has yet to be determined. Furthermore, a direct anti-fibrotic effect (independent of BNP) of Wnt-c59 is also possible as the latter has been shown to prevent the TGF-β induced transformation of cardiac fibroblasts into profibrotic myofibroblasts (Blyszczuk *et al.* 2017). Taken together, the data demonstrates for the first time that administration of a PORCN inhibitor, Wnt-c59, improves diastolic function in a mouse model of HFpEF. Further investigation is needed to fully elucidate the mechanism(s) involved in this cardioprotective effect.

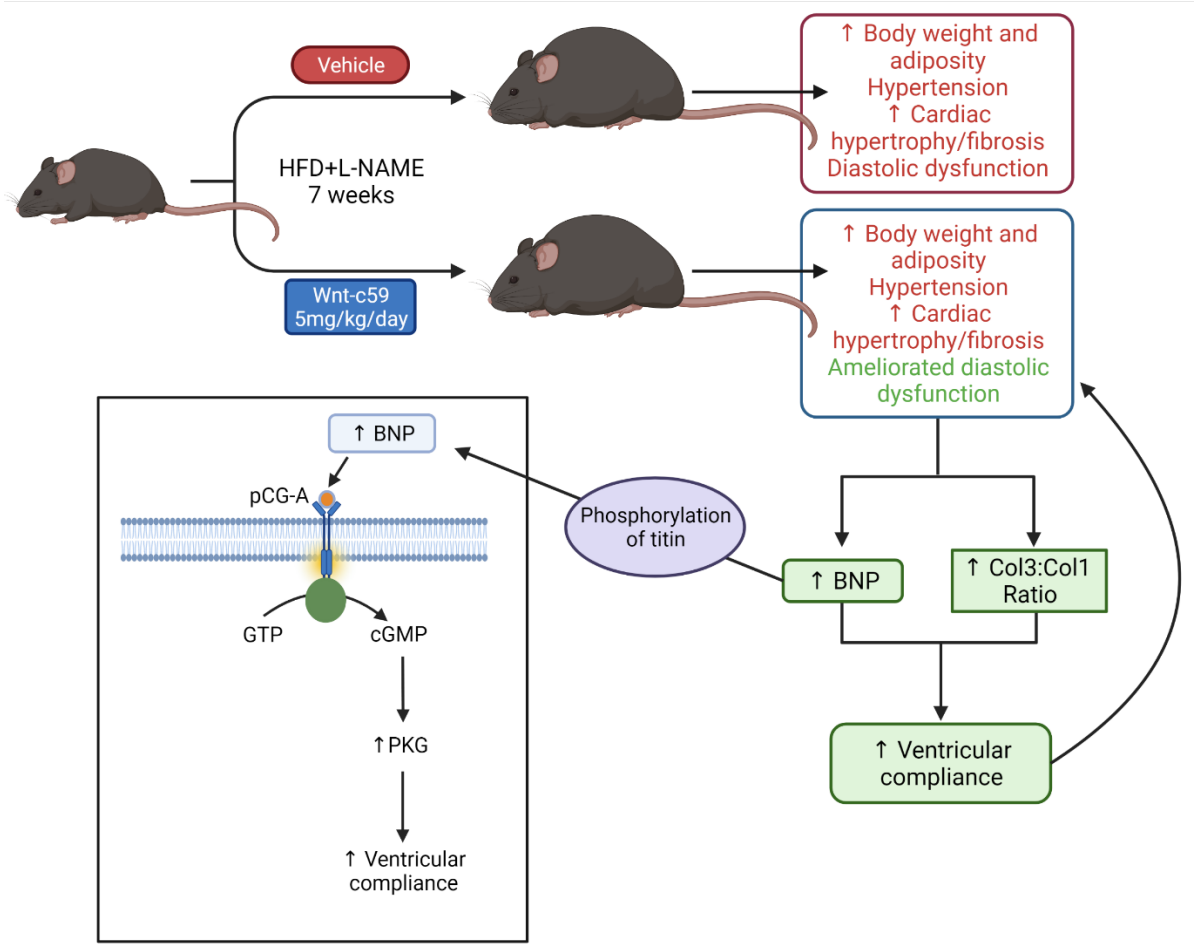

Figure 7.2. Graphical display of the proposed mechanisms involved in Wnt-c59 induced amelioration of diastolic dysfunction. A dietary intervention of HFD+L-NAME resulted in increased body weight and adiposity, hypertension, increased cardiac hypertrophy/fibrosis, and diastolic dysfunction in mice. However, treatment with Wnt-c59 ameliorated this diastolic dysfunction and the possible mechanisms involved are described above. One possible explanation for this could involve the increased ratio of Col3 to Col1 expression (Col3:Col1) observed in the hearts of Wnt-c59 treated mice. Col3 is more elastic than Col1, therefore an increase in the Col3:Col1 ratio would result in an increase in ventricular compliance. The other possible mechanism is via the phosphorylation of titin which is induced via PKG. In this proposed mechanism, Wnt-c59 induced BNP would bind to the particulate guanylyl cyclase A (pCG-A) receptor converting guanosine-5'-triphosphate (GTP) to cGMP and activating PKG. PKG would then phosphorylate the N2B isoform of titin (which is the stiffer form of titin) resulting in increased ventricular compliance. The contribution of one or both of these mechanisms to increased ventricular compliance would then subsequently improve diastolic function.

7.2. Limitations of the study

One of the main limitations of this study is the use of young male mice for the *in vivo* model of HFpEF, as clinically the latter mainly affects older women. One of the many justifications for the predominant use of male mice in *in vivo* experiments is the assertion that results from female mice tend to be more variable as a consequence of both female hormones and the oestrous cycle. However, a meta-analysis conducted on neuroscience and biomedical research concluded that the variability in female mice is similar to that observed in male mice (Prendergast *et al*. 2014) and in 2016 the NIH issued a mandate that future grant proposals should incorporate animals of both sexes or demonstrate a valid reason not to (Clayton 2018). In this study, there was a valid reason to exclude female mice based on results reported by Tong et al. (2019), that demonstrated that female mice were more resistant to the effects of the HFD+L-NAME intervention and only developed some of the key features of HFpEF and to a lesser degree than those observed in male mice. Furthermore, this female-related protection persisted in the absence of oestrogen in mice that had undergone ovariectomies.

Another limitation of the study relates to the use of cardiomyoblast cells rather than cardiomyocytes for the *in vitro* work investigating the role of Wnt signalling in cardiomyocyte hypertrophy. Undifferentiated rat H9c2 cells, although widely used as an *in vitro* model of cardiomyocytes, are an immortalised cell line with a myoblast phenotype originally derived from rat embryonic ventricular tissue and so not entirely representative of adult cardiomyocytes. Initial experiments were conducted to differentiate (via the addition of RA and low serum media) H9c2 cells into a more cardiomyocyte-like phenotype, and, while this was successful, it was not possible to induce hypertrophy in these cells and thus undifferentiated H9c2 cells were used instead. Furthermore, to confirm cardiomyocyte hypertrophy was present, measurement of cardiomyocyte area (via histological staining with fluorescently labelled wheat germ agglutinin) in addition to the measurement of fetal gene expression could also have been conducted to strengthen the results. Finally, the *in vitro* work only focused on the potential role of Wnt signalling in cardiomyocyte hypertrophy*,* however cardiac fibrosis is also a key feature of HFpEF, therefore future studies could investigate the role of this signalling pathway in a co-culture of cardiomyocytes and fibroblasts which would more accurately reflect the cellular environment in which HFpEF develops.

In this study, seven weeks of treatment with HFD+L-NAME was sufficient to induce both cardiac hypertrophy/fibrosis and diastolic dysfunction in mice, however increased lung weight (which is indicative of pulmonary oedema and a key feature of HFpEF) was not observed in

these animals. Conversely, Schiattarella et al. (2019) demonstrated that high fat feeding and L-NAME administration for 5 weeks was sufficient to induce all of the key features of HFpEF, including a significant increase in lung weight. One potential reason for the lack of change in lung weight in the present study may have been due to the lungs briefly being washed in PBS after removal from the mouse and thus potentially additional liquid was absorbed by the tissues. Wnt signalling was not activated in this model of HFpEF after 7 weeks, however appeared to be increased in the pilot study after 5 weeks of HFD+L-NAME, therefore increasing the duration time of the model could have an effect on Wnt signalling, however as this is the first study to investigate Wnt signalling in this model, further studies would need to be conducted. The time course for the treatment of Wnt-c59 in the *in vivo* experiment was chosen based on results shown by Proffitt et al. (2013) that reported that the same concentration of Wnt-c59 reduced tumour volume size as early as 7 days post commencement of treatment. However, Zhao et al. (2020) reported that adverse functional and structural changes induced by a TAC pressure overload model were mitigated after 4 weeks of treatment with Wnt-c59. While a treatment period of 2 weeks appeared to be long enough for Wnt-c59 to alter ventricular compliance/diastolic function, it may not have been long enough for it to have any effect on the adverse structural changes (i.e. cardiac hypertrophy) associated with HFpEF. However, as one of the key contributors to the development of cardiac hypertrophy in this model is the L-NAME induced pressure overload and Wnt-c59 did not alter BP, it seems unlikely that increasing the duration of the Wnt-c59 intervention would alter the maladaptive structural changes in this model of HFpEF.

7.3. Future Studies

7.3.1. Investigation of the relationship between Wnt-c59 and cGMP-PKG signalling

Future studies could investigate if there is a link between Wnt-c59 induced BNP expression and activation of cGMP-PKG signalling. As previously stated, the hearts of HFpEF patients are characterised by reduced cGMP-PKG signalling resulting in increased titin-based stiffness and impaired ventricular compliance (van Heerebeck *et al*. 2012), thus pharmacological interventions that promote cGMP-PKG signalling are likely to be beneficial in HFpEF. In this study Wnt-c59 increased the expression of myocardial BNP, which has previously been shown to generate the second messenger cGMP (Chen and Burnett 2018) and increase PKG (Chang *et al.* 2019) and thus it is possible that Wnt-c59 induced BNP may activate cGMP-PKG signalling in HFpEF (illustrated in figure 7.2.). At present, a human recombinant form of BNP (Nestiride) has been approved as a treatment for congestive HF caused by systolic dysfunction (Elkayam *et al*. 2002), which has been reported to increase cGMP and its usage leads to

natriuresis, diuresis, vasorelaxation, and a reduction in plasma aldosterone and ET-1 levels (reviewed by Burnett 2005). Furthermore, chronic administration of BNP in patients has been shown to improve LV remodelling, reduce LV filling pressures, suppress the RAAS (Chen *et al*. 2012), and improve diastolic dysfunction as indicated by a decrease in the E/e' ratio (Wan *et al.* 2016). Despite the positive effects of BNP, a major limitation associated with it is the means via which it is administered. In particular, BNP is either administered intravenously (Nestiride) or as twice daily subcutaneous injections (Chen *et al.,* 2012; Wan *et al.,* 2016). Therefore, an orally active pharmacological agent such as Wnt-c59 that can induce BNP expression could prove highly beneficial in HFpEF patients.

7.4. Clinical Relevance

A recent study has reported promising results for a possible therapeutic intervention for HFpEF. In this study, Empaglifloazin, a sodium-glucose cotransporter 2 inhibitor, was shown to reduce the combined risk of death or hospitalisations in patients with HFpEF (Anker *et al*. 2021). These findings are encouraging as to date there have been no previous drugs which have demonstrated a clear therapeutic benefit in a HFpEF clinical trial. As a consequence, therapeutic options for HFpEF patients are limited and represent a strong unmet clinical need. The findings from the present study further highlight the divergence in the pathophysiological mechanisms underlying both HFrEF and HFpEF, with canonical Wnt signalling appearing to be a chief mediator of the former (based on published literature) but not the latter. Notwithstanding this, findings from the present study do suggest a potential therapeutic option (i.e. Wnt-c59) that may, following further investigation, prove to be beneficial to HFpEF patients in the long-term.

7.5. Conclusion

In conclusion, this study demonstrated that AngII induces an increase in markers of cardiomyocyte hypertrophy, in part, via the upregulation of Wnt3a (which on its own was also shown to exert hypertrophic effects), indicating a link between RAAS activation and the initiation of Wnt signalling. Furthermore, these findings appear to translate to HCMs, which would suggest that the relationship between the RAAS and Wnt signalling systems is not confined to rodents. However, although Wnt3a induces an increase in a marker of cardiomyocyte hypertrophy, activation of canonical Wnt signalling does not appear to contribute to cardiac hypertrophy in the setting of experimental HFpEF. In the present study, the 'two-hit' experimental model of HFpEF was characterised by HTN, increased adiposity,

cardiac hypertrophy and fibrosis, and diastolic dysfunction, however there was no evidence of activation of canonical Wnt signalling in this model. Notwithstanding this, treatment of HFpEF mice with Wnt-c59 (a PORCN inhibitor that abrogates Wnt signalling), did ameliorate diastolic dysfunction via mechanisms that may contribute to increased ventricular compliance such as BNP induced phosphorylation of titin and/or favourable regulation of the ratio of collagen subtype expression. Further investigation is needed to identify the exact mechanism(s) involved in the cardioprotective effect of Wnt-c59.

Chapter 8: References

ABOU ZIKI, M.D. and MANI, A., 2017. Wnt signaling, a novel pathway regulating blood pressure? State of the art review. *Atherosclerosis,* 262, pp.171-178.

ABRAHAM, D.M. et al., 2016. β-Arrestin mediates the Frank–Starling mechanism of cardiac contractility. *PNAS,* 113(50), pp. 14426-14431.

ABRAITYTE, A. et al., 2017a. Wnt5a is elevated in heart failure and affects cardiac fibroblast function. *Journal of Molecular Medicine,* 95, pp.767-777.

ABRAITYTE, A. et al., 2017b. Wnt5a is associated with right ventricular dysfunction and adverse outcome in dilated cardiomyopathy. *Scientific Reports,* 7.

AGGARWAL, P. et al., 2014. RNA Expression Profiling of Human iPSC-Derived Cardiomyocytes in a Cardiac Hypertrophy Model. *PLoS ONE,* 9(9).

AISAGBONHI, O. et al., 2011. Experimental myocardial infarction triggers canonical Wnt signaling and endothelial-to-mesenchymal transition. *Disease Models and Mechanisms,* 4(4), pp.469-483.

AKOUMIANAKIS, I. et al., 2019. Adipose tissue-derived WNT5A regulates vascular redox signaling in obesity via USP17/RAC1-mediated activation of NADPH oxidases. *Science Translational Medicine,* 11(510).

ALEX, L. et al., 2018. Characterization of a mouse model of obesity-related fibrotic cardiomyopathy that recapitulates features of human heart failure with preserved ejection fraction. *American Journal of Physiology. Heart and Circulatory Physiology,* 315(4), pp.H934-949.

ALFARO, M.P. et al., 2010. sFRP2 suppression of bone morphogenic protein (BMP) and Wnt signaling mediates mesenchymal stem cell (MSC) self-renewal promoting engraftment and myocardial repair. *Journal of Biological Chemistry,* 285(46), pp.35645-35653.

ALI, D. et al., 2019. Heart failure with preserved ejection fraction (HFpEF) pathophysiology study (IDENTIFY-HF): does increased arterial stiffness associate with HFpEF, in addition to ageing and vascular effects of comorbidities? Rationale and design. *British Medical Journal,* 9(11), pp. e027984.

ALLAN, A. et al., 2005. Reversal of cardiac dysfunction by selective ET-A receptor antagonism. *British Journal of Pharmacology,* 146(6), pp.846-853.

ANDERSEN, M.J. et al., 2013. Sildenafil and diastolic dysfunction after acute myocardial infarction in patients with preserved ejection fraction: the Sildenafil and Diastolic Dysfunction After Acute Myocardial Infarction (SIDAMI) trial. *Circulation,* 127(11), pp.1200-1208.

ANESTOPOULOS, I. et al., 2013. Silibinin protects H9c2 cardiac cells from oxidative stress and inhibits phenylephrine-induced hypertrophy: potential mechanisms. *The Journal of Nutritional Biochemistry,* 24(3), 586-594.

ANG, S.Y. et al., 2017. Signal transduction pathways activated by insulin-like peptide 5 at the relaxin family peptide RXFP4 receptor. *British Journal of Pharmacology,* 174, pp.1077-1089.

ANKER, S.D. et al., 2021. Empagliflozin in Heart Failure with a Preserved Ejection Fraction. *The New England Journal of Medicine,* 385(16), pp.1451-1461.

ARCHER, C.R. et al., 2017. Endothelin-1 Promotes Hypertrophic Remodelling of Cardiac Myocytes by Activating Sustained Signalling and Transcription Downstream of Endothelin type A receptors. *Cell Signalling,* 36, pp.240-254.

ARIMOTO, T. et al., 2006. Cardiac-specific overexpression of diacylglycerol kinase zeta prevents Gq protein-coupled receptor agonist-induced cardiac hypertrophy in transgenic mice. *Circulation,* 113(1), pp.60-6.

ARUMUGAM, S. et al., 2012. Candesartan cilexetil protects from cardiac myosin induced cardiotoxicity via reduction of endoplasmic reticulum stress and apoptosis in rats: involvement of ACE2-Ang (1-7)-mas axis. *Toxicology,* 291(1-3), pp.139-145.

ASKEVOLD, E.T. et al., 2014. The cardiokine secreted Frizzled-related protein 3, a modulator of Wnt signalling, in clinical and experimental heart failure. *Journal of Internal Medicine,* 275(6), pp.621-630.

ATHILINGAM,P. et al., 2013. Predictive Validity of NYHA and ACC/AHA Classifications of Physical and Cognitive Functioning in Heart Failure. *International Journal of Nursing Science,* 3(1), pp.22-32.

AUBERT, G. et al., 2010. Neuroendocrine characterization and anorexigenic effects of telmisartan in diet- and glitazone-induced weight gain. *Metabolism,* 59(1), pp.25-32.

AUMILLER, V. et al., 2013. WNT/β-catenin signaling induces IL-1β expression by alveolar epithelial cells in pulmonary fibrosis. *American Journal of Respiratory Cell and Molecular Biology,* 49(1), pp.96-104.

BAE, E.H. et al., 2012. Renoprotective Effects of Sildenafil in DOCA-Salt Hypertensive Rats. *Kidney and Blood Pressure Research,* 36(1).

BAI, B. et al., 2019. Seipin Knockout Mice Develop Heart Failure With Preserved Ejection Fraction. *JACC: Basic to Translational Science,* 4(8), pp.924-937.

BALMAIN, S. et al., 2007. Differences in arterial compliance, microvascular function and venous capacitance between patients with heart failure and either preserved or reduced left ventricular systolic function. *European Journal of Heart Failure,* 9(9), pp.865-871.

BARANDON, L. et al., 2003. Reduction of infarct size and prevention of cardiac rupture in transgenic mice overexpressing FrzA. *Circulation,* 108(18), pp.2282-2289.

BARANDON, L. et al., 2011. Secreted frizzled-related protein-1 improves postinfarction scar formation through a modulation of inflammatory response. *Arteriosclerosis, Thrombosis, and Vascular Biology,* 31(11), pp.e80-87.

BARHOUMI, T. et al., 2017. Matrix metalloproteinase-2 knockout prevents angiotensin II-induced vascular injury. *Cardiovascular Research,* 113(14), pp.1753-1762.

BAROUCH, L.A. et al., 2003. Disruption of leptin signaling contributes to cardiac hypertrophy independently of body weight in mice. *Circulation,* 108(6), pp.754-759.

BARTA, T. et al., 2018. Endothelin-1-induced hypertrophic alterations and heme oxygenase-1 expression in cardiomyoblasts are counteracted by beta estradiol: in vitro and in vivo studies. *Naunyn-Schmiedeberg's Archives of Pharmacology,* 391(4), pp.371-383.

BASTOS, M.B. et al., 2020. Invasive left ventricle pressure-volume analysis: overview and practical clinical implications. *European Heart Journal,* 41(12), pp. 1286-1297.

BAUMANN, D.C. et al., 2020. Renal Denervation Attenuates DOCA-salt Hypertension in the Mouse. *The FASEB Journal,* 34(S1).

BEALE, A.L. et al., 2018. Sex Differences in Cardiovascular Pathophysiology: Why Women are Overrepresented in Heart Failure with Preserved Ejection Fraction. *Circulation,* 138(2), pp.198-205.

BEAM, J. et al., 2015. Excess Linoleic Acid Increases Collagen I/III Ratio and "Stiffens" the Heart Muscle Following High Fat Diets. *The Journal of Biological Chemistry,* 290(38), pp.23371-23384.

BECHER, P.M. et al., 2012. Role of heart rate reduction in the prevention of experimental heart failure: comparison between If-channel blockade and β-receptor blockade. *Hypertension,* 59(5), pp.949-957.

BEHRENS, A.N. et al., 2013. Nkx2-5 mediates differential cardiac differentiation through interaction with Hoxa10. *Stem Cells and Development,* 22(15), pp.2211-2220.

BENNETT, C.N. et al., 2002. Regulation of Wnt signaling during adipogenesis. *Journal of Biological Chemistry,* 277(34), pp.30998-31004.

BERENYIOVA, A. et al., 2018. The Effect of Chronic NO Synthase Inhibition on the Vasoactive and Structural Properties of Thoracic Aorta, NO Synthase Activity, and Oxidative Stress Biomarkers in Young SHR. *Oxidative Medicine and Cellular Longevity,* 2018.

BERS, D.M., 2002. Cardiac excitation–contraction coupling. *Nature,* 415, pp. 198-205.

BHAT, S.A. et al., 2018. Angiotensin Receptor Blockade by Inhibiting Glial Activation Promotes Hippocampal Neurogenesis Via Activation of Wnt/β-Catenin Signaling in Hypertension. *Molecular Neurobiology,* 55(6), pp.5282-5298.

BHATNAGAR, P. et al., 2015. The epidemiology of cardiovascular disease in the UK 2014. *Heart*, 101(15), pp.1182-1189.

BHUIYAN, T. and MAURER, M.S., 2011. Heart Failure with Preserved Ejection Fraction: Persistent Diagnosis, Therapeutic Enigma. *Current Cardiovascular Risk Reports,* 5(5), pp. 440-449.

BIENVENU, L.A. et al., 2017. Chronic in vivo nitric oxide deficiency impairs cardiac functional recovery after ischemia in female (but not male) mice. *Journal of Molecular and Cellular Cardiology,* 112, pp.8-15.

BISHU, K. et al., 2011. Sildenafil and B-type natriuretic peptide acutely phosphorylate titin and improve diastolic distensibility in vivo. *Circulation,* 124(25), pp.2882-2891.

BISPING, E. et al., 2014. Targeting cardiac hypertrophy: toward a causal heart failure therapy. *Journal of Cardiovascular Pharmacology,* 64(4), pp. 293-305.

BISTOLA, B. et al., 2019. Inotropes in Acute Heart Failure: From Guidelines to Practical Use: Therapeutic Options and Clinical Practice. *Cardiac Failure Review,* 5(3), pp.133-139.

BLAIR, M., 2016. Diabetes Mellitus Review. *Urologic Nursing,* 36(1), pp.27-36.

BLASI, E.R. et al., 2003. Aldosterone/salt induces renal inflammation and fibrosis in hypertensive rats. *Kidney International,* 63(5), pp.1791-1800.

BLYSZCZUK, P. et al., 2017. Transforming growth factor-β-dependent Wnt secretion controls myofibroblast formation and myocardial fibrosis progression in experimental autoimmune myocarditis. *European Heart Journal,* 38(18), pp.1413-1425.

BONNANS, C., CHOU, J. and WERB, Z., 2014. Remodelling the extracellular matrix in development and disease. *Nature reviews molecular cell biology,* 15(2014), pp.786-801.

BORBELY, A. et al., 2009. Hypophosphorylation of the Stiff N2B titin isoform raises cardiomyocyte resting tension in failing human myocardium. *Circulation Research,* 104(6), pp.780-786.

BORLAUG, B.A. and REDFIELD, M.M., 2011. Diastolic and Systolic Heart Failure are Distinct Phenotypes Within the Heart Failure Spectrum. *Circulation,* 123(18), pp.2006-2014.

BOUVET, C. et al., 2005. Different involvement of extracellular matrix components in small and large arteries during chronic NO synthase inhibition. *Hypertension,* 45(3), pp.432-437.

BOVOLENTA, P. et al., 2008. Beyond Wnt inhibition: new functions of secreted Frizzled-related proteins in development and disease. *Journal of Cell Science,* 121(Pt6), pp.737-746.

BOWLING, N. et al., 1999. Increased protein kinase C activity and expression of Ca2+-sensitive isoforms in the failing human heart. *Circulation,* 99(3), pp.384-91.

BRADFORD, M.M., 1976. A rapid and sensitive method for the quantitation of microgram quantities of protein utilizing the principle of protein-dye binding. *Analytical Biochemisty,* 72, pp.248-254.

BRAGAZZI, N.L., 2021. Burden of heart failure and underlying causes in 195 countries and territories from 1990 to 2017**.** *European Journal of Preventive Cardiology,* 2021, zwaa147.

BRAINARD, R.E. et al., 2013. High fat feeding in mice is insufficient to induce cardiac dysfunction and does not exacerbate heart failure. *PLoS One,* 8(12), pp.e83174.

BRANCO, A.F. et al., 2015. Gene Expression Profiling of H9c2 Myoblast Differentiation towards a Cardiac-Like Phenotype. *PLoS ONE,* 10(6).

BRAZ, J.C. et al., 2002. PKC alpha regulates the hypertrophic growth of cardiomyocytes through extracellular signal-regulated kinase1/2 (ERK1/2). *Journal of Cell Biology,* 156(5), pp.905-19.

BRAZ, J.C. et al., 2004. PKC-alpha regulates cardiac contractility and propensity toward heart failure. *Nature Medicine,* 10(3), pp.248-54.

BREDY, C. et al., 2018. New York Heart Association (NYHA) Classification in Adults with Congenital Heart Disease: Relation to Objective Measures of Exercise and Outcomes. *European Heart Journal,* 4, pp.51-58.

BREIJO-MARQUEZ, F.L. 2018. Breijo Electrocardiographic Pattern. In: U. LAKSHMANADOSS. ed. *Cardiac Arrhythmias.* InTechOpen. Chapter 8.

BRETONES, G., DELGADO, M.D. and LEON, J., 2015. Myc and cell cycle control. *Biochimica et Biophysica Acta,* 1849(5), pp.506-516.

BRETON-ROMERO, R. et al., 2016. Endothelial Dysfunction in Human Diabetes Is Mediated by Wnt5a-JNK Signaling. *Arteriosclerosis, thrombosis and vascular biology,* 36(3), pp.561-569.

BRITISH HEART FOUNDATION (BHF), 2021. *UK Factsheet*. [online]. London: BHF. Available from: https://www.bhf.org.uk/what-we-do/our-research/heart-statistics [Accessed 4th June 2020].

BRODERICK, T.L. et al., 2012. Downregulation in GATA4 and Downstream Structural and Contractile Genes in the db/db Mouse Heart. *ISRN Endocrinology,* 2012.

BRODERICK, T.L. et al., 2014. Unexpected effects of voluntary exercise training on natriuretic peptide and receptor mRNA expression in the ob/ob mouse heart. *Regulatory Peptides,* 188, pp.52-59.

BROWN, B.A. et al., 2019. Aging differentially modulates the Wnt pro-survival signalling pathways in vascular smooth muscle cells. *Aging Cell,* 18(1), pp. e12844.

BROWN, L. et al., 2001. Reversal of cardiovascular remodelling with Candesartan. *Journal of the Renin-Angiotensin-Aldosterone System,* 2, pp.S141-147.

BUPHA-INTR, T., HAIZLIP, K.M. and JANSSEN, P.M.L., 2012. Role of Endothelin in the Induction of Cardiac Hypertrophy *In Vitro. PLos One,* 7(8).

BURGER, A.J. et al., 2002. Effect of nesiritide (B-type natriuretic peptide) and dobutamine on ventricular arrhythmias in the treatment of patients with acutely decompensated congestive heart failure: the PRECEDENT study. *American Heart Journal,* 144(6), pp.1102-1108.

BURNETT, J.C., 2005. Nesiritide: new hope for acute heart failure syndromes? *European Heart Journal Supplements,* 7, pp.B25-30.

CAI, J-I. et al., 2021. Atorvastatin inhibits mice cardiac remodeling induced by metabolic syndrome. *Fudan University Journal of Medical Sciences,* 48(5), pp.569-577.

CALLERA, G.E. et al., 2016. Differential renal effects of Candesartan at high and ultra-high doses in diabetic mice-potential role of the ACE2/AT2R/Mas axis. *Bioscience Reports,* 36(5).

CALLIGARIS, S.D. et al., 2013. Mice long-term high-fat diet feeding recapitulates human cardiovascular alterations: an animal model to study the early phases of diabetic cardiomyopathy. *PLoS One,* 8(4).

CAMBIER, L. et al., 2018. Angiotensin II-Induced End-Organ Damage in Mice Is Attenuated by Human Exosomes and by an Exosomal Y RNA Fragment. *Hypertension,* 72(2), pp.370-380.

CAMPBELL, D.J., 2006. L-NAME hypertension: trying to fit the pieces together. *Journal of Hypertension,* 24(1), pp.33-36.

CANNAVO, A. et al., 2018. Aldosterone and Mineralocorticoid Receptor System in Cardiovascular Physiology and Pathophysiology. *Oxidative Medicine and Cellular Longevity,* 2018, pp. 1204598.

CARLSON, C. et al., 2013. Phenotypic Screening with Human iPS Cell–Derived Cardiomyocytes: HTS-Compatible Assays for Interrogating Cardiac Hypertrophy. *Journal of Biomolecular Screening*, 18(10), pp. 1203-1211.

CARRICK-RANSON, G. et al., 2012. Effect of healthy aging on left ventricular relaxation and diastolic suction. *American Journal of Physiology Heart and Circulatory Physiology,* 303(3), pp.H315-H322.

CARSTENSEN-KIRBERG, M. et al., 2017. Inverse associations between serum levels of secreted frizzled-related protein-5 (SFRP5) and multiple cardiometabolic risk factors: KORA F4 study. *Cardiovascular Diabetology,* 16(1).

CARTER, R.L. et al., 2014. Dynamic mass redistribution analysis of endogenous β-adrenergic receptor signaling in neonatal rat cardiac fibroblasts. *Pharmacology Research and Perspectives,* 2(1), pp. e00024.

CARTHY, J.M. et al., 2011. Wnt3a induces myofibroblast differentiation by upregulating TGF-β signaling through SMAD2 in a β-catenin-dependent manner. *PLoS One,* 6(5).

CASELLAS, D. et al., 2001. Candesartan prevents L-NAME-induced cardio-renal injury in spontaneously hypertensive rats beyond hypotensive effects. *Journal of the Renin-Angiotensin-Aldosterone System,* 2, pp.S84-90.

CATALAN, V. et al., 2014. Activation of noncanonical Wnt signaling through WNT5A in visceral adipose tissue of obese subjects is related to inflammation. *Journal of Clinical Endocrinology and Metabolism,* 99(8), pp. E1407-1417.

CELUTKIENE, J. et al., 2017. Challenges of Treating Acute Heart Failure Patients with Chronic Obstructive Pulmonary Disease. *Cardiac Failure Review,* 3(1), pp.56-61.

CHANG, P. et al., 2019. B-type natriuretic peptide attenuates endoplasmic reticulum stress in H9c2 cardiomyocytes underwent hypoxia/reoxygenation injury under high glucose/high fat conditions. *Peptides,* 111, pp.103-111.

CHEN, C. et al., 2004. Gene Expression Changes Associated with Fibronectin-induced Cardiac Myocyte Hypertrophy. *Physiological Genomics,* 18(3), pp.273-283.

CHEN, C-C., KUO, C-Y. and CHEN, R-F., 2016. Role of CAPE on cardiomyocyte protection via connexin 43 regulation under hypoxia. *International Journal of Science,* 13(10), pp. 754-758.

CHEN, H.H. et al., 2012. Novel protein therapeutics for systolic heart failure: chronic subcutaneous B-type natriuretic peptide. *Journal of the American College of Cardiology,* 60(22), pp.2305-2312.

CHEN, L. et al., 2017. STAT3 Balances Myocyte Hypertrophy vis-à-vis Autophagy in Response to Angiotensin II by Modulating the AMPKα/mTOR axis. *PLoS One*, 12(7), pp. e0179835.

CHEN, M. et al., 2020. CTNNB1/ β -catenin dysfunction contributes to adiposity by regulating the cross-talk of mature adipocytes and preadipocytes. *Science Advances,* 6(2).

CHEN, X. et al., 2006. The beta-catenin/T-cell factor/lymphocyte enhancer factor signaling pathway is required for normal and stress-induced cardiac hypertrophy. *Molecular and Cellular Biology,* 26(12), pp.4462-4473.

CHEN, Y. and BURNETT, J.C., 2018. Particulate Guanylyl Cyclase A/cGMP Signaling Pathway in the Kidney: Physiologic and Therapeutic Indications. *International Journal of Molecular Sciences,* 19(4), pp.1006.

CHENG, K-C. et al., 2019. TGR5 Activation Ameliorates Hyperglycemia-induced Cardiac Hypertrophy in H9c2 cells. *Scientific Report,* 9(2019).

CHENG, Y. et al., 2015. Wnt-C59 arrests stemness and suppresses growth of nasopharyngeal carcinoma in mice by inhibiting the Wnt pathway in the tumor microenvironment. *Oncotarget,* 6(16), pp.14428-14439.

CHIRINOS, J.A. and ZAMANI, P., 2016. The Nitrate-Nitrite-NO Pathway and Its Implications for Heart Failure and Preserved Ejection Fraction. *Current heart failure reports,* 13(1), pp.47-59.

CHO, Y.K. et al., 2018. Effect of SFRP5 (Secreted Frizzled-Related Protein 5) on the WNT5A (Wingless-Type Family Member 5A)-Induced Endothelial Dysfunction and Its Relevance With

Arterial Stiffness in Human Subjects. *Arteriosclerosis, thrombosis and vascular biology,* 38(6), pp.1358-1367.

CHODAVARAPU, H. et al., 2016. High-fat diet-induced glucose dysregulation is independent of changes in islet ACE2 in mice. *American Journal of Physiology. Regulatory, integrative and comparative physiology,* 311(6), pp.R1223-1233.

CHOI, Y.S. et al., 2016. Preservation of myocardial fatty acid oxidation prevents diastolic dysfunction in mice subjected to angiotensin II infusion. *Journal of Molecular and Cellular Biology,* 100, pp.64-71.

CHOPRA, S. et al., 2013. Physiology and clinical significance of natriuretic hormones. *Indian Journal of Endocrinology and Metabolism,* 17(1), pp.83–90.

CHOUDHARY, R. et al., 2008. All-trans retinoic acid prevents development of cardiac remodeling in aortic banded rats by inhibiting the renin-angiotensin system. *American Journal of Physiology. Heart and Circulatory Physiology,* 294(2), pp.H633-644.

CHRISTOFFERSEN, C. et al., 2003. Cardiac lipid accumulation associated with diastolic dysfunction in obese mice. *Endocrinology,* 144(8), pp.3483-3490.

CHUNG, J-H. et al., 2016. Myofilament Calcium Sensitivity: Role in Regulation of *In vivo* Cardiac Contraction and Relaxation. *Frontiers in Physiology,* 7, Article 562.

CIKES, M. and SOLOMON, S.D., 2016. Beyond Ejection Fraction: An Integrative Approach for Assessment of Cardiac Structure and Function in Heart Failure. *European Heart Journal,* 37(21), pp.1642-1650.

CLAYCOMB, W.C. et al., 1998. HL-1 cells: a cardiac muscle cell line that contracts and retains phenotypic characteristics of the adult cardiomyocyte. *PNAS,* 95(6), pp.2979-2984.

CLAYTON, J.A., 2018. Applying the new SABV (sex as a biological variable) policy to research and clinical care. *Physiology and Behavior,* 187, pp.2-5.

CLEMENT, K., 2006. Genetics of human obesity. *Comptes rendus biologiues,* 329(8), pp.608-622.

CLEMENT, S. et al., 2001. Angiotensin II stimulates α-skeletal actin expression in cardiomyocytes in vitro and in vivo in the absence of hypertension. *Differentiation,* 69(1), pp. 66-74.

COLSTON, J.T. et al., 2007. Wnt-induced secreted protein-1 is a prohypertrophic and profibrotic growth factor. *American Journal of Physiology. Heart and Circulatory Physiology,* 293(3), pp.H1839-1846.

COLUCCI, W.S, et al., 2000. Intravenous nesiritide, a natriuretic peptide, in the treatment of decompensated congestive heart failure. Nesiritide Study Group. *The New England Journal of Medicine,* 343(4), pp.246-253.

CONNELLY, K.A. et al., 2019. Empagliflozin Improves Diastolic Function in a Nondiabetic Rodent Model of Heart Failure With Preserved Ejection Fraction. *JACC. Basic to translational science,* 4(1), pp.27-37.

CONRAD, N. et al., 2018. Temporal trends and patterns in heart failure incidence: a population-based study of 4 million individuals. *The Lancet.* 391(10120), pp. 572-580.

CORDERO-HERRERA, I. et al., 2019. AMP-activated protein kinase activation and NADPH oxidase inhibition by inorganic nitrate and nitrite prevent liver steatosis. *PNAS,* 116(1), pp217-226.

CORDERO-HERRERA, I. et al., 2020. Head-to-head comparison of inorganic nitrate and metformin in a mouse model of cardiometabolic disease. *Nitric Oxide,* 97, pp.48-56.

CORNELISSEN, C.G. et al., 2013. Fibronectin Coating of Oxygenator Membranes Enhances Endothelial Cell Attachment. *BioMedical Engineering Online*, 12(7).

CORNING EPIC TECHNOLOGY., 2012. *Corning Epic® BT System Label-free Detection in a Benchtop System.* [online]. Available at: https://www.corning.com/media/worldwide/cls/documents/CLS-ES-038REV3.pdf [Accessed 9th December 2021].

CORNUAULT, L. et al., 2021. Diastolic dysfunction in high fat diet + L-NAME treated mice is associated with endothelial dysfunction. *Archives of Cardiovascular Disease Supplements,* 13(2).

CORREA, M.V. et al., 2014. Endogenous endothelin 1 mediates angiotensin II-induced hypertrophy in electrically paced cardiac myocytes through EGFR transactivation, reactive oxygen species and NHE-1. *European Journal of Physiology,* 466(9), pp.1819-1830

COX, E.J. and MARSH, S.A., 2014. A systematic review of fetal genes as biomarkers of cardiac hypertrophy in rodent models of diabetes. *PLos One,* 9(3), pp.e92903.

CRUCIAT, C-M. and NIEHRS, C., 2013. Secreted and transmembrane wnt inhibitors and activators. *Cold Spring Harbor Perspective in Biology,* 5(3), pp. a015081.

CUEVAS, C.A. et al., 2015. Angiotensin II increases fibronectin and collagen I through the β-catenin-dependent signaling in mouse collecting duct cells. *American Journal of Physiology. Renal Physiology,* 308(4), pp.F358-365.

DA SILVA, G.J.J. et al., 2021. Atrial Natriuretic Peptide 31-67: A Novel Therapeutic Factor for Cardiovascular Diseases. *Frontiers in Physiology,* 12.

DAMBROT, C. et al., 2014. Serum supplemented culture medium masks hypertrophic phenotypes in human pluripotent stem cell derived cardiomyocytes. *Journal of Cellular and Molecular Medicine,* 18(8), pp.1509-1218.

DAVARGAON, R.S., SAMBE, A.D. and MUTHANGI, S., 2019. Toxic Effect of High Glucose on Cardiomyocytes, H9c2 cells: Induction of Oxidative Stress and Ameliorative Effect of Trolox. *Journal of Biochemical and Molecular Toxicology,* 33(4), pp.e22272.

DAVIS, M.E. et al., 2006. Introduction of metoprolol increases plasma B-type cardiac natriuretic peptides in mild, stable heart failure. *Circulation,* 113(7), pp.977-985.

DAVIS, R.C., HOBBS, F.D.R. and LIP, G.Y.H., 2000. ABC of Heart Failure History and Epidemiology, *British Medical Journal.* 320.

DAWSON, K., AFLAKI, M. and NATTEL, S., 2013. Role of the Wnt-Frizzled system in cardiac pathophysiology: a rapidly developing, poorly understood area with enormous potential. *The Journal of Physiology,* 591(Pt6), pp.1409-1432.

DE JONG, A.M. et al., 2013. Atrial remodeling is directly related to end-diastolic left ventricular pressure in a mouse model of ventricular pressure overload. *PLoS One,* 8(9), pp.e72651.

DE KLOET, A.D. et al., 2009. The effect of angiotensin-converting enzyme inhibition using captopril on energy balance and glucose homeostasis. *Endocrinology,* 150(9), pp.4114-4123.

DE LANGHE, E. et al., 2014. Secreted frizzled related proteins inhibit fibrosis in vitro but appear redundant in vivo. *Fibrogenesis and Tissue Repair,* 7(14).

DE, A., 2011. Wnt/Ca2+ signaling pathway: a brief overview. *Acta Biochimica et Biophysica Sinica*, 43(10), pp.745-756.

DESAI, A.S. et al., 2015. Effect of the angiotensin-receptor-neprilysin inhibitor LCZ696 compared with enalapril on mode of death in heart failure patients. *European Heart Journal,* 36(30), pp.1990-1997.

DEY, N. et al., 2013. Wnt signaling in triple negative breast cancer is associated with metastasis. *BMC Cancer,* 13.

DI GIACOMO, V. et al., 2010. PKC-δ signalling pathway is involved in H9c2 cells differentiation. *Differentiation,* 80(4-5), pp.204-212.

DIEP, Q.N. et al., 2001. Expression of Cell Cycle Proteins in Blood Vessels of Angiotensin II–Infused Rats. *Hypertension,* 37(2), pp.604-608.

DIEZ-VILLANUEVA, P. and ALFONSO, F., 2016. Heart Failure in the Elderly. *Journal of Geriatric Cardiology,* 13, pp.115-117.

DIVORTY, N. et al., 2018. The Orphan Receptor GPR35 Contributes to Angiotensin II-Induced Hypertension and Cardiac Dysfunction in Mice. *American Journal of Hypertension,* 31(9), pp.1049-1058.

DONG, C. et al., 2015. Phylogenetic and Evolutionary Analyses of the Frizzled Gene Family in Common Carp (Cyprinus carpio) Provide Insights into Gene Expansion from Whole-Genome Duplications. *PLoS One,* 10(12), pp.e0144037.

DONG, F. et al., 2006. Impaired cardiac contractile function in ventricular myocytes from leptin-deficient ob/ob obese mice. *Journal of Endocrinology,* 188(1), pp.25-36.

DONG, Z-X. et al., 2017. (-)-Epicatechin Suppresses Angiotensin II-induced Cardiac Hypertrophy via the Activation of the SP1/SIRT1 Signaling Pathway. *Cell Physiology and Biochemistry,* 41(5), pp.2004-2015.

DRIESEN, R.B. et al., 2009. Re-expression of alpha skeletal actin as a marker for dedifferentiation in cardiac pathologies. *Journal of Cellular and Molecular Biology,* 13(5), pp.896-908.

DU, M. et al., 2013. Nardosinone protects H9c2 cardiac cells from angiotensin II-induced hypertrophy. *Journal of Huazhong University of science and technology. Medical Sciences,* 33(6), pp.822-826.

DUAN, H. et al., 2015. Rcan1-1L Overexpression Induces Mitochondrial Autophagy and Improves Cell Survival in Angiotensin II-exposed Cardiomyocytes. *Experimental Cell Research,* 335(1), pp.99-106.

DUAN, J. et al., 2012. Wnt1/βcatenin injury response activates the epicardium and cardiac fibroblasts to promote cardiac repair. *The EMBO Journal,* 31(2), pp.429-442.

DUERRSCHMID, C. et al., 2013. TNF receptor 1 signaling is critically involved in mediating angiotensin-II-induced cardiac fibrosis. *Journal of Moelcular and Cellular Cardiology,* 57, pp.59-67.

DUNLAY, S.M., ROGER, V.L. and REDFIELD, M.M., 2017. Epidemiology of Heart Failure with Preserved Ejection Fraction. *Nature Reviews. Cardiology,* 14(10), pp.591-602.

DUPREZ, D.A. et al., 2018. Predictive Value of Collagen Biomarkers for Heart Failure With and Without Preserved Ejection Fraction: MESA (Multi-Ethnic Study of Atherosclerosis). *Journal of the American Heart Association,* 7(5), pp. e007885.

EBONG, I.A. et al., 2014. Mechanisms of heart failure in obesity. *Obesity Research and Clinical Practise,* 8(6), pp.e540-548.

ECCLESTON, H.B. et al., 2011. Chronic exposure to a high-fat diet induces hepatic steatosis, impairs nitric oxide bioavailability, and modifies the mitochondrial proteome in mice. *Antioxidants and Redox Signalling,* 15(2), pp.447-459.

ECG AND ECHO LEARNING. *ECG and clinical characteristics of left ventricular hypertrophy.* [online]. Available from: https://ecgwaves.com/topic/ecg-left-ventricular-hypertrophy-lvh-clinical-characteristics/ [Accessed 24th November 2021].

EDVINSSON, M-L. et al., 2014. Brain natriuretic peptide is a potent vasodilator in aged human microcirculation and shows a blunted response in heart failure patients. *Journal of Geriatric Cardiology,* 11(1), pp.50-56.

EHRLUND, A. et al., 2013. Characterization of the Wnt inhibitors secreted frizzled-related proteins (SFRPs) in human adipose tissue. *Journal of Clinical Endocrinology and Metabolism,* 98(3), pp. E503-508.

ELKAYAM, U. et al., 2002. Nesiritide: a new drug for the treatment of decompensated heart failure. *Journal of Cardiovascular Pharmacology and Therapeutics,* 7(3), pp.181-194.

ENGLAND, J. and LOUGHNA, S., 2013. Heavy and light roles: myosin in the morphogenesis of the heart. *Cellular and Molecular Life Sciences,* 70(7), pp.1221-1239.

ESSICK, E.E. et al., 2013. Adiponectin Modulates Oxidative Stress-Induced Autophagy in Cardiomyocytes. *PLoS One,* 8(7), pp.e68697.

EZAN, J. et al., 2004. FrzA/sFRP-1, a secreted antagonist of the Wnt-Frizzled pathway, controls vascular cell proliferation in vitro and in vivo. *Cardiovascular Research,* 63(4), pp.731-738.

FALCAO-PIRES, I. et al., 2011. Diabetes mellitus worsens diastolic left ventricular dysfunction in aortic stenosis through altered myocardial structure and cardiomyocyte stiffness. *Circulation,* 124(10), pp.1151-1159.

FAN, D. et al., 2012. Cardiac fibroblasts, fibrosis and extracellular matrix remodeling in heart disease. *Fibrogenesis and tissue repair,* 5(1).

FAN, D. et al., 2014. Differential role of TIMP2 and TIMP3 in cardiac hypertrophy, fibrosis, and diastolic dysfunction. *Cardiovascular Research,* 103(2), pp.268-280.

FAN, Y. et al., 2018. Wnt/β-catenin-mediated signaling re-activates proliferation of matured cardiomyocytes. *Stem Cells Research and Therapy,* 9(1), pp.338.

FANG, Q. et al., 2020. LncRNA TUG1 alleviates cardiac hypertrophy by targeting miR-34a/DKK1/Wnt-β-catenin signalling. *Journal of Cellular and Molecular Medicine,* 24(6), pp.3678-3691.

FARB, M.G. et al., 2016. WNT5A-JNK regulation of vascular insulin resistance in human obesity. *Vascular Medicine,* 21(6), pp.489-496.

FATIMA, A. et al., 2016. Murine transgenic iPS cell line for monitoring and selection of cardiomyocytes. *Stem Cell Research,* 17(2), pp.266-272.

FIELDS, L.A., KOSCHINSKI, A. and ZACCOLO, M., 2016. Sustained exposure to catecholamines affects cAMP/PKA compartmentalised signalling in adult rat ventricular myocytes. *Cellular Signalling,* 28(7), pp.725-732.

FLACK, J.M. and ADEKOLA, B., 2020. Blood pressure and the new ACC/AHA hypertension guidelines. *Trends in Cardiovascular Medicine,* 30(3), pp.160-164.

FLORES-MUNOZ, M. et al., 2011. Angiotensin1-9 antagonises pro-hypertrophic signalling in cardiomyocytes via the angiotensin type 2 receptor. *The Journal of Physiology,* 589, pp.939-951.

FOGLIA, M.J. and POSS, K.D., 2016. Building and Re-Building the Heart by Cardiomyocyte Proliferation. *Development,* 143, pp.729-740.

FORONJY, R. et al., 2010. The divergent roles of secreted frizzled related protein-1 (SFRP1) in lung morphogenesis and emphysema. *The American Journal of Pathology,* 177(2), pp.598-607.

FOULQUIER, S. et al., 2018. WNT Signaling in Cardiac and Vascular Disease. *Pharmacological Reviews,* 70(1), pp.68-141.

FRANK, D. et al., 2007. Calsarcin-1 protects against angiotensin-II induced cardiac hypertrophy. *Circulation,* 116(22), pp.2587-2596.

FRANSSEN, C. et al., 2016. Myocardial Microvascular Inflammatory Endothelial Activation in Heart Failure With Preserved Ejection Fraction. *JACC. Heart Failure,* 4(4), pp.12-24.

FREY, N. et al., 2004. Hypertrophy of the Heart A New Therapeutic Target? *Circulation,* 109, pp.1580-1589.

FU, S. et al., 2018. Brain Natriuretic Peptide and Its Biochemical, Analytical, and Clinical Issues in Heart Failure: A Narrative Review. *Frontiers in Physiology,* 9, pp. 692.

FUKUSHIMA, A. et al., 2018. Acetylation contributes to hypertrophy-caused maturational delay of cardiac energy metabolism. *JCI Insight,* 3(10), pp.e99239.

FUNCK-BRENTANO, T. et al., 2018. Porcupine inhibitors impair trabecular and cortical bone mass and strength in mice. *The Journal of Endocrinology,* 238(1), pp.13-23.

FUNKE-KAISER, H. et al., 2003. Endothelin- converting enzyme 1 is a downstream target of the homeobox transcription factor Nkx2.5. *Federation of American Sciences for Experimental Biology,* 17(11).

FUSTER, J.J. et al., 2015. Noncanonical Wnt signaling promotes obesity-induced adipose tissue inflammation and metabolic dysfunction independent of adipose tissue expansion. *Diabetes,* 64(4), pp.1235-1248.

GALLI, L.M. et al., 2006. Differential inhibition of Wnt-3a by Sfrp-1, Sfrp-2, and Sfrp-3. *Developmental Dynamics,* 235(3), pp.681-690.

GALLI, L.M. et al., 2016. Divergent effects of Porcupine and Wntless on WNT1 trafficking, secretion, and signaling. *Experimental Cell Research,* 347(1), pp.171-183.

GARAWI, F. et al., 2014. Global Differences between Women and Men in the Prevalence of Obesity: is there an association with gender inequality? *European Journal of Clinical Nutrition,* 68, pp. 1101-1106.

GAUGER, K.J. et al., 2013. Mice deficient in Sfrp1 exhibit increased adiposity, dysregulated glucose metabolism, and enhanced macrophage infiltration. *PLoS One,* 8(12), pp. e78320.

GEORGE, J, and STRUTHERS, A.D., 2007. Natriuretic Peptides. In G. Y. H. Lip, & J. E. Hall. *Comprehensive Hypertension* (pp. 349-362). Mosby Elsevier.

GERENA, Y. et al., 2017. Losartan counteracts the effects of cardiomyocyte swelling on glucose uptake and insulin receptor substrate-1 levels. *Peptides,* 96, pp.38-43.

GESMUNDO, I. et al., 2017. Growth hormone-releasing hormone attenuates cardiac hypertrophy and improves heart function in pressure overload-induced heart failure. *PNAS,* 114(45), pp.12033-12038.

GHOSH, A.K. et al., 2014. Midlife blood pressure change and left ventricular mass and remodelling in older age in the 1946 British Birth Cohort Study. *European Heart Journal,* 35(46), pp.3287-3295.

GIANI, J.F. et al., 2014. Renal Generation of Angiotensin II and the Pathogenesis of Hypertension. *Current Hypertension Reports,* 16(9), pp.477.

GIBB, A.A., LAZAROPOULOS, M.P. and ELROD, J.W., 2020. Myofibroblasts and Fibrosis: Mitochondrial and Metabolic Control of Cellular Differentiation. *Circulation Research,* 127(3), pp.427-447.

GIGUERE, H. et al., 2018. ADAP1 limits neonatal cardiomyocyte hypertrophy by reducing integrin cell surface expression. *Scientific Reports,* 8, pp.13605.

GLENN, D.J. et al., 2015. Cardiac steatosis potentiates angiotensin II effects in the heart. *American Journal of Physiology. Heart and Circulatory Physiology,* 308(4), pp.H339-350.

GOLDSBERRY, W.N. et al., 2020. Inhibiting WNT Ligand Production for Improved Immune Recognition in the Ovarian Tumor Microenvironment. *Cancer,* 12(3), pp.766.

GOLIASCH, G. et al., 2012. Premature myocardial infarction is associated with low serum levels of Wnt-1. *Atherosclerosis,* 222(1), pp.251-256.

GONG, B., WU, Z. and LI, Z., 2016. Efficacy and safety of nesiritide in patients with decompensated heart failure: a meta-analysis of randomised trials. *BMJ Open,* 6(1).

GONZALEZ, D.R. et al., 2010. Impaired S-Nitrosylation of the Ryanodine Receptor Caused by Xanthine Oxidase Activity Contributes to Calcium Leak in Heart Failure. *Journal of Biological Chemistry,* 285(37), pp. 28938–28945.

GRAY, M.O. et al., 1998. Angiotensin II stimulates cardiac myocyte hypertrophy via paracrine release of TGF-beta 1 and endothelin-1 from fibroblasts. *Cardiovascular Research,* 40(2), pp.352-363.

GREEN, J., NUSSE, R. and VAN AMERONGEN, R., 2014. The role of Ryk and Ror receptor tyrosine kinases in Wnt signal transduction. *Cold Spring Harbor Perspective in Biology,* 6(2), pp. a009175.

GROBE, J.L. et al., 2006. Chronic angiotensin-(1–7) prevents cardiac fibrosis in DOCA-salt model of hypertension. *American Journal of Physiology. Heart and Circulatory Physiology,* 290(6), pp.H2417-2423.

GU, S. et al., 2014. EPC-Derived Microvesicles Protect Cardiomyocytes from Ang II-Induced Hypertrophy and Apoptosis. *PLoS One,* 9(1), pp. e85396.

GUAN, X-H. et al., 2017. CD38 promotes angiotensin II-induced cardiac hypertrophy. *Journal of Cellular and Molecular Medicine*, 21(8), pp.1492-1502.

GUATIMOSIM, S., GUATIMOSIM, C. and SONG, L-S., 2011. Imaging calcium sparks in cardiac myocytes. *Methods in Molecular Biology,* 689, pp.205-214.

GUAZZI, M., 2014. Pulmonary hypertension in heart failure preserved ejection fraction: prevalence, pathophysiology, and clinical perspectives. *Circulation: Heart Failure,* 7(2), pp.367-377.

GUO, Z-P. et al., 2017. Plasma protein profiling in patients undergoing coronary artery bypass grafting surgery and clinical significance. *Oncotarget,* 8(36), pp.60528-60538.

GUTIERREZ, C. and BLANCHARD, D.G.,2004. Diastolic Heart Failure: Challenges of Diagnosis and Treatment. *American Family Physician,* 69(11), pp. 2609-2617.

GUTKOWSKA, J. et al., 2009. Downregulation of oxytocin and natriuretic peptides in diabetes: possible implications in cardiomyopathy. *The Journal of Physiology,* 587, pp.4725-4736.

HAASS, M. et al., 2011. Body mass index and adverse cardiovascular outcomes in heart failure patients with preserved ejection fraction: results from the Irbesartan in Heart Failure with Preserved Ejection Fraction (I-PRESERVE) trial. *Circulation: Heart Failur,* 4(3), pp.324-331.

HAGENMULLER, M. et al., 2013. Dapper-1 induces myocardial remodeling through activation of canonical Wnt signaling in cardiomyocytes. *Hypertension,* 61(6), pp.1177-1183.

HAHN, N.E. et al., 2014. Early NADPH oxidase-2 activation is crucial in phenylephrine-induced hypertrophy of H9c2 cells. *Cell Signalling,* 26(9), pp.1818-1824.

HAMADA, N. et al., 2012. Disrupted regulation of ghrelin production under antihypertensive treatment in spontaneously hypertensive rats. *Circulation Journal: Official Journal of the Japanese Circulation Society,* 76(6), pp.1423-1429.

HAMBLETON, M. et al., 2007. Inducible and myocyte-specific inhibition of PKCalpha enhances cardiac contractility and protects against infarction-induced heart failure. *American Journal of Physiology Heart and Circulatory Physiology*, 293(6), pp.H3768-3771.

HAMDANI, M.et al., 2013. Deranged myofilament phosphorylation and function in experimental heart failure with preserved ejection fraction. *Cardiovascular Research,* 97(3), pp. 464-471.

HAMILTON, D.J. et al., 2016. Combination of angiotensin II andL-NG-nitroarginine methyl ester exacerbates mitochondrial dysfunction and oxidative stress to cause heart failure. *American Journal of Physiology. Heart and Circulatory Physiology,* 310, pp.H667-680.

HAN, D. et al., 2016. Jujuboside A Protects H9C2 Cells from Isoproterenol-Induced Injury via Activating PI3K/Akt/mTOR Signaling Pathway. *Evidence-based and Complementary and Alternative Medicine,* 2016.

HANKENSON, F.C. et al., 2018. Effects of Rodent Thermoregulation on Animal Models in the Research Environment. *Comparative Medicine,* 68(6):425-438.

HAQ, S. et al., 2001. Differential activation of signal transduction pathways in human hearts with hypertrophy versus advanced heart failure. *Circulation,* 103(5), pp.670-676.

HAQ, S. et al., 2003. Stabilization of beta-catenin by a Wnt-independent mechanism regulates cardiomyocyte growth. *PNAS,* 100(8), pp.4610-4615.

HARVEY, A. et al., 2016. Vascular Fibrosis in Aging and Hypertension: Molecular Mechanisms and Clinical Implications. *The Canadian Journal of Cardiology,* 32(5), pp. 659-668.

HE, H. et al., 2010b. Telmisartan prevents weight gain and obesity through activation of peroxisome proliferator-activated receptor-delta-dependent pathways. *Hypertension,* 55(4), pp.869-879.

HE, J. et al., 2015. Expression of Wnt and NCX1 and its correlation with cardiomyocyte apoptosis in mouse with myocardial hypertrophy. *Asian Pacific Journal of Tropical Medicine,* 8(11), pp.930-936.

HE, W. et al., 2009. Wnt/beta-catenin signaling promotes renal interstitial fibrosis. *Journal of the American Society of Nephrology,* 20(4), pp.765-776.

HE, W. et al., 2010a. Exogenously administered secreted frizzled related protein 2 (Sfrp2) reduces fibrosis and improves cardiac function in a rat model of myocardial infarction, *PNAS.* 107(49), pp. 21110-21115.

HEDHLI, N. et al., 2011. Endothelium-derived neuregulin protects the heart against ischemic injury. *Circulation,* 123(20), pp.2254-2262.

HERMANS, K.C.M. and BLANKESTEIJN, W.M., 2015. Wnt Signaling in Cardiac Disease. *Comprehensive Physiology,* 5(3), pp.1183-1209.

HERNANDEZ, J.S. et al., 2014. Crosstalk between AMPK activation and angiotensin II-induced hypertrophy in cardiomyocytes: the role of mitochondria. *Journal of Cellular and Molecular Medicine,* 18(4), pp.709-720.

HIGUCHI, Y. et al., 2002. Involvement of reactive oxygen species-mediated NF-kappa B activation in TNF-alpha-induced cardiomyocyte hypertrophy. *Journal of Molecular and Cellular Cardiology,* 34(2), pp.233-240.

HILAL-DANDON, R. and BRUNTON, L.L.,2012. Endothelin A Receptor (ETAR). In: Choi S. *Encyclopedia of Signaling Molecules*. Springer, New York.

HOFFMANN, F., 2018. A concise discussion of the regulatory role of cGMP kinase I in cardiac physiology and pathology. *Basic Research in Cardiology,* 113(4), pp.31.

HOFFMANN, M.M. et al., 2014. Association of secreted frizzled-related protein 4 (SFRP4) with type 2 diabetes in patients with stable coronary artery disease. *Cardiovascular Diabetology,* 13(155).

HOU, J. et al., 1995. Angiotensin II-induced cardiac fibrosis in the rat is increased by chronic inhibition of nitric oxide synthase.. *The Journal of Clinical Investigation,* 96(5), pp.2469-2477.

HU, B. et al., 2017. Sodium Ferulate Protects against Angiotensin II-Induced Cardiac Hypertrophy in Mice by Regulating the MAPK/ERK and JNK Pathways. *BioMed Research International,* 2017, pp. 3754942.

HU, W. et al., 2013. Circulating Sfrp5 is a signature of obesity-related metabolic disorders and is regulated by glucose and liraglutide in humans. *Journal of Clinical Endocrinology and Metabolism,* 98(1), pp.290-298.

HUANG, J. et al., 2014. miR-34a Modulates Angiotensin II-Induced Myocardial Hypertrophy by Direct Inhibition of ATG9A Expression and Autophagic Activity. *PLoS One,* 9(4), pp.e94382.

HUANG, Y. et al., 2011. Suppression of endothelin-1-induced cardiac myocyte hypertrophy by PPAR agonists: role of diacylglycerol kinase zeta. *Cardiovascular Research,* 90(2), pp.267-275.

HUANG, Y. et al., 2021. An herbal preparation ameliorates heart failure with preserved ejection fraction by alleviating microvascular endothelial inflammation and activating NO-cGMP-PKG pathway. *Phytomedicine,* 91.

HUBERT, F. et al., 2014. Alteration of vascular reactivity in heart failure: role of phosphodiesterases 3 and 4. *British Journal of Pharmacology,* 171(23), pp.5361-5375.

HUGGINS, C.E. et al., 2003. Elevated intracardiac angiotensin II leads to cardiac hypertrophy and mechanical dysfunction in normotensive mice. *Journal of the Renin Angiotensin Aldosterone System,* 4(3), pp.186-190.

HUTCHINGS, D.C. et al., 2018. Phosphodiesterase-5 inhibitors and the heart: compound cardioprotection? *Heart,* 104(15), pp.1244-1250

ILIESIU, A.M. and HODOROGEA, A.S., 2018. Treatment of Heart Failure with Preserved Ejection Fraction. *Advances in Experimental Biology and Medicine,* 1067, pp.67-87.

IP, W., CHIANG, Y-T.A. and JIN, T., 2012. The involvement of the wnt signaling pathway and TCF7L2 in diabetes mellitus: The current understanding, dispute, and perspective. *Cell and Bioscience,* 2.

IQBAL, S.T.A. et al., 2020. Paeonol Reverses Adriamycin Induced Cardiac Pathological Remodeling through Notch1 Signaling Reactivation in H9c2 Cells and Adult Zebrafish Heart. *Chemical Research in Toxicology,* 33(2), pp.312-323.

ISHIGURO, K. et al., 2007. Developmental activity of the renin-angiotensin system during the "critical period" modulates later L-NAME-induced hypertension and renal injury. *Hypertension Research,* 30(1), pp.63-75.

ISOBE, N. et al., 2002. Candesartan cilexetil improves left ventricular function, left ventricular hypertrophy, and endothelial function in patients with hypertensive heart disease. *Circulation Journal: Official Journal of the Japanese Circulation Society,* 66(11), pp.993-999.

IVASHCHENKO, C.Y. et al., 2013. Human-induced Pluripotent Stem Cell-Derived Cardiomyocytes Exhibit Temporal Changes in Phenotype. *American Journal of Physiology-Heart and Circulatory Physiology,* 305(6), pp. H913-H922.

IWANO, H. and LITTLE, W.C., 2013. Heart Failure: What Does Ejection Fraction have to do with it? *Journal of Cardiology,* 62(2013), pp.1-3.

IZUMIYA, Y. et al., 2003. Apoptosis signal-regulating kinase 1 plays a pivotal role in angiotensin II-induced cardiac hypertrophy and remodelling. *Circulation Research,* 93(9), pp. 874-883.

JANDA, C.Y. et al., 2012. Structural basis of Wnt recognition by Frizzled. *Science,* 337(6090), pp.59-64.

JANI, B. and RAJKUMAR, C., 2006. Ageing and vascular ageing. *Postgraduate Medical Journal,* 82(968), pp.357-362.

JANUZZI, J.L. et al., 2006. NT-proBNP Testing for Diagnosis and Short Term Prognosis in Acute Destabilized Heart Failure: an International Pooled Analysis of 1256 Patients. *European Heart Journal,* 27, pp.330-337.

JEN, H-L. et al., 2017. Endothelin-1-Induced Cell Hypertrophy in Cardiomyocytes is Improved by Fenofibrate: Possible Roles of Adiponectin. *Journal of Atherosclerosis and Thrombosis,* 24(5), pp.508-517.

JEONG, E-M. et al., 2013. Tetrahydrobiopterin improves diastolic dysfunction by reversing changes in myofilament properties. *Journal of Molecular and Cellular Cardiology,* 56, pp.44-54.

JEONG, W-J., RO, E.J. and CHOI, K-Y., 2018. Interaction between Wnt/β-catenin and RAS-ERK pathways and an anti-cancer strategy via degradations of β-catenin and RAS by targeting the Wnt/β-catenin pathway. *npj Precison Oncology,* 2.

JESSUP, M. et al., 2009. ACCF/AHA Guidelines for the Diagnosis and Management of Heart Failure in Adults. *Circulation,* 119, pp. 1977-2016.

JHO, E-H. et al., 2002. Wnt/beta-catenin/Tcf signaling induces the transcription of Axin2, a negative regulator of the signaling pathway. *Molecular and Cellular Biology,* 22(4), pp.1172-1183.

JIA, G. et al., 2018. Role of Renin-Angiotensin-Aldosterone System Activation in Promoting Cardiovascular Fibrosis and Stiffness. *Hypertension,* 72(3), pp.537-548.

JIA, N. et al., 2012. Allopurinol attenuates oxidative stress and cardiac fibrosis in angiotensin II-induced cardiac diastolic dysfunction. *Cardiovascular Therapeutics,* 30(2), pp.117-123.

JIANG, J. et al., 2018. A novel porcupine inhibitor blocks WNT pathways and attenuates cardiac hypertrophy. *Biochimica et Biophysica Acta (BBA) - Molecular Basis of Disease,* 1864(10), pp.3459-3467.

JIANG, Q. et al., 2021. Ginkgolide B Protects Cardiomyocytes from Angiotensin II-Induced Hypertrophy via Regulation of Autophagy through SIRT1-FoxO1. *Cardiovascular Therapeutics,* 2021.

JIN, L. et al., 2018. Gallic acid improves cardiac dysfunction and fibrosis in pressure overload-induced heart failure. *Nature Scientific Reports,* 8.

JOHANSSON, M. et al., 2020. Cardiac hypertrophy in a dish: a human stem cell based model. *Biology Open,* 9(9).

JUN, H-O. et al., 2011. Clusterin Protects H9c2 Cardiomyocytes from Oxidative Stress-Induced Apoptosis via Akt/GSK-3β Signaling Pathway. *Experimental & Molecular Medicine,* 43(1), pp.53-61.

JUNG, E.K. et al., 2017. WNT1-inducible signaling pathway protein-1 contributes to tumor progression and treatment failure in oral squamous cell carcinoma. *Oncology Letters,* 14(2), pp.1719-1724.

KADOGUCHI, T. et al., 2015. Angiotensin II can directly induce mitochondrial dysfunction, decrease oxidative fibre number and induce atrophy in mouse hindlimb skeletal muscle. *Experimental Physiology,* 100(3), pp.312-322.

KAGIYAMA, S. et al., 2002. Aldosterone-and-salt-induced cardiac fibrosis is independent from angiotensin II type 1a receptor signaling in mice. *Hypertension Research,* 30(10), pp.979-989.

KAHN,M., 2014. Can we safely target the WNT pathway? *Nature Reviews. Drug Discovery,* 13(7), pp.513-532.

KAMIYA, M. et al., 2021. β 3-Adrenergic Receptor Agonist Prevents Diastolic Dysfunction in an Angiotensin II-Induced Cardiomyopathy Mouse Model. *The Journal of Pharmacology and Experimental Therapeutics,* 376(3), pp.473-481.

KANKEU, C. et al., 2018. Quantitative proteomics and systems analysis of cultured H9C2 cardiomyoblasts during differentiation over time supports a 'function follows form' model of differentiation. *Molecular Omics,* 14(3), pp.181-196.

KANNEL, W.B. and MCGEE, D.L., 1979. Diabetes and cardiovascular disease. The Framingham study. *JAMA,* 241(19), pp.2035-2038.

KAPOUN, A.M. et al., 2004. B-type natriuretic peptide exerts broad functional opposition to transforming growth factor-beta in primary human cardiac fibroblasts: fibrosis, myofibroblast conversion, proliferation, and inflammation. *Circulation Research,* 94(4), pp.453-461.

KARAGIANNIS, T.C. et al., 2010. Trichostatin A accentuates doxorubicin-induced hypertrophy in cardiac myocytes. *Aging,* 2(10), pp.659-668.

KATRUKHA, I.A., 2013. Human cardiac troponin complex. Structure and functions. *Biochemistry (Moscow),* 78(13), pp.1447-1465.

KAUTZKY-WILLER, A., HARREITER, J. and PACINI, G., 2016. Sex and Gender Differences in Risk, Pathophysiology and Complications of Type 2 Diabetes Mellitus. *Endocrine Reviews,* 37(3), pp.278-316.

KEBIG, A. et al., 2009. An optical dynamic mass redistribution assay reveals biased signaling of dualsteric GPCR activators. *Journal of Receptor and Signal Transduction Research,* 23(3-4), pp.140-145.

KEMP, C.D. and CONTE, J.V., 2012. The Pathophysiology of Heart Failure. *Cardiovascular Pathology,* 21(5), pp.365-371.

KESSLER-ICEKSON, G. et al., 2002. ANP expression in the hypertensive heart. *Experimental and Clinical Cardiology,* 7(2-3), pp.80-84.

KHAN, K. et al., 2019. The cytoprotective impact of yes-associated protein 1 after ischemia-reperfusion injury in AC16 human cardiomyocytes. *Experimental Biology and Medicine,* 244(10), pp.802-212.

KIM, J. et al., 2012. Wnt5a activates THP-1 monocytic cells via a β-catenin-independent pathway involving JNK and NF-κB activation. *Cytokine,* 60(1), pp.242-248.

KIM, J.I., 2017. High fat diet confers vascular hyper-contractility against angiotensin II through upregulation of MLCK and CPI-17. *Korean Journal of Physiology and Pharmacology,* 21(1), pp.99-106.

KIMES, B.W. and BRANDT, B.L., 1976. Properties of a clonal muscle cell line from rat heart. *Experimental Cell Research,* 98(2), pp.367-381.

KITAKATA, H. et al., 2021. Imeglimin prevents heart failure with preserved ejection fraction by recovering the impaired unfolded protein response in mice subjected to cardiometabolic stress. *Biochemical and biophysical research communications,* 572, pp.185-190.

KLEIN, A.B. et al., 2016. Demonstration of the dynamic mass redistribution label-free technology as a useful cell-based pharmacological assay for endogenously expressed GABAA receptors. *MedChemComm,* 7(3), pp.426-432.

KLEIN, G. et al., 2005. Increased collagen deposition and diastolic dysfunction but preserved myocardial hypertrophy after pressure overload in mice lacking PKCepsilon. *Circulation Research,* 96(7), pp.748-755.

KLEMM, F. et al., 2011. β-catenin-independent WNT signaling in basal-like breast cancer and brain metastasis. *Carcinogenesis,* 32(3), pp.434-442.

KONIGSHOFF, M. et al., 2008. Functional Wnt signaling is increased in idiopathic pulmonary fibrosis. *PLoS One,* 3(5), pp. e2142.

KONSTAM, M.A. et al., 2011. Left Ventricular Remodeling in Heart Failure. *JACC: Cardiovascular Imaging,* 4(1), pp.98-108.

KONSTANDIN, M.H. et al., 2013. Fibronectin Contributes to Pathological Cardiac Hypertrophy but Not Physiological Growth. *Basic Research in Cardiology,* 108(5).

KONUKOGLU, D. and UZUN, H., 2017. Endothelial Dysfunction and Hypertension. *Advances in Experimental Medicine and Biology,* 956, pp.511-540.

KOPINCOVA, J., PUZSEROVA, A. and BERNATOVA, I., 2012. L-NAME in the cardiovascular system - nitric oxide synthase activator? *Pharmacological Reports,* 64(3), pp.511-520.

KRATTINGER, N. et al., 2009. Increased expression of renal cyclooxygenase-2 and neuronal nitric oxide synthase in hypertensive Cx40-deficient mice. *Journal of Vascular Research,* 46(3), pp.188-198.

KRUGER, M. et al., 2009. Protein kinase G modulates human myocardial passive stiffness by phosphorylation of the titin springs. *Circulation Research,* 104(1), pp.87-94.

KUZMENKIN, A. et al., 2009. Functional Characterization of Cardiomyocytes Derived From Murine Induced Pluripotent Stem Cells in Vitro**.** *Federation of American Societies for Experimental Biology,* 23(12), pp. 4168-1480.

LACOLLEY, P., REGNAULT, V. and AVOLIO, A.P., 2018. Smooth Muscle Cell and Arterial Aging: Basic and Clinical Aspects. *Cardiovascular Research,* 114, pp.513-528.

LACOMBE, P., TARIQ, M.A. and LAPPIN, S.L., 2021. Physiology, Afterload Reduction. In: StatPearls [Online]. Treasure Island (FL): StatPearls Publishing. Available from: https://www.ncbi.nlm.nih.gov/books/NBK493174/

LAGATHU, C. et al., 2010. Secreted frizzled-related protein 1 regulates adipose tissue expansion and is dysregulated in severe obesity. *International Journal of Obesity,* 34(12), pp.1695-1705.

LAKATTA, E.G., SPURGEON, H.A. and JANCZEWSKI, A.M., 2014. Changes in the Heart That Accompany Advancing Age: Humans to Molecules. In: BI Jugdutt, ed. *Aging and Heart Failure.* New York: Springer, pp.319-337.

LAKSITORINI, M.D. et al., 2019. Modulation of Wnt/β-catenin signaling promotes blood-brain barrier phenotype in cultured brain endothelial cells. *Scientific Reports,* 9.

LANG, P. et al., 2019. Effects of different diets used in diet-induced obesity models on insulin resistance and vascular dysfunction in C57BL/6 mice. *Scientific Reports,* 9.

LAYLAND, J., SOLARO, R.J. and SHAH, A.M., 2005. Regulation of cardiac contractile function by troponin I phosphorylation. *Cardiovascular Research,* 66(1), pp.12-21.

LAZAR, E., SADEK, H.A. and BERGMANN, O., 2017. Cardiomyocyte renewal in the human heart: insights from the fall-out. *European Heart Journal,* 38(30), pp.2333-2342.

LE, T.Y.L. and CHONG, J.J.H., 2016. Cardiac progenitor cells for heart repair. *Cell Death Discovery,* 2.

LE, T.Y.L. and CHONG, J.J.H., 2016. Cardiac progenitor cells for heart repair. *Cell Death Discovery,* 2.

LEE, H.X. et al., 2006. Embryonic dorsal-ventral signaling: secreted frizzled-related proteins as inhibitors of tolloid proteinases. *Cell,* 124(1), pp.147-159.

LEE, J. et al., 2002. Upregulation of vascular renin-angiotensin and endothelin systems in rats inhibited of nitric oxide synthesis. *Pharmacology Research,* 46(5), pp.383-387.

LEE, N.S. and DANIELS, L.B., 2016. Current Understanding of the Compensatory Actions of Cardiac Natriuretic Peptides in Cardiac Failure: A Clinical Perspective. *Cardiac Failure Review,* 2(1), pp. 14-19.

LEE, S-H. et al., 2008. Islet specific Wnt activation in human type II diabetes. *Experimental Diabetes Research,* 2008.

LEE, Y-S. et al., 2012. The Wnt inhibitor secreted Frizzled-Related Protein 1 (sFRP1) promotes human Th17 differentiation. *European Journal of Immunology,* 42(10), pp.2564-2573.

LEUNG, J.Y. et al., 2002. Activation of AXIN2 expression by beta-catenin-T cell factor. A feedback repressor pathway regulating Wnt signaling. *The Journal of Biological Chemistry,* 277(14), pp.21657-21665.

LEVIN, E.R., GARDNER, D.G. and SAMSON, W.K., 1998. Natriuretic peptides. *The New England Journal of Medicine,* 339(5), pp.321-328.

LEWINTER, M.M. and MEYER, M., 2013. Mechanisms of Diastolic Dysfunction in HFpEF: If It's Not One Thing It's Another. *Circulation: Heart Failure,* 6(6), pp. 1112-1115.

LI, B. et al., 2020. Hypertensive Rats Treated Chronically With N ω-Nitro-L-Arginine Methyl Ester (L-NAME) Induced Disorder of Hepatic Fatty Acid Metabolism and Intestinal Pathophysiology. *Frontiers in Pharmacology,* 10.

LI, J. et al., 2017b. The Inhibitory Effect of WenxinKeli on H9c2 Cardiomyocytes Hypertrophy Induced by Angiotensin II through Regulating Autophagy Activity. *Oxidative Medicine and Cellular Longevity*, 2017.

LI, L. et al., 2015. Thymosin β4 Prevents Angiotensin II-Induced Cardiomyocyte Growth by Regulating Wnt/WISP Signaling. *Journal of Cellular Physiology,* 231(8), pp.1737-1744.

LI, R. et al., 2019. The Glp-1 Analog Liraglutide Protects Against Angiotensin II and Pressure Overload-Induced Cardiac Hypertrophy via PI3K/Akt1 and AMPKa Signaling. *Frontiers in Pharmacology,* 10.

LI, T. et al., 2021. Wnt3a upregulation is involved in TGFβ1-induced cardiac hypertrophy. *Cytokine,* 138, pp.155376.

LI, W. et al., 2017c. Folic acid prevents cardiac dysfunction and reduces myocardial fibrosis in a mouse model of high-fat diet-induced obesity. *Nutrition and Metabolism,* 14.

LI, X. et al., 2017a. Telmisartan suppresses cardiac hypertrophy by inhibiting cardiomyocyte apoptosis via the NFAT/ANP/BNP signaling pathway. *Molecular Medicine Reports,* 15(5), pp.2574-2582.

LIAN, X. et al., 2012. Robust cardiomyocyte differentiation from human pluripotent stem cells via temporal modulation of canonical Wnt signaling. *PNAS,* 109(27), pp.E1848-1857.

LIANG, W., CHO, H.C. and MARBAN, E., 2015. Wnt signalling suppresses voltage-dependent Na+ channel expression in postnatal rat cardiomyocytes. *The Journal of Physiology,* 593, pp.1147-1157.

LIAO, S. et al., 2021. β-Hydroxybutyrate Mitigated Heart Failure with Preserved Ejection Fraction by Increasing Treg Cells via Nox2/GSK-3β. *Journal of Inflammation Research,* 14, pp.4697-4706.

LIEN, C.L. et al., 1999. Control of early cardiac-specific transcription of Nkx2-5 by a GATA-dependent enhancer. *Development,* 126(1), pp.75-84.

LIM.S.L. et al., 2017. Association Between Use of Long-Acting Nitrates and Outcomes in Heart Failure With Preserved Ejection Fraction. *Circulation: Heart Failure,* 10(4).

LINDSTROM, P., 2007. The physiology of obese-hyperglycemic mice [ob/ob mice]. *Scientific World Journal,* 7, pp.666-685.

LIOU, S-H. et al., 2015. KMUP-1 Attenuates Endothelin-1-Induced Cardiomyocyte Hypertrophy through Activation of Heme Oxygenase-1 and Suppression of the Akt/GSK-3β, Calcineurin/NFATc4 and RhoA/ROCK Pathways. *Molecules,* 20(6), pp.10435-10449.

LIP, G.Y.H., GIBBS, C.R. and BEEVERS, D.G., 2000. ABC of Heart Failure Aetiology. *British Medical Journal,* 320, pp. 104-107.

LIU, C. et al., 2018. Alamandine Attenuates Hypertension and Cardiac Hypertrophy in Hypertensive Rats. *Amino Acids,* 50(8), pp.1071-1081.

LIU, F. et al., 2020. STVNa Attenuates Isoproterenol-Induced Cardiac Hypertrophy Response through the HDAC4 and Prdx2/ROS/Trx1 Pathways. *International Journal of Molecular Sciences,* 21(2), pp.682.

LIU, J. et al., 2013. Targeting Wnt-driven cancer through the inhibition of Porcupine by LGK974. *PNAS,* 110(50), pp.20224-20229.

LIU, L. et al., 2012. Activation of Wnt3a signaling stimulates intestinal epithelial repair by promoting c-Myc-regulated gene expression. *American Journal of Physiology. Cell Physiology,* 302(1), pp.C277-285.

LIU, L., 2015. Calhex$_{231}$ Ameliorates Cardiac Hypertrophy by Inhibiting Cellular Autophagy in Vivo and in Vitro. *Cellular Physiology and Biochemistry,* 36(4), pp.1597-1612.

LIU, M-H. et al., 2016. Hydrogen Sulfide Protects H9c2 Cardiac Cells Against Doxorubicin-Induced Cytotoxicity Through the PI3K/Akt/FoxO3a Pathway. *International Journal of Molecular Medicine,* 37(6), pp.1661-1668.

LIU, X. et al., 2006. Neuregulin-1/erbB-activation improves cardiac function and survival in models of ischemic, dilated, and viral cardiomyopathy. *Journal of American College of Cardiology,* 48(7), pp.1438-1447.

LOPEZ, J.L. et al., 2012. β-Myosin Heavy Chain Is Induced by Pressure Overload in a Minor Sub-Population of Smaller Mouse Cardiac Myocytes. *Circulation Research,* 109(6), pp.629-638.

LOUCH, W.E., SHEEHAN, K.A. and WOLSKA, B.M., 2011. Methods in cardiomyocyte isolation, culture, and gene transfer. *Journal of Molecular and Cellular Cardiology,* 51(3), pp.288-298.

LOVELOCK, J.D. et al., 2012. Ranolazine improves cardiac diastolic dysfunction through modulation of myofilament calcium sensitivity. *Circulation Research,* 110(6), pp.841-850.

LOVIC, D. et al., 2017. Left ventricular hypertrophy in athletes and hypertensive patients. *Journal of Clinical Hypertension,* 19(4), pp. 413-417.

LU, Z. et al., 2008. Extracellular superoxide dismutase deficiency exacerbates pressure overload-induced left ventricular hypertrophy and dysfunction. *Hypertension,* 51(1), pp.19-25.

LU, Z. et al., 2018. Deficiency of PKD2L1 (TRPP3) Exacerbates Pathological Cardiac Hypertrophy by Augmenting NCX1-Mediated Mitochondrial Calcium Overload. *Cell Reports,* 24(6), pp.1639-1652.

LUO, C. et al., 2021. Therapeutic of Candesartan and Music Therapy in Diabetic Retinopathy with Depression in Rats. *Evidence-based Complementary and Alternative Medicine,* 2021.

LUO, J-Y. et al., 2015. Regulators and effectors of bone morphogenetic protein signalling in the cardiovascular system. *The Journal of Physiology,* 593(14), pp.2995-3011.

LUSTIG, B. et al., 2002. Negative feedback loop of Wnt signaling through upregulation of conductin/axin2 in colorectal and liver tumors. *Molecular and Cellular Biology,* 22(4), pp.1184-1193.

MACDONALD, B.T. and HE, X., 2012. Frizzled and LRP5/6 receptors for Wnt/β-catenin signaling. *Cold Spring Harbor Perspectives in Biology,* 4(12).

MACDONALD, B.T., TAMAI, K. and HE, X., 2009. Wnt/beta-catenin signaling: components, mechanisms, and diseases. *Developmental Cell,* 17(1), pp.9-26.

MACHIRAJU, P. and GREENWAY, S.C., 2019. Current methods for the maturation of induced pluripotent stem cell-derived cardiomyocytes. *World Journal of Stem Cells,* 11(1), pp.33-43.

MAHDI, T. et al., 2012. Secreted frizzled-related protein 4 reduces insulin secretion and is overexpressed in type 2 diabetes. *Cell Metabolism,* 16(5), pp.625-633.

MAISEL, A.S. et al., 2002. Rapid Measurement of B-type Natriuretic Peptide in the Emergency Diagnosis of Heart Failure. *The New England Journal of Medicine,* 347(3), pp.161-167.

MAITI, G., NASKAR, D. and SEN.M., 2012. The Wingless homolog Wnt5a stimulates phagocytosis but not bacterial killing. *PNAS,* 109(41), pp.16600-16605.

MALEKAR, P. et al., 2010. Wnt signaling is critical for maladaptive cardiac hypertrophy and accelerates myocardial remodelling. *Hypertension,* 55(4), pp.939-945.

MANEESAI, P. et al., 2016. Synergistic Antihypertensive Effect of Carthamus tinctorius L. Extract and Captopril in L-NAME-Induced Hypertensive Rats via Restoration of eNOS and AT_1R Expression. *Nutrients,* 8(3), pp.122.

MANOLESCU, D-C. et al., 2014. All-trans retinoic acid stimulates gene expression of the cardioprotective natriuretic peptide system and prevents fibrosis and apoptosis in cardiomyocytes of obese ob/ob mice. *Applied Physiology, nutrition and metabolism,* 39(10), pp.1127-1136.

MAQUIGUSSA, E. et al., 2018. Klotho and PPAR Gamma Activation Mediate the Renoprotective Effect of Losartan in the 5/6 Nephrectomy Model. *Frontiers in Physiology,* 9.

MARCHESI, C. et al., 2012. Plasma levels of matrix metalloproteinases and their inhibitors in hypertension: a systematic review and meta-analysis. *Journal of Hypertension,* 30(1), pp.3.-16.

MARTINS, F. et al., 2015. Dieta Hiperlipídica Promove Remodelação Cardíaca em Modelo Experimental de Obesidade. *Arquivos Brasileiros de Cardiologia,* 105(5).

MASANI, N. et al., 2011. *Echocardiography: Guidelines for Chamber Quantification.* [online]. British Heart Foundation. Available from: file:///H:/Downloads/g407_echocardiography_guidelines_for_chamber_quantification_poster_0411%20(4).pdf

MASILAMANI, T.J., LOISELLE, J.J. and SUTHERLAND, L.C., 2014. Assessment of reference genes for real-time quantitative PCR gene expression normalization during C2C12 and H9c2 skeletal muscle differentiation. *Molecular Biotechnology,* 56(4), pp.329-339.

MASTAITIS, J. et al., 2015. Loss of SFRP4 Alters Body Size, Food Intake, and Energy Expenditure in Diet-Induced Obese Male Mice. *Endocrinology,* 156(12), pp.4502-4510.

MATHEW, T. et al., 2013. *A Guideline Protocol for the Echocardiographic assessment of Diastolic Dysfunction.* [online]. British Society of Echocardiography. Available from: https://www.bsecho.org/common/Uploaded%20files/Education/Protocols%20and%20guidelines/Diastolic%20dysfunction.pdf [Accessed 7th December 2021].

MATHIEU, S. et al., 2018. Angiotensin II Overstimulation Leads to an Increased Susceptibility to Dilated Cardiomyopathy and Higher Mortality in Female Mice. *Scientific Reports,* 8(1), pp.952.

MATIAS, A.M. et al., 2020. Hypercaloric diet models do not develop heart failure, but the excess sucrose promotes contractility dysfunction. *PLoS One,* 15(2).

MATSUMOTO, E. et al., 2013. Angiotensin II-induced cardiac hypertrophy and fibrosis are promoted in mice lacking Fgf16. *Genes Cells,* 18(7), pp.544-553.

MATSUSAKA, H. et al., 2006. Targeted deletion of matrix metalloproteinase 2 ameliorates myocardial remodeling in mice with chronic pressure overload. *Hypertension,* 47(4), pp.711-717.

MAYET, J. and HUGHES, A., 2003. Cardiac and vascular pathophysiology in hypertension. *Heart,* 89(9), pp. 1104-1109.

MAZZOTTA, S. et al., 2016. Distinctive Roles of Canonical and Noncanonical Wnt Signaling in Human Embryonic Cardiomyocyte Development. *Stem Cell Reports,* 7(4), pp.764-776.

MCCLEAN, D.R. et al., 2002. Vasopeptidase inhibition with omapatrilat in chronic heart failure: acute and long-term hemodynamic and neurohumoral effects. *Journal of the American College of Cardiology,* 39(12), pp.2034-2041.

MCDONAGH, T.A. et al., 2021. 2021 ESC Guidelines for the diagnosis and treatment of acute and chronic heart failure. *European Heart Journal,* 42(36), pp. 3599-3726.

MCHUGH, K. et al., 2019. Heart Failure With Preserved Ejection Fraction and Diabetes: JACC State-of-the-Art Review. *Journal of the American College of Cardiology,* 73(5), pp.602-611.

MCMURRAY, J.J.V. et al., 2012. ESC Guidelines for the Diagnosis and Treatment of Acute and Chronic Heart Failure 2012: The Task Force for the Diagnosis and Treatment of Acute and Chronic Heart Failure 2012 of the European Society of Cardiology. *European Journal of Heart Failure,* 14(8), pp.803-869.

MCMURRAY, J.J.V. et al., 2014. Angiotensin-neprilysin Inhibition Versus Enalapril in Heart Failure. *The New England Journal of Medicine,* 371(11), pp.993-1004.

MEHROTRA, A., JOE, B. and DE LA SERNA, I.L., 2013. SWI/SNF Chromatin Remodeling Enzymes are Associated with Cardiac Hypertrophy in a Genetic Rat Model of Hypertension. *Journal of Cell Physiology,* 228(12), pp.2337-2342.

MEHTA, A., VERMA,V. and NANDIHALLI, M., 2014. A Systemic Evaluation of Cardiac Differentiation from mRNA Reprogrammed Human Induced Pluripotent Stem Cells. *PLoS One,* 9(7), pp. e103485.

MENARD, C. et al., 1999. Modulation of L-type Calcium Channel Expression During Retinoic Acid-Induced Differentiation of H9C2 Cardiac Cells**.** *The Journal of Biochemical Chemistry,* 274(41), pp.29063-29070.

METHATHAM, T. et al., 2021. Inhibition of the canonical Wnt signaling pathway by a β-catenin/CBP inhibitor prevents heart failure by ameliorating cardiac hypertrophy and fibrosis. *Scientific Reports,* 11.

MICHAELS, A.D. et al., 2003. Effects of intravenous nesiritide on human coronary vasomotor regulation and myocardial oxygen uptake. *Circulation,* 107(21), pp.2697-2701.

MILL, C. et al., 2014. Wnt5a-induced Wnt1-inducible secreted protein-1 suppresses vascular smooth muscle cell apoptosis induced by oxidative stress. *Arteriosclerosis, Thrombosis, and Vascular Biology,* 34(11), pp.2449-2456.

MISAKA, T. et al., 2013. Deficiency of senescence marker protein 30 exacerbates angiotensin II-induced cardiac remodelling. *Cardiovascular Research,* 99(3), pp.461-470.

MITTER, S.S. et al., 2017. E/A and E/e to Assess Diastolic Dysfunction and LV Filling Pressure. *Journal of the American College of Cardiology,* 69(11), 1451-1464.

MIYATA, S. et al., 2000. Myosin Heavy Chain Isoform Expression in the Failing and Nonfailing Human Heart. *Circulation Research,* 86(4), pp.386-390.

MIZUTANI, M., WU, J.C. and NUSSE, R., 2016. Fibrosis of the Neonatal Mouse Heart After Cryoinjury Is Accompanied by Wnt Signaling Activation and Epicardial-to-Mesenchymal Transition. *Journal of the American Heart Association,* 5(3).

MOHAMMED, S.F. et al., 2010. Mineralocorticoid accelerates transition to heart failure with preserved ejection fraction via "nongenomic effects". *Circulation,* 122(4), pp.370-378.

MOHAMMED, S.H. and HUSSEIN, R.H., 2020. Anti-hypertensive and anti-oxidant activities of walnut almond oil, and corn and Candesartan on LNAME induced hypertensive rats. *Journal of Zankoy Sulaimani,* 22(2).

MOJARRAB, M. et al., 2013. Extracts of *Artemisia ciniformis* Protect Cytotoxicity Induced by Hydrogen Peroxide in H9c2 Cardiac Muscle Cells through the Inhibition of Reactive Oxygen Species. *Advances in Pharmacological Sciences,* 2013, pp.141683.

MONFREDI, O., MALTSEV, V.A. and LAKATTA,E.G., 2013. Modern Concepts Concerning the Origin of the Heartbeat. *Physiology,* 28(2), pp.74-92.

MONTAG, J. et al., 2018. Successful Knock-In of Hypertrophic Cardiomyopathy-mutation R723G Into the MYH7 Gene Mimics HCM Pathology in Pigs**.** *Scientific Reports,* 8(1), pp.4786.

MOON, J. et al., 2017. Blockade to pathological remodeling of infarcted heart tissue using a porcupine antagonist. *PNAS,* 114(7), pp.1649-1654.

MORIS, D. et al., 2017. The role of reactive oxygen species in the pathophysiology of cardiovascular diseases and the clinical significance of myocardial redox. *Annals of Translational Medicine,* 5(16), pp.326.

MUL, J.D. et al., 2013. Angiotensin-converting enzyme inhibition reduces food intake and weight gain and improves glucose tolerance in melanocortin-4 receptor deficient female rats. *Physiology and Behaviour,* 121, pp.43-48.

MULLER-FIELITZ, H. et al., 2011. Weight loss and hypophagia after high-dose AT1-blockade is only observed after high dosing and depends on regular leptin signalling but not blood pressure. *Naunyn-Schmiedebergs Archives of Pharmacology,* 383(4), pp.373-384.

MUSHTAQ, S. et al., 2015. N-Acetyl Cysteine Inhibits Endothelin-1-Induced ROS Dependent Cardiac Hypertrophy through Superoxide Dismutase Regulation. *Cell Journal,* 17(2), pp.355-360.

NACHER, W. et al., 2019. Cardiac inflammation and diastolic dysfunction in hypercholesterolemic rabbits. *PLoS One,* 14(8).

NAGANO, K. et al., 2013. Apelin elevates blood pressure in ICR mice with L-NAME-induced endothelial dysfunction. *Molecular Medicine Reports,* 7(5), pp.1371-1375.

NAGUEH, S.F. et al., 2016. Recommendations for the Evaluation of Left Ventricular Diastolic Function by Echocardiography: An Update from the American Society of Echocardiography and the European Association of Cardiovascular Imaging. *Journal of the American Society of Echocardiography,* 29(4), pp. 277-314.

NAITO, A. et al., 2012. Complement C1q activates canonical Wnt signaling and promotes aging-related phenotypes. *Cell,* 149(6), pp.1298-1313.

NAKAGAWA, A. et al., 2016. Activation of endothelial β-catenin signaling induces heart failure. *Scientific Reports*, 6, pp.25009.

NAKAGAWA, Y., NISHIKIMI, T. and KUWAHARA, K., 2019. Atrial and Brain Natriuretic Peptides: Hormones Secreted From the Heart. *Peptides,* 111, pp.18-25.

NAKAMURA, K. et al., 2016. Secreted Frizzled-related Protein 5 Diminishes Cardiac Inflammation and Protects the Heart from Ischemia/Reperfusion Injury. *Journal of Biological Chemistry,* 291(6), pp. 2566-2575.

NAKAMURA, M. and SADOSHIMA, J., 2018. Mechanisms of physiological and pathological cardiac hypertrophy. *Nature Reviews. Cardiology,* 15(7), pp.387-407.

NATIONAL HEALTH SERVICE (NHS), 2018. *Symptoms Heart Failure*. [online]. Available from: https://www.nhs.uk/conditions/heart-failure/symptoms/ [Accessed 6th June 2020].

NATIONAL INSTITUTE FOR CARDIOVASCULAR OUTCOMES RESEARCH (NICOR), 2019/2020. *National Heart Failure Audit (NHFA) 2019/2020 Summary Report.* [online]. London: NICOR. Available from: https://www.nicor.org.uk/wp-content/uploads/2021/10/NHFA-Domain-Report_2021_FINAL.pdf [Accessed 11th June 2020].

NATIONAL INSTITUTE FOR HEALTH AND CARE EXCELLENCE (NICE), 2019. *Hypertension in adults: diagnosis and management NICE guideline* [online]. NICE. Available from:https://www.nice.org.uk/guidance/ng136/resources/hypertension-in-adults-diagnosis-and-management-pdf-66141722710213 [Accessed 19th December 2021].

NATIONAL INSTITUTES OF HEALTH (NIH), 2016. *World's older population grows dramatically*. [online]. Maryland, USA: NIH. Available from: https://www.nih.gov/news-events/news-releases/worlds-older-population-grows-dramatically [Accessed 4th June 2020].

NEHME, A. et al., 2019. An Update on the Tissue Renin Angiotensin System and Its Role in Physiology and Pathology. *Journal of Cardiovascular Development and Disease,* 6(2).

NEHRA, S. et al., 2015. Nanocurcumin Prevents Hypoxia Induced Stress in Primary Human Ventricular Cardiomyocytes by Maintaining Mitochondrial Homeostasis. *PLos One,* 10(9). pp.e0139121.

NEWMAN, D.R. et al., 2016. Expression of WNT5A in Idiopathic Pulmonary Fibrosis and Its Control by TGF-β and WNT7B in Human Lung Fibroblasts. *The Journal of Histochemistry and Cytochemistry,* 64(2), pp.99-111.

NICKS, A.M. et al., 2020. Pressure overload by suprarenal aortic constriction in mice leads to left ventricular hypertrophy without c-Kit expression in cardiomyocytes. *Scientific Reports,* 10(1).

NISHIKIMI, T., MAEDA, N. and MATSUOKA, H., 2006. The role of natriuretic peptides in cardioprotection. *Cardiovascular Research,* 69(2), pp.318-328.

NOLLET, E.E. et al., 2020. Large-Scale Contractility Measurements Reveal Large Atrioventricular and Subtle Interventricular Differences in Cultured Unloaded Rat Cardiomyocytes. *Frontiers in Physiology,* 11, pp.815.

NORTH, B.J. and SINCLAIR, D.A., 2012. The Intersection Between Aging and Cardiovascular Disease. *Circulation Research,* 110(8), pp. 1097-1108.

O'CONNOR, T.G. et al., 2011. Effect of nesiritide in patients with acute decompensated heart failure. *The New England Journal of Medicine,* 365(1), pp.32-43.

O'NEAL, W.T. et al., 2017. Electrocardiographic Predictors of Heart Failure With Reduced Versus Preserved Ejection Fraction: The Multi-Ethnic Study of Atherosclerosis. *Journal of the American Heart Association,* 6(6), pp. e006023.

OCK, S. et al., 2021. IGF-1 protects against angiotensin II-induced cardiac fibrosis by targeting αSMA. *Cell Death and Disease,* 12(7).

ODAGIRI, F. et al., 2014. Effects of Candesartan on electrical remodeling in the hearts of inherited dilated cardiomyopathy model mice. *PLoS One,* 9(7).

OELZE, M. et al., 2013. Chronic therapy with isosorbide-5-mononitrate causes endothelial dysfunction, oxidative stress, and a marked increase in vascular endothelin-1 expression. *European Heart Journal,* 34(41), pp.3206-3216.

OGAWA, E. et al., 2000. Outside-in Signalling of Fibronectin Stimulates Cardiomyocyte Hypertrophy in Cultured Neonatal Rat Ventricular Myocytes. *Journal of Molecular and Cellular Cardiology*, 32(5), pp. 765-776.

OJALA, M. et al., 2014. Modeling hypertrophic cardiomyopathy with human induced pluripotent stem cells. *Cardiovascular Research,* 103, pp.S105.

OKAZAKI, H. et al., 2006. Angiotensin II type 1 receptor blocker prevents atrial structural remodeling in rats with hypertension induced by chronic nitric oxide inhibition. *Hypertension Research* 29(4), pp.277-284.

OKTAY, A., RICH, J.D. and SHAH, S.J.,2013. The Emerging Epidemic of Heart Failure with Preserved Ejection Fraction. *Current Heart Failure Reports,* 10, pp.401-410.

ONISHI, K., HOLLIS, E. and ZOU, Y., 2014. Axon guidance and injury-lessons from Wnts and Wnt signaling. *Current Opinion in Neurobiology,* 27, pp.232-240.

OUCHI, N. et al., 2010. Sfrp5 is an anti-inflammatory adipokine that modulates metabolic dysfunction in obesity. *Science,* 329(5990), pp.454-457.

PACKER, M., 2018. Do sodium-glucose co-transporter-2 inhibitors prevent heart failure with a preserved ejection fraction by counterbalancing the effects of leptin? A novel hypothesis. *Diabetes, Obesity and Metabolism,* 20(6), pp.1361-1366.

PACURARI, M. et al., 2014. The Renin-Angiotensin-aldosterone system in vascular inflammation and remodelling. *International Journal of Inflammation,* 2014, pp.689360.

PAGANO, M. et al., 2004. Differentiation of H9c2 cardiomyoblasts: The role of adenylate cyclase system. *Journal of Cell Physiology,* 198(3), pp. 408-416.

PAIGE, S.L. et al., 2010. Endogenous Wnt/beta-catenin signaling is required for cardiac differentiation in human embryonic stem cells. *PLoS One,* 5(6), pp.e11134.

PAIVA, S.A.R. et al., 2005. Retinoic acid supplementation attenuates ventricular remodeling after myocardial infarction in rats. *The Journal of Nutrition,* 135(10), pp.2326-2328.

PALM-LEIS, A. et al., 2004. Mitogen-activated protein kinases and mitogen-activated protein kinase phosphatases mediate the inhibitory effects of all-trans retinoic acid on the hypertrophic growth of cardiomyocytes. *The Journal of Biological Chemistry,* 279(52), pp.54905-54917.

PAN, S. et al., 2018. Sfrp1 attenuates TAC-induced cardiac dysfunction by inhibiting Wnt signaling pathway- mediated myocardial apoptosis in mice. *Lipids in Health and Disease,* 17(1), pp.202.

PAN, W. et al., 2013. MiR-30-regulated autophagy mediates angiotensin II-induced myocardial hypertrophy. *PLoS One,* 8(1), pp.e53950.

PANDY, K.N., 2011. The Functional Genomics of Guanylyl Cyclase/Natriuretic Peptide Receptor-A: Perspectives and Paradigms. *The FEBS Journal,* 278(11), pp. 1792-1807.

PAPAY, R.S. et al., 2013. α_1A-adrenergic receptors regulate cardiac hypertrophy in vivo through interleukin-6 secretion. *Molecular Pharmacology,* 83(5), pp.939-948.

PAPINSKA, A.M. et al., 2016. Long-term administration of angiotensin (1-7) prevents heart and lung dysfunction in a mouse model of type 2 diabetes (db/db) by reducing oxidative stress, inflammation and pathological remodeling. *Pharmacology Research,* 107, pp.372-380.

PARK, S. et al., 2020. Cardiac Fibrosis Is Associated With Decreased Circulating Levels of Full-Length CILP in Heart Failure. *JACC Basic to Translational Science,* 5(5), pp.432-443.

PARROTTA, E.I. et al., 2020. Modeling Cardiac Disease Mechanisms Using Induced Pluripotent Stem Cell-Derived Cardiomyocytes: Progress, Promises and Challenges. *International Journal of Molecular Sciences, 21(12), pp.4534.*

PATRA, C., RICCIARDI, F. and ENGEL, F.B., 2012. The functional properties of nephronectin: An adhesion molecule for cardiac tissue engineering. *Biomaterials,* 33(17), pp.4327-4335.

PATTEN, V. et al., 2017. Cardiomyocyte differentiation: Experience and observations from 2 laboratories. *Journal of South African Heart Association,* 14(2).

PECHANOVA, O., VRANKOVA, S. and CEBOVA, M., 2020. Chronic L-Name-Treatment Produces Hypertension by Different Mechanisms in Peripheral Tissues and Brain: Role of Central eNOS. *Pathophysiology,* 27(1), pp.46-54.

PEI, J. and GRISHIN, N.V., 2012. Cysteine-rich domains related to Frizzled receptors and Hedgehog-interacting proteins. *Protein Science,* 21(8), pp.1172-1184.

PENG, C. et al., 2017. Phenylephrine-induced Cardiac Hypertrophy Is Attenuated by a Histone Acetylase Inhibitor Anacardic Acid in Mice. *Molecular bioSystems,* 13(4), pp. 714-724.

PENG, H. et al., 2011. Angiotensin II-induced dilated cardiomyopathy in Balb/c but not C57BL/6J mice. *Experimental Physiology,* 96(8), pp.756-764.

PENG, K. et al., 2016. Novel EGFR Inhibitors Attenuate Cardiac Hypertrophy Induced by Angiotensin II. *Journal of Cellular and Molecular Medicine,* 20(3), pp.482-494.

PEOTTA, V.A., VASQUEZ, E.C. and MEYRELLES, S.S., 2001. Cardiovascular neural reflexes in L-NAME-induced hypertension in mice. *Hypertension,* 38, pp.555-559.

PERCIE DU SERT, N. et al., 2020. The ARRIVE guidelines 2.0: Updated guidelines for reporting animal research. *PLoS Biology,* 18(7).

PEREIRA, C. et al., 2008. Wnt5A/CaMKII signaling contributes to the inflammatory response of macrophages and is a target for the antiinflammatory action of activated protein C and interleukin-10. *Arteriosclerosis, Thrombosis, and Vascular Biology,* 28(3), pp.504-510.

PEREIRA, S.L. et al., 2011. Metabolic Remodeling During H9c2 Myoblast Differentiation: Relevance for in Vitro Toxicity Studies. *Cardiovascular Toxicology,* 11(2), pp.180-190.

PERRELLI, M-G., PAGLIARO, P. and PENNA, C., 2011. Ischemia/reperfusion injury and cardioprotective mechanisms: Role of mitochondria and reactive oxygen species. *World Journal of Cardiology,* 3(6), pp.186-200.

PESSANHA, M.G., HAHN, M.D. and MANDARIM-DE-LACERDA, C.A.., 1999. Myocardial repair with long-term and low-dose administration of a nitric oxide synthesis inhibitor. Myofibroblasts, type III collagen and fibronectin. *Arquivos Brasileiros de Cardiologia,* 73(1), pp.87-96.

PETER, A.K., BJERKE. M.A. and LEINWAND, L.A., 2016. Biology of the cardiac myocyte in heart disease. *Molecular Biology of the Cell,* 27(14), pp.2148-2160.

PFAFFL, M.W., 2001. A new mathematical model for relative quantification in real-time RT–PCR. *Nucleic Acid Research,* 29(9), pp. e45.

PFEFFER, M.A. and BRAUNWALD, E., 1990. Ventricular remodeling after myocardial infarction. Experimental observations and clinical implications. *Circulation,* 81(4), pp.1161-1172.

PIASTOWSKA-CIESIELSKA, A.W. et al., 2014. Angiotensin modulates human mammary epithelial cell motility. *Journal of the Renin Angiotensin-Aldosterone Systems,* 15(4), pp.419-429.

PIGNATELLI, P. et al., 2018. Oxidative stress and cardiovascular disease: new insights. *Kardiologia Polska,* 76(4), pp.713-722.

PIRKMAJER, S. and CHIBALIN, A.V., 2011. Serum starvation: caveat emptor. *American Journal of Physiology. Cell Physiology,* 301(2), pp.C272-279.

PLANTE, E. et al., 2015. Oxytocin treatment prevents the cardiomyopathy observed in obese diabetic male db/db mice. *Endocrinology,* 156(4), pp.1416-1428.

POLAKIS, P., 2012. Wnt signaling in cancer. *Cold Spring Harbor Perspectives in Biology,* 4(5), pp. a008052.

POLLOCK, D.M. et al., 1993. Angiotensin blockade reverses hypertension during long-term nitric oxide synthase inhibition. *Hypertension,* 21(5), pp.660-666.

PONIKOWSKI, P. et al.,2016. ESC Guidelines for the Diagnosis and Treatment of Acute and Chronic Heart Failure. *European Heart Journal,* 37, pp.2129-2200.

POURRIER, M. et al., 2013. CrossTalk proposal: The late sodium current is an important player in the development of diastolic heart failure (heart failure with a preserved ejection fraction). *The Journal of Physiology,* 592(3), pp.411-414.

PRASAD, A.M. et al., 2007. Phenylephrine hypertrophy, Ca2+-ATPase (SERCA2), and Ca2+ signaling in neonatal rat cardiac myocytes. *American Journal of Physiology. Cell Physiology,* 292(6), pp.C2269-2275.

PRATHAPAN, A. et al., 2014. Protective effect of Boerhaavia diffusa L. against mitochondrial dysfunction in angiotensin II induced hypertrophy in H9c2 cardiomyoblast cells. *PLoS One,* 9(4), pp.e96220.

PRATHAPAN, A. et al., 2018. Apoptosis in angiotensin II-stimulated hypertrophic cardiac cells -modulation by phenolics rich extract of Boerhavia diffusa L. *Biomedicine and Pharmacotherapy,* 108, pp.1097-1104.

PRENDERGAST, B.J., ONISHI, K.G. and ZUCKER, I., 2014. Female mice liberated for inclusion in neuroscience and biomedical research. *Neuroscience and Biobehavioural Reviews,* 40, pp.1-5.

PROFFITT, K.D. et al., 2013. Pharmacological inhibition of the Wnt acyltransferase PORCN prevents growth of WNT-driven mammary cancer. *Cancer Research,* 73(2), pp.502-507.

PUPPALA, D. et al., 2013. Comparative Gene Expression Profiling in Human-Induced Pluripotent Stem Cell–Derived Cardiomyocytes and Human and Cynomolgus Heart Tissue. *Toxicology Science,* 131(1), pp.292-301.

QIAN, W. et al., 2018. Wogonin Attenuates Isoprenaline-Induced Myocardial Hypertrophy in Mice by Suppressing the PI3K/Akt Pathway. *Frontiers Pharmacology,* 9, pp.896.

QIN, F. et al., 2006. NADPH oxidase is involved in angiotensin II-induced apoptosis in H9C2 cardiac muscle cells: effects of apocynin. *Free Radical Biology and Medicine,* 40(2), pp.236-246.

QU, J. et al., 2007. Cardiac-specific haploinsufficiency of beta-catenin attenuates cardiac hypertrophy but enhances fetal gene expression in response to aortic constriction. *Journal of Molecular and Cellular Cardiology,* 43(3), pp.319-326.

QUEREJETA, R. et al., 2004. Increased collagen type I synthesis in patients with heart failure of hypertensive origin: relation to myocardial fibrosis. *Circulation,* 110(10), pp.1263-1268.

RAPHAEL, C. et al., 2007. Limitations of the New York Heart Association Functional Classification System and Self-Reported Walking Distances in Chronic Heart Failure. *Heart*, 93, pp.476-482.

RAVICHANDRAN, L.V. and PUVANAKRISHNAN, R., 1991. In vivo labeling studies on the biosynthesis and degradation of collagen in experimental myocardial infarction. *Biochemistry International,* 24(3), pp.405-414.

REDFIELD, M.M. et al., 2005. Age and Gender-Related Ventricular-Vascular Stiffening. *Circulation,* 112, pp.2254-2262.

REDFIELD, M.M. et al., 2013. Effect of phosphodiesterase-5 inhibition on exercise capacity and clinical status in heart failure with preserved ejection fraction: a randomized clinical trial. *JAMA,* 309(12), pp.1268-1277.

REGAN, J.A. et al., 2015. A mouse model of heart failure with preserved ejection fraction due to chronic infusion of a low subpressor dose of angiotensin II. *American Journal of Physiology. Heart and Circulatory Physiology,* 309(5), pp.H771-778.

REIL, J-C. et al., 2013. Heart rate reduction by If-inhibition improves vascular stiffness and left ventricular systolic and diastolic function in a mouse model of heart failure with preserved ejection fraction. *European Heart Journal,* 34(36), pp.2839-2849.

REISCHMANN, R. et al., 2015. Measured Effects of Wnt3a on Proliferation of HEK293T Cells Depend on the Applied Assay. *International Journal of Cell Biology,* 2015, pp.928502.

RELLING, I. et al., 2018. Role of wnt5a in Metabolic Inflammation in Humans. *Journal of Clinical Endocrinology and Metabolism,* 103(11), pp.4253-4264.

REN, J. et al., 2015. Nitric oxide synthase inhibition abolishes exercise-mediated protection against isoproterenol-induced cardiac hypertrophy in female mice. *Cardiology,* 130(3), pp.175-184.

RICHARDS, D.A. et al., 2019. Distinct Phenotypes Induced by Three Degrees of Transverse Aortic Constriction in Mice. *Scientific Reports,* 9.

RING, A., KIM, Y-M. and KAHN, M., 2014. Wnt/catenin signaling in adult stem cell physiology and disease. *Stem Cell Reviews and Reports,* 10(4), pp.512-525.

RIOS-ESTEVES, J. and RESH, M.D., 2013. Stearoyl CoA Desaturase Is Required to Produce Active, Lipid-Modified Wnt Proteins. *Cell Reports,* 4(6), pp.1072-1081.

RISS, T.L. et al., 2004. Cell Viability Assays. In: S.MARKOSSIAN, ed. *Assay Guidance Manual.* Bethesda: Eli Lilly and Company.

RIVERA-JARDON, F.F. et al., 2009. Angiotensin II augments renal vasoconstriction via AT1 receptors in L-NAME-induced hypertensive rats. *Proceedings of the Western Pharmacology Society,* 52, pp.47-49.

RODGERS, J.L. et al., 2019. Cardiovascular Risks Associated with Gender and Aging. *Journal of Cardiovascular Development and Disease,* 6(2).

ROSANO, G.MC., VITALE, C. and SEFEROVIC, P., 2017. Heart Failure in Patients with Diabetes Mellitus. *Cardiac Failure Review,* 3(1), pp.52-55.

ROSENBAUM, Z. et al., 2019. Association of body mass index and diastolic function in metabolically healthy obese with preserved ejection fraction. *International Journal of Cardiology,* 277, pp.147-152.

ROSS, S.E. et al., 2000. Inhibition of adipogenesis by Wnt signaling. *Science,* 289(5481), pp.950-953.

RUSCONI, F. et al., 2013. CIP4 is required for the hypertrophic growth of neonatal cardiac myocytes. *Journal of Biomedical Science,* 20(1), pp.56.

RUSSO, I. and FRANGOGIANNIS, N.G., 2016. Diabetes-associated cardiac fibrosis: Cellular effectors, molecular mechanisms and therapeutic opportunities. *Journal of Molecular and Cell Cardiology,* 90, pp.84-93.

SACCHETTO, C. et al., 2020. Modeling Cardiovascular Diseases with hiPSC-Derived Cardiomyocytes in 2D and 3D Cultures. *International Journal of Molecular Sciences,* 21(9), pp.3404.

SACKNER-BERSTEIN, J.D. et al., 2005b. Short-term risk of death after treatment with nesiritide for decompensated heart failure: a pooled analysis of randomized controlled trials. *JAMA,* 293(15), pp.1900-1905.

SACKNER-BERSTEIN, J.D., SKOPICKI, H.A. and AARONSON, K.D., 2005a. Risk of worsening renal function with nesiritide in patients with acutely decompensated heart failure. *Circulation,* 111(12), pp.1487-1491.

SAEGUSA, S. et al., 2007. Oral administration of Candesartan improves the survival of mice with viral myocarditis through modification of cardiac adiponectin expression. *Cardiovascular Drugs and Therapy,* 21(3), pp.155-160.

SAFAR, M.E. et al., 2018. Interaction Between Hypertension and Arterial Stiffness. *Hypertension,* 72(4), pp.796-805.

SANTOS, I.B. et al., 2020. Açaí seed extract prevents the renin-angiotensin system activation, oxidative stress and inflammation in white adipose tissue of high-fat diet-fed mice. *Nutrition Research,* 79, pp.35-49.

SAVJI, N. et al., 2018. The Association of Obesity and Cardiometabolic Traits With Incident HFpEF and HFrEF. *JACC Heart Failure,* 6(8), pp.701-709.

SAWADA, H. et al., 2015. Iron restriction inhibits renal injury in aldosterone/salt-induced hypertensive mice. *Hypertension Research,* 38(5), pp.317-322.

SCHIATTARELLA, G.G. et al., 2019. Nitrosative stress drives heart failure with preserved ejection fraction. *Nature,* 568(7752), pp.351-356.

SCHRODER, R. et al., 2011. Applying label-free dynamic mass redistribution technology to frame signaling of G protein–coupled receptors noninvasively in living cells. *Nature Protocols,* 6(2011), pp.1748-1760.

SCHULTE, D.M. et al., 2012. Pro-inflammatory wnt5a and anti-inflammatory sFRP5 are differentially regulated by nutritional factors in obese human subjects. *PLoS One,* 7(2), pp. e32437.

SCIARRETTA, S. et al., 2009. Role of the renin-angiotensin-aldosterone system and inflammatory processes in the development and progression of diastolic dysfunction. *Clinical Science,* 116(6), pp.467-477.

SHARIFI, A.M., AKBARLOO, N. and DARABI, R., 2005. Investigation of local ACE activity and structural alterations during development of L-NAME-induced hypertension. *Pharmacology Research,* 52(5), pp.438-444.

SHEIKH, F., LYON, R.C. and CHEN, J., 2015. Functions of Myosin Light Chain-2 (MYL2) In Cardiac Muscle and Disease. *Gene,* 569(1), pp.14-20.

SHEN, Y. et al., 2016. Granzyme B Deficiency Protects against Angiotensin II-Induced Cardiac Fibrosis. *The American Journal of Pathology,* 186(1), pp.87-100.

SHEN, Y. et al., 2017. c-Myc promotes renal fibrosis by inducing integrin αv-mediated transforming growth factor-β signaling. *Kidney International,* 92(4), pp.888-899.

SHENG, L. et al., 2008. Peroxisome proliferator-activated receptor beta/delta activation improves angiotensin II-induced cardiac hypertrophy in vitro. *Clinical and Experimental Hypertension,* 30(2), pp.109-119.

SHUAI, W. et al., 2020. Loss of myeloid differentiation protein 1 promotes atrial fibrillation in heart failure with preserved ejection fraction. *ESC Heart Failure,* 7(2), pp.626-638.

SILBERMAN, G.A. et al., 2010. Uncoupled cardiac nitric oxide synthase mediates diastolic dysfunction. *Circulation,* 121(4), pp.519-528.

SILVA, R.A.C. et al., 2017. Cardiac Remodeling Induced by All-Trans Retinoic Acid is Detrimental in Normal Rats. *Cellular Physiology and Biochemistry,* 43, pp.1449-1459.

SILVANI, A. et al., 2009. Sleep modulates hypertension in leptin-deficient obese mice. *Hypertension,* pp.53(2), pp.251-255.

SIMKO, F. et al., 2018. Effect of Ivabradine on a Hypertensive Heart and the Renin-Angiotensin-Aldosterone System in L-NAME-Induced Hypertension. *International Journal of Molecular Sciences,* 19(10).

SIMONDS, S.E. et al., 2014. Leptin mediates the increase in blood pressure associated with obesity. *Cell,* 159(6), pp.1404-1416.

SINGH, K. et al., 2020. Arginyltransferase knockdown attenuates cardiac hypertrophy and fibrosis through TAK1-JNK1/2 pathway. *Nature Scientific Reports,* 10.

SINGH, R.M. et al., 2017. Protein kinase C and cardiac dysfunction: a review. *Heart Failure Reviews,* 22(6), pp.843-859.

SKALOVA, S. et al., 2015. Induced Pluripotent tem Cells and Their Use in Cardiac and Neural Regenerative Medicine. *International Journal of Molecular Sciences,* 16(2), pp.4043-4067.

SKLEPKIEWICZ, P. et al., 2015. Loss of secreted frizzled-related protein-1 leads to deterioration of cardiac function in mice and plays a role in human cardiomyopathy. *Circulation: Heart Failure,* 8(2), pp.362-372.

SMYRNIAS, I., BOOTMAN, M.D. AND RODERICK, H.L., 2012. Excitation-Contraction Coupling. In: F.C. MOOREN, ed. *Encyclopedia of Exercise Medicine in Health and Disease*. 2012 Edition. Berlin: Springer, pp. 310-314.

SNEDEKER, J.G. and GAUTIERI, A., 2014. The Role of Collagen Crosslinks in Ageing and Diabetes – the good, the bad and the ugly. *Muscles, Ligaments and Tendons Journal,* 4(3), pp.303-308.

SO, K.H. et al., 2011. Generation of functional cardiomyocytes from mouse induced pluripotent stem cells. *International Journal of Cardiology,* 153(3), pp.277-285.

SOLIMAN, E. et al., 2019. PPAR-γ agonist, pioglitazone, reduced oxidative and endoplasmic reticulum stress associated with L-NAME-induced hypertension in rats. *Life Sciences,* 239.

SOLOMON, S.D. et al., 2012. The angiotensin receptor neprilysin inhibitor LCZ696 in heart failure with preserved ejection fraction: a phase 2 double-blind randomised controlled trial. *Lancet,* 280(9851), pp.1387-1395.

SOLOMON, S.D. et al., 2019. Angiotensin–Neprilysin Inhibition in Heart Failure with Preserved Ejection Fraction. *The New England Journal of Medicine,* 381, pp.1609-1620.

SON, Y. et al., 2011. Mitogen-Activated Protein Kinases and Reactive Oxygen Species: How Can ROS Activate MAPK Pathways? *Journal of Signal Transduction,* 2011, pp. 792639.

SONG, H-P. et al., 2017. Label-free pharmacological profiling based on dynamic mass redistribution for characterization and authentication of hazardous natural products. *Journal of Hazardous Materials,* 333, pp.265-274.

SONG, R. et al., 2015. H2O2 Induces Myocardial Hypertrophy in H9c2 Cells: A Potential Role of Ube3a. *Cardiovascular Toxicology*, 15(1), pp.23-28.

SOWAH, D. et al., 2014. Resistance to cardiomyocyte hypertrophy in ae3-/- mice, deficient in the AE3 Cl-/HCO3- exchanger. *BMC Cardiovascular Disorders,* 14, pp.89.

SPRENGER, J.U. et al., 2016. Interactions of Calcium Fluctuations during Cardiomyocyte Contraction with Real-Time cAMP Dynamics Detected by FRET. *PLoS One,* 11(12), pp.e0167974.

SRIVASTAVA, S. et al., 2016. Cardioprotective effects of Cu (II) ATSM in human vascular smooth muscle cells and cardiomyocytes mediated by Nrf2 and DJ-1. *Scientific Reports,* 6(1).

ST PAUL, A. et al., 2020. Angiotensin II, Hypercholesterolemia, and Vascular Smooth Muscle Cells: A Perfect Trio for Vascular Pathology. *International Journal of Molecular Sciences,* 21(12), pp. 4525.

STAMOS, J.L. and WEIS, W.I., 2013. The β-catenin destruction complex. *Cold Spring Harbor Perspective in Biology,* 5(1), pp. a007898.

STEINBERG, S.F., 2012. Cardiac actions of protein kinase C isoforms. *Physiology,* 27(3), pp.130-139.

SUHAERI, M. et al., 2015. Cardiomyoblast (h9c2) differentiation on tunable extracellular matrix microenvironment. *Tissue Engineering,* 21(11-12), pp.1940-1951.

SUMIDA, T. et al., 2015. Complement C1q-induced activation of β-catenin signalling causes hypertensive arterial remodelling. *Nature Communications,* 6.

SUNG, J.H. et al., 2013. Effect of Lutein on L-NAME-Induced Hypertensive Rats. *Korean Journal of Physiology and Pharmacology,* 17(4), pp.339-345.

SUO, M. et al., 2002. N(G)-nitro-L-arginine methyl ester-induced hypertension and natriuretic peptide gene expression: inhibition by angiotensin II type 1 receptor antagonism. *Journal of Cardiovascular Pharmacology,* 40(3), pp.478-486.

SURENDRAN, K., MCCAUL, S.P. and SIMON, T.C., 2002. A role for Wnt-4 in renal fibrosis. *American Journal of Physiology. Renal Physiology,* 282(3), pp.F431-441.

SZYMANSKI, P. et al., 2012. Adaptation of high-throughput screening in drug discovery-toxicological screening tests. *International Journal of Molecular Science,* 13(1), pp.427-452.

TABATABAI, E. et al., 2021. Inhibition of angiotensin II type 1 receptor by Candesartan reduces tumor growth and ameliorates fibrosis in colorectal cancer. *EXCLi Journal,* 20, pp.863-878.

TAKADA, S. et al., 2017. Differences in the secretion and transport of Wnt proteins. *Journal of Biochemistry,* 161(1), pp.1-7.

TAKAHASHI, K. and YAMANAKA, S., 2006. Induction of pluripotent stem cells from mouse embryonic and adult fibroblast cultures by defined factors. *Cell,* 126(4), pp.663-676.

TAKAHASHI, K. et al., 2007. Induction of Pluripotent Stem Cells From Adult Human Fibroblasts by Defined Factors. *Cell,* 131(5), pp.861-872.

TAKEDA, Y. et al., 2007. Effects of aldosterone and angiotensin II receptor blockade on cardiac angiotensinogen and angiotensin-converting enzyme 2 expression in Dahl salt-sensitive hypertensive rats. *American Journal of Hypertension,* 20(10), pp.1119-1124.

TAKIMOTO, E. et al., 2005. Oxidant stress from nitric oxide synthase-3 uncoupling stimulates cardiac pathologic remodeling from chronic pressure load. *The Journal of Clinical Investigation,* 115(5), pp.1221-1231.

TAMAMORI-ADACHI, M. et al., 2002. Expression of cyclin D1 and CDK4 causes hypertrophic growth of cardiomyocytes in culture: a possible implication for cardiac hypertrophy. *Biochemical and Biophysical Research Communications,* 292(2), pp.274-280.

TANAKA, K. et al., 2000. The evolutionarily conserved porcupine gene family is involved in the processing of the Wnt family. *European Journal of Biochemistry,* 267(13), pp.4300-4311.

TANASE, D.M. et al., 2019. Natriuretic Peptides in Heart Failure with Preserved Left Ventricular Ejection Fraction: From Molecular Evidences to Clinical Implications. *International Journal of Molecular Science,* 20(11), pp.2629.

TANG, Q. et al., 2018. Wnt5a regulates the cell proliferation and adipogenesis via MAPK-independent pathway in early stage of obesity. *Cell Biology International,* 42(1), pp.63-74.

TEBROKE, J. et al., 2019. Wnt-3a Induces Cytokine Release in Human Mast Cells. *Cells,* 8(11), pp.1372.

THAM, Y.K. et al., 2015. Pathophysiology of cardiac hypertrophy and heart failure: signaling pathways and novel therapeutic targets. *Archives of Toxicology,* 89(9), pp.1401-1438.

THOONEN, R. et al., 2013. Pathophysiology of hypertension in the absence of nitric oxide/cyclic GMP signaling. *Current Hypertension Reports,* 15(1), pp.47-58.

TIAN, H. et al., 2018. Angiotensin II upregulates cyclophilin A by enhancing ROS production in rat cardiomyocytes. *Molecular Medicine Reports,* 18(5), pp.4349–4355.

TILLEY, D.G., REPAS, A.A. and CARTER, R.L., 2015. Label-Free Profiling of Endogenous Receptor Responses in Primary Isolated Cardiac Cells. In: Y.FANG, ed. *Methods in Pharmacology and Toxicology.* New York: Springer. Chapter 9.

TOMEK, J and BUB, G., 2017. Hypertension-induced remodelling: on the interactions of cardiac risk factors. *The Journal of Physiology.* 595(12), pp.4027-4036.

TONG, D. et al., 2019. Female Sex Is Protective in a Preclinical Model of Heart Failure With Preserved Ejection Fraction. *Circulation,* 140, pp.1769-1771.

TORNERO-ESTEBAN, P. et al., 2015. Altered Expression of Wnt Signaling Pathway Components in Osteogenesis of Mesenchymal Stem Cells in Osteoarthritis Patients. *PLoS One,* 10(9), pp. e0137170.

TOUYZ, R.M. and MONTEZANO, A.C., 2018. Angiotensin-(1-7) and Vascular Function: The Clinical Context. *Hypertension,* 71(1), pp.68-69.

TRAN, T.H. et al., 2009. Wnt3a-induced mesoderm formation and cardiomyogenesis in human embryonic stem cells. *Stem Cells,* 27(8), pp.1869-1878.

TSAI, T-Y. et al., 2015. Parthenolide-Induced Cytotoxicity in H9c2 Cardiomyoblasts Involves Oxidative Stress. *Acta Cardiologica Sinica,* 31(1), pp.33-41.

TSUCHIYA, K. et al., 2007. Chronic blockade of nitric oxide synthesis reduces adiposity and improves insulin resistance in high fat-induced obese mice. *Endocrinology,* 148(10), pp.4548-4556.

TSUKAMOTO, Y. et al., 2013. A novel heart failure mice model of hypertensive heart disease by angiotensin II infusion, nephrectomy, and salt loading. *American Journal of Physiology Heart and Circulatory Physiology,* 305(11), pp.H1658-1667.

TSURUDA, T. et al., 2016. Angiotensin II Stimulation of Cardiac Hypertrophy and Functional Decompensation in Osteoprotegerin-Deficient Mice. *Hypertension,* 67(5), pp.848-856.

UCHINAKA, A. et al., 2018. Overexpression of collagen type III in injured myocardium prevents cardiac systolic dysfunction by changing the balance of collagen distribution. *The Journal of Thoracic and Cardiovascular Surgery,* 156(1), pp.217-226.

VALERO-MUNOZ, M. et al., 2016. Dual Endothelin-A/Endothelin-B Receptor Blockade and Cardiac Remodeling in Heart Failure With Preserved Ejection Fraction. *Circulation: Heart Failure,* 9(11), pp.e003381.

VALERO-MUNOZ, M., BACKMAN, W. and SAM, F., 2017. Murine Models of Heart Failure with Preserved Ejection Fraction: a "Fishing Expedition". *JACC: Basic to Translational Science,* 2(6), pp.770-789.

VALIENTE-ALANDI, I. et al., 2018. Inhibiting Fibronectin Attenuates Fibrosis and Improves Cardiac Function in a Model of Heart Failure. *Circulation,* 138(12), pp.1236-1252.

VAN BILSEN, M. et al., 2014. Hypertension is a conditional factor for the development of cardiac hypertrophy in type 2 diabetic mice. *PLoS One,* 9(1).

VAN DE SCHANS, V.A.M. et al., 2007. Interruption of Wnt signaling attenuates the onset of pressure overload-induced cardiac hypertrophy. *Hypertension,* 49(3), pp.473-480.

VAN DER POL, A. et al., 2019. Treating oxidative stress in heart failure: past, present and future. *European Journal of Heart Failure,* 21(4), pp. 425-435.

VAN HEEREBEEK, L. and PAULUS, W,J., 2016. Understanding Heart Failure with Preserved Ejection Fraction: Where are we today? *Netherlands Heart Journal,* 24, pp.227-236.

VAN HEEREBEEK, L. et al., 2012. Low myocardial protein kinase G activity in heart failure with preserved ejection fraction. *Circulation,* 126(7), pp.830-839.

VERK, B. et al., 2017. Markers of oxidative stress in dogs with heart failure. *Journal of Veterinary Diagnostic Investigation,* 29(5), pp.636-644.

VERMEULEN, J. et al., 2011. Measurable Impact of RNA Quality on Gene Expression Results From Quantitative PCR. *Nucleic Acids Research,* 39(9), pp. e63.

VINCENT, J-L., 2008. Understanding cardiac output. *Critical Care,* 12(4), pp. 174.

VOLPE, M., CARNOVALI, M. and MASTROMARINO, V., 2016. The natriuretic peptides system in the pathophysiology of heart failure: from molecular basis to treatment. *Clinical Science,* 130(2), pp.57-77.

WAN, S-H. et al., 2016. Chronic Peptide Therapy With B-Type Natriuretic Peptide in Patients With Pre-Clinical Diastolic Dysfunction (Stage B Heart Failure). *JACC. Heart Failure,* 4(7), pp.539-547.

WANG, C. et al., 2020. Low-dose L-NAME induces salt sensitivity associated with sustained increased blood volume and sodium-chloride cotransporter activity in rodents. *Kidney International,* 98(5), pp.1242-1252.

WANG, F-S. et al., 2005. Secreted frizzled-related protein 1 modulates glucocorticoid attenuation of osteogenic activities and bone mass. *Endocrinology,* 146(5), pp.2415-2423.

WANG, H-J., ZHU, Y-C. and YAO, T., 2002. Effects of all-trans retinoic acid on angiotensin II-induced myocyte hypertrophy. *Journal of Applied Physiology,* 92, pp.2162-2168.

WANG, J, et al., 2003. Increased expression of protein kinase C isoforms in heart failure due to myocardial infarction. *American Journal of Physiology Heart and Circulatory Physiology,* 284, pp. H2277–H2287.

WANG, R. et al., 2014a. Inhibition of angiotensin II-induced cardiac hypertrophy and associated ventricular arrhythmias by a p21 activated kinase 1 bioactive peptide. *PLoS One,* 9(7), pp.e101974.

WANG, R. et al., 2014b. SFRP5 acts as a mature adipocyte marker but not as a regulator in adipogenesis. *Journal of Molecular Endocrinology,* 53(3), pp.405-415.

WANG, X. et al., 2018. Ghrelin Alleviates Angiotensin II-Induced H9c2 Apoptosis: Impact of the miR-208 Family. *Medical Science Monitor: international medical journal of experimental and clinical research,* 24, pp.6707-6716.

WANG, Z. et al., 2012. Effects of angiotensin II AT1 receptor inhibition and exercise training on insulin action in rats on high-fat diet. *Life Sciences,* 90(9-10), pp.322-327.

WANG,Z. et al., 2015. Chronic high fat diet induces cardiac hypertrophy and fibrosis in mice. *Metabolism,* 64(8), pp.917-925.

WATKINS, S.J. et al., 2012. Angiotensin II-induced cardiomyocyte hypertrophy in vitro is TAK1-dependent and Smad2/3-independent. *Hypertension Research,* 35(4), pp.393-398.

WATKINS, S.J., BORTHWICK, G.M. and ARTHUR, H.M., 2011. The H9C2 Cell Line and Primary Neonatal Cardiomyocyte Cells Show Similar Hypertrophic Responses in Vitro. *In Vitro Cellular & Developmental Biology,* 47, pp.125-131.

WATSON, C.J. et al., 2012. Mechanical stretch up-regulates the B-type natriuretic peptide system in human cardiac fibroblasts: a possible defense against transforming growth factor-β mediated fibrosis. *Fibrogenesis and Tissue Repair,* 5.

WAWRZAK, D. et al., 2007. Wnt3a binds to several sFRPs in the nanomolar range. *Biochemical and biophysical research communications,* 357(4), pp.1119-1123.

WEI, W-Y. et al., 2019. Secreted frizzled-related protein 2 prevents pressure-overload-induced cardiac hypertrophy by targeting the Wnt/β-catenin pathway. *Molecular and Cellular Biochemistry,* 472, pp.241-251.

WEN, H., GWATHMEY, J.K. and XIE, L-H., 2012. Oxidative stress-mediated effects of angiotensin II in the cardiovascular system. *World Journal of Hypertension,* 2(4), pp. 34-44.

WESTERMANN, D. et al., 2012. Selective PDE5A inhibition with sildenafil rescues left ventricular dysfunction, inflammatory immune response and cardiac remodeling in angiotensin II-induced heart failure in vivo. *Basic Research in Cardiology,* 107(6), pp.308.

WETTERSTEN, N, and MAISEL, A.S., 2016. Biomarkers for Heart Failure: An Update for Practitioners of Internal Medicine. *The American Journal of Medicine,* 129(6), pp.560-567.

WHITE, S.M., CONSTANTIN, P.E. and CLAYCOMB, W.C., 2004. Cardiac physiology at the cellular level: use of cultured HL-1 cardiomyocytes for studies of cardiac muscle cell structure and function. *American Journal of Physiology. Heart and Circulation Physiology,* 286(3), pp.H823-829.

WILLIAMS, H., 2015. Hypertension: Pathophysiology and diagnosis. *Clinical Pharmacist,* 7(1), pp.11-14.

WILSON, R.M. et al., 2009. Effects of fixed-dose isosorbide dinitrate/hydralazine on diastolic function and exercise capacity in hypertension-induced diastolic heart failure. *Hypertension,* 54(3), pp.583-590.

WISDOM, R., JOHNSON, R.S. and MOORE, C.,1999. c-Jun regulates cell cycle progression and apoptosis by distinct mechanisms. *The EMBO Journal,* 18(1), pp.188-197.

WITEK, P. et al., 2016. The effect of a number of H9C2 rat cardiomyocytes passage on repeatability of cytotoxicity study results. *Cytotechnology,* 68(6), pp.2407-2415.

WITHAAR, C. et al., 2021a. Heart failure with preserved ejection fraction in humans and mice: embracing clinical complexity in mouse models. *European Heart Journal,* 42(43), pp.4420-4430.

WITHAAR, C. et al., 2021b. The effects of liraglutide and dapagliflozin on cardiac function and structure in a multi-hit mouse model of heart failure with preserved ejection fraction. *Cardiovascular Research,* 117(9), pp.2108-2124.

WITTIG, C. and SZULCEK, R., 2021. Extracellular Matrix Protein Ratios in the Human Heart and Vessels: How to Distinguish Pathological From Physiological Changes? *Frontiers in Physiology,* 12.

WOO, S-L. et al., 2014. Metformin Ameliorates Hepatic Steatosis and Inflammation without Altering Adipose Phenotype in Diet-Induced Obesity. *PLoS One,* 9(3), pp.e9111.

WORLD HEALTH ORGANISATION (WHO), 2017. *Cardiovascular Diseases (CVDs).* [online]. Geneva: WHO. Available from: https://www.who.int/en/news-room/fact-sheets/detail/cardiovascular-diseases-(cvds) [Accessed 4th June 2020].

WRIGHT, J.T. et al., 2015. A Randomized Trial of Intensive versus Standard Blood-Pressure Control. *The New England Journal of Medicine,* 373, pp.2103-2116.

WU, C., DONG, S. and LI, Y., 2015. Effects of miRNA-455 on cardiac hypertrophy induced by pressure overload. *International Journal of Molecular Medicine,* 5(4), pp.893-900.

WU, J. et al., 1996. 1,25(OH)2D3 suppresses expression and secretion of atrial natriuretic peptide from cardiac myocytes. *The American Journal of Physiology,* 268, pp.E1108-1113.

WU, L. et al., 2018. C1QTNF1 attenuates angiotensin II-induced cardiac hypertrophy via activation of the AMPKa pathway. *Free Radical Biology and Medicine,* 121, pp.215-230.

WU, M-P. et al., 2017. Vinpocetine Attenuates Pathological Cardiac Remodeling by Inhibiting Cardiac Hypertrophy and Fibrosis. *Cardiovascular Drugs and Therapy,* 31(2), pp.157-166.

WU, Q-Q. et al., 2014. Sulforaphane protects H9c2 cardiomyocytes from angiotensin II-induced hypertrophy. *Herz,* 39(3), pp.390-396

WU, T. et al., 2020. An MRTF-A-Sp1-PDE5 Axis Mediates Angiotensin-II-Induced Cardiomyocyte Hypertrophy. *Frontiers in Cell and Developmental Biology,* 8, pp.839.

WU, X. et al., 2010. Cardiomyocyte Contractile Status Is Associated With Differences in Fibronectin and Integrin Interactions. *American journal of physiology. Heart and circulatory physiology,* 298(6), pp.H2071-H2081.

XAVIER, C.P. et al., 2014. Secreted Frizzled-related protein potentiation versus inhibition of Wnt3a/β-catenin signaling. *Cell Signalling,* 26(1), pp.94-101.

XIANG, F-L., FANG, M. and YUTZEY, K.E., 2017. Loss of β-catenin in resident cardiac fibroblasts attenuates fibrosis induced by pressure overload in mice. *Nature Communications,* 8.

XIANG, G. et al., 2011. Lentivirus-mediated Wnt11 gene transfer enhances Cardiomyogenic differentiation of skeletal muscle-derived stem cells. *Molecular Therapy,* 19(4), pp.790-796.

XIAO, G. et al., 2001. Inducible activation of c-Myc in adult myocardium in vivo provokes cardiac myocyte hypertrophy and reactivation of DNA synthesis. *Circulation Research,* 89(12), pp.1122-1129.

XIAO, L. et al., 2019. Wnt/β-catenin regulates blood pressure and kidney injury in rats. *Biochimica et Biophysica Acta - Molecular Basis of Disease*, 1865(6), pp.1313-1322.

XIE, Y. et al., 2019. Rare mutations of ADAM17 from TOFs induce hypertrophy in human embryonic stem cell-derived cardiomyocytes via HB-EGF signaling. *Clinical Science,* 133(2), pp.225-238.

XU, C. et al., 2002. Characterization and enrichment of cardiomyocytes derived from human embryonic stem cells. *Circulation Research,* 91(6), pp.501-508.

Xu, M. et al., 2019. Oridonin protects against cardiac hypertrophy by promoting P21-related autophagy. *Cell Death and Disease,* 10(403).

XU, S. and GOTLIEB, A.I., 2013. Wnt3a/β-catenin increases proliferation in heart valve interstitial cells. *Cardiovascular Pathology,* 22(2), pp.156-166.

XU, X, et al., 2014. Macrophage migration inhibitory factor deletion exacerbates pressure overload-induced cardiac hypertrophy through mitigating autophagy. *Hypertension,* 63(3), pp.490-499.

XU, Z. et al., 2008. Pravastatin attenuates left ventricular remodeling and diastolic dysfunction in angiotensin II-induced hypertensive mice. *Journal of Cardiovascular Pharmacology,* 51(1), pp.62-70.

XUE, B. et al., 2021. Maternal Angiotensin II-Induced Hypertension Sensitizes Postweaning High-Fat Diet-Elicited Hypertensive Response Through Increased Brain Reactivity in Rat Offspring. *Journal of the American Heart Association,* 10(18).

YAMAMOTO, M. et al., 2017. Effect of Dipeptidyl Peptidase-4 Inhibitors on Cardiovascular Outcome and Cardiac Function in Patients With Diabetes and Heart Failure - Insights From

the Ibaraki Cardiac Assessment Study-Heart Failure (ICAS-HF) Registry. *Circulation Journal.* 81(11), pp.1662-1669.

YAN, L. et al., 2013. Quercetin inhibits left ventricular hypertrophy in spontaneously hypertensive rats and inhibits angiotensin II-induced H9C2 cells hypertrophy by enhancing PPAR-γ expression and suppressing AP-1 activity. *PLoS One,* 8(9), pp.e72548.

YANG, D. et al., 2017. Therapeutic effect of a novel Wnt pathway inhibitor on cardiac regeneration after myocardial infarction. *Clinical Science,* 131(24), pp.2919-2932.

YANG, K., HITOMI, M. and STACEY, D.W., 2006. Variations in cyclin D1 levels through the cell cycle determine the proliferative fate of a cell. *Cell Division,* 1, pp.32.

YANG, L. et al., 2016. All-trans retinoic acid protects against doxorubicin-induced cardiotoxicity by activating the ERK2 signalling pathway. *British Journal of Pharmacology,* 173(2), pp.357-371.

YE, N. et al., 2014. Small molecule inhibitors targeting activator protein 1 (AP-1). *Journal of Medicinal Chemistry,* 57(16), pp.6930-6948.

YI, H. et al., 2007. Characterization of Wnt signaling during photoreceptor degeneration. *Investigative Ophthalmology & Visual Science,* 48(12), pp.5733-5741.

YIN, F.C. et al., 1982. Use of tibial length to quantify cardiac hypertrophy: application in the aging rat. *The American Journal of Physiology,* 243(6), pp.H941-947.

YONG, C. et al., 2016. SNF5 alleviates Ang II-induced myocardial hypertrophy by inactivation of MAPK/mTOR pathway. *International Journal of Clinical and Experimental Pathology,* 9(12), pp.12602-12608.

YU, J. and VIRSHUP, D.M., 2014. Updating the Wnt pathways. *Bioscience Reports,* 34(5), pp. e00142.

YU, X-M. et al., 2013. Wnt5a inhibits hypoxia-induced pulmonary arterial smooth muscle cell proliferation by downregulation of β-catenin. *American Journal of Physiology. Lung cellular and molecular physiology,* 304(2), pp. L103-111.

YUN, M-S. et al., 2005. Both ERK and Wnt/beta-catenin pathways are involved in Wnt3a-induced proliferation. *Journal of Cell Science,* 118, pp.313-322.

ZABLOCKI, D. and SADOSHIMA, J., 2013. Angiotensin II and Oxidative Stress in the Failing Heart. *Antioxidants and Redox Signaling,* 19(10), pp.1095-1109.

ZAKERI, A. et al., 2015. Nitrate's effect on activity tolerance in heart failure with preserved ejection fraction trial: rationale and design. *Circulation. Heart Failure,* 8(1), pp.221-228.

ZELARAYAN, L., GEHRKE, C. and BERGMANN, M.W., 2007. Role of beta-catenin in adult cardiac remodelling. *Cell Cycle,* 6(17), pp.2120-2126.

ZHANG, J. et al., 2020. Neohesperidin inhibits cardiac remodeling induced by Ang II in vivo and in vitro. *Biomedical and Pharmacotherapy,* 129.

ZHANG, L. et al., 2018b. Protective Effect of Rosamultin against H_2O_2- Induced Oxidative Stress and Apoptosis in H9c2 Cardiomyocytes. *Oxidative Medicine and Cellular Longevity.* 2018, pp.8415610.

ZHANG, X. et al., 2018a. Identification and Evaluation of Cytotoxicity of Peptide Liposome Incorporated Citron Extracts in an in Vitro System. *International Journal of Molecular Sciences,* 19(2), pp.626.

ZHANG, Y. et al., 2019. Captopril attenuates TAC-induced heart failure via inhibiting Wnt3a/β-catenin and Jak2/Stat3 pathways. *Biomedicine and Pharmacotherapy,* 133, pp.108780.

ZHAO, M. et al., 2019b. Deciphering Role of Wnt Signalling in Cardiac Mesoderm and Cardiomyocyte Differentiation from Human iPSCs: Four-dimensional control of Wnt pathway for hiPSC-CMs differentiation. *Scientific Reports,* 9(1), pp.19389.

ZHAO, X. and WANG, X., 2018. Candesartan targeting of angiotensin II type 1 receptor demonstrates benefits for hypertension in pregnancy via the NF-κB signaling pathway. *Molecular Medicine Reports,* 18(1), pp.705-714.

ZHAO, Y. et al., 2018. An essential role for Wnt/β-catenin signaling in mediating hypertensive heart disease. *Nature Scientific Reports,* 8(8996).

ZHAO, Y. et al., 2019a. Wnt/β-catenin signaling mediates both heart and kidney injury in type 2 cardiorenal syndrome. *Kidney International,* 95(4), pp.815-829.

ZHAO, Z. et al., 2020. Wnt-C59 Attenuates Pressure Overload-Induced Cardiac Hypertrophy via Interruption of Wnt Pathway. *Medical Science Monitor,* 26, pp.e923025.

ZHENG, Q. et al., 2013. Expression and redistribution of β-catenin in the cardiac myocytes of left ventricle of spontaneously hypertensive rat. *Journal of Molecular Histology,* 44(5), pp.565-573.

ZHONG, W. et al., 2006. Hypertrophic growth in cardiac myocytes is mediated by Myc through a Cyclin D2-dependent pathway. *The EMBO Journal,* 25(16), pp.3869-2879.

ZHOU, H. et al., 2014. Icariin attenuates angiotensin II-induced hypertrophy and apoptosis in H9c2 cardiomyocytes by inhibiting reactive oxygen species-dependent JNK and p38 pathways. *Experimental and Therapeutic Medicine,* 7(5), pp.1116-1122.

ZHOU, L. and LIU, Y., 2016. Wnt/β-catenin signaling and renin-angiotensin system in chronic kidney disease. *Current opinion in nephrology and hypertension,* 25(2), pp.100-106.

ZHOU, L. et al., 2015. Multiple genes of the renin-angiotensin system are novel targets of Wnt/β-catenin signaling. *Journal of the American Society of Nephrology,* 26(1), pp.107-120.

ZHOU, M.D. et al., 1995. Retinoid-dependent pathways suppress myocardial cell hypertrophy. *PNAS,* 92(16), pp.7391-7395.

ZHOU, T. et al., 2012. Implication of dysregulation of the canonical wingless-type MMTV integration site (WNT) pathway in diabetic nephropathy. *Diabetologia*, 55(1), pp.255-266.

ZHU, X-H. et al., 2016. LncRNA MIAT enhances cardiac hypertrophy partly through sponging miR-150. *European Review for Medical and Pharmacological Sciences,* 20(17), pp.3653-3660.

ZIAEIAN, B. and FONAROW, G.C., 2016. Epidemiology and Aetiology of Heart Failure. *Nature Reviews. Cardiology,* 13(6), pp.368-378.

ZUO, S. et al., 2012. Paracrine effect of Wnt11-overexpressing mesenchymal stem cells on ischemic injury. *Stem Cells and Development,* 21(4), pp.598-608.